REPORT DOCUMENTATION PAGE

AD-A255 383

1. AGENCY USE ONLY (Leave blank)	2. REPORT DATE	3. REPORT TYPE AND DATES COVERED
		Quarterly 2 Mar - 5 Mar 92

4. TITLE AND SUBTITLE	5. FUNDING NUMBERS
Physics of X-Ray Multilayer Structures	F49620-92-J-0264

6. AUTHOR(S)

Dr Quinn

7. PERFORMING ORGANIZATION NAME(S) AND ADDRESS(ES)	8. PERFORMING ORGANIZATION REPORT NUMBER
Optical Society of America 2010 Massachusetts Ave N.W. Washington, DC 20036	AFOSR-TR· 2 0737

9. SPONSORING/MONITORING AGENCY NAME(S) AND ADDRESS(ES)	10. SPONSORING/MONITORING AGENCY REPORT NUMBER
AFOSR/NE Bldg 410 Bolling AFB DC 20332-6448	2301/AS

DTIC
ELECTE
AUG 11 1992
S A D

11. SUPPLEMENTARY NOTES

12a. DISTRIBUTION/AVAILABILITY STATEMENT	12b. DISTRIBUTION CODE
UNLIMITED	

13. ABSTRACT (Maximum 200 words)

CONFERENCE WAS HELD

14. SUBJECT TERMS	15. NUMBER OF PAGES
	16. PRICE CODE

17. SECURITY CLASSIFICATION OF REPORT	18. SECURITY CLASSIFICATION OF THIS PAGE	19. SECURITY CLASSIFICATION OF ABSTRACT	20. LIMITATION OF ABSTRACT
UNCLASS	UNCLASS	UNCLASS	UL

Physics of X-ray Multilayer Structures

Summaries of papers presented at the
Physics of X-ray Multilayer Structures Topical Meeting

March 2–5, 1992
Jackson Hole, Wyoming

1992 Technical Digest Series
Volume 7

CONFERENCE EDITION

92-22465

Articles in this publication may be cited in other publications. In order to facilitate access to the original publication source, the following form for the citation is suggested:

Name of Author(s), "Title of Paper," in <u>Physics of X-ray Multilayer Structures Technical Digest 1992</u> (Optical Society of America, Washington, D.C., 1992), Vol. 7, pp. xx–xx.

CONTENTS

DTIC QUALITY INSPECTED 5

Distribution /

Availability Codes

Dist	Avail and / or Special
A-1	

iii

TECHNICAL PROGRAM COMMITTEE

TETON ROOM

6:00 pm–8:00 pm   BEER AND PRETZELS WELCOME
RECEPTION

MEZZANINE

6:00 pm–8:00 pm   REGISTRATION

MONDAY, MARCH 2, 1992

RESTAURANT

7:00 am–8:00 am   BREAKFAST

MEZZANINE

7:00 am–11:30 am   REGISTRATION/SPEAKER CHECK-IN

GRAND ROOM

8:00 am–9:00 am
MA, INTRODUCTION AND OPENING REMARKS
Daniel G. Stearns, *Lawrence Livermore National
Laboratory, Presider*

8:15 am   (Invited Paper)
MA1   Physical optics of x-ray multilayer structures, Eberhard Spiller, *IBM Watson Research Center.* Overview about design and characterization, deposition techniques, present performance, possible future performance, and applications of multilayer structures in x-ray optics is presented. (p. 2)

GRAND ROOM

9:00 am–11:30 am
MB, GROWTH AND STRUCTURE: 1
Daniel G. Stearns, *Lawrence Livermore National
Laboratory, Presider*

9:00 am   (Invited Paper)
MB1   Relationship between soft x-ray reflectance and structural parameters of nanometer-period multilayers for x-ray mirrors, Philippe Houdy, Pierre Boher, *Laboratoires d'Electronique Philips, France.* Multilayers alternating materials at atomic scale have been deposited using UHV diode rf sputtering, to be used as soft x-ray mirrors. We have investigated the relationship between the stack performances (reflectivity, selectivity) and the structural characteristics of the stacks. (p. 4)

TETON ROOM

9:45 am–10:15 am   COFFEE BREAK

GRAND ROOM

10:15 am
MB2   Effects of sputtering pressure on roughness and re-sputtering of multilayers, M. M. Hasan, R. J. Highmore, R. E. Somekh, *Univ. Cambridge, U.K.* We have studied the effects of roughness and resputtering in UHV dc magnetron sputtered multilayers of W-Si (for x-ray mirrors) and Co–Cu (for giant magnetoresistance). (p. 8)

10:45 am
MB3   Stress, morphology, and optical properties of Mo/Si x-ray multilayers, D. L. Windt, R. R. Kola, W. K. Waskiewicz, R. Hull, J. Griffith, D. A. Grigg, *AT&T Bell Laboratories.* The stress and stress-relaxation characteristics have been correlated with the structural and optical properties of Mo/Si multilayers. The dependence of stress with multilayer period, Mo:Si ratio, sputter gas, gas pressure, and magnetron cathode power density during growth has been investigated. (p. 12)

11:15 am
MB4   Experimental setup for the production of large size x-ray multilayer structures, E. Ziegler, J. Ch. Peffen, P. Hoghoj, *European Synchrotron Radiation Facility, France.* A novel method for depositing large size multilayers is described. A plasma produced by distributed electron cyclotron resonance will soon allow the chemical vapor deposition and the sputtering of nanometer thin-films over and area of 250 cm². (p. 16)

11:45 am–7:00 pm   AFTERNOON FREE

MEZZANINE

7:00 pm–10:00 pm   REGISTRATION/SPEAKER CHECK-IN

TETON ROOM

7:00 pm–7:30 pm
MC, POSTER SESSION AND REFRESHMENTS

MC1   Investigation of the effect of large x-ray fluences on multilayer structures, B. J. MacGowan, S. Mrowka, T. Barbee Jr., L. B. Da Silva, D. C. Eder, J. A. Koch, L. Pan, J. Underwood, P. E. Young, *Lawrence Livermore National Laboratory.* X-ray damage processes in multilayer mirrors, for use in x-ray laser cavities, have been studied experimentally using short-duration (500 psec) bursts of soft x-rays. (p. 22)

MC2 Analytical observations and depth profile simulation in regular-d and graded-d metal/carbon multilayers prepared by laser pulse vapor deposition, R. Dietsch, H. Mai, W. Pompe, B. Schoneich, S. Vollmar, *Fraunhofer-Einrichtung fur Werkstoffphysik und Schichttechnologie;* S. Hopfe. P. Werner, *Institut fur Festkorperphysik und Elektronenmikroskopie;* G. Oertel, *Zentralinstitut fur Elektronenphysik;* B. Wehner, *Technische Univ. Dresoen;* P. Weibbrodt, *Jenoptik Carl Zeiss JENA GmbH, Germany.* Multilayer structures are characterized by TEM, XD, AES, and SNMS. Results obtained for x-ray optical behavior, layer stack morphology, and microstructure of individual layers are described, and their explanation is supported by computer simulation data. (p. 23)

MC3 Diffusion behavior of metal–carbon multilayers, A. D. Akhsakhalyan, A. A. Fraerman, Yu. Ya. Platonov, N. I. Polushkin, N. N. Salashchenko, *USSR Academy of Sciences, USSR.* The effect of annealing on the x-ray optical characteristics of artificial multilayer structures composed of metal (Cr, Fe, Ni, Mo, Rh, W, Pt and others) and carbon is studied. To analyze the changes at annealing, a small-angle x-ray diffraction was used. The observed x-ray reflectivity enhancement can be explained by the uphill diffusion of metal atoms. (p. 27)

MC4 Interfacial roughness and interdiffusion derived from a comparison of the measured and calculated reflectances of Mo/Si multilayer coatings, J. F. Seely, M. P. Kowalski, J. C. Rife, *U.S. Naval Research Laboratory;* T. W. Barbee, *Lawrence Livermore National Laboratory;* W. R. Hunter, *SFA, Inc.* The reflectances of Mo/Si multilayers were modeled and compared to synchrotron radiation measurements with the intention of inferring the effects of interfacial roughness and interdiffusion. (p. 31)

MC5 A system for rapid characterization of multilayer mirrors and other soft x-ray optical components, S. Mrowka, B. J. MacGowan, L. B. Da Silva, J. A. Koch, *Lawrence Livermore National Laboratory.* A laser-produced plasma soft x-ray system for the very rapid characterization of multilayers and other optical components is described. (p. 35)

MC6 Sputtering deposited Ta/Si multilayer soft x-ray mirrors, Shao Jianda, Fan Zhengxiu, *Academia Sinica, China.* Tantalum/silicon multilayers to be used as normal-incidence mirrors for 234A x-ray have been fabricated using a plane magnetron sputtering system. The test and evaluation of characterizations have been given by small-angle diffraction and Cu–Ka radiation, transmission electron microscopy, and auger electron spectroscopy. (p. 39)

MC7 Stability of the long-period modulated structures in ordering systems, S. S. Andreev, N. I. Polushkin, N. N. Salashchenko, S. I. Shinkarev, *USSR Academy of Sciences, USSR.* The anomalies in diffusion behavior of compositionally modulated structures in ordering systems W/Sb and Co/Pt are discussed. There are stable subnanometer modulated structures in W/Sb alloys. It has allowed the construction of normal-incidence x-ray mirrors. (p. 40)

MC8 Study of ultrathin films in multilayer structures by standing-waves and small-angle x-ray scattering techniques, A. A. Fraerman, Yu. Ya. Platonov, N. I. Polushkin, N. N. Salashchenko, S. I. Zheludeva, M. V. Kovalchuk, N. N. Novikova, I. V. Bashelhanov, *USSR Academy of Sciences, USSR.* A method for determining the parameters (concentration of atoms in the layers; thickness of the layers and thickness of the interface between constituent layers; characteristics of the layer thickness fluctuations) of real layered synthetic microstructures of superthin films (the layer thickness is about 1–10 nm) is discussed. (p. 44)

MC9 Modeling of x-ray diffraction by multilayer mirrors, gratings, and zone plates, A. Sammar, B. Pardo, J.-M. Andre, *Univ. Paris, France.* The Born approximation is applied to describe the diffractive properties of multilayer mirrors, gratings, and zone plates. A rigorous theory is given for the gratings. (p. 48)

MC10 X-ray and TEM analysis of small period W–Si and W–B₄C multilayers, James Wood, Kevin Parker, James Scholhamer, *Ovonic Synthetic Materials Co., Inc.;* John F. Mansfield, *Univ. Michigan.* Achievement of high reflectivity by small period multilayer coatings for uses in x-ray spectroscopy and microscopy has been limited by layer-interface imperfections. During a systematic investigation to better understand the influence of process conditions on these imperfections, we produced W–Si and W–B₄C multilayers with a range of d-spacings (15A < d < 22Å) via magnetron sputtering. An analysis of experimental and calculated x-ray reflectivities at 1.54Å and 8.34Å compared to high-resolution TEM images of the multilayers illustrates the relationship between layer roughness propagation and x-ray performance for the two material systems. (p. 52)

MC11 XUV Mo/Si multilayer mirrors deposited by rf magnetron sputtering, Claude Montcalm, Brian T. Sullivan, J. A. Dobrowolski, *National Research Council of Canada;* H. Pepin, *Univ. Quebec, Canada.* Characterization results of Mo/Si multilayer mirrors deposited under different deposition conditions are presented. Substrate rotation and oscillation were used to achieve large-area uniform coatings. (p. 55)

MC12 Layered optics for nuclear monochromatization of synchrotron radiation, E. E. Alp, E. Witthoff, T. Mooney, *Argonne National Laboratory;* H. Homma, M. Kentjana, *CUNY-Brooklyn.* Monochromatization of synchrotron radiation with $\Delta E/E = 10^{-10}$–10^{-12} at energies above 10 keV using nuclear coherent scattering from grazing incidence antireflection (GIAR) films is discussed. (p. 57)

GRAND ROOM

7:30 pm–10:30 pm
MD, GROWTH AND STRUCTURE: 2
Jeffrey B. Kortright, *Lawrence Berkeley Laboratory,*
Presider

7:30 pm (Invited Paper)
MD1 Application of *in-situ* ellipsometry to the study of ultrathin layers and soft x-ray multilayers, Masaki Yamamoto, *Tohoku Univ., Japan. In-situ* ellipsometry with 633 nm He–Ne laser light has been applied to the study of minimum thicknesses of optical uniformity, interdiffusions and stability of ultrathin multilayers. **(p. 60)**

8:15 pm
MD2 Optimization of growth conditions of vapor-deposited Mo/Si multilayers, M. B. Stearns, *Arizona State Univ.;* D. G. Stearns, *Lawrence Livermore National Laboratory.* The dependence of the layer structure and interfaces of e-beam and sputter-deposited Mo/Si multilayers on the growth conditions was investigated. **(p. 64)**

8:45 pm–9:30 pm COFFEE BREAK

9:00 pm (Invited Paper)
MD3 Pulse laser deposition of layered synthetic microstructures, S. V. Gaponov, E. B. Kluenkov, Yu. Ya. Platonov, N. N. Salashchenko, *USSR Academy of Science, USSR.* The physical grounds of the pulse laser deposition of layered synthetic microstructures (LSM) are discussed. The experimental data are compared by means of soft x-ray reflection from LSM synthesized by pulse laser deposition (PLD), magnetron sputtering (MS) and e-beam evaporation. **(p. 66)**

9:45 pm
MD4 Ion-assisted sputter deposition of Mo-Si multilayers, S. P. Vernon, *Vernon Applied Physics;* D. G. Stearns, R. S. Rosen, *Lawrence Livermore National Laboratory.* The structural and x-ray optical properties of Mo-Si multilayers grown by dc magnetron sputter deposition at varying substrate bias have been investigated. **(p. 70)**

10:15 pm
MD5 Simulation of mixing at Mo/Si interfaces, D. B. Boercker, *Lawrence Livermore National Laboratory;* W. L. Morgan, *Kinema Research.* We have performed molecular dynamics simulations of the mixing at Mo/Si interfaces, and we have reproduced the observed asymmetry in interlayer thicknesses. **(p. 72)**

RESTAURANT

7:00 am–8:00 am BREAKFAST

MEZZANINE

7:00 am–11:15 am REGISTRATION/SPEAKER CHECK-IN

GRAND ROOM

8:00 am–9:45 am
TuA, ROUGHNESS AND NONSPECULAR SCATTERING: 1
Jon M. Slaughter, *University of Arizona, Presider*

8:00 am (Invited Paper)
TuA1 Roughness evolution in films and multilayer structures, M. G. Lagally, *Univ. Wisconsin-Madison.* STM and diffraction are used to probe the evolution of roughness in growing films and to determine correlation lengths and degree of correlation in multilayers. **(p. 78)**

8:45 am
TuA2 X-ray scattering studies of correlated interface roughness in multilayers, S. K. Sinha, *Exxon Research & Engineering Company;* M. K. Sanyal, *Brookhaven National Laboratory;* S. K. Satija, C. F. Majkrzak, *U.S. National Institute for Standards and Technology;* I. K. Schuller, *UC-San Diego;* H. Homma, *Brooklyn College;* C. M. Falco, B. N. Edngel, *Univ. Arizona.* We discuss the formalism for specular and diffuse x-ray scattering from multilayers with correlated interface roughness and demonstrate good agreement with x-ray studies on such systems. **(p. 82)**

9:15 am
TuA3 Theory of nonspecular x-ray scattering from multilayer structures, D. G. Stearns, *Lawrence Livermore National Laboratory.* The scattering of x-rays from interfacial roughness in multilayer structures is treated theoretically, and calculations for specific interface configurations are presented. **(p. 86)**

TETON ROOM

9:45 am–10:15 am COFFEE BREAK

GRAND ROOM

10:15 am–11:30 am
TuB, TEM CHARACTERIZATION
D. J. Eaglesham, *AT&T Bell Laboratories, Presider*

10:15 am (Invited Paper)
TuB1 **High-resolution electron microscope imaging and quantification of interface structure in x-ray multilayers,** R. Hull, D. L. Windt, R. Kola, W. K. Waskiewicz, *AT&T Bell Laboratories.* We discuss the applications and limits of high-resolution electron microscopy to quantifying atomic-scale structure in x-ray mirror multilayer structures. (p. 90)

11:00 am
TuB2 **Effects of Fresnel fringes on TEM images of interfaces in x-ray multilayers,** Tai D. Nguyen, Michael A. O'Keefe, Roar Kilaas, Ronald Gronsky, Jeffrey B. Kortright, *Lawrence Berkeley Laboratory.* X-ray multilayers of alternating layers of very different materials are prone to Fresnel fringe effects in TEM images. The effects result in different apparent interfacial profiles with defocus and thus complicate quantitative interpretation of interfacial profiles. Modeling of the fringes provides a useful tool to characterize the interfaces. (p. 94)

11:30 am–7:00 pm Afternoon Free

MEZZANINE

7:00 pm–10:00 pm REGISTRATION/SPEAKER CHECK-IN

TETON ROOM

7:00 pm–7:30 pm
POSTER SESSION AND REFRESHMENTS

GRAND ROOM

7:30 pm–10:15 pm
TuC, ROUGHNESS AND NONSPECULAR SCATTERING: 2
David L. Windt, *AT&T Bell Laboratories, Presider*

7:30 pm (Invited Paper)
TuC1 **Surface roughness and x-ray scattering,** E. L. Church, *USA ARDEC;* P. Z. Takacs, *Brookhaven National Laboratory.* Methods developed for measuring, characterizing and predicting the performance of glancing-incidence x-ray synchrotron mirrors are discussed with reference to multilayer stacks. (p. 98)

8:15 pm
TuC2 **Substrate effects on x-ray specular reflectance and nonspecular scattering from x-ray multilayers,** J. B. Kortright, T. D. Nguyen, I. M. Tidswell, C. A. Lucas, *Lawrence Berkeley Laboratory.* Measured specular and nonspecular scattering from a set of rough substrates, and from tungsten/carbon multilayers deposited onto those substrates, provides details on how substrate roughness limits the reflectance obtainable from high-quality x-ray multilayers. (p. 102)

TETON ROOM

8:45 pm–9:00 pm COFFEE BREAK

GRAND ROOM

9:00 pm (Invited Paper)
TuC3 **Synchrotron study of roughness in Fe-Cr multilayers,** B. M. Clemens, A. P. Payne, *Stanford Univ.;* S. Brennan, *Stanford Synchrotron Radiation Laboratory.* We have performed specular and nonspecular low-angle x-ray scattering on Fe-Cr multilayers. The samples are found to exhibit both conformal and nonconformal roughness. By fitting the data, we extract quantitative estimates of the magnitude and lateral length scale of the roughness. (p. 105)

9:45 pm
TuC4 **Mosaic reflectivity of x-ray multilayer structures,** F. E. Christensen, H. W. Schnopper, *Danish Space Research Institute, Denmark.* Experimental study of mosaic reflectivity of Ni/C multilayers at line energies from B-K$_\alpha$ to Cu-K$_\alpha$ is presented. A novel theoretical model is compared with data. (p. 109)

RESTAURANT

7:00 am–8:00 am   BREAKFAST

MEZZANINE

7:00 am–11:45 am   REGISTRATION/SPEAKER CHECK-IN

GRAND ROOM

8:00 am–11:45 am
WA, GROWTH AND STRUCTURE: 3
R. E. Somekh, *University of Cambridge, U.K., Presider*

8:00 am   (Invited Paper)
WA1   Morphology of thin-film growth, R. W. Collins, Ilsin
An, Y. M. Li, *The Pennsylvania State Univ.* Real-time spectro-
scopic ellipsometry has been developed as a probe that pro-
vides information on thin-film nucleation, coalescence, and
surface roughness evolution with submonolayer sensitivity.
(p. 114)

8:45 am
WA2   Growth and epitaxy of materials for multilayer x-ray
optics, Jon M. Slaughter, Patrick A. Kearney, Judith A. Ruff-
ner, Charles M. Falco, *Univ. Arizona.* Growth of Si, Be, and
B-based materials pairs has been studied using molecular
beam epitaxy. Interface structure, overlayer morphology, and
crystal structure have been determined. (p. 118)

9:15 am
WA3   Interface roughness and void formation in Si deposi-
tion at low temperatures, D. J. Eaglesham, D. L. Windt, *AT&T
Bell Laboratories.* Si depostion at given rate and temperature
can lead to either amorphous or crystalline films. Geometric
roughness and void formation can occur in both cases, but
are considerably more marked for a-Si. (p. 121)

TETON ROOM

9:45 am–10:15 am   COFFEE BREAK

GRAND ROOM

10:15 am
WA4   In-situ grazing incidence x-ray diffraction during sput-
ter deposition, B. M. Clemens, A. P. Payne, T. C. Hufnagel, J.
A. Bain, *Stanford Univ.;* S. Brennan, *Stanford Synchrotron
Radiation Laboratory.* A specially designed UHV deposition
chamber has been designed to perform grazing incidence
x-ray scattering in-situ concurrently with sputter deposition.
The apparatus and technique are described as well as in-situ
results from Gd/Co and Mo/Ni metal/metal systems. (p. 125)

10:45 am
WA5   Stability of metallic superlattices, P. E. A. Turchi, M.
Sluiter, *Lawrence Livermore National Laboratory.* The in-
fluence of the layer repeat period, growth orientation, and
chemical order on the stability of metallic superlattices is
discussed within a first principles approach. (p. 128)

11:15 am
WA6   Elastic properties of strained metallic superlattices,
D. Ariosa, *Univ. de Neuchatel, Switzerland.* A model relating
uniform strain and misfit dislocations at sharp interfaces of
Mo/Ni superlattices is found to agree with earlier data on
elastic softening. (p. 132)

11:45 am–7:00 pm   Afternoon Free

MEZZANINE

7:00 pm–10:00 pm   REGISTRATION/SPEAKER CHECK-IN

TETON ROOM

7:00 pm–7:30 pm
POSTER SESSION

GRAND ROOM

7:30 pm–10:15 pm
WB, X-RAY CHARACTERIZATION
Takeshi Namioka, *NASA Goddard Space Flight Center,
Presider*

7:30 pm
WB1   Multilayer x-ray mirror absolute reflectivity, energy
band pass, and overlapping order determination using an
x-ray tube and a Si(Li) detector, P. Dhez, H. Duval, J. C.
Malaurent, *Univ. Paris, France.* X-ray interference mirrors are
a particular case of artificial multilayered media for which
the wanted property is a high intensity of the diffraction
phenomenon itself. We attempt to demonstrate how such
x-ray reflectivity tests can be achieved on a laboratory ap-
paratus to get absolute reflectivity and without the need of a
synchrotron source. (p. 138)

8:00 pm
WB2   Soft x-ray and XUV reflectometer using a laser-
produced plasma source and a high-throughput
monochromator, E. M. Gullikson, J. H. Underwood, P. C. Bat-
son, V. Nikitin, *Lawrence Berkeley Laboratory.* We describe a
soft x-ray general purpose calibration facility using a laser-
produced plasma as the x-ray/XUV source, a high-throughput
monochromator, and a 2-axis goniometer in vacuum. The
performance of the instrument is described, examples of
measurements are taken on a variety of multilayers, and
other x-ray optical components are presented. (p. 142)

TETON ROOM

8:30 pm–8:45 pm   COFFEE BREAK

GRAND ROOM

8:45 pm
WB3   Preparation and characterization of platinum–carbon multilayers, K. Yamashita, G. S. Lodha, T. Suzuki, *Institute of Space and Astronautical Science, Japan,* I. Hatsukade, *Miyazaki Univ., Japan;* M. Ohtani, *NIKON Corp., Japan.* Characterization of platinum–carbon multilayers (2d-50-150A, N = 5-25) was done by measuring x-ray reflectivity in 0.9–8 keV region. The interfacial roughness depends on 2d, N, and deposition method. **(p. 144)**

9:15 pm
WB4   Experimental and theoretical soft x-ray reflectivities for Mo–B$_4$C multilayer structures, D. B. Brown, J. V. Gilfrich, R. K. Freitag, H. B. Rosenstock, J. H. Konnert, P. D'Antonio, P. B. Burkhalter, C. M. Dozier, *U.S. Naval Research Laboratory.* Soft x-ray reflectivity from Mo–B$_4$C was 20% greater than from W–C. Predictions for ideal and imperfect structures were compared. Interfacial roughness was measured with AFM. **(p. 147)**

9:45 pm
WB5   Soft x-ray multilayer mirrors, Fan Zhengxiu, Shao Jianda, *Academia Sincia, China.* The present status of studies on soft x-ray multilayer mirrors in our institute are described. These include the optimum design, deposition technique, and the preliminary characterizations. W/C, Ta/Si, Mo/Si, Mo/Al multilayers, which are designed as mirrors at 105A, 135A and 234A respectively, have been fabricated with dc- and rf-plane magnetron sputtering systems. **(p. 151)**

RESTAURANT

7:00 am–8:00 am   BREAKFAST

MEZZANINE

7:00 am–11:45 am   REGISTRATION/SPEAKER CHECK-IN

GRAND ROOM

8:00 am–11:45 am
ThA, STABILITY
Eric Ziegler, *European Synchrotron Radiation Facility, France, Presider*

8:00 am   (Invited Paper)
ThA1   Thermal stability of Mo-based multilayers fabricated by rf sputtering, Yoshikazu Ishii, Hisataka Ta!--naka, Tomoaki Kawamura, *NTT Interdisciplinary Research Laboratories, Japan;* Hiroo Kinoshita, *'TT LSI Laboratories,* Thermal annealing of Mo/Si and Mo/B$_4$C was performed in an Ar atmosphere. The x-ray reflectivity and structure of these multilayers were examined using x-ray diffraction and TEM. **(p. 154)**

8:45 am
ThA2   Interdiffusion kinetics in Mo/Si multilayers, R. S. Rosen, D. G. Stearns, *Lawrence Livermore National Laboratory;* M. A. Viliardos, M. E. Kassner, *Oregon State Univ.;* S. P. Vernon, *Vernon Applied Physics.* The interdiffusion kinetics in Mo/Si multilayers were determined from interlayer growth rates at temperatures of ~200–500 °C and times from 1–1000 hours. **(p. 157)**

9:15 am
ThA3   Comparison of microstructure and thermal stability of short period x-ray multilayers, Tai D. Nguyen, Ronald Gronsky, Jeffrey B. Kortright, *Lawrence Berkeley Laboratory.* The microstructures in short period multilayers depend on the period and show different behaviors for different multilayer systems. The response to thermal treatment likewise depends on multilayers materials and periods. Comparison among W/C, WC/C, Ru/C, and Ru/B$_4$C multilayers is presented and discussed in this study. **(p. 160)**

TETON ROOM

9:45 am–10:15 am   COFFEE BREAK

GRAND ROOM

10:15 am
ThA5   Modeling of multilayer mirror damage by a short pulse of x-rays, D. C. Eder, B. J. MacGowan, L. B. DaSilva, S. Mrowka, T. Barbee Jr., *Lawrence Livermore National Laboratory.* X-rays from a gold target heated by a 0.5-ns laser are calculated to result in significant reduction in the reflectivity of multilayer mirrors. **(p. 163)**

10:45 am
ThA6   Low-radiation-damage multilayer coatings for the soft x-ray region, W. R. Hunter, _SFA Inc.;_ J. F. Seely, _U.S. Naval Research Laboratory._ Highly reflecting multilayer coatings can have large electric fields at layer boundaries. Slight alterations in the uppermost layer thicknesses can reduce the fields and prevent damage. **(p. 165)**

11:45 am–7:00 pm   Afternoon Free

TETON ROOM

6:00 pm–7:30 pm   CONFERENCE RECEPTION

MEZZANINE

7:00 pm–9:30 pm   REGISTRATION/SPEAKER CHECK-IN

GRAND ROOM

7:30 pm–9:45 pm
ThB, NOVEL PROPERTIES
Natale M. Ceglio, _Lawrence Livermore National Laboratory,_ Presider

7:30 pm
ThB1   Bragg-Fresnel multilayer optics for x-ray microscopy and spectroscopy, B. Vidal, P. Vincent, _Univ. Marseille, France;_ M. Brunel, _Laboratoire de Cristallographie CNRS, France;_ A. Erko, D. Rochtchoopkine, _USSR Academy of Sciences, USSR;_ J. Susini, _European Synchrotron Radiation Facility, France._ This report gives examples of fabrication, computer simulation, and tests for two kinds of BFMO: Lamellar multilayer gratings and Lamellar Bragg-Fresnel multilayer lenses. All theoretical calculations are verified by experimental tests. **(p. 170)**

8:00 pm
ThB2   A multilayer quarter-wave plate of transmission type at a wavelength of 12.4 nm, Hiroaki Kimura, _The Graduate Univ. Advanced Studies, Japan;_ Masaki Yamamoto, Hiroshi Nomura, Ko Mayama, Mihiro Yanagihara, _Tohoku Univ., Japan._ Useful designs for multilayer quarter-wave plates of transmission type are presented. High throughput (50%) or high-incident angle tolerance are possible at a wavelength of 12.4 nm. **(p. 174)**

TETON ROOM

8:30 pm–8:45 pm   COFFEE BREAK

GRAND ROOM

8:45 pm
ThB3   Observation of nuclear diffraction from multilayers containing ^{57}**Fe,** R. Rohlsberger, E. Witthoff, E. Luken, E. Gerdau, _Institut fur Experimentalphysik, Germany._ A ^{56}FE/^{57}FE multilayer structure exhibits a nuclear Bragg reflection in the vicinity of the 14.4 keV resonance of the ^{57}Fe nucleus. Corresponding experiments are described. **(p. 178)**

9:15 pm
ThB4   Multilayer structures traversed by electron beams as narrow line x-ray sources, A. E. Kaplan, C. T. Law, _The Johns Hopkins Univ._ We investigate the optimal geometric configuration and materials composition of multilayer structures for generation of narrow line x-ray radiation from electron beams traversing these structures. **(p. 182)**

Introduction

MA   8:00am–9:00am
Grand Room

Daniel G. Stearns, *Presider*
Lawrence Livermore National Laboratory

Physical Optics of X-Ray Multilayer Structures

Eberhard Spiller

IBM Research Division, T. J. Watson Research Center
P.O. Box 218, Yorktown Heights, NY 10598

The paper will review the present state-of-the-art of multilayer optics. Different theories to model the performance of multilayer structures will be compared and the influence of imperfections will be discussed. Optimized coating designs for the XUV will be compared to perfect crystals, as used in x-ray diffraction and laser mirrors, as used for visible light. Practically all deposition methods have been used for the fabrication of x-ray multilayer structures and we will summarize their strengths and weaknesses. Material combinations for a specific application are first selected by the optical constants at a specific wavelength and then by the requirement that the materials chosen must form atomically abrupt, smooth and stable boundaries. Only a handful of combinations are in practical use. The limit on the performance of multilayer structures is given by absorption and by the roughness of the boundaries. The shortest practically useful multilayer period ($\Lambda \approx 25\text{Å}$) is limited by boundary roughness and a drastic improvement at shorter periods can only be expected if we learn to place atoms by a non-random process.

Multilayer structures have permitted the extension of classical optics into the soft x-ray range. The shorter wavelengths should make it possible to build instruments with a resolution that is 100 times better than that of similar instruments for visible light. However, this goal can only be reached with 100 times tighter fabrication tolerances. It appears that recent progress in metrology will make such a performance available during the next decade. Multilayer structures have been used in x-ray astronomy, microscopy, spectroscopy and plasma diagnostics and have been proposed for the fabrication of integrated circuits. We will discuss these applications and present examples of first results.

Growth and Structure 1

MB 9:00am–11:45am
Grand Room

Daniel G. Stearns, *Presider*
Lawrence Livermore National Laborotory

Relationship between soft X-ray reflectance and structural parameters of nanometer-period multilayers for X-ray mirrors

Philippe Houdy and Pierre Boher

Laboratoires d'Electronique Philips, 22 Avenue Descartes 94453 Limeil-Brévannes cedex France

Multilayers alternating materials at atomic scale have been deposited, using UHV diode rf sputtering, to be used as soft X-ray mirrors [1,2,3,4]. We have investigated the relationship between the stack performances (reflectivity, selectivity) and the structural chara cteristics of the stacks. The use of graphite instead of amorphous carbon in Ni/C multilayers results in an increase of the performances as well as cooling the sample during the deposition. A similar effect is observed in W/BN multilayers introducing nitrogen during the growth to saturate the nitride. In the case of Si/SiN stacks, narrow Bragg peaks and a higher reflectivity are obtained anealing the samples up to 800°C. At least, a comparison is made between Mo/Si and Co/Si multilayers in order to show the importance of interface compound formation.

I. GENERALITIES

A UHV r.f. diode sputtering system has been used to fabricate the multilayers. This system is equiped with special gas inlets to introduce gas (N,O,H) at the top of the sample during the deposition from an argon plasma. The multilayer growth is in situ observed using kinetic ellipsometry. [5] . All samples have been grown on commercially available Si wafers with a chemical native oxide removal prior to introduction into the system. The multilayer structure has been characterized in situ by kinetic ellipsometry (KE) and ex situ using by grazing X-ray reflection (GXR), X-ray diffraction (XRD), Auger profile analysis (APA), Mössbauer spectrometry (MS), and transmission electron microscopy (TEM). The reflectivity performances of the multilayers have been measured usin synchrotron radiation or a conventionnal X-ray tube.

II. CRISTALLINITY IN Ni/C MULTILAYERS
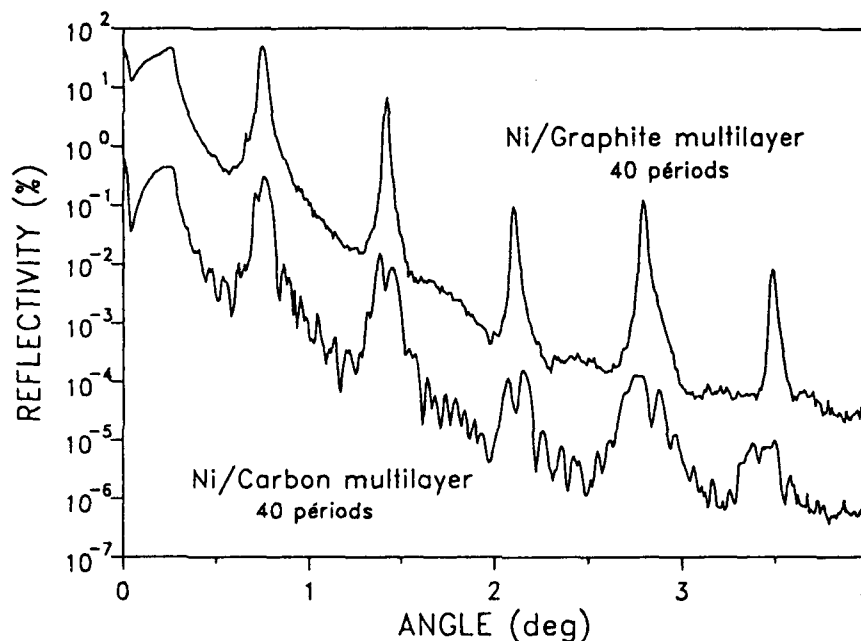
FIG.1.Grazing X-ray reflection curve of two Ni/C multilayers (40x6.5 nm, up using graphite, down using amorphous carbon)

For use such as monochromator at 4.47 nm we have deposited Ni/C multilayers. Using an amorphous carbon target we observe (KE,TEM) the nickel crystallization for very low thickness (1.5 nm) and then interfacial roughness increase all along the stack. The GXR curve (fig.1) is very perturbed and the Bragg peak intensities are low. If we use graphite we get narrow peaks with high intensity corresponding to a low stable interface roughness (0.4 nm). In the case of amorphous carbon, the autobias voltage is 1.6 kV. Using amorphous carbon, we get high energy atoms bombarding the surface, favouring the nickel crystallization and the roughness increase. This problem is solved using graphite where autobias voltage is only 0.9 kV for similar deposition rate.

III. NITRIDE STOICHIOMETRY IN W/BN MULTILAYERS

Simulations show that W/BN multilayers reach high reflectivities (around 30%) for boron line (6.7 nm) and nitrogen line (3.1 nm), and 60 % for aluminium line (0.83 nm). We have deposited W/BN multilayers from boron nitride target. We observe a lack of nitrogen in the boron nitride layers, decreasing W/BN optical contrast and then the reflectivity. Then, we have used a special pipe to introduce nitrogen at the top of the sample during the boron nitride deposition. In this case we can control the nitrogen concentration in the BN layer and get the optimal index in the soft X-ray range. Fig.2 shows the reflectivity at 0.82 nm wavelength for three different nitrogen partial pressure in the deposition chamber. The X-ray optimum reflectivity is obtained for 10 % partial pressure.
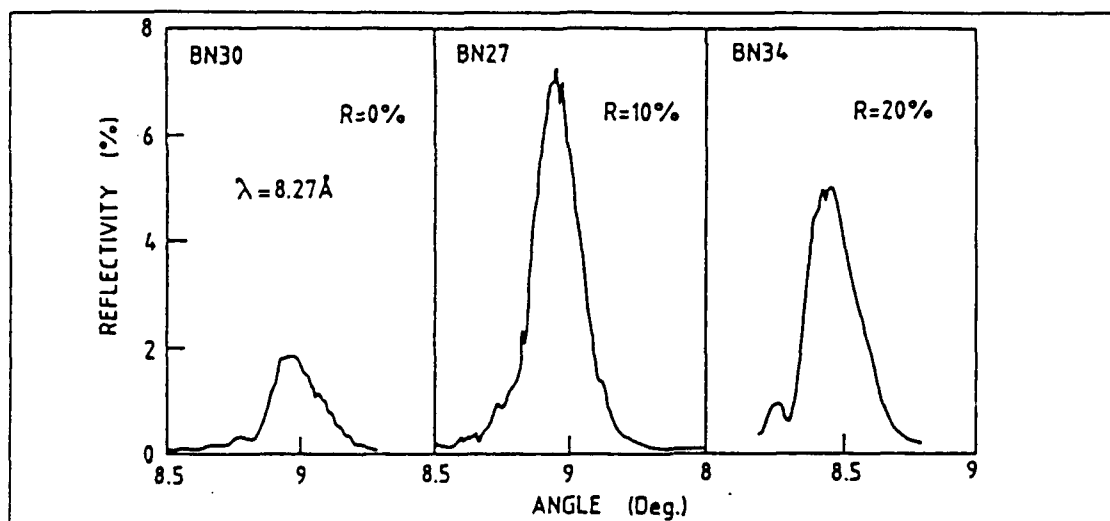
FIG.2.Soft X-ray curves of W/BN multilayers for three nitrogen
partial pressure ratios (0%,10%,20%)

IV. THERMAL BEHAVIOUR OF Si/SiN MULTILAYERS

For special applications in synchrotron or X-ray laser, we need multilayers capable to keep stable under intense X-rays flux. We have start the study of nitride and carbide compounds with Si/SiN alternances. From KE and TEM, we observe very narrow interface region (0.3 nm) with abrupt nitrogen concentration variation. The multilayers have been annealed up to 900°C without damage in the structure and in the performances. On the contrary we can observe (fig.3) that after 800°C annealing, the Bragg peaks are thinner and the intensities higher. A light change in Si/SiN thicknesses ratio is also observed cooresponding to 7 % silicon layer thickness increase, nitride layers being stable. With these multilayers, we get also very high selectivity (2 to 3 time Mo/Si one) in the range 12nm-32nm.
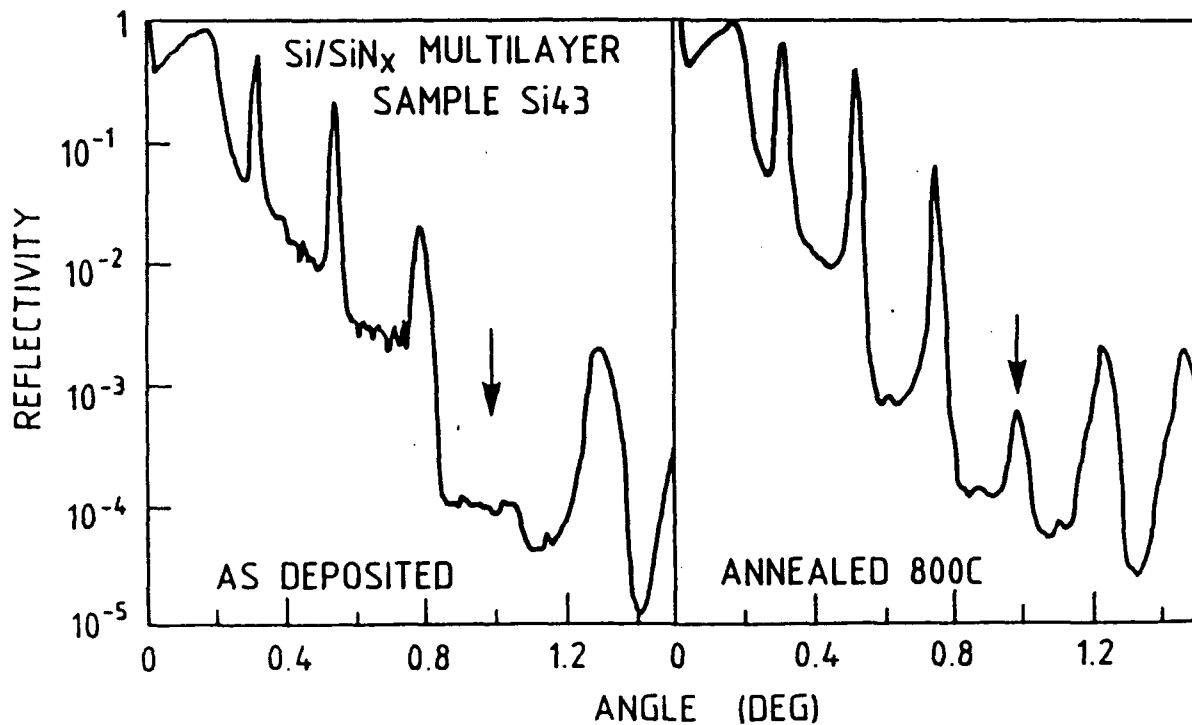
FIG.3.Grazing X-ray reflection curves of a Si/SiN multilayer
(left : as deposited, right : annealed at 800°C)

V. INTERFACE COMPOUND IN Mo/Si AND Co/Si MULTILAYERS

For astrophysic applications, we have deposited Mo/Si and Co/Si multilayers, to be used at high wavelength (16nm-18nm). For Mo/Si multilayers, we observe (KE) the formation of a $MoSi_2$ compound at both interface. The interface when depositing molybdenum on silicon is two time thicker than the other one (1 nm instead of 0.5 nm). The crystallization of molybdenum also occurs for 2.5 nm pure Mo layer. In the case of Co/Si multilayer, the interfaces are symetric, being both 1.5nm thick and cobalt crystallization is not observed. The interdiffusion is much more high in Co/Si multilayers with high interface roughness. Due to the larger interface in Co/Si we observe a strong decrease of the reflectivity (see fig.4) compared to a perfectly sharp interface model (10 % instead of 25 %). In the case of Mo/Si multilayers, the molybdenum crystallization reduces silicon diffusion and then the interface thickness, we just observe a light decrease of the reflectivity compared to a perfect stack model (45 % instead of 50%). In any case such multilayers (Mo/Si or Co/Si) have limited thermal stability (destroyed above 500°C).
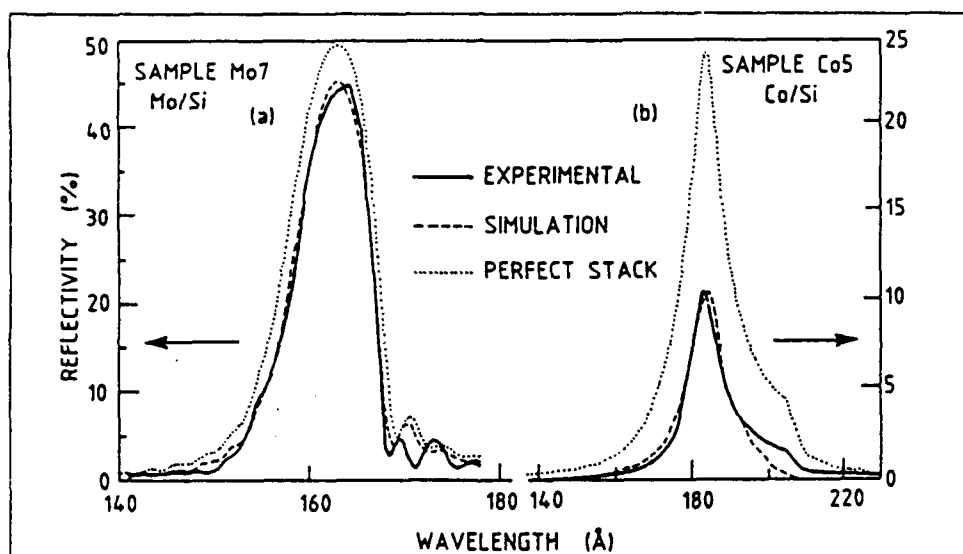
FIG.4.Soft X-ray reflection curves of Mo/Si and Co/Si multilayers
(normal incidence)

VII. CONCLUSION

An important aspect of multilayers, for application such as mirrors in synchrotron, is the temperature stability. Stacks made of nitrides or carbides will be of first interest in a near future especially for nitrogen and carbon wavelength. With multilayers alternating Ti/TiC, Ti/TiN etc, mirrors would get hich reflectivities and also high temperature stability.

ACKNOWLEDGMENT

REFERENCES

1.   T.W.Barbee, SPIE n° 563, 2, San Diego (Aug. 1985)
2.   E.Spiller, SPIE n°563, 135, San Diego (Aug. 1985)
3.   F.E.Fernandez, C.Falco, SPIE n°563, 195 San Diego (Aug. 1985)
4.   Ph.Houdy, J.P.Chauvineau, SFV le vide les couches minces n°245, 69-86, (Jan-Feb 1989)
5.   P.Boher, Ph.Houdy, P.Kaikati, R.Barchewitz, J.J.Van Ijzendoorn, Z.G.Li, D.J.Smith, J.C.Joud, 1990 SPIE conf. proceed. San Diego (8-11 july 1990)
6.   Ph.Houdy, Revue Phys. Appl. 23, 1653-1659 (Oct. 1988)

EFFECTS OF SPUTTERING PRESSURE ON ROUGHNESS AND RESPUTTERING OF MULTILAYERS

M.M. Hasan, R.J. Highmore and R.E. Somekh,
University of Cambridge,
Department of Materials Science and Metallurgy,
Pembroke Street, Cambridge, CB2 3QZ, U.K.
Telephone 0223-334374.   .

This summary outlines studies of W-Si and Co-Cu multilayers. We recognize that W-Si is unlikely to make optimal x-ray mirrors, because Si is more strongly absorbing than, say, carbon for most radiation wavelengths, and because the known propensity of metal-silicon couples to interdiffuse to form silicides suggests that interfaces are unlikely to be very sharp. W-Si is, though, a useful model system. A more extensive account of our work with W-Si and related systems is contained in [1]. Interfacial roughness is important in determining the properties not only of x-ray mirrors, but also of multilayer systems which exhibit so-called "giant magnetoresistance". We are using Co-Cu as a model system with which to study this phenomenon.

Multilayers were deposited onto pieces of Si wafer and strips of Cu in two-target UHV dc magnetron sputtering systems. The systems are similar, but not identical, to the one described in [2]; substrates sit on a rotating substrate holder and pass alternately beneath the two magnetrons. The sputtering gas was Ar and the target-substrate distances were 30 mm for W, Si and Co and 42 mm for Cu.

Fig. 1 is a plot of apparent Si layer thickness (at constant Si magnetron power) versus apparent W layer thickness, for W-Si multilayers deposited using 0.65 Pa of Ar and substrate holder rotation periods of 20, 40 and 64 s. The data are consistent with a two-stage process in which atoms from the most recently deposited Si layer are first transported through the growing layer of W to the instantaneous surface of the film, and are then removed by the resputtering action of energetic atoms (mainly reflected neutral Ar atoms) striking the surface. Si can be removed as long as W is being deposited, but the rate of removal decreases as the distance which atoms must travel through the W to the surface grows larger. Si ceases to be removed from the film in appreciable quantities once the thickness of the W layer exceeds some 10 to 15 Å. The initial rate of decrease of Si thickness with respect to W thickness is greatest for a rotation period of 20 s, and least for a rotation period of 64 s. The magnetron power needed to deposit a given thickness of W is inversely proportional to the rotation period; this observation suggests, therefore, that more Si is removed from the film by a large flux of bombarding particles acting for a short time than by a smaller flux acting for a proportionally longer time. This may be a material effect, or it could be a consequence of the sputtering gas becoming hotter and thus less dense as the magnetron power is raised, thereby reducing the thermalizing effect of the gas. After depositing W-Si multilayers we found Si beside the slot through which W had been deposited, but no W beside the slot through which Si had been deposited: these findings are consistent with there being substantial resputtering of Si whilst W is being deposited, but no noticable resputtering of W during deposition of Si. The possibility that removal of Si during deposition of W may be limited by the speed with which Si can be transported through the growing W layer led us to study the temperature dependence of the resputtering phenomenon. Reducing the temperature from 50°C to -90°C caused only slightly less Si to be removed, which suggests that transport of Si through the W layer occurs via a mechanism which requires little thermal activation, e.g., energetic atoms striking the surface of the film and mixing or "churning" the top few layers of atoms. This explanation is consistent with the resputtering reported above, since both resputtering and churning require that the film be bombarded by substantial fluxes of energetic (> 70 eV atom^{-1}) neutrals.

We expect ideal superlattice peak intensities to decay with increasing angle as something like [3]

$$I \propto \frac{1}{\sin^4\theta} \exp\left(-2\left[\frac{2\pi}{\lambda}\sigma\sin\theta\right]^2\right) \qquad (1),$$

where I is the superlattice peak intensity, θ the Bragg angle, λ the radiation wavelength and σ the interfacial roughness. Our vertical x-ray diffractometer has a beam width which is greater than the size of the multilayer samples which we study, and we therefore expect the denominator in equation (1) to be $\sin^3\theta$, rather than $\sin^4\theta$. A plot of $\ln(I\sin^3\theta)$ versus $\sin^2\theta$ should thus approximate a straight line whose gradient becomes steeper as σ grows larger. Fig. 2 shows such plots for W-Si multilayers with periods of about 30 Å deposited using different Ar pressures. Raising the pressure from 0.65 to 2.0 Pa altered σ from 4.1 ± 0.2 Å to 4.2 ± 0.3 Å, whilst using a gas pressure of 3.2 Pa increased the roughness to 5.4 ± 0.3 Å. This dependence of film quality on Ar pressure is largely a consequence of the greater energies with which reflected neutral Ar atoms bombard the growing films at lower pressures. Energetic bombardment has the virtuous effect of aiding surface mobility and the consequent growth of dense, smooth layers, but may also cause mixing at interfaces on a scale of 10 to 15 Å [1].

Our polycrystalline Co-Cu multilayers had 40 periods and approximate effective layer thicknesses of 19.0 Å for Co and 9.5 Å for Cu. The structural parameters which changed most as the sputtering pressure was increased from 0.4 to 2.5 Pa were the rocking curve width of the (111) Co-Cu peak (which grew from 12° to 23°, see fig. 3) and the superlattice peak intensities (which decreased by a factor of about 25 for the 1st order peak). By comparison, the interfacial roughness increased only slowly with rising sputtering pressure (see fig. 4). After depositing the multilayers we found (at least for Ar pressures of 1 Pa or less) Cu beside the slot through which Co had been deposited, but no Co beside the slot through which Cu had been deposited. This observation is consistent with there being resputtering of Cu during deposition of Co, but no resputtering of Co during deposition of Cu. The asymmetry may result from the target-substrate distance being smaller for Co than for Cu, and from Co being more refractory than Cu. The large values of interfacial roughness relative to Cu layer thickness for these films indicate that sputtered polycrystalline Co-Cu multilayers do not approximate stacks of perfectly smooth layers of pure elements. Rather, they are substantially intermixed structures with rounded composition profiles. Experiments with the highest quality Fe-Cr structures [4,5] have shown two-monolayer-period oscillations in exchange coupling as a function of non-ferromagnetic element layer thickness, but such oscillations will be washed out by the roughnesses of ~6 Å which we find in our films. The longer-period (~10 Å) oscillations as a function of Cu layer thickness do survive, but we expect fluctuations in Cu layer thickness to result in there being both ferromagnetic and antiferromagnetic coupling between adjacent Co layers at different points in the same film. Zhang and Levy [6] have deduced the existence of such mixed coupling in sputtered Co-Cu multilayers.

There is an optimal value of interfacial roughness in systems such as Fe-Cr and Co-Cu at which magnetoresistance is a maximum, since this roughness causes spin-dependent scattering of conduction electrons [7,8]. Experiments with multilayers grown using molecular beam epitaxy suggest that the optimum for Fe-Cr lies between 1 and 4 Å [7]. Our sputtered polycrystalline films probably show no maximum in magnetoresistance as a function of sputtering pressure (see fig. 5) because their interfaces are always too rough.

Why does the magnetoresistance increase as the sputtering pressure is reduced? As explained above, decreasing the pressure seemingly reduces the interfacial roughness towards a more optimal value. Decreasing the sputtering pressure causes the stress state of a sputtered film to become more compressive [9]; this stress can act through the magnetostriction to increase the in-plane magnetic anisotropy [10] and so facilitate magnetization rotation. The more perfect structures which are obtained at lower sputtering pressures (as evidenced by more intense superlattice lines and narrower rocking curves) are likely to aid magnetization rotation (via reduced pinning and anisotropy dispersion) and to result in longer mean free paths for conduction electrons.

Conduction electrons with long mean free paths can sample many magnetized layers and thereby enhance magnetoresistance [8].

References

1. M.M Hasan, R.J. Highmore and R.E. Somekh,*Vacuum*, in press.
2. R.E. Somekh and Z.H. Barber, *J. Phys. E* **21**, 1029 (1988).
3. E. Spiller and A.E. Rosenbluth, *Proc. SPIE* **563**, 221 (1985).
4. J. Unguris, R.J. Celotta and D.T. Pierce, *Phys. Rev. Lett.* **67**, 140 (1991).
5. S.T. Purcell, W. Folkerts, M.T. Johnson, N.W.E. McGee, K. Jager, J. aan de Stegge, W.B. Zeper, W. Hoving and P. Grünberg, *Phys. Rev. Lett.* **67**, 903 (1991).
6. S. Zhang and P.M. Levy, *Proc. MRS Spring '91 Meeting*, in press.
7. F. Petroff, A. Barthélémy, A. Hamzic, A. Fert, P. Etienne, S. Lequien and G. Creuzet, *J. Mag. Magn. Mater.* **93**, 95 (1991).
8. P.M. Levy and S. Zhang, *J. Mag. Magn. Mater.* **93**, 67 (1991).
9. D.W. Hoffman, in *Proc. 7th Int. Conf. on Vacuum Metallurgy*, The Iron and Steel Institute of Japan, Tokyo, p. 145 (1982).
10. C.H. Lee, H. He, F.J. Lamlas, W. Vavra, C. Uher and R. Clarke, *Phys. Rev. B* **42**, 1066 (1990).
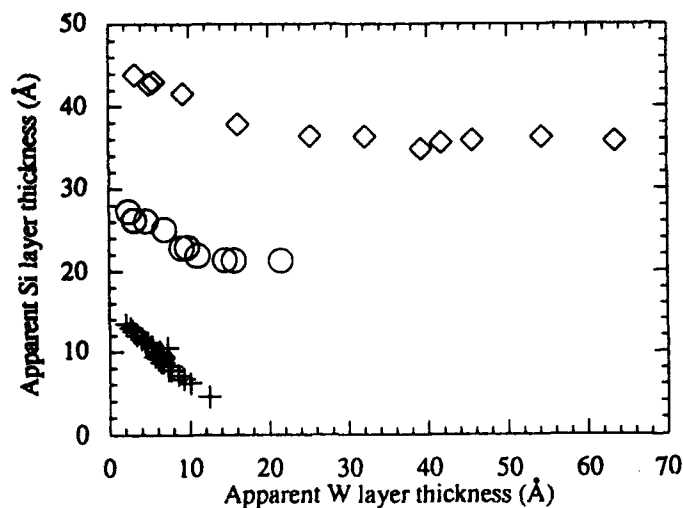
Figure 1: Plots of apparent Si layer thickness (at a Si magnetron power of 40 W) versus apparent W layer thickness for W-Si multilayers deposited using a sputtering pressure of 0.65 Pa and substrate holder rotation periods of 20s (crosses), 40s (circles) and 64s (diamonds).
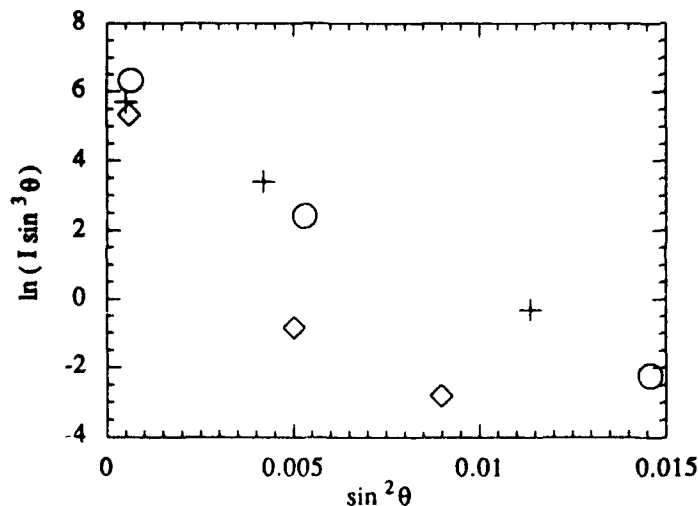
Figure 2: Plots of $\ln(I\sin^3\theta)$ versus $\sin^2\theta$ for W-Si multilayers with periods of about 30 Å and approximately equal apparent thicknesses of W and Si. The films were deposited using Ar pressures of 0.65 Pa (crosses), 2.0 Pa (circles) and 3.2 Pa (diamonds). It can be seen that the film deposited at 3.2 Pa is the roughest of the three.
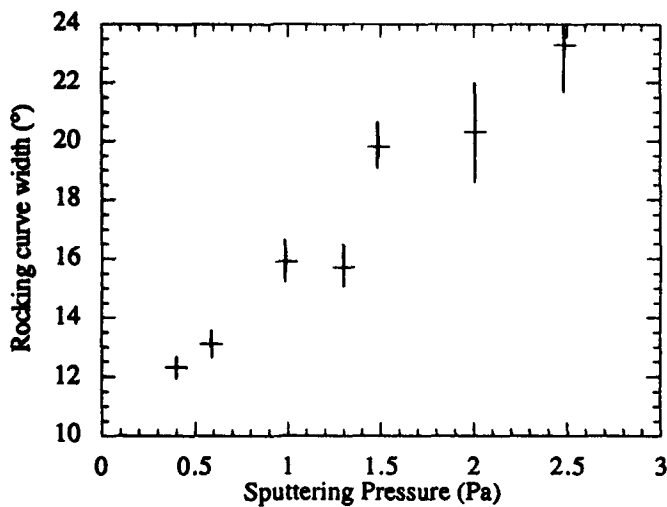
Figure 3: A plot of rocking curve width (full-width half-maximum) versus sputtering pressure for the (111) Co-Cu peak of the Co-Cu multilayers described in the text.
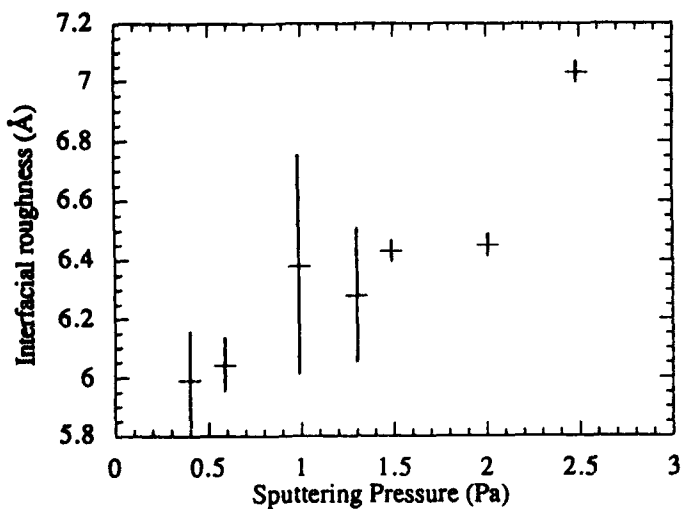
Figure 4: A plot of interfacial roughness versus sputtering pressure for the Co-Cu multilayers described in the text. The roughness was calculated using the intensities of the first two superlattice lines, and equation (1) with the denominator as $\sin^3\theta$. We did not expect a 3rd order line because the Co layers are approximately twice as thick as the Cu layers. The roughnesses of the most rough films could not be calculated, because they gave no 2nd order line.
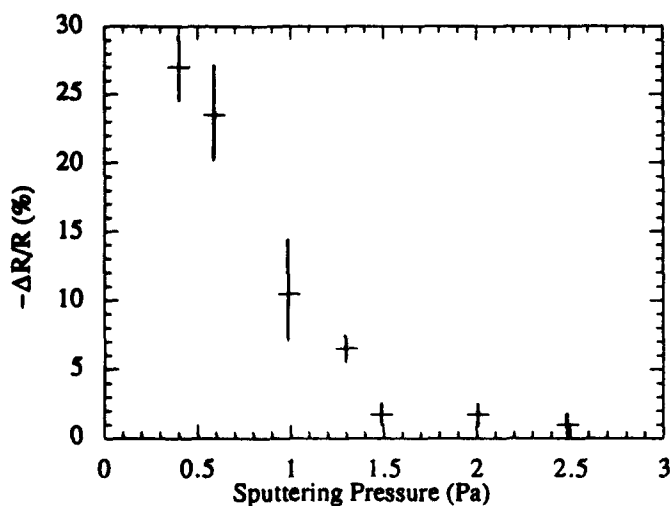
Figure 5: A plot of room temperature magnetoresistance (in a field of 0.3 T) versus sputtering pressure for the Co-Cu multilayers described in the text. The spread of data is most probably caused by films which occupied different positions on the substrate holder during deposition having different layer thicknesses and experiencing different amounts of bombardment.

Stress, Morphology, and Optical Properties of Mo/Si X-Ray Multilayers

D.L. Windt, R. R. Kola, W.K. Waskiewicz, R. Hull, J. Griffith and D. A. Grigg

AT&T Bell Laboratories, Room 1D-456, 600 Mountain Ave, Murray Hill, NJ 07974

(908) 582-2367

Due to its high X-ray reflectance (~60%) for wavelengths longer than the Si-L absorption edge near 125 Å, the Mo/Si X-ray multilayer (XML) system is now used in a diverse range of advanced applications, including soft X-ray projection lithography and X-ray astronomy. Consequently, the stability and the structural and optical properties of this system have been extensively studied [1-7]. High resolution transmission electron microscopy (HRTEM) of sputter-deposited Mo/Si XMLs reveals that the Mo layers are polycrystalline, the Si layers amorphous, and the interface region composed of an amorphous mixture of Mo and Si. Further investigations have indicated that this interlayer material is, in fact, amorphous $MoSi_2$. Thermal anneal studies have revealed the absence of solid-state amorphization, in spite of the presence of the amorphous alloy interfacial layers. Instead, the amorphous interlayers crystallize, and growth of the crystalline product, $MoSi_2$ proceeds in the temperature range 275-550°C. At higher temperatures (600°C), the Mo_5Si_3 phase appears as well. However, at lower temperatures (<200°C), no structural or optical changes have thus far been reported.

Understanding the stress in Mo/Si XMLs can elucidate the dynamics of the growth process and the consequent effect on the structural and optical properties of these structures. Furthermore, the stress in these coatings is of prime importance with regard to the advanced applications mentioned above. In general, the in-plane stress in a coating affects the film adhesion (e.g. peeling, crazing, etc.), while the normal stress affects its ultimate strength. In the Mo/Si system, large in-plane stresses in the coating can, depending on the characteristics of the substrate, distort the surface figure of the highly precise optical substrates required for diffraction-limited imaging at soft X-ray wavelengths.

Although the intrinsic stress in pure Mo [8] and amorphous Si (a-Si) [9,10] coatings has been measured previously, to the best of our knowledge, the stress in Mo/Si XMLs has not. In this work, therefore, we report on recent investigations directed at measuring the stress in Mo/Si XMLs grown under a variety of deposition conditions. Using several experimental techniques, we have begun to correlate the observed stress-temperature behavior with the morphology and optical properties of these structures.

The stress in Mo/Si multilayers, and also pure Mo and a-Si films, was determined by measuring the change in substrate curvature after film deposition, using a laser-scanning technique [11]; the film stress is obtained from Stoney's formula [12]:

$$\sigma_f = (1/6) [E_s / (1-v_s)] (t_s^2 / t_f) (1/R) \qquad (1)$$

where σ_f is the film stress, E_s, v_s and t_s are Young's modulus, Poisson's ratio, and substrate thickness, respectively, t_f the film thickness, and R the change in substrate curvature due to film stress.

Mo/Si multilayers, and Mo and Si thin films, were deposited by DC magnetron sputtering using a deposition system that has been described previously [13]. The films were deposited using various sputtering gases (argon, xenon and krypton), at varying gas pressures (3-9 mTorr), and with various magnetron cathode power densities. Multilayers containing 40 bilayers of Mo/Si, with periods ranging from approximately 30 to 150 Å, and with various Mo:Si ratios were deposited onto polished 75-mm-diameter Si (100) wafers.

Stress vs. temperature measurements were made by monitoring substrate curvature while the samples were heated at a rate of 3°C/min in an ambient argon atmosphere maintained at 15 psi. Soft X-ray reflectance measurements were made near normal incidence using a laser-plasma reflectometer system that has been described previously [14]. Grazing incidence X-ray reflectance-vs-incidence angle measurements were made using a 4-circle diffractometer with a rotating anode Cu-target source (λ=1.54 Å), in the θ-2θ geometry. HRTEM measurements were performed on cross-sectional samples prepared using an ion-milling technique. Images were obtained using an Akashi 002B electron microscope operating at 200 kV. In addition to investigating the layer morphology from these images, digital image analysis techniques were used to measure the interfacial roughness and interface diffuseness of XML samples. (The HRTEM measurement techniques are further described in a related paper in this program [15].) Surface topography was measured using both an optical profilometer (Wyko TOPO-3D, 20X and 200X objectives) and an atomic force microscope, thereby covering a continuous range of spatial wavelengths extending from ~50 Å to 500 μm. The force microscope scans were performed in air with an instrument employing a rocking beam force sensor [16]. The probe tips were electrochemically etched W and Ir, which have a radius at the apex of approximately 100 nm. Because of

the extremely flat topography, sharper probes were not needed. The results included in the remainder of this summary are, however, confined to the stress-temperature and reflectance measurements only.

Fig. 1 shows the stress vs. temperature curve obtained for a Mo/Si XML having a period of 75 Å (45% Mo), deposited using argon gas at 3 mTorr, appropriate
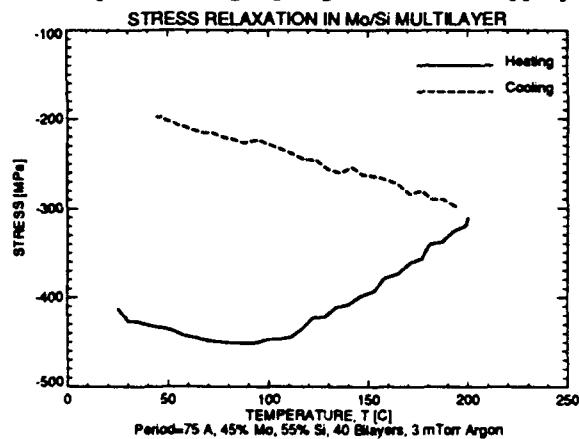
STRESS RELAXATION IN Mo/Si MULTILAYER

Period=75 A, 45% Mo, 55% Si, 40 Bilayers, 3 mTorr Argon

Figure 1.

for use as a normal incidence reflection coating at a wavelength of ~135 Å. The as-deposited in-plane stress was measured to be -410 ± 8 MPa (compressive), and decreased to -200 ± 4 MPa after a thermal cycling to 200°C. This sample was found to have high reflectance, as shown in Fig. 2a which is a plot of the soft X-ray reflectance versus wavelength measured at 5° incidence. No significant change in the peak reflectance was ob-
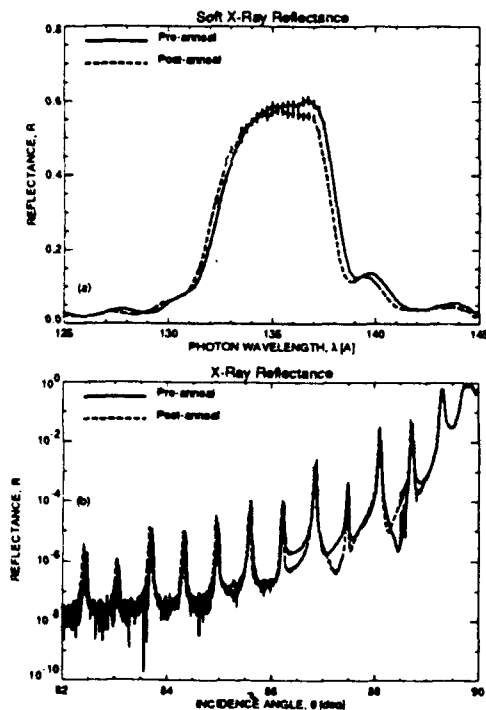
Soft X-Ray Reflectance

X-Ray Reflectance

Figure 2.

served (within experimental uncertainty) as a result of the 200°C thermal cycling, indicating that interdiffusion or interfacial reaction at the Mo/Si interface has not occurred. However, it can be seen that the location of the Bragg peaks in both Figs. 2a and 2b (X-ray reflectance) have shifted slightly; from model fits to the reflectance data (using recursive application of the Fresnel equations), the period of the multilayer was found to decrease by ~0.25 Å, indicating a change in the out-of-plane strain due to densification.

The stress-temperature behavior of the Mo/Si XML can be understood in terms of the behavior of the individual Mo and a-Si layers. Shown in Fig. 3 are the stress-temperature curves obtained for 3000-Å-thick films (the same thickness as the Mo/Si XML of Figs. 1 and 2) of the pure materials. The shape of the stress-temperature curve for the multilayer (Fig. 1) is obtained, qualitatively at least, from the superposition of the stress-temperature curves for the Mo and a-Si films (Fig. 3). Stress relaxation, observed in *both* the Mo and Si films, is attributed to densification and plastic flow, in general. However, as the relative amount of relaxation in the Mo film (5%) is small compared with that ob-

STRESS RELAXATION IN Mo FILM

STRESS RELAXATION IN Si FILM
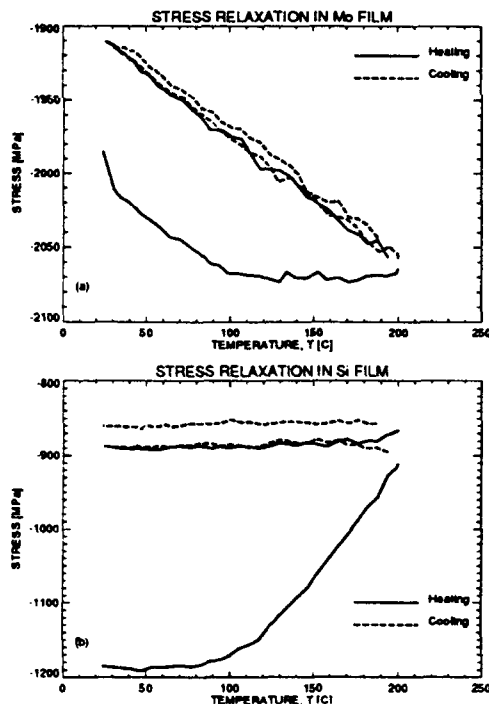

Figure 3.

served in the a-Si film (25%), we conclude that the stress-relaxation observed in the multilayer is due to densification and plastic flow occurring predominantly in the a-Si layers. (Note that the stress measured in the 3000-Å-thick films is considerably larger than that found in the Mo/Si XML. This difference is due to differences in the growth dynamics and therefore the

microstructure of these samples and the thin (i.e. ~35 Å) layers that comprise the multilayer.)

Further investigations are underway to probe the dependance of the intrinsic stress and stress-relaxation behavior in Mo/Si XMLs with various multilayer parameters and with deposition conditions. Preliminary results are shown in Figs. 4 through 6, which reveal sensitive
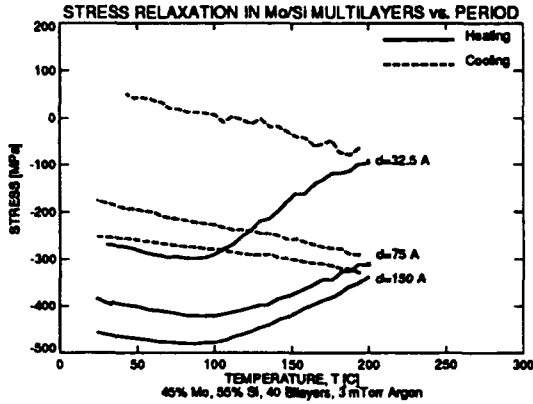
Figure 4.
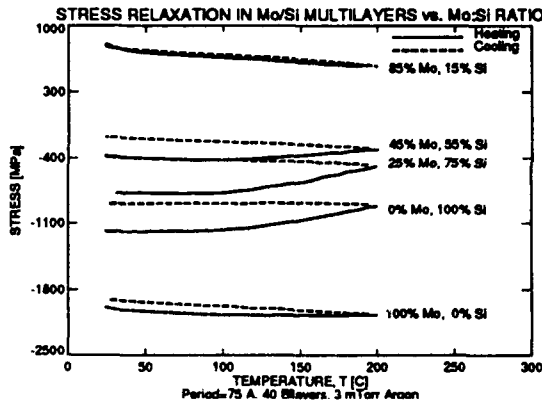
Figure 5.
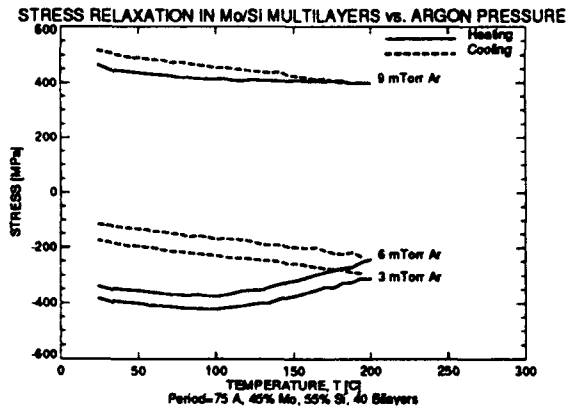
Figure 6.

dependencies of stress and stress-relaxation behavior with multilayer period, Mo:Si ratio, and argon pressure, respectively. These results are now being correlated with the multilayer structural and optical properties, using the
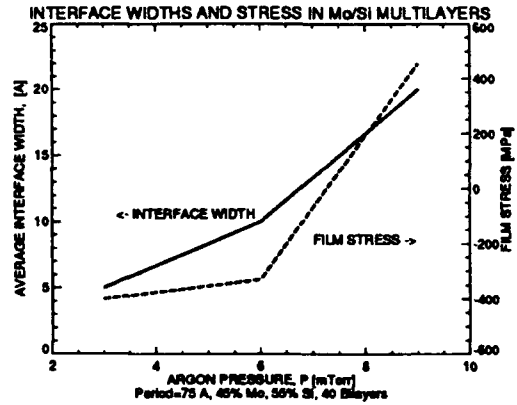
Figure 7.

experimental techniques described above. For example, the dependance of stress with argon pressure is highly correlated with the previously observed dependance of interfacial roughness (and consequently the X-ray reflectance) with argon pressure [4]. This correlation is illustrated in Fig. 7, where the intrinsic stress and interfacial roughness deduced from X-ray reflectance measurements are plotted versus argon pressure. The stress in these structures is compressive at low pressures and undergoes a transition to tensile stress at higher pressures. Investigation of the stress-temperature behav-
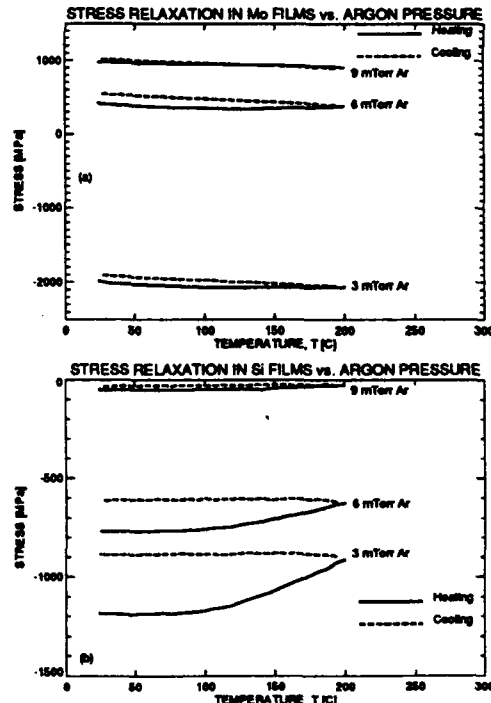
Figure 8.

ior of individual Mo and a-Si films with argon pressure, shown in Fig. 8, reveals that the transition from compressive to tensile stress observed in the multilayers is due to a trend towards tensile stress occurring in the individual Mo and a-Si layers, though the transition to

tensile stress is not observed in the a-Si films.

In summary, the stress in Mo/Si XMLs was found to be compressive with a value of approximately -410 MPa. The stress was observed to relax to -200 MPa as a result of thermal cycling to 200°C, with no significant change in soft X-ray reflectance. By examining the stress-temperature behavior of individual Mo and a-Si films, the stress relaxation observed in the multilayer is attributed to densification and plastic flow occurring predominantly in the a-Si layers. The stress and stress-temperature behavior of Mo/Si XMLs is quite sensitive to many parameters, including multilayer period, Mo:Si ratio, and argon pressure. These dependencies are now being correlated with the structural and optical properties of these coatings, using a variety of experimental techniques.

References

[1] A. K. Petford-Long, M. B. Stearns, C. H. Chang, S. R. Nutt, D. G. Stearns, N. M. Ceglio, and A. M. Hawryluk, *J. Appl. Phys.*, **61**, 1422 (1987)

[2] K. Holloway, K. B. Do, and R. Sinclair, *J. Appl. Phys.*, **65**, 474 (1989)

[3] D. G. Stearns, M. B. Stearns, Y. Cheng, J. H. Stith, and N. Ceglio, *J. Appl. Phys.*, **67**, 2415 (1990)

[4] D. G. Stearns, R. S. Rosen, and S. P. Vernon, *J. Vac. Sci. Technol. A*, **9**, 2662 (1991)

[5] R. S. Rosen, M. A. Viliardos, D. G. Stearns, M. E. Kassner, and S. P. Vernon, *Proc. SPIE* **1547** (1991)

[6] D. L. Windt, R. Hull, and W. K. Waskiewicz, *J. Appl. Phys.*, in press

[7] J. M. Slaughter, A. Shapiro, P. A. Kearney, and C. M. Falco, *Phys. Rev. B*, in press

[8] T. J. Vink and J. B. A. D. van Zon, *J. Vac. Sci. Technol. A*, **9**, 124 (1991)

[9] A. Witvrouw and F. Spaepen, in *Kinetics of Phase Transformations, MRS Proc. edited by M.O. Thompson, M.J. Aziz, and G.B. Stephenson*, Materials Research Society, Pittsburgh, PA 1991

[10] C. A. Volkert, *J. Appl. Phys.*, **70**, 3521 (1991)

[11] J. T. Pan and I. Blech, *J. Appl. Phys.*, **55**, 2874 (1984)

[12] G. G. Stoney, *Proc. Roy. Soc. London, A*, **82**, 172 (1909)

[13] W. K. Waskiewicz, *et al.*, *Proc. OSA Topical Meeting on Soft X-Ray Projection Lithography, Monterey, CA*, Optical Society of America, Washington D.C., 1991

[14] D. L. Windt and W. K. Waskiewicz, *Proc. SPIE*, 1547-19 (1991)

[15] R. Hull, D. L. Windt, W. K. Waskiewicz, and R. Kola, this program

[16] G. L. Miller, J. E. Griffith, E. R. Wagner, and D. A. Grigg, *Rev. Sci. Instrum.*, **62**, 705 (1991)

An Experimental Set-up for the Production
of Large Size X-Ray Multilayer Structures

E. Ziegler, J.Ch. Peffen, and P. Høghøj

European Synchrotron Radiation Facility, BP 220, 38043 Grenoble Cedex, France

Phone (33)7688-2170

INTRODUCTION

Multilayer-based x-ray optical components call for heterostructures made of smooth and uniform layers with an abrupt interface, which imposes severe restrictions to the choice of materials. The multilayers have to be very uniform (1%) over the area that will be illuminated by an X-ray beam. For hard x-rays the small angle of incidence implies multilayers that are several tens of centimeter long, even when using a small d-spacing. When the beam is produced by a synchrotron storage ring source the high heat flux connected with the intense x-ray beams requires materials that are chemically very stable.

X-ray multilayer deposition has been successfully achieved by plasma sputtering[1], laser ablation[2], and electron beam evaporation[3], including very recently molecular beam epitaxy[4]. In every system the coating uniformity is often improved by moving the sample during deposition. Yet, a moving sample is difficult to cool or to heat or to combine with the use of in-situ characterization methods, which are likely to require a precise alignment. The static ways of improving the level of uniformity consist of increasing the distance between source and sample when using evaporation or laser ablation or of increasing the cathode size with respect to that of the sample when using dc or rf sputtering methods. However, the deposition rate will decrease unless a larger power supply or a stronger laser is used, which usually is not favourable to stability. In the cases of evaporation and sputtering techniques the consumption of material increases, and also the contamination of the vacuum vessel. With nanosecond pulse laser ablation limited improvement also might be obtained by rotating the target to vary the direction of the plume or by increasing the distance to the sample, also with an expected drop in the deposition rate.

Apparently, until now the smallest d-spacings have been achieved by sputtering[5]. The most promising technique for an atomic layer control of the films might be molecular beam epitaxy, although restricted to few materials and limited size. The production of thin-films and interference coatings with in-depth dimensions on the nanometer scale and lateral dimensions of few tens of centimeters has modified the methods used for fabrication and characterization. After a complete analysis of the existing technologies and processes we decided to build a multilayer fabrication facility using a large size microwave multipolar plasma capable of assisting the chemical vapor deposition or the reactive sputterring deposition of materials such as refractory metals and silicides.

PRODUCTION OF MICROWAVE MULTIPOLAR PLASMA

The technique of distributed electron cyclotron resonance (DECR) has been used in the past for the dry etching process in semiconductor technology. It has recently been applied to the epitaxy of silicon[6]. The method is based on the ability to transfer energy to electrons in a magnetic field. Because the cyclotron frequency is independent of energy, the electrons can be accelerated at each point of their orbit and therefore gain energy while increasing the radius of their trajectory. At a frequency of 2.45 GHz the field necessary for the electrons to be in resonance is 875 G. The multipolar magnetic confinement is classically obtained in a circular cylindrical chamber with an array of fixed permanent magnets with alternating polarity at the perimeter of the discharge chamber. The microwave excitation is produced by a series of individual antennas positioned in the plasma region, parallel to the magnets.

In most x-ray mirror applications for the hard x-ray region, the sample is long in the direction of the beam and narrow in tranverse direction. To reduce the reactor dimensions, we have designed a rectangular shape where the two long walls contain the magnets bars and water-cooling for preventing gas phase reactions and deposition. The chamber has an internal section of 50 cm x 50 cm and a length of 90 cm. The wall thickness of the vacuum vessel and the strength of the magnets have been chosen so that they can be located outside the chamber. The microwave

power is delivered by a series of individual power generators and magnetrons to each antenna using low leak rate connector feedthroughs. The 25 cm x 10 cm sample is oriented with its longer side parallel to the walls and located in the central region where the magnetic field is negligible. To obtain a uniform plasma in a plane perpendicular to the walls many parameters had to be optimized[7], such as the distance between panels, the number of magnets, and the magnet-antenna distance. For a minimum disturbance of the magnetic field controlling the plasma confinement, it is important that the components and the materials in the vacuum chamber have a low magnetic permeability. Yet, with the ability of varying the power on each individual antenna, local corrections to the plasma density are possible. The electron resonance condition is satisfied in a region located in-between the magnets and the antennas, called the source region. At high pressure the coupling of the electrons with the microwave field is poor due to the high collision rate, whereas a moderate low pressure (10^{-4}-10^{-5} hPa) favours the diffusion transport of the low energy ions away from the source. Using a Langmuir probe we measured the I(V) characteristics at different locations within the plasma. With a $7.3 \cdot 10^{-4}$ hPa nitrogen pressure and a power of 150 W applied to each antenna we obtained a positive ion density of $2.9 \cdot 10^{10}$ cm^{-3} ($\pm$ 4.5%), an electronic temperature of 3.08 ± 0.05 eV, and a plasma potential of 17.57 ± 0.17 V over a distance of 15 cm along the direction of the smaller side of the sample.

DECR-BASED DEPOSITION PROCESSES

While the plasma production is dominated by the electrons, the particles of interest for the thin-film deposition process are the ions having energies in the 0.1 eV- 10 eV range[8]. Two deposition methods are currently developed for using the glow discharge produced by ECR, namely reactive sputtering and plasma assisted chemical vapor deposition (PACVD).

The main advantage of the DECR plasma over the classical diode plasma sputtering is the ability to increase the flux of ions to the cathode without increasing the ion energy. Therefore, it is possible to avoid the emission of secondary electrons, a cause of layer damage during sputter deposition. In our system it is also possible to vary the distance between sample and cathode for optimizing the growth.

In PACVD the plasma is used to break down the gas molecules and to stimulate the reaction at the sample surface. The plasma allows the reaction to occur at a lower temperature than in conventional CVD. We plan to produce W/Si multilayers using WF_6 and SiH_4 as gas carriers, the constant mixture ratio between the gases being controlled by two mass flow meters and monitored by a mass spectrometer. As the mass spectrometer is equipped with a cylindrical mirror analyzer it is also possible to measure the energy distribution for the species present in the discharge. A differential pumping stage allows operation at up to 10^{-3} hPa.

With both methods an additional control of the interaction with the sample surface is possible. This consists of biasing the sample with a 13.56 MHz rf potential, without any coupling to the 2.45 GHz microwave excitation frequency. By adjusting the power, so that the energy of the ions striking the sample remains below 100 eV, one can enhance the surface mobility and hopefully obtain a better surface coverage. In addition we built a sample heater capable of regulating the temperature from ambient up to 800 °C.

IN-SITU CONTROL METHODS

The thickness repeatability over many layers can either be achieved by the stabilization of the deposition parameters during the time needed for deposition or by using in-situ characterization method capable of detecting thickness fluctuations. As most surface analysis techniques measure an electron or an ion current they cannot be used in a plasma environment. The same limitation applies for a soft x-ray reflectometer due to absorption from the plasma gas pressure. The production of amorphous structures precludes the use of some techniques such as

the reflection of high electron energy diffraction (RHEED). For crystalline materials RHEED might be applicable providing that the species present in the plasma do not disturb the detection of the signal.

We plan to use two in-situ methods that do not have this limitation, namely ellipsometry and grazing incidence hard x-ray scattering techniques. As they are presently in the design phase, only planning can be described.

As mentioned by various authors[9] ellipsometry can be used as an in-situ probe of the nucleation and growth of thin-films. The technique is sensitive to the interface structure[10] and can detect changes at the monolayer-level. For determining the film thickness we will preferably measure and analyze the intensity signal obtained after reflection of grazing incidence x-rays at 8 or 10 keV in the 0 to 5 degree angular range. The combination of ellipsometry and grazing incidence x-rays will be used to derive both the optical constants and the layer thickness.

The sample holder is capable of pitch and yaw alignment with respect to an incident X-ray or light beam. It is also integrated into the sample vertical translation, so that little modification of the alignement is necessary when changing the position of the sample inside the chamber.

EX-SITU CONTROL METHODS

We use ex-situ methods for calibration. An Auger electron spectrometer (AES) is available in an analysis chamber that is directly connected to the deposition chamber. It is used to control the residual carbon and oxygen composition of the sample surface with a monolayer sensitivity. It is also used to analyze the composition of the layers for various growth conditions, although it is very time consuming process due to the time necessary before transferring the sample from the process chamber to the AES chamber. An x-y scanning stage allows the mapping of the 10 cm x 25 cm sample size.

Low and high angle x-ray scattering measurements also can be made in our laboratory using a triple-axis x-ray diffractometer.

ACKNOWLEDGMENTS

REFERENCES

1. T.W. Barbee, AIP Proc. vol.75, p.131, Low Energy X-ray Diagnostics (1981), edited by D.T. Attwood and B.L. Henke
2. S.V. Gaponov, Y.A. Platonov, and N.N. Salashchenko, Proceedings of the International Conference on Synchrotron radiation, SR-90, Moscow, 26-29 June 1990
3. E. Spiller, Mat. Res. Soc. Symp. Proc. vol.56, 419-433(1986)
4. D.W.Schulze, J.M. Slaughter, and C.M. Falco , SPIE vol.984, 75, 17 -19 August 1988, F.E. Christensen Editor
5. T.W. Barbee, Private Communication
6. R. Burke and C.Pomot, Solid State Technology, 67-71, Feb.1988
7. The chamber has been manufactured by SNLS, F-38160 Saint-Romans under CNET/CNRS licence
8. See for example Thin Films Processes II, edited by J.L. Vossen and W. Kern, Academic Press publisher (1991)
9. B. Drevillon, J.Non-Cryst. Solids 114, 139(1989)
10. Ph. Houdy, this conference

Poster Session

MC 7:00pm–7:30pm
Teton Room

Investigation of the effect of large x-ray fluences on multilayer structures.

B.J. MacGowan, S. Mrowka, T. Barbee Jr., L.B. Da Silva, D.C. Eder,
J.A. Koch, L. Pan, J. Underwood, and P.E. Young.
*Lawrence Livermore National Laboratory, University of California,
L-483, P.O. Box 808, Livermore, California 94550, U.S.A.*

The use of multilayer mirrors in x-ray laser cavities is complicated by extremely intense optical and x-ray pulses that damage the multilayer mirror before it has done its job. The issue of damage of the mirror by x-ray emission from the plasma amplifier has been studied experimentally using short duration (500 psec) bursts of soft x-rays from a laser produced Au plasma. Different damage/failure mechanisms have been observed and identified for Mo/Si, $MoSi_2$/Si, W/C, WC/C and Cr_3C_2/C multilayers and damage thresholds quantified. The effect of the x-ray flux on the peak mirror reflectivity together with the position and shape of the bandpass has been resolved both temporally and spectrally. The shape of the bandpass has been fitted to solutions to the Fresnel equations for aperiodic stacks in order to infer the time history of the stack. Rapid diffusion of Mo into Si in Mo/Si multilayers has been observed to occur in time scales of order 70 psec.
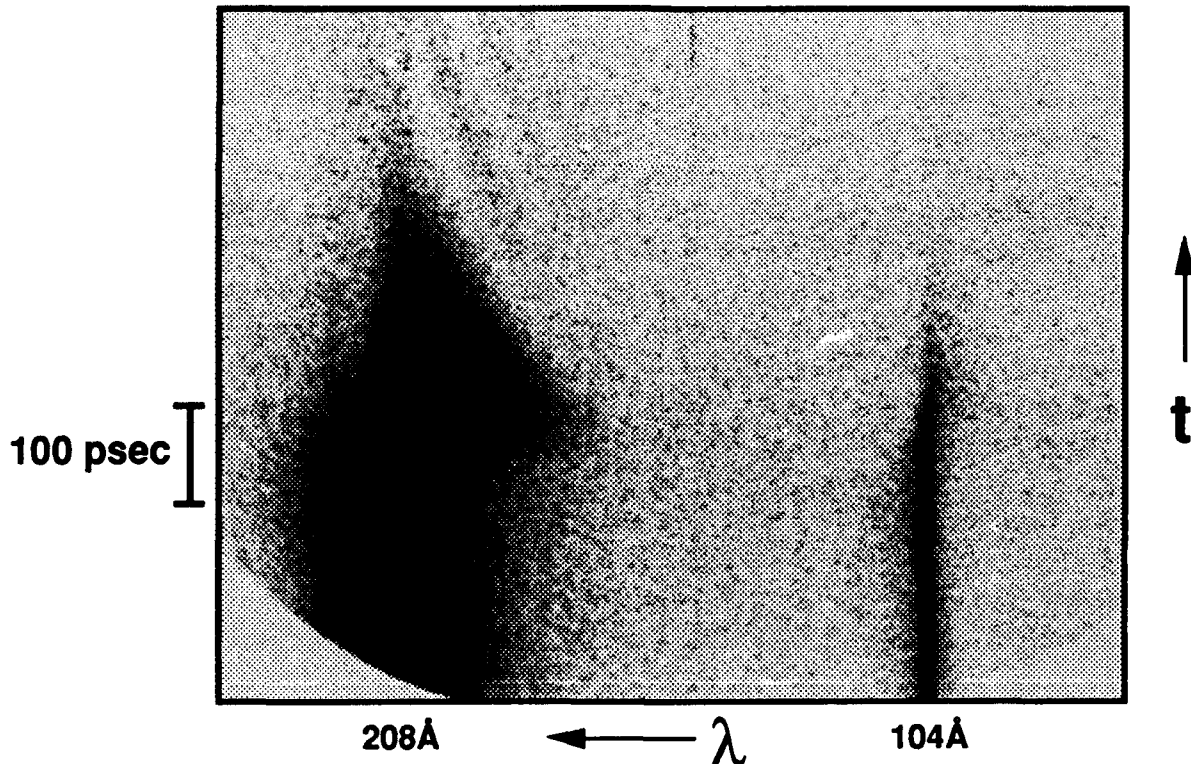

Figure illustrating the effect of a fluence of 0.4 Jcm^{-2} of 300 eV x-rays on a Mo/Si multilayer. The figure is the output from an x-ray streak camera that is spectrally resolving the first and second order Bragg reflections at normal incidence from the multilayer. The dark areas of exposure indicate wavelengths that are reflected by the multilayer. The rapid movement of the mirror bandpass to short wavelength and suppression of the 2nd order 104 Å signal occur after an integrated x-ray fluence of ~ 0.15 Jcm^{-2}. The mirror reflectivity is significantly reduced after an integrated fluence of ~0.3 Jcm^{-2}.

Analytical Observations and Depth Profile Simulation in regular-d and graded-d Metal/Carbon Multilayers prepared by Laser Pulse Vapour Deposition

R.Dietsch[1], S.Hopfe[2], H.Mai[1], G.Oertel[3], W.Pompe[1], M.Prokop[3], B.Schöneich[1], S.Völlmar[1], B.Wehner[4], P.Weißbrodt[5], P.Werner[2]

1   Fraunhofer- Einrichtung für Werkstoffphysik und Schicht-
    technologie
    Helmholtzstr. 20, O- 8027 Dresden, Germany
    Tel. (51)-2322-371

2   Institut für Festkörperphysik und Elektronenmikroskopie
    Weinberg 2, PF 250, O- 4020 Halle, Germany
    Tel. (46)-601312

3   Zentralinstitut für Elektronenphysik
    Rudower Chaussee, O- 1199 Berlin, Germany
    Tel. (2)-674-0

4   Technische Universität Dresden
    Institut für Werkstoffphysik
    Mommsenstr. 13, O- 8027 Dresden, Germany
    Tel. (51)-463-5679

5   Jenoptik Carl Zeiss JENA GmbH, Dünnschichtzentrum
    Göschwitzer Str. 33, O- 6905 Jena- Göschwitz, Germany
    Tel. (978)-77-472

The metal/carbon multilayers were prepared by Laser Pulse Vapour Deposition (LPVD).

Experimental equipment:

a) high vacuum system (base pressure $p \approx 5 \times 10^{-8}$ mbar)
   combined with a CO_2-TEA- Laser

b) ultra high vacuum system (base pressure $p \approx 4 \times 10^{-10}$ mbar)
   combined with a Nd-YAG- Laser

Characteristic laser pulse parameters:

	CO_2-TEA- Laser	Nd-YAG- Laser
wave length	10600 nm	1064 nm
pulse energy	4...5 J	970 mJ
pulse width	1 us	5...7 ns
pulse rep. rate	2 Hz	30 Hz

Deposition rates at the substrate in the order of 0,01...0,4 nm/s were achieved for focused power densities at the target in the order of $5\times10^8...10^9$ W/cm^2.

Both LPVD- reactors involve a particular target handling system which allows the elongation of the plasma plume direction due to a curved target surface.

The in-situ film thickness control is carried out by a quartz oszillator. A quite different behaviour was observed for film thickness measurement of both materials with only one quartz oszillator head and the thickness control by separate quartz heads, i.e. one for each material.
The ratio between the film thickness measured by quartz oszilator and the film thickness at the substrate was determined by ellipsometry, X- ray diffraction and profilometry at single layers.
The thickness profile across the substrate area measured by ellipsometry shows a thickness homogeneity in the order of a few percent.

Multilayers of regular-d and graded-d structures were prepared from the materials C, Ni and W.
The analytical characterization has been carried out by X-ray diffraction, TEM- cross section, AES, SNMS and ellipsometry.
Results obtained show that the layer stacks have a low interface roughness, a good reproducibility of individual layer thickness and a quite reproducible thickness ratio of the individual metal and carbon layers.

The efficiency of that technique will be demonstraded by presentation of results obtained from selected layer stack specimens.

The analytical results indicate:
- that the microstructure of the multilayers can be resolved with atomic resolution
- that analytical detection of very thin layers and layered inclusions in a layer stack and their direct observation by TEM can be achieved (Fig. 1)
- that selected order suppression is possible for a predesigned thickness ratio of metal and carbon layers (Fig. 2)
- that depth profile measurements with steady depth resolution of the order of 1 nm throughout the whole multilayer are possible

The interpretation of the measured results is improved by the computer simulation of the X- ray diffraction curves and AES and SNMS depth profiles.
Quantitative microanalysis of the AES intensity depth profiles is realized by application of factor analysis algorithms (Fig. 3).

Fig. 1.
TEM- cross section
micrograph of a
substrate near
region of a Ni/C
layer stack,
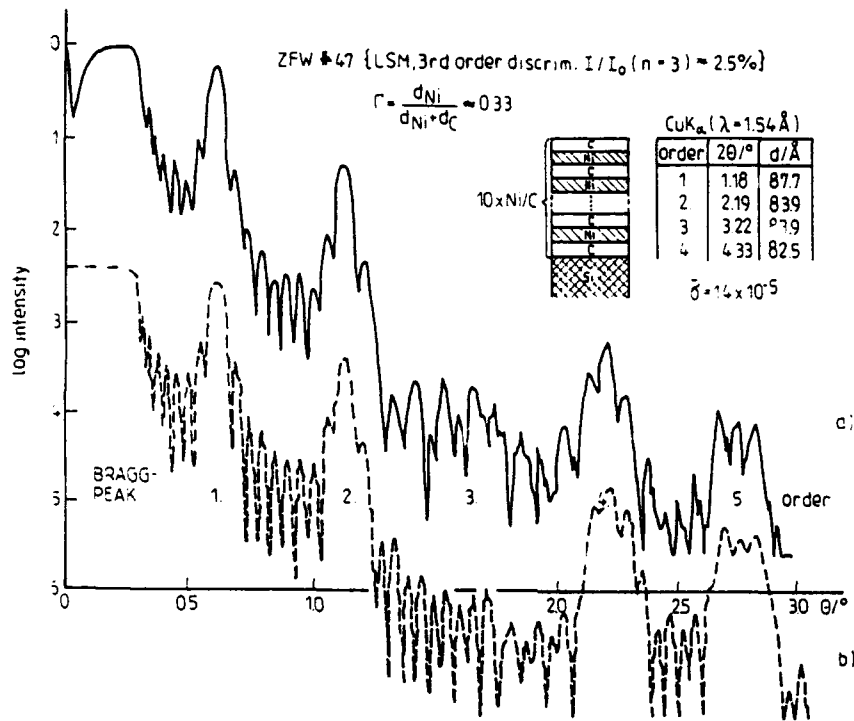detection of very
thin layered
inclusion

ZFW #47 {LSM,3rd order discrim. I/I_0(n = 3) = 2.5%}

$$\Gamma = \frac{d_{Ni}}{d_{Ni}+d_C} \approx 0.33$$

CuK_α (λ = 1.54Å)

order	2θ/°	d/Å
1	1.18	87.7
2	2.19	83.9
3	3.22	83.9
4	4.33	82.5

10 x Ni/C

$\bar{\delta}$ = 1.4 x 10⁻⁵

Fig. 2. X- Ray Diffraction curve of Ni/C multilayer with
predesigned ratio of individual layer thickness
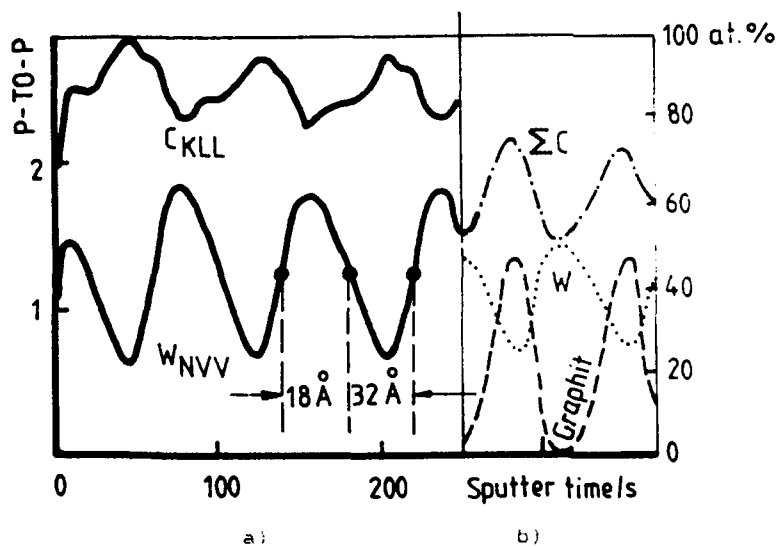a) experimental curve, b) simulation data

Fig. 3. AES depth profiling results
a) AE- intensity   b) concentration profiles
profiles   obtained by factor analysis

DIFFUSION BEHAVIOR OF METAL-CARBON MULTILAYERS.

A.D. Akhsakhalyan,A.A. Fraerman,Yu.Ya. Platonov
N.I. Polushkin and N.N. Salashchenko

Institut of Applied Physics,USSR Academy of Sciences,
USSR,Nizhny Novgorod,603600,46 Yljanov Street,tel.36-80-10.

The effect of annealing on the X-ray optical characteristics
of artificial multilayer structures composed of metal (Cr,Fe,Ni,Mo,Rh,
W,Pt and others) and carbon is studied.To analyze the changes at
annealing a small-angle X-ray diffraction was used.The observed X-ray
reflectivity enhancement can be explained by the uphill diffusion
of metal atoms.

1.   INTRODUCTION

One of the main requirements for X-ray mirrors is the stability
of their characteristics when they acted upon externally,specifi-
cally.when thermal action is involved [1,2].On the other hand,the multi-
layer samples present an unique possibility to study the diffusion
in supertnin films [3].Small variations in X-ray reflectivity from the
multilayer mirror,which occur at each boundary,lead to its considerable
variation as a whole ,since the reflectivity of the total structure
is proportional to one from interface multiplied by the square number
of effectively reflecting interfaces.

This study deals with the time evolution the reflection characte-
ristics in metal-carbon multilayers at different temperatures.To
interprete the results Auger electron spectrcscopy,small-angle X-ray
scattering and Raman spectroscopy were used.

2.   EXPERIMENT

Metal(Ni,Cr,Fe,Mo,W,Pt)-carbon multilayers were prepared by a pulse laser deposition technique [4].A solid-state pulsed Nd laser (λ =1.06 m) with the energy density 10^9 W/cm and pulse duration 30 ns was used. The films were annealed in 100... 600°C temperature range for time varied from 10^{-1} to 10^3 minutes. For film characterization a small-angle X-ray diffraction technique was used.A standard diffractometer (the power was 30 kV*40 mA) with a Ge (111) monochromator was operated in the $\theta/2\theta$ mode using CuKα radiation (λ = 0.154 nm).Soft X-ray diffraction measurements were performed in a RSM-500 spectrometer within the range of 1...10 nm wavelengths.

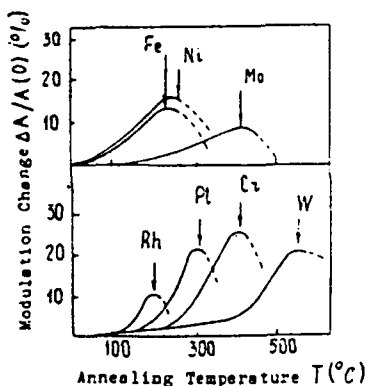The main result of the metal-carbon film experiments is presented in Fig. 1.The values of temperature T_c, at which the modulation $\Delta A/A$ decrease begin,as well as modulation amplitude enhancement at $T<T_c$ depend on structure period and average composition. The value of ($\Delta A/A)_{T=T_c}$ is defined by start one of modulation amplitude A also. The modulation changes are accompanied by the modulation period growth $\Delta d/d$,where d is the start value of period:

Fig.1 Experimental dependences of modulation amplitude on annealing temperature for different metals.

Metal	Cr	Fe	Ni	Mo	Rh	W	Pt
$\Delta d/d$,%	3.5	4.6	3.7	3.3	4.8	5.1	9.0

Here the value of $\Delta d/d$ is taken at $T=T_c$.

Fig.2 shows the changes in soft X-ray diffraction spectra at λ =1.33 nm for Pt/C and λ=4.47 nm for Ni/C films. As it shown,the peak intensity increases and the peak shifts towards lower glancing angles.

The time dependences of modulation amplitude and period are illustrated on a Ni-C sample (Fig.3).With annealing at 150°C a rapid growth of these magnitudes for a time t<1 min. takes place.
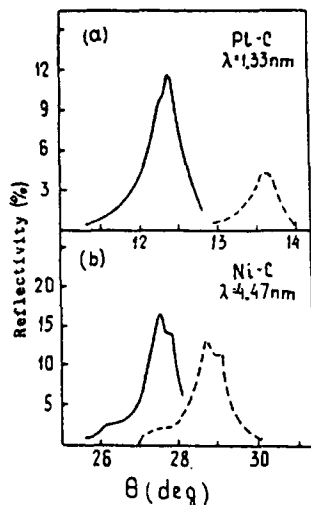
Fig.2 Soft X-ray diffrac-
tion spectra for
Pt/C at λ =1.33 nm
(a) and Ni/C at
λ =4.47 nm (b) before
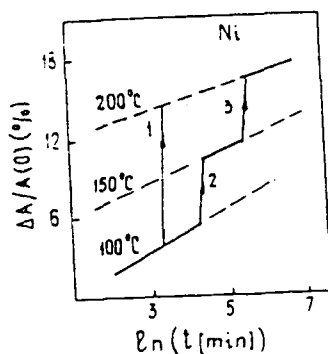(dashed curves) and
after annealing (full
curves).

Fig.3 Dependences of the
modulation amplitude
on the logarithm of
the time int at T=100°C,
150°C and 200°C for a
multilayer structure
Ni/C.

Then the slow growth stage comes.This
situation repeats at increasing of
temperature to 200°C(transition 3 in
Fig.3).

3.   DISCUSSION.

Analysing the X-ray diffraction spectra
at $\lambda\sim$ 0.1 nm,one can determine the chan-
ges in electron density distribution at
annealing (Fig.4) [4]. The main effect
consist the electron density decrease in
C region.We assume the two possible
reasons of this:

1.the structure change in carbon layer
which lead to carbon density decrease
[5] ;2.metal or carbon atom displace-
ment from C-rich region to metal-rich
one.The results of the sample characte-
rization with Auger and Raman spectro-
scopies don't contradict neither the
first version nor the second one.

We have carried out the additional
verification of metal atom diffusion
possibility.For this the weak-modulated
Ni/C film,in which the modulation ampli-
tude much less than average electron
density,has been prepared.A relatively
strong enhancement of X-ray reflectance
was observed (in 10 times) for this
sample after annealing at 180°C.Auger
spectra for the as-prepared and annealed

film show that X-ray reflectance
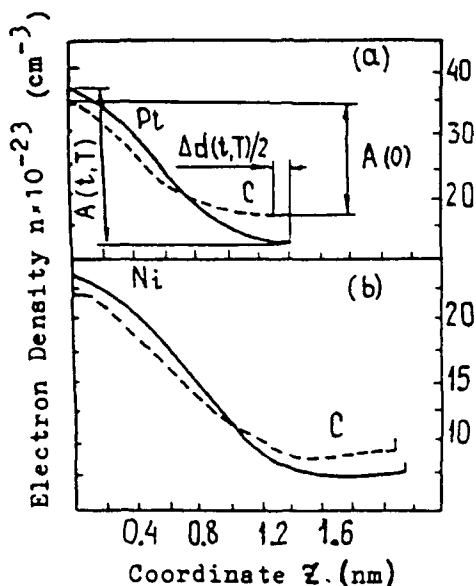increase is a result of uphill diffu-
sion metal and carbon atoms.

We compared the modulation change evolution in weak-modulated films with one in multilayer structures and couldn't find a qualitative difference in the modulation amplitude behavior. Moreover,the period variations are identical.The identical dependence of $\Delta A/A$ at $T<T_c$ and T_c values on the modulation period was found for two types of structures.These experiments let us to assume that the electron density decrease in Fig.3 is connected with the metal atom diffusion from C-rich region.

The general features of modulation amplitude and period with increasing annealing time are in qualitative accord with nonlinear theories of spinodal decomposition (for example,[6]).

Fig.4 Electron density distributions n(z) for Pt/C (a) and Ni/C (b) before (dashed curves) and after annealing (full curves).

1. J.B. Kortright and E. Ziegler, J. Appl. Phys.,69(1),1991,168.
2. A.F. Jankowski,L.R. Schrawyer and M.A. Wall,J.Appl.Phys.,68(10), 1990,5162.
3. H.E. Cook and J.E. Hilliard,J.Appl.Phys.,40(5),1969,2191.
4. A.D. Akhasakhalyan,A.A. Fraerman,Yu.Ya. Platonov,N.I. Polushkin and N.N. Salaschenko,Thin Sol. Films,203,1991,317.
5. Z. Jiang,X. Jiang,W. Liu and Z. Wu,J.Appl.Phys.65(1),1989,196.
6. J. Marro,A.B. Bortz,M.H. Kalos and J.L. Lebowitz,Phys.Rev.B12, 1975,2000.

Interfacial Roughness and Interdiffusion Derived from a Comparison of the Measured and Calculated Reflectances of Mo/Si Multilayer Coatings

J. F. Seely[1], M. P. Kowalski[1], T. W. Barbee[2], J. C. Rife[1], and W. R. Hunter[3]

[1]Naval Research Laboratory, Washington, DC 20375 (tel. 202-7673529)
[2]Lawrence Livermore National Laboratory, Livermore, CA 94550 (510-4237796)
[3]SFA Inc., 1401 McCormick Drive, Landover, MD 20785 (202-7672545)

Mo/Si multilayer coatings were fabricated at LLNL and were characterized using the Grating/Crystal Monochromator and Reflectometer attached to the Naval Research Laboratory beamline X24C at the National Synchrotron Light Source. The reflectances were measured at several angles of incidence and for both s and p polarizations. The measured reflectances were compared to calculations that included the effects of interdiffusion layers and of roughness at each interface and that were based on Henke's optical constants.

The dispersive element was a 2400 groove/mm gold-coated grating operated on-blaze, and the resolving power of the monochromator was 600. The reflectometer was rotated by 90° about the incident radiation beam to measure reflectances in both polarization orientations. An aluminum, silicon, or boron filter was used to attenuate higher order radiation.

Shown in Fig. 1 is the measured polarization of the light emerging from the exit slit of the monochromator, $(I_h-I_v)/(I_h+I_v)$, at the time when the data was taken. I_h refers to the intensity of light with the electric vector in the horizontal plane, and I_v refers to the intensity with the electric vector in the vertical plane. Polarization was determined by measuring the reflectance of a gold mirror at 45° angle of indidence in two orientations of the reflectometer with the plane of reflectance either vertical or horizontal ("s" or "p"). The orientation can be changed under vacuum. The incident beam was approximately 80% polarized in the horizontal plane except near the silicon L absorption edge. The polarization can be made greater than 95% by adjusting the beamline.

Shown in Figs. 2(a) and 3(a) are typical reflectance measurements for two of the optical samples that were characterized. The first sample (Fig. 2) consisted of 50 Mo/Si periods deposited on a superpolished fused quartz substrate. The period was d=106 Å, and the ratio of the Mo thickness to the d spacing was γ=0.23. A thin carbon layer was deposited on the top of the multilayer stack. The reflectance was measured at three angles of incidence (10°, 25°, and 45°) and for both polarizations. The calculated reflectances are shown in Fig. 2(b), where the amplitude reflectance at each interface was

multiplied by a Debye-Waller factor with a 10 Å roughness parameter. The calculated peak reflectances and the widths of the reflectance profiles are in good agreement with the observations. The calculated reflectances are somewhat higher than observed on the long wavelength side of the peaks.

The second sample (Fig. 3) consisted of 40 Mo/Si periods deposited on a superpolished fused quartz substrate. The period was d=178 Å and γ=0.20. The reflectance was measured with 80% p polarized incident radiation and for three angles of incidence (10°, 25°, and 45°). The reflectances at wavelengths corresponding to the first and second multilayer orders were measured. The reflectance was calculated assuming a 60 Å carbon layer and a Debye-Waller factor with a 10 Å roughness parameter. As shown in Fig. 3, the calculated and observed peak reflectances are in good agreement, while the calculated reflectance between the peaks are lower than observed. The relatively high reflectance observed between the peaks may be due to non-specular scattering resulting from in-plane structural inhomogenieties.

The comparison of the calculated and observed reflectances of a number of Mo/Si multilayer coatings will be discussed with the intention of inferring the characteristics of the coatings.
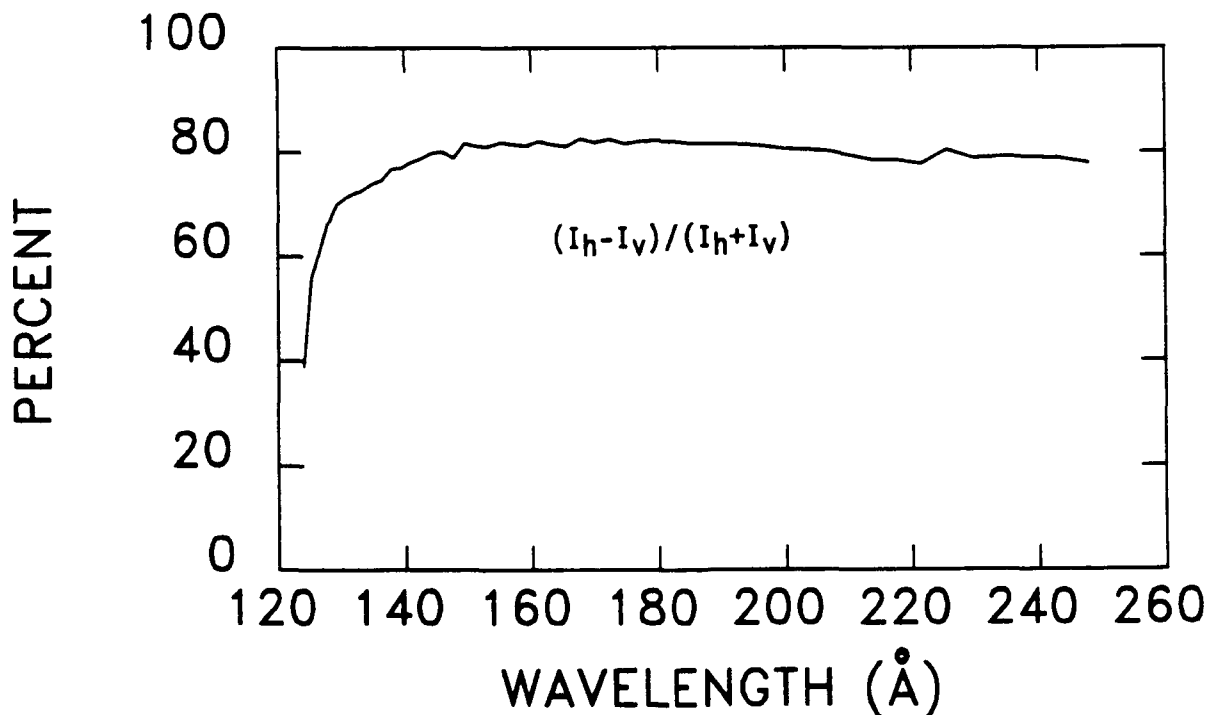

Fig. 1. Polarization $(I_h-I_v)/(I_h+I_v)$ of the incident radiation beam measured using a gold-coated flat at 45° angle of incidence.

Fig. 2. The measured (a) and calculated (b) reflectance of a multilayer coating consisting of 50 Mo/Si periods with d=106 Å and γ=0.23. The angles of incidence are 10°, 25°, and 45°. The reflectance profiles with the highest peak reflectance are for 80% s polarized incident radiation, and the lower profiles are for 80% p polarized radiation.
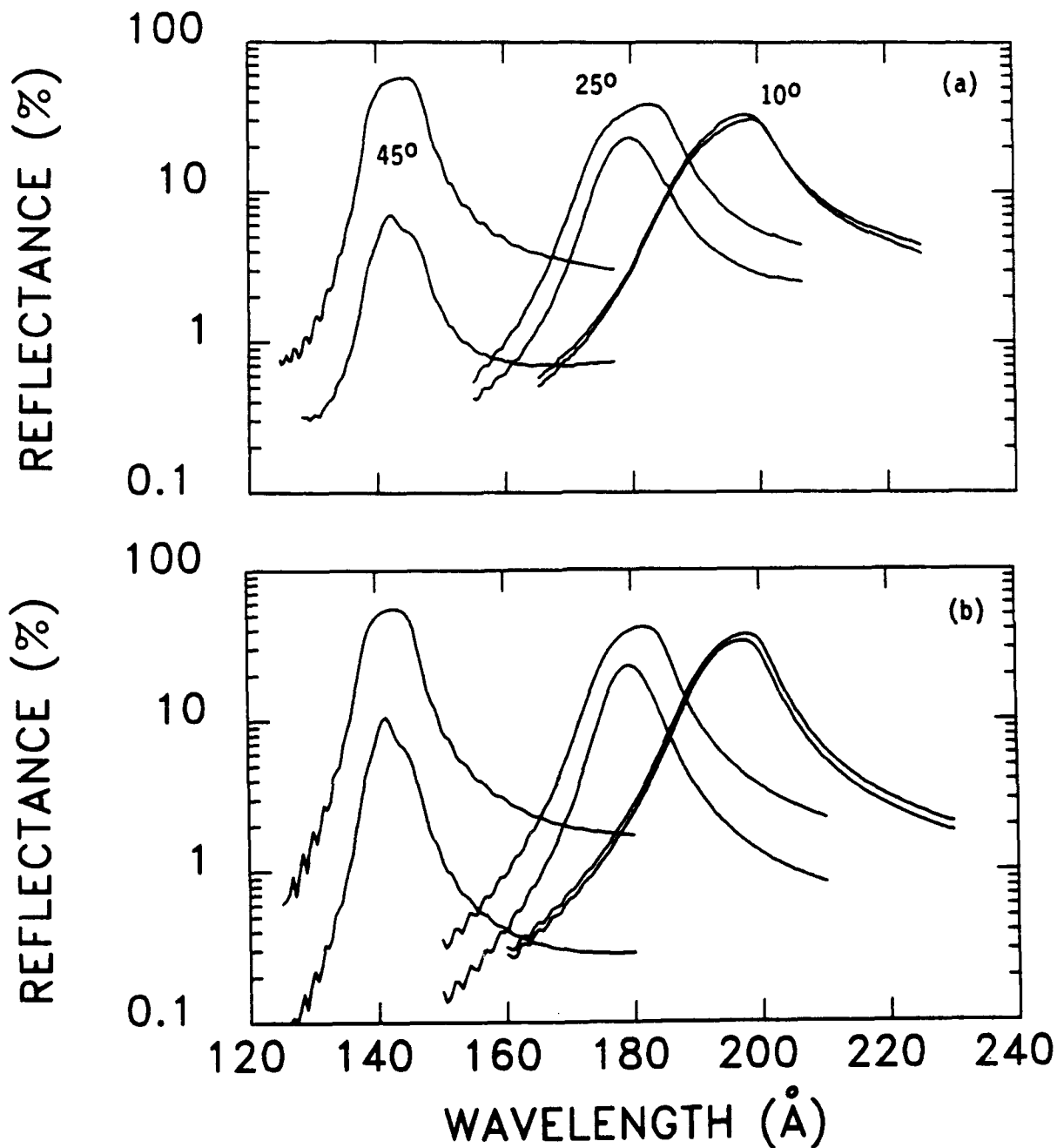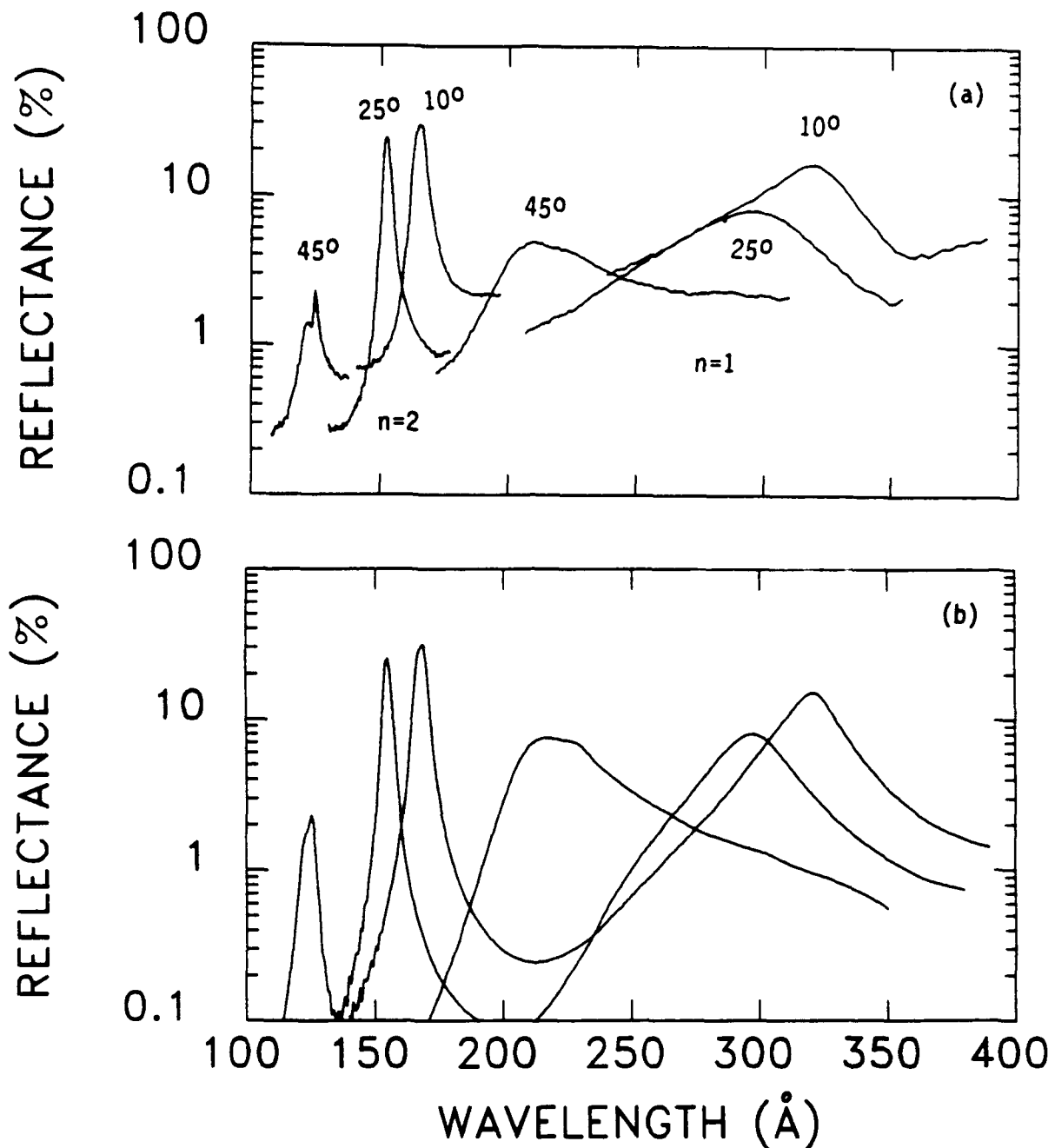
Fig. 3. The measured (a) and calculated (b) reflectance for a multilayer coating consisting of 40 Mo/Si periods with d=178 Å and γ=0.20. The incident radiation is 80% p polarized, and the angles of incidence are 10°, 25°, and 45°. The first (n=1) and second (n=2) multilayer orders are indicated.

A system for rapid characterization of multilayer mirrors and other soft x-ray optical components

S. Mrowka, B. J. MacGowan, L. B. Da Silva, J. A. Koch
Lawrence Livermore National Laboratory
University of California
L-476, P.O.Box 808, Livermore, CA94550, USA

We have developed a system capable of rapid characterization of optics in the soft x-ray region. X-rays from a laser produced plasma source are dispersed by a grating spectrograph onto a microchannel plate detector which is coupled to a CCD detector, figure 1. The CCD image is then read by a Macintosh computer. Part of the x-ray flux from the plasma is passed through the optic under test before being analyzed by the grating. In this way, spectral images with and without the test component in the optical path can be recorded simultaneously and compared to give throughput, figure 2. A .7 Joule Nd:Yag laser with 8ns pulse width, frequency doubled and capable of 10Hz operation, is focussed onto various targets to produce the x-ray pulses. A thin film filter is used to stop visible laser light from reaching the detector. Multiple diffraction orders from the grating are recorded so that the wavelength scale on the detector can be determined with high precision.

To date we have used our facility primarily for the evaluation of normal incidence multi-layer mirrors to be used in our x-ray laser and microscopy programs. Because the mirror testing is so rapid, we have been able to make substantial progress in development of short wavelength mirror coatings. Our system shows directly the reflectivity, bandpass and the wavelength at peak reflectivity. The actual wavelength at peak reflectivity is major issue for our x-ray laser optics and also for any application which requires reflectivity at a specified spectral line, such as astronomical spectroscopy. The problem assumes major proportions at short wavelengths (~45Å) where reflectivities are low and coatings with hundreds of layer pairs have to be made with the consequence that band-widths become very narrow.

In order to precisely match the mirror d spacing to the laser wavelength, we test the mirrors immediately after coating so that, if necessary, adjustments may be made to the coating parameters while the deposition system is unchanged. This development would have been quite impractical if synchrotron facilities were relied on, where typical turn around times might be weeks in comparison to hours.

The other major issue with which we have had to deal is the uniformity of coatings over large areas. At short wavelengths, this problem is particularly acute for mirrors with large numbers of layers. In our system, it is a straightforward matter to scan large areas, even on curved mirrors, by using an alignment telescope to set up the correct mirror angle.

The CCD image in figure 3 shows the incident continuum radiation and the reflected

x-ray radiation from a Mo/Si mirror made to reflect at around 135Å. Figure 4 shows line outs taken through the images. The calculated reflectivity is superimposed and shows the mirror to have a reflectivity close to theoretical. A single shot was required to take this data which then takes only a few minutes to analyse and compare with calculations. Even a large mirror (limited by our current chamber to ~4" diameter) can be examined in great detail in a relatively short time.

The system described is pumped by a turbomolecular pump and operates in the pressure range 10^{-5} to 10^{-6} torr. Contamination from the laser produced plasma appears to be insignificant as we have not observed any effects on reflectivity even after 100 pulses.
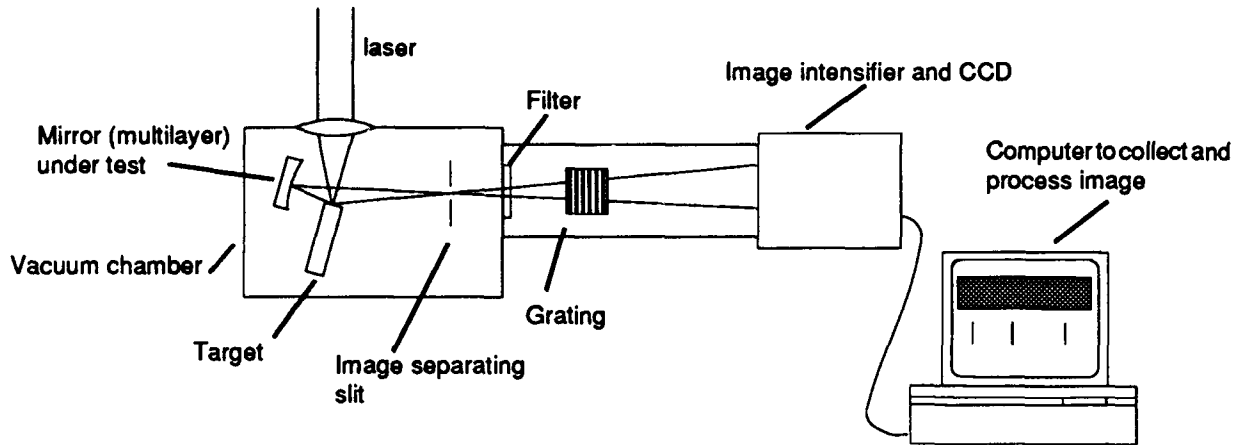
Figure 1. Laser produced plasma soft xray calibration system.
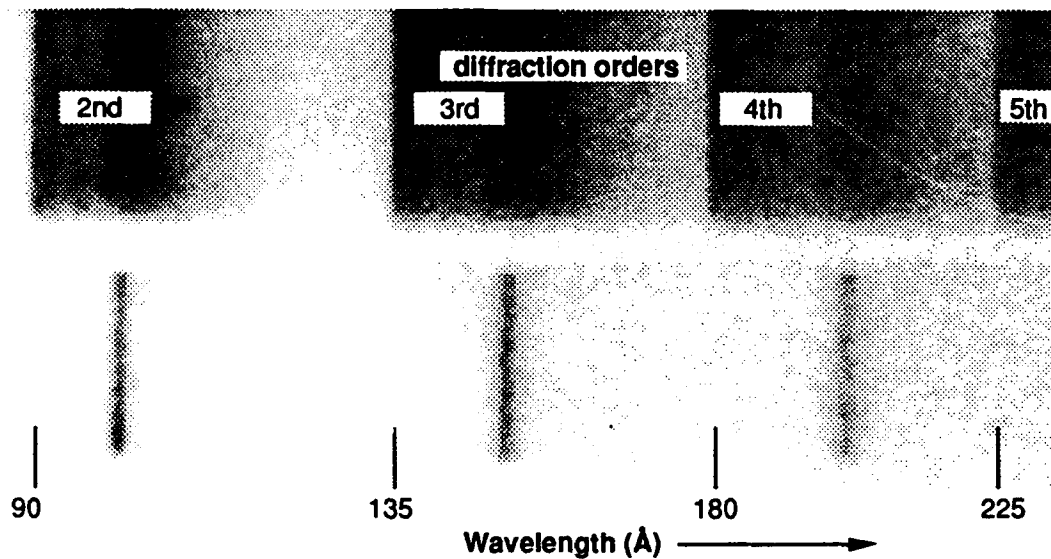
Figure 2. Direct spectrum of tungsten (top) and spectrum reflected in multilayer mirror (bottom). Up to 5 diffraction orders are recorded which allow the wavelength scale to be precisely calibrated. The mirror is W/C, reflecting at ~50Å.
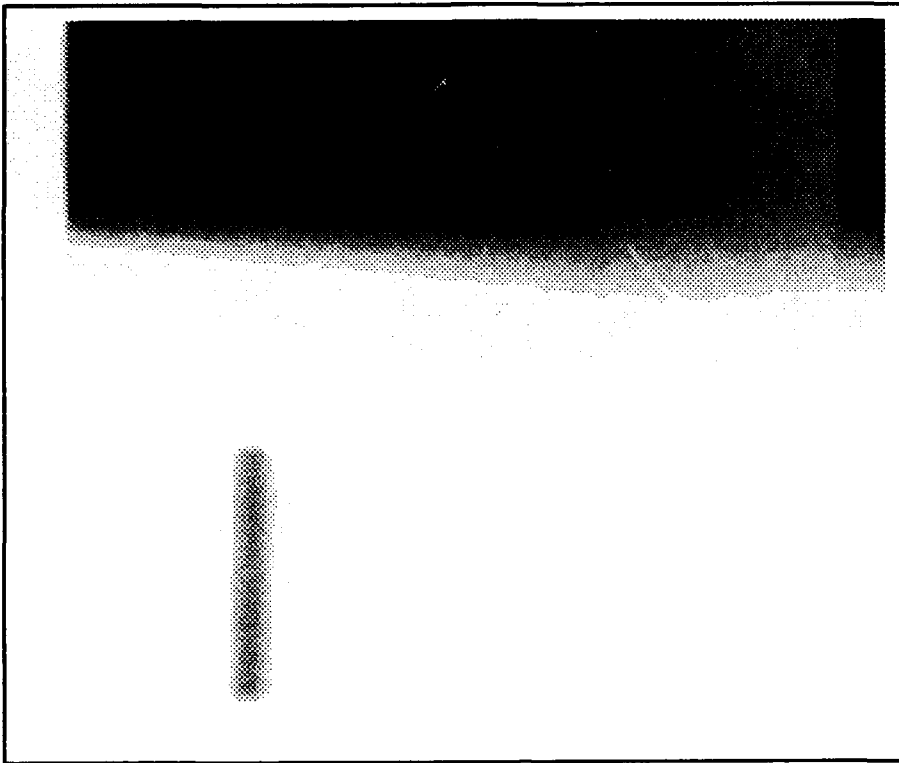
Figure 3. Image of incident continuum radiation and reflected x-rays from Mo/Si mirror (made by T W Barbee Jr, LLNL)
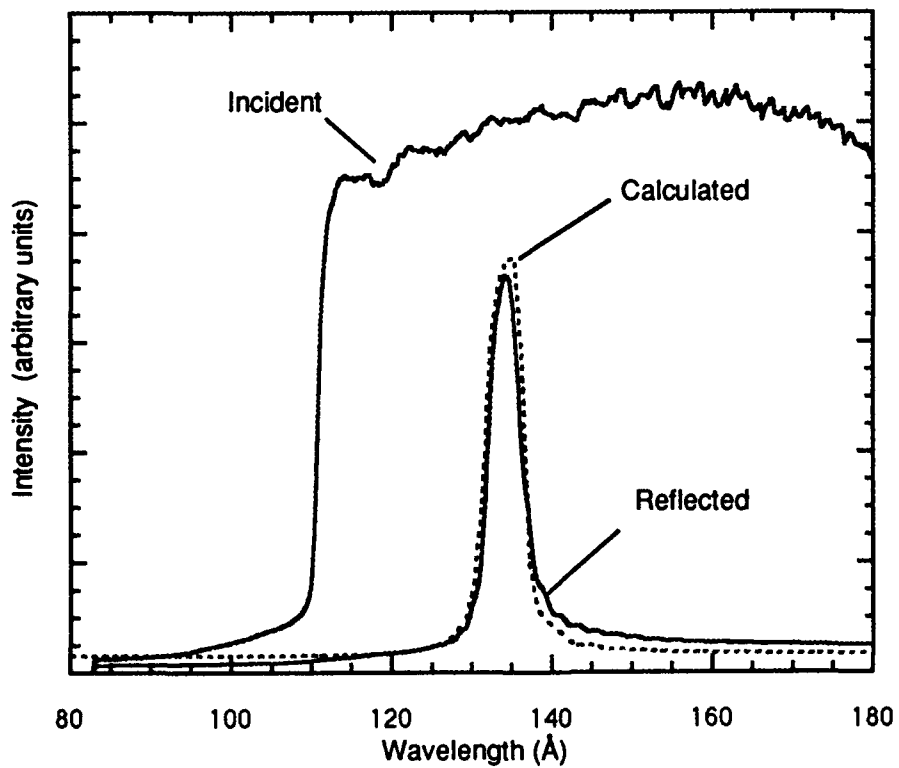
Figure 4. Lineouts from the images shown in figure 3. The calculated reflectivity is indicated by the dashed line.

SPUTTERING DEPOSITED Ta/Si MULTILAYER SOFT X-RAY MIRRORS

Shao Jianda   Fan Zhengxiu
Shanghai Institute of Optics and Fine Mechanics,
Academia Sinica, P.O.Box 800-211,
Shanghai, P.R.China

Tantalum/Silicon multilayers to be used as normal-incidence mirrors for 234A X-ray have been fabricated using plane magnetron sputtering system. The test and evaluation of characterizations have been given by Small Angle Diffraction with Cu-Ka radiation, Transmission Electron Microscopy and Auger Electron Spectrooscopy.

STABILITY OF THE LONG PERIOD MODULATED STRUCTURES

IN ORDERING SYSTEMS.

S.S. Andreev, N.I. Polushkin, N.N. Salashchenko and
S.I. Shinkarev.
Institut of Applied Physics, USSR Academy of Sciences,
USSR, Nizhny Novgorod, 603600, 46 Uljanov street, tel.36-80-10.

The anomalies in diffusion behavior of compositionally modulated structures in ordering systems W/Sb and Co/Pt are discussed. There are stable subnanometer modulated structures in W/Sb alloys. It has allowed to construct normal incidence X-ray mirrors. Co/Pt alloys are characterised by arising of self-organizated modulated structures with d=3.8 - 4.2 nm.

1. INTRODUCTION

The creation of equiblibrium ingomogeneous states with nanometer-scale periodicities attracts considerable attention in X-ray multilayer structure physics. The artificial modulated structure (MS) stability [1,2] or self-organizated MS in binary alloys behavior [2,3] is defined by temperature, average composition (or layer thickness ratio in multilayer structures), modulation period d and magnitude and sign of the mixing energy $U=E_{AB}-(1/2)(E_{AA}+E_{BB})$, where E's are the interatomic potentials.

In ordering systems ($U<0$), as it have been shown in the framework of linearized early stage theory Cahn's and Hilliard's theory [4], for MS with $d<d_c$ interdiffusion coefficient D is negative value (the modulation amlitude A(t) increases for a time t.), and $D>0$ for $d>d_c$ (Fig.1). If atomic interactic is other than those between nearest neighbors are neglected, then d_c close to the interatomic distance. Interdiffusion coefficient calculated from the formula

$$D = - \ln[A(t)/A(0)] \, (1/2 \, q^2 t)$$

where $q=2\pi/d$.

This paper studies the stability of modulated films in ordering systems Co/Pt and W/Sb under the heat treatment.The problem of MS self-organization in ordering systems is discussed also.

1.   EXPERIMENT

The modulated films Co/Pt and W/Sb with average composition 0.3-0.4 produced on glass and Si (111) substrates by a dc magnetron sputtering at a pressure of 5 mTorr of argon gas.Except this,the Co/Pt films were prepared by an excimer laser with λ=248 nm deposition.The films were annealed at 200°C for a duration of 1 hour.For MS characterization a small-angle X-ray diffraction technique was used.A standard diffractometer (the power was 30 kV*40 mA) with a Ge (111) monochromator was operated in the θ / 2θ mode using CuKα radiation (λ =0.154 nm).Soft X-ray diffraction spectra were measured by a RSM-500 spectrometer at OKα -edge of absorption.
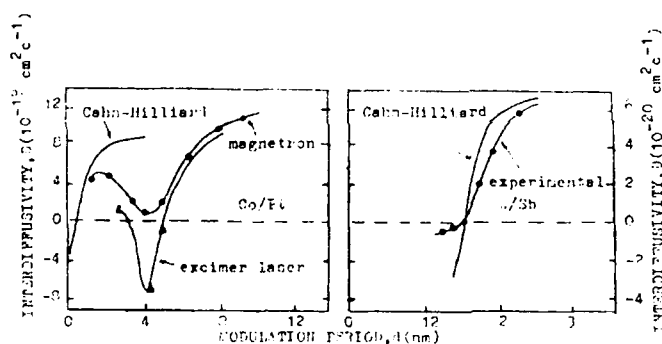
Fig.1   The dependence of interdiffusion coefficient at 200°C on modulation period for Co/Pt and W/Sb MS.

In Fig.1 experimental and calculated in accord with Kahn's and Hilliard's model curves D(d) for Co/Pt and W/Sb films are shown.Experimental curves were determined from the diffraction spectra at λ =0.154 nm. One can note the anomal behavior of D(d) in d region 3...6 nm for Co/Pt films.In ones, prepared by an excimer laser deposition, the self- organizated MS with d=3.8 ... 4.2 nm can arise besides of artificial one (Fig.2). The X-ray reflectivity in these MS doesn't decrease at temperatures less than 700°C,while the degradation temperature of artificial MS with the

same d is 300°C.For dc magnetron sputtered Co/Pt films we couldn't

find of modulation amplitude increasing.However,their behavior qualitatively coincides with ones, which were prepared by an excimer laser deposition.

Fig.2   Grasing incidence $\theta/2\theta$ diffraction spectrum at λ =0.154 nm of the as-prepared by an excimer laser deposition 30-layer pair 1.5-nm Co/Pt multilayer film.
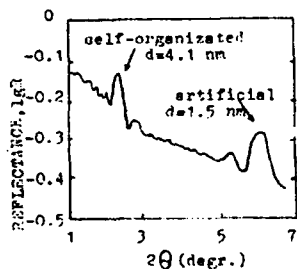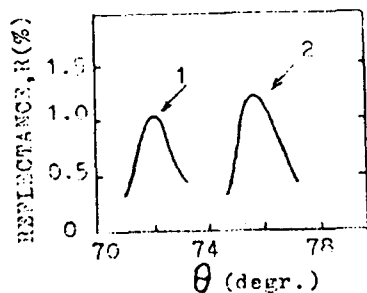
.   The observed in W/Sb films X-ray reflectivity enhancement is not large (Fig.3).It may be explained by a relatively high modulation amplitude in as- prepared W/Sb films.

Fig.3 Diffraction spectra at λ =2.36 nm (O Kα) of the 60-layer pair 1.2-nm W/Sb multi-layer film:1- as-prepared, 2-annealing at 200°C in duration of 1 hour.

3.   DISCUSSION

The enhancement of amplitude modulation in ordering systems for periods much greater than interatomic distance can be hardly understood in the framework of regular solution model with nearest neigbor interac-tions.In a more general form the model can include longer range interactions,characterised by a r.m.s. interaction distance

$$\delta = \sqrt{\sum_n Z_n r_n^2 U_n / \sum_n Z_n U_n}$$

where Z_n is the number of atoms in the nth coordination shell at a radius r_n.Interdiffusion coefficient is defined as $D(q)=D_0 \cdot (1-q^2 \delta^2)$ and $d_c \sim 2\pi\delta$ .Consequently, for W/Sb alloys δ is 0.6 nm.

The calculated from the experiments with Co/Pt structures of d=1.5 and 1.7 nm Cahn-Hilliard's curve intersects the dashed line D=0 at d=0.5 nm.It means that one can wait of MS with d<0.5 nm arising. Superstructures in ordering systems with periods ,which do not exceed an interatomic distance,are well-known(for example,the ordered phase CoPt).The Co/Pt film structure with self-organized MS was examined by an electron microscope.These investigations have shown that two

phases - disordered (A1) and ordered CoPt (L1) are in the films.
One can assume that such films comprise of alternating layers of the
two phases with different composition of Co and Pt atoms.

1. J.B. Kortright and E. Ziegler, J. Appl. Phys.,69(1),1991,168.
2. A.L. Greer, Ann. Rev. Mater. Sci.,1987,17:219-33.
3. L.H. Shwartz,Proc. of the NATO Advanced Study Institute on
   Modulation Structure Materials,Maleme-Chania,Greece,June 15-25,
   1983,p.411.
4. J.W. Cahn and J.E. Hilliard,J. of Chem. Phys.,28(2),1958,258.

Study of ultra-thin films in multilayer   structures by
standing -waves and small- angle x-ray scattering techniques

A. A. Fraerman, Yu. Ya. Platonov, N. I. Polushkin, N. N. Salashchenko
Institute of Applied Physics, AS USSR,
Ul'yanov 46, 603600, Nizhny Novgorod, USSR
S. I. Zheludeva, M. V. Kovalchuk, N. N. Novikova, I. V. Bashelhanov
A. V. Shubnikov Institute of Cristallography, AS USSR
Leninsky 59, 117333, Moscow, USSR

I. INTRODUCTION

The traditional method for LSM parameters investigation uses
small angle x-ray diffraction at $\lambda=0.1$nm. The parameters of
interest have been determined by comparing the theoretical
angular dependencies of reflectivity as a functions of these
parameters with the experimental curves.

In this paper we discuss the possibilities of solving the
inverse problem, i.e. the electron density or permittivity
distribution have been determined directly from the small angle
x-ray diffraction spectra. Also a new possibilities of ultrathin
film thickness and density determination are demonstrated by
means of x-ray method in form of x-ray standing wave technique
(XSW) and total external fluorescence study (NTEF).

II. DETERMING THE PARAMETERS OF REAL LSMs BY
A SMALL-ANGLE X-RAY SCATTERING TECHNIQUE

The parameters of multilayer structures were determined by
analyzing the angular dependence of x-ray reflectivity (≈ 1Å) in
the region of total external reflection and several Bragg peaks.
The essence of the procedure for processing the angular depen-
dence is as follows: 1. the LSM average electron density is
determined from the total external reflection angle; 2. the
moduli of Fourier harmonics of electron density are determined
from the integral reflection coefficients; 3. from the formula
of the reflectivity angular dependence withing Bragg peak region
a dispersion of the film thickness fluctuations in the structu-
re (ξ^2) is determined.

The roughness height distribution of the interface boundaries was supposed to be distributed according to the normal law, and the thickness of the boundary transition layer σ did not depend upon the boundary number.

Having obtained from the experiment the moduli of harmonic amplitudes at least in three orders of Bragg diffraction we determine the width of the boundary transition layer σ, ratio of the thicknesses β and the value of the electron density difference n_1-n_2.

The calculated values of the layer thickness and density are presented in Table I.for Ni/Ti and Ni/C LSM.These results were tested by difraction experiments using soft x-ray spectrometer. Fig.2 gives experimental (broken curve) and calculated (full curves) soft x-ray difraction spectra at $\lambda=1.76$ nm for Ni/C LSM.

TABLE I.

Parameters for the density distribution in LSM's

Sample	Ni/Ti	Ni/C
h_1 (nm)	1.76	1.63
ρ_1 (g cm^{-3})	6.9	7.5
2σ (nm)	0.8	0.6
h_2 (nm)	2.64	3.17
ρ_2 (g cm^{-3})	4.9	2.8
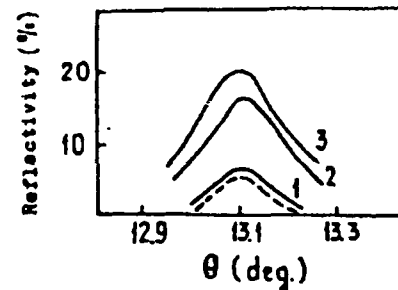
Fig.1.Soft x-ray spectra at $\lambda=1.76$ nm for Ni/C LSM: 1-$2\sigma=.6$nm, $\xi^2=.06$nm^2, $\rho_{Ni}=$ 7.5g cm^{-3}, $\rho_C=2.8$g cm^{-3}; 2-$2\sigma=.6$nm, $\xi^2=$ .06nm^2, $\rho_{Ni}=8.9$g cm^{-3}, $\rho_C=2.3$g cm^{-3}; 3- $2\sigma=0$, $\xi^2=0$, $\rho_{Ni}=8.9$g cm^{-3}, $\rho_C=2.3$g cm^{-3}.

III.Thickness and density determination of ultrathin solid films comprising LSM by XSW and NTEF techniques.

XSW is formed in a perfect crystal as a result of dynamic interaction between incident and reflected beams.Its nodes and antinodes are moving towards the lattice planes as an incident angle is scanned through Bragg diffraction region leading to a drastic change in photoelectron interaction of x-rays with crystal atoms and hence to peculiar angular dependence of secondary radiations yield.

We propose to apply SW formed in LSM for thickness determination of ultrathing films on the top of it. Of cause the deposition of a film will modify SW pattern. However for film of thickness and densities under consideration the alteration of SW amplitude is negligible and the phase shift is too small compared to Bragg angle.

The experiment was carried on a double-crystal diffractometer with CuK_α radiation and Si(111) crystal as monochromator. The fluorescence was registered with Si(Li) solid state detector. The investigated sample was an iron film deposited by pulse laser evaporation technique on Rh/C LSM prepared by the same method on Si substrate (see Fig.2). Two fragments of the sample (1 and 2) had initially iron films with the same thickness, but one of them (2) was covered with carbon layer and the other remained bare. The third fragment (3) had another film thickness and was also covered with carbon. Thus, two layers of iron had different thicknesses and were just in the situation they are inside multilayer structure.

D(LSM)= 59Å
D(Rh)= 11Å
N=20
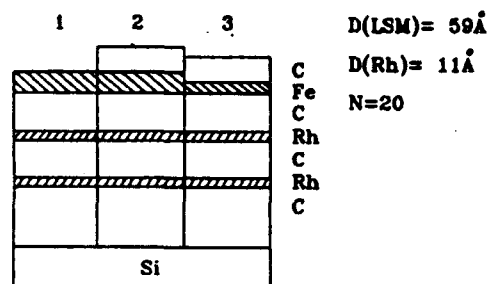
Fig.2.Schematic showing iron films deposited on Rh/C LSM

In fact the quality of XSW and, hence, the sensitivity of the technique depends on the structure perfection of periodic matrix. The "scale" (XSW) should be carefully calibrated before using. So, as preliminary the Rh/C LSM was investigated by a small-angle x-ray scattering technique.

Experimental results for the case when XSW is generated in LSM and determines fluorescence from iron film are represented in Fig.3. Calculations revealed that the thickness of uncovered film is sufficiently greater than that of covered film is (36Å ± 3Å and 22Å ± 3Å, respectively). The third covered film was determined to be 16Å±2Å thick.
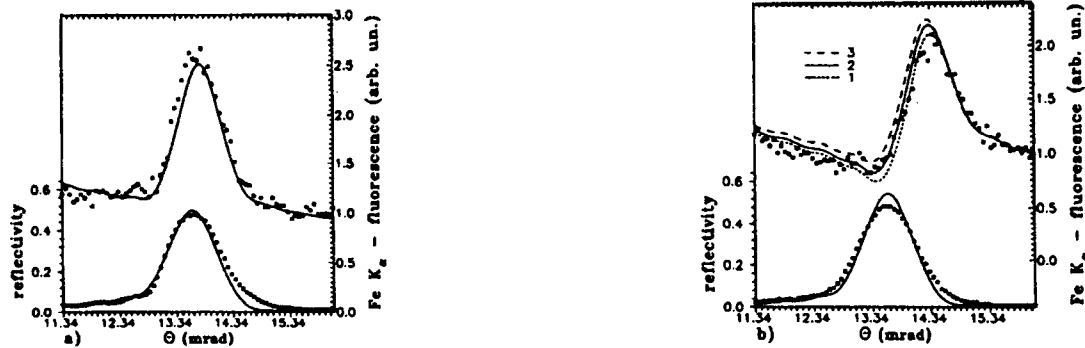
Fig.3. X-ray reflection and FeK$_\alpha$ fluorescence (upper curves) at Bragg difraction condition. (a)-dotts-experimental results for sample 1;calculated curves corresponds to iron film thickness 36 Å. (b)-dotts-experimental results for sample 2;calculated curves 1,2,3 correspond to iron film thickness 19Å, 22Å and 25Å respectively.

NTEF results are presented in Fig.4 for bare iron film having a remarkable change in film density. Calculation showed that ρ is only 45% ± 5% from that of the bulk material ρ_0. Pay attention that calculated x-ray reflection curves for both cases differ at much less extend than fluorescence angular dependencies.For a film 25Å thick covered with carbon the best fit between theory and experiment corresponds to ρ= 85% ± 5% ρ_0.
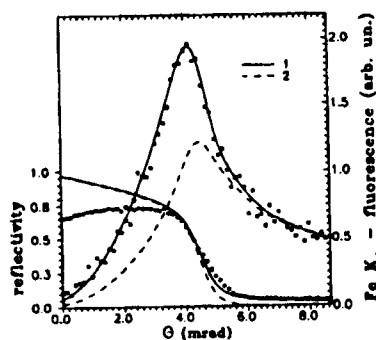
Fig.4.Experimental (dotts) and calculated results for bare iron film 36Å ± 3Å thick.Curve 1 corresponds to film density ρ=45% ρ_0 and curve 2 to ρ=ρ_0.

Thus,Bragg SW fluorescence measurements give the possibility to determine film thickness with high precision typical for XSW technique, NTEF study possesses information about film density. The main advantage is that these two parameters can be determined independently and the investigated film is not in the "model" situation,but just in the real conditions it is inside LSM structure.

Modeling of x-ray diffraction by multilayer mirrors, gratings and zone plates

A. Sammar *, B. Pardo ** , J-M. André *

* Laboratoire de Chimie Physique, Université Paris 6, CNRS URA 176, 11 rue Pierre et Marie Curie, 75231 Paris Cédex 05, France.

** Institut d'Optique Théorique et Appliquée, Université Paris 11, CNRS URA 14, Bât. 503, 91405 Orsay Cédex, France.

I. First Born approximation :

I.1. Generality: The diffraction problem consists in solving the Helmholtz equation for the tangential electric field component φ in the TE polarization case. The equation is :

$$\left[\Delta + k^2 \varepsilon(R)\right] \varphi = 0$$

where k is the wavenumber, $\varepsilon(R)$ is the complex dielectric constant and R is the position vector. Noting that $|1 - \varepsilon(R)|$ is generally small with respect to unity in the x-ray region, it is interesting to rewrite this equation in the following manner :

$$(E - H_0) \varphi = V \varphi$$

with : $H_0 = - \Delta$, $V = (1 - \varepsilon(R)) k^2$ and $E = k^2$. It is worth noting that this equation looks like the Schrödinger equation and the problem can be treated in a similar manner as the scattering problem in Quantum Mechanics. The field φ can be expessed as :

$$\varphi(r) = \exp(i\, k.r) + \frac{\exp(i\,k\,r)}{r} \, f(k_d, k, r)$$

where k_d, k are the scattered and incident wavevectors, r is the observation point, and $f(k_d, k, r)$ the so-called scattering amplitude. By means of the integral equation formalism, one shows [1] that the scattering amplitude $f(k_d, k, r)$ satisfies the self-consistent equation :

$$f(k_d, k, r) = - \frac{\tilde{V}(k_d - k, r)}{4\pi} + \lim_{s \to 0^+} \frac{1}{(2\pi)^2} \int dK \, \frac{V(k_d - K, r)}{k^2 - K^2 + i\,s} \, f(K, k, r)$$

where $\tilde{V}(q, r)$ is the Fourier transform of the Fresnel potential $\tilde{V}(R, r) = \exp\left(i\,k\frac{R^2}{r}\right) V(R)$.

If $Q = k_d - k$, $-\tilde{V}(Q, r) / (4\pi)$ can be considered as the first term of the Born expansion of $f(k_d, k, r)$.

I.2. Application to the mirrors, gratings and zone plates:

fn(x) =tg δ x + nd
gn(x) =tg δ x + nd+da
f(x) =-tgη x
g(x) =-tgη (x - D')

multilayer period: d= da+db
α= 1/tg δ +tgγ
d* = d /cosδ

Fig. 1a

Fig 1.b. Zone Plate
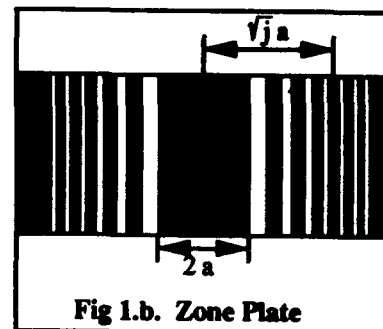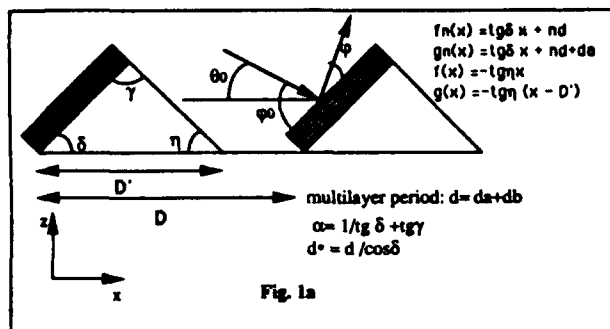
I.2.a Application to the mirrors and gratings : In this case we are concerned with Fraunhofer (R<<r) diffraction and $\tilde{V} \cong V$. The general model that we study here is given by the figure 1a.; it covers the so-called multilayer mirrors, laminar and sawtooth profile gratings by a judicious choice of the geometrical parameters.It is convenient for the following calculations to write the potential by means of a convolution product :

$$V(R) = V(x,z) = V_D(x,z) \otimes \Pi\Pi_D(x)$$

where $\Pi\Pi_D$ (x) is the Dirac comb of period D since we consider gratings with an infinite number of line (ideal periodic medium) and $V_D(x,z)$ is the potential distribution within the unit grating cell (See fig.1a.) that is easily expressed by the help of the Heaviside function H as follows:

$$V_D(x,z) = \sum_{n=0}^{N} (V_a + V_b T_a) H(z - f_n(x)) H(g_n(x) - z) H(z - f(x)) H(g(x) - z)$$

with $V_a = (1-\varepsilon_a) k^2$ and $V_b = (1-\varepsilon_b) k^2$; N is the number of bilayers in the multilayer structure. The functions fn(x), gn(x), f(x) and g(x) describe the geometry of the unit cell and T_a is a translation operator defined by the vector Va whose components are (See fig.1a.): $(d_a\cos\delta, d_a\sin\delta)$ in the reference frame considered.First of all, let us calculate the Fourier transform of V(R) :

$$V(K) = \int_{-\infty}^{\infty} dx \int_{-\infty}^{\infty} dz \ V_D(x,z) \exp\left(i (K_x x + K_z z)\right) . \Pi\Pi_{2\pi/D}(K_x)$$

where the wellknown properties of the Fourier transforms in particular the convolution theorem, were used. Integration by parts over x and z gives after tedious algebra :

$$V(K) = i\Pi\Pi_{2\pi/D}(K_x) \exp[-i(K_x - K_z \, tg\gamma)\alpha \, \tfrac{d_a^*}{2}] \left[\frac{1 - \exp(-i (K_x + K_z \, tg\delta)\alpha tg\gamma D')}{4\pi \, \alpha \, (K_x + K_z \, tg\delta)} \right] U_{N-1}\left[(K_x - K_z \, tg\gamma)\alpha \, \tfrac{d_a^*}{2} \right]$$

$$\left[V_a \frac{(1 - \exp(-i (K_x - K_z \, tg\gamma)\alpha \, d_a^*)}{(K_x - K_z \, tg\gamma)} + \exp(-i (K_x \sin\delta - K_z \cos\delta) d_a^*) V_b \frac{(1 - \exp(-i (K_x - K_z \, tg\gamma)\alpha \, d_b^*)}{(K_x - K_z \, tg\gamma)} \right]$$

where U_n stands for the Chebychev polynomial of first kind. The diffracted intensity in the first Born approximation is $I^{(1)} = |V(Q)|/4\pi^2$. The latter formula makes it possible to understand the kinematical behavior of the multilayer gratings. The diffracted directions are given by cancelling the argument of the Dirac comb which gives :

$$D (\cos \theta - \cos \theta_0) = p \lambda$$

which is nothing else but the usual grating rule. The condition of diffraction by the multilayer structure reads in the real direct space :

$$(\sin \varphi + \sin\varphi_0) d = m \lambda$$

This equation is the generalized Bragg law. At this stage we must consider the different cases:
-i: multilayer laminar grating: in this case $\varphi_0 = \theta_0$ and $\varphi = \theta$ so that one finds the generalized Bragg law in the form initially given by Warburton [2].

-ii: multilayer mirror: in this particular case one has moreover the specular condition $\theta = \theta_0$ and one recovers the standard Bragg law : $2d \sin\theta_0 = m\lambda$

-iii: multilayer sawtooth profile grating: in this most general case $\varphi_0 \neq \theta_0$ which means that the Bragg law is formaly identical to the generalized Bragg law obtained for the laminar grating provided that the angles are evaluated with respect to the face planes of the grating. To obtain a high efficiency of the grating it is necessary that the term $Q_x + Q_z \, tg\delta = 0$ vanishes. This condition is equivalent to the blaze condition of the grating, i.e. the reflection is specular for the facets of the grating ($\varphi = \varphi_0$). To match the blaze condition and the generalized Bragg law, it is necessary that the following condition be satisfied: $2\,d \sin \varphi_0^{Bl} = m\,\lambda$, which has the form of the standard Bragg law but written with the so-called Bragg blazed φ_0^{Bl} angle. In the case of laminar gratings this blazed angle is nothing else but the Bragg angle of the zeroth grating order. The grating rule in the blaze condition can be written as $2\,D \sin\delta \sin\varphi_0^{Bl} = p\,\lambda$, which shows that to match the grating rule, the Bragg law of the multilayer structure and the blaze condition, it is necessary that the following relation be satisfied :

$$\frac{D \sin \delta}{d} = \frac{p}{m}$$

II.2.b: Application to the zone plates: In this case we deal with a Fresnel diffraction problem. We consider positive linear zone plates with straight edges [3] as shown in fig.1b. As for the gratings it is worth to calculate the Fourier transform of the potential ; but as we deal with Fresnel diffraction we have mainly to consider the Fourier transform of the Fresnel potential $\tilde{V}(K)$:

$$\tilde{V}(K) = \int_{-\infty}^{\infty} dx \int_{-\infty}^{\infty} dz \, \exp(i\frac{kR^2}{r}) \, X(x) \, Z(z) \, \exp\left(i\,(K_x\, x + K_z\, z)\right)$$

where $X(x) = \sum_{j=0}^{L} \left[\Pi(\frac{x}{a\sqrt{2j+1}}) - \Pi(\frac{x}{a\sqrt{2j}}) \right]$ and $Z(z) = \sum_{n=0}^{N} (V_a + V_b\, T_a) H(z-f_n) H(g_n-z)$

$f_n = n\,d$ and $g_n = n\,d + d_a$, L is the number of lines. Clearly the integral can be separated:

$$\tilde{V}(K) = \tilde{V}_x(K_x)\, \tilde{V}_z(K_z)$$

where $\tilde{V}_x(K_x) = \exp(-i\frac{k}{2r}\xi^2) \int \exp(i\frac{k}{2r}(x-\xi)^2)\, X(x)\, dx$ and $\tilde{V}_z(K) \equiv V_z(K) = \int \exp(i\,K_z\, z)\, Z(z)\, dz$

with $\xi = K_x\, r / k$. It is valid to approximate $\tilde{V}_z(K_z)$ by $V_z(K_z)$ as long as the distance r is large with respect to the total thickness of the multilayer structure which is generally the case. It is convenient to introduce the Fresnel integrals :

$$Fr(w) = C(w) + i\, S(w) = \int_0^w \cos(\frac{\pi}{2} x^2)\, dx + i \int_0^w \sin(\frac{\pi}{2} x^2)\, dx$$

With the change of variable $\frac{k}{2r}(x-\xi)^2 = \frac{\pi}{2} x^2$ one gets the following expression for $\tilde{V}_x(K_x)$:

$$\tilde{V}_x(K_x) = i\, \exp(-i\frac{k}{2r}\xi^2) \sum_j (-1)^j \left[Fr\left((a\sqrt{j} - \xi)\sqrt{\frac{k}{\pi r}}\right) + Fr\left((a\sqrt{j} + \xi)\sqrt{\frac{k}{\pi r}}\right) \right]$$

A calculation similar to the one carried out in § I.1 for the multilayer grating gives for V_z:

$$V_z(K_z) = - \left[V_a \frac{(1- \exp(iK_z\, d_a))}{K_z} + V_b \exp(iK_z\, d_a) \frac{(1- \exp(iK_z\, d_b))}{K_z} \right] U_{N-1}(K_z \frac{d}{2})$$

These results allow the calculation of the diffracted intensity in the first Born approximation.

### III. Rigorous dynamical theory :

A rigorous electromagnetic theory has been recently developed to treat the problem of diffraction by multilayer gratings using a matricial formalism [4], [5]. The method takes advantage of the lateral periodicity of the grating, by expanding the field in terms of Bloch functions. Unfortunately this periodicity is lost for Fresnel zone plates and thus this expansion is not valid. In principle this approach can be applied to both the laminar and the sawtooth profile gratings but in the latter case the computing time becomes very large. So one hopes that a Born approximation treatment carried out at higher orders will be sufficient for both the sawtooth profile gratings and the zone plates. This study is underway.

IV. Numerical applications:

Fig.2 gives a comparison at 620 eV photon energy between rigorous calculation (2a) and first Born approximation (2b) for a multilayer mirror and a sawtooth grating at blaze condition at the 5 th order; the parameters are the following: multilayer with 20 W/C bilayers (dw = 2nm, dc =3 nm), grating period D = 1000 nm and δ = 2.86.
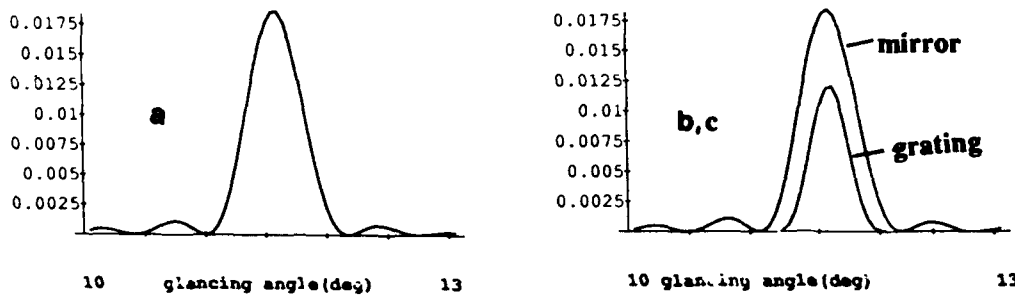
One notes a good agreement between the two approachs but at lower energy discrepancies appear. Fig.3 displays the intensity distribution along the focalisation axis of a linear zone plate with a= 14 μm and L= 15 and the same multilayer at the same energy.
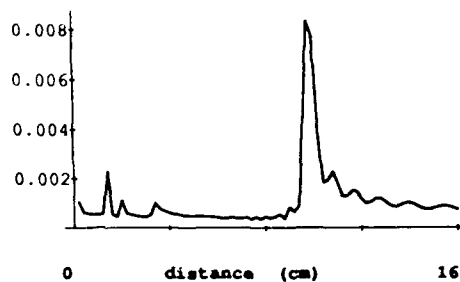
References
[1] A. Sammar, J-M. André, JOSA to be published.
[2] W.K. Warburton, Nucl. Instr. and method A 291, p 278 (1990).
[3] V.V. Aristov, A.I. Erko, V.V. Martinov, Rev. Phys. Appl. 23, p 289 (1988).
[4] B. Pardo, J-M. André, A. Sammar, J. Optics (Paris) 22 (3), p 141 (1991).
[5] A. Sammar, J-M. André, B. Pardo, Opt. Comm. 86 (2), p 245 (1991)

X-Ray and TEM Analysis of small period W-Si and W-B$_4$C multilayers

James Wood, Kevin Parker, James Scholhamer
Ovonic Synthetic Materials Co., Inc., Troy, Michigan 48084
(313) 362-1290

John Mansfield
Electron Microbeam Analysis Laboratory
University of Michigan, Ann Arbor, Michigan 48109-2143
(313) 936-3352

INTRODUCTION

In recent reports of the manufacture and characterization of small period multilayers, researchers have utilized high resolution TEM and an analysis of Cu-Kα X-Ray data to interpret and explain variations of reflectivity from theoretical predictions. These theoretical analyses are based on a dynamical reflectivity calculation which incorporates the Debye-Waller factor to simulate layer/interface roughness. Using the same analysis techniques we have evaluated how layer roughness varies with d-spacing and film thickness for small period (15Å<d<22Å) multilayers.

THE EXPERIMENT

W/B$_4$C and W/Si multilayer samples were produced on <100> silicon wafers in a planar-magnetron sputtering system. The ratio of tungsten thickness to bilayer thickness d, Γ, was determined to be 0.4 for W/B$_4$C and 0.3 for W/Si. Samples with intended d-spacings of 15, 18.5, and 22Å were produced. Process conditions were kept constant for all samples except for sputter time per layer. Samples with 25, 50, and 180 bilayers with an intended d-spacing of 22Å were also produced. The wafers were measured prior to coating with a WYKO Topo 2D profilometer. The measured substrate surface roughnesses ranged from 6Å to 8Å rms.

Cu-Kα X-Ray reflectivity measurements were performed at Ovonic Synthetic Materials Co. using a Huber diffraction system with a germanium <111> pre-monochromator. Transmission Electron Microscopy images were produced at the Electron Microbeam Analysis Laboratory of the University of Michigan using a JEOL 4000EX high resolution electron microscope.

The dynamical X-Ray reflectivity calculation includes a Debye-Waller factor

$$DW=e^{\left(-2\left(\frac{2\pi\sigma\cos\alpha}{\lambda}\right)^2\right)}$$

which was used to determine the roughness parameter σ. The measured and calculated values for reflectivity R(%), different

bilayer periods d($\overset{\circ}{A}$), and number of bilayers N, are shown in Table-1. Here R_σ is the measured reflectivity and $R_{\sigma=0}$ is the calculated zero roughness reflectivity.

Table 1

ID#	mat'l	N	d	$R_{\sigma=0}$	R_σ	σ
1	W/B$_4$C	265	15.1	84.1	20.0	4.3
2		215	18.1	84.5	39.6	4.4
3		180	21.3	84.7	49.0	4.7
4		50	21.3	68.6	32.6	4.2
5		25	21.3	36.7	13.3	4.1
6	W/Si	265	15.2	83.8	4.6	5.2
7		215	18.8	84.7	25.6	5.1
8		180	22.3	84.9	44.1	4.9
9		50	22.3	66.0		
10		25	22.3	33.4	9.6	4.2

From the data in Table 1, Figures 1 and 2 illustrate the relationship between calculated and measured reflectivity as it relates to d-spacing and number of bilayers.
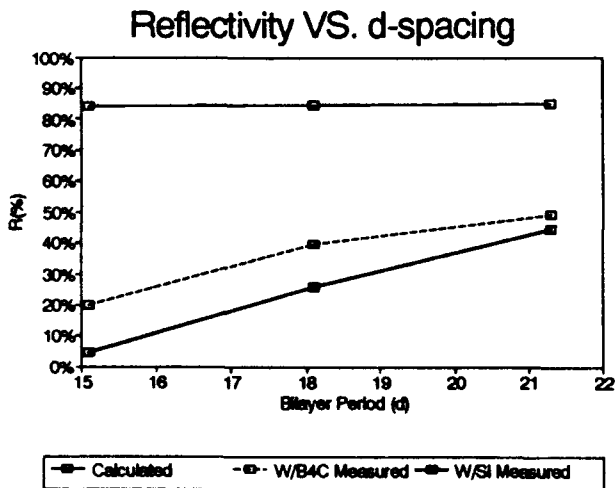
Figure 1
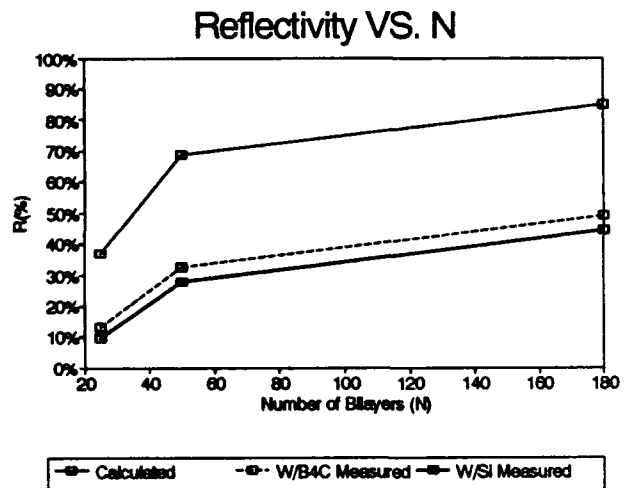
Figure 2

From the HRTEM images of W/B$_4$C multilayers shown in Figures 3 and 4, one can see that the quality of layering or interfacial roughness for the 15Å and 20Å period multilayers is similar. This evidence, along with the similar calculated roughness values from Table 1, suggests that the X-ray reflectivity reduction with d-spacing closely follows the Debye-Waller trend.

Figure 3: d=15Å W/B$_4$C multilayer   Figure 4: d=20Å W/B$_4$C multilayer

DISCUSSION

Evidence is shown that 25 to 180 bilayer W/B$_4$C and W/Si small period multilayers exhibit an increase in layer roughness or decrease in layer quality as the number of bilayer periods increases. In addition, measured reflectivities and calculated values for roughness parameter σ indicate that the reflectivity reduction as multilayer period decreases from 22Å to 15Å follows the Debye-Waller trend. The trend for σ vs. d-spacing indicates a slight roughness decrease with d-spacing for W/B$_4$C while the opposite is true for W/Si.

REFERENCES

1. Jankowski, A.F., et. al., "Subnanometer multilayers for x-ray mirrors: Amorphous crystals", J. Appl. Phys., 65(11), 1 June 1989, pp 4450-4451

2. Vidal, B., Marfaing, J., "Comparison of ultrathin W/Si and W/C multilayers for x-ray optics", Opt. Eng., Vol.30 No.5, May 1991

3. Jankowski, A.F., Makowiecki, D.M., "W/B$_4$C multilayer x-ray mirrors", Opt. Eng., Vol.30 No.12, December 1991

XUV Mo/Si Multilayer Mirrors Deposited
by RF Magnetron Sputtering

Claude Montcalm*†, Brian T. Sullivan*,
Henri Pépin†, J.A. Dobrowolski*.

* Institute for Microstructural Sciences, National Research Council of Canada,
Montreal Road, Ottawa, Ontario, Canada, K1A 0R6, (613) 993-9658.

† Institut National de la Recherche Scientifique-Énergie, Université du Québec,
P.O. Box 1020, Varennes, Québec, Canada, J3X 1S2, (514) 468-7721.

SUMMARY

Mo/Si multilayer mirrors with a high reflectance at 132 Å were deposited using rf magnetron sputtering. The reflectance as a function of the deposition conditions was studied by varying both the argon partial pressure and the target power. To provide uniform coatings, the samples were rotated about their axis during deposition. In addition, the substrates could also be oscillated back and forth over the target giving rise to multiple passes during the deposition of each layer. With specially designed masks placed between the substrate and the target, this oscillation provides a further improvement in the uniformity. Furthermore, the multiple passes help average out any fluctuations in the deposition rate. Uniformity measurements of samples, made with and without the oscillations, will be presented.

The multilayer mirrors were characterized by x-ray diffraction (XRD), TEM and reflectance measurements using synchrotron radiation. A new cleaving technique was used to prepare the samples for the TEM studies [1]. In addition to being quick, this method introduces less sample damage than the standard ion milling technique.

Asymmetry in the interfaes of the multilayer mirrors can be observed with TEM and, indirectly, with XRD. Theoretically, with XRD the asymmetry in the interdiffusion of the Mo/Si interfaces results in a decreased modulation in the amplitude of the Bragg peaks, as shown in the curves of Figure 1. The modulation evident in curve b for symmetric interfaces is nearly absent in curve d, corresponding to a large asymmetry in the interfaces.
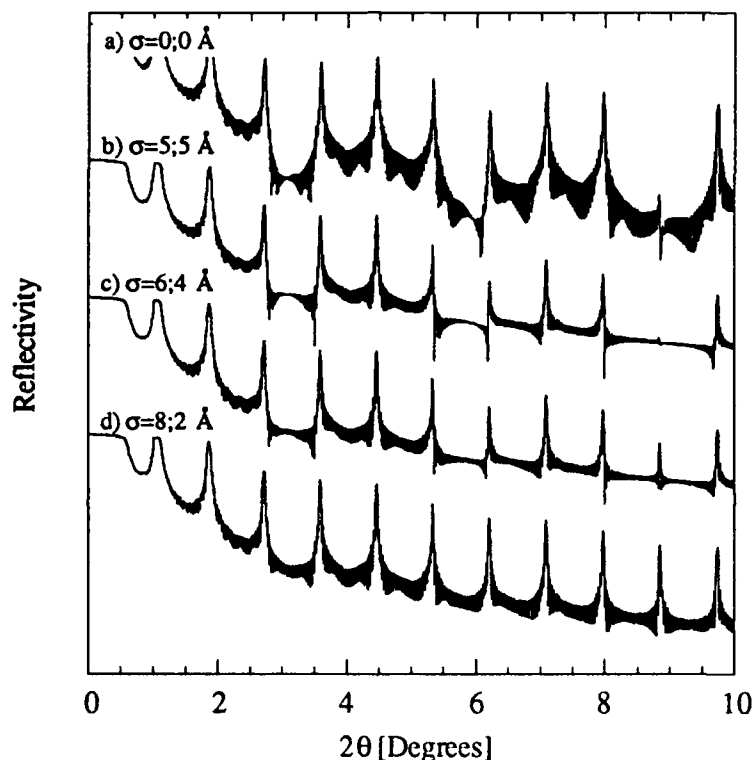
Figure 1. Calculated reflectivity of a 30 period Mo/Si multilayer ([Mo(30Å)/Si(70Å)]$_{30}$) for various interface thicknesses $\sigma = \sigma_{Mo/Si}; \sigma_{Si/Mo}$. The spatial profile of each interface has been modeled using an exponential variation [2]. The first two curves a and b correspond to symmetrical interfaces ($\sigma_{Mo/Si} = \sigma_{Si/Mo}$) with thicknesses of 0 Å and 5 Å, respectively. Curves c and d show the effect of asymmetry in the interfaces ($\sigma_{Mo/Si} \neq \sigma_{Si/Mo}$), keeping the sum of the interface thicknesses constant.

References

1. J.P. McCaffrey, "Small-angle cleavage of semiconductor for transmission electron microscopy", Ultramicroscopy (1991), in press.
2. D.G. Stearns, "The scattering of x-rays from non-ideal multilayer structures", J. Appl. Phys. **65**(2), 491-506 (1989).

LAYERED OPTICS FOR NUCLEAR MONOCHROMATIZATION OF SYNCHROTRON RADIATION

E. E. Alp, E. Witthoff[*], T. Mooney,
Advanced Photon Source,
Argonne National Laboratory, Argonne, Illinois, 60439

H. Homma, M. Kentjana
Brooklyn College, CUNY, Brooklyn. NY 11210

SUMMARY:

The insertion device based third generation synchrotron radiation sources currently under construction in Europe, USA, and Japan brings new opportunities and challenges in the design and manufacturing of x-ray optics. These high brightness sources demand more stringent parameters on the quality of multilayered optics in terms of size, uniformity, and surface and interface roughness.

We will present the design principles, and characterization and performance of SnO_2 / Pd / quartz Grazing Incidence Anti Reflection, GIAR, films[1]. These films are designed to produce high energy resolution with $\Delta E/E = 10^{-11} - 10^{-12}$ at 23.870 keV via ^{119}Sn Mossbauer transition. The energy resolution is tunable between few tens of nano-eV up to μeV level by changing the incident angle. The difficulties associated with premonochromatization using multiple bounce Si crystals, and ways to increase angular acceptance, while maintaining high energy resolution will be discussed. The characterization of films in terms of the degree of electronic reflectivity suppression, and nuclear reflectivity will be presented. The expected nuclear reflectivity as a function of photon energy and incidence angle is presented in Fig. 1. The time response of nuclear decay, and the limitations imposed on the time-coincidence detector system will be explained.

The measurements of surface, and interface roughness via x-ray reflectivity are carried out for numerous samples prepared under various sputtering conditions. The effect of oxygen partial pressure, substrate temperature, and subsequent annealing on chemical composition of the film is investigated via conversion electron Mossbauer Spectroscopy, CEMS. The performance of GIAR films will then be compared to resonant/non-resonant multilayers.

---

[*] Permanent address: II. Institut f. Experimentalphysik, Hamburg University

(1) J. P. Hannon, G. T. Trammel, E. Gerdau, M. Müller, R. Rüffer, H. Winkler, Phys. Rev. B, **32**, 363 (1985).

SnO2 GIAR Nuclear Monochromator
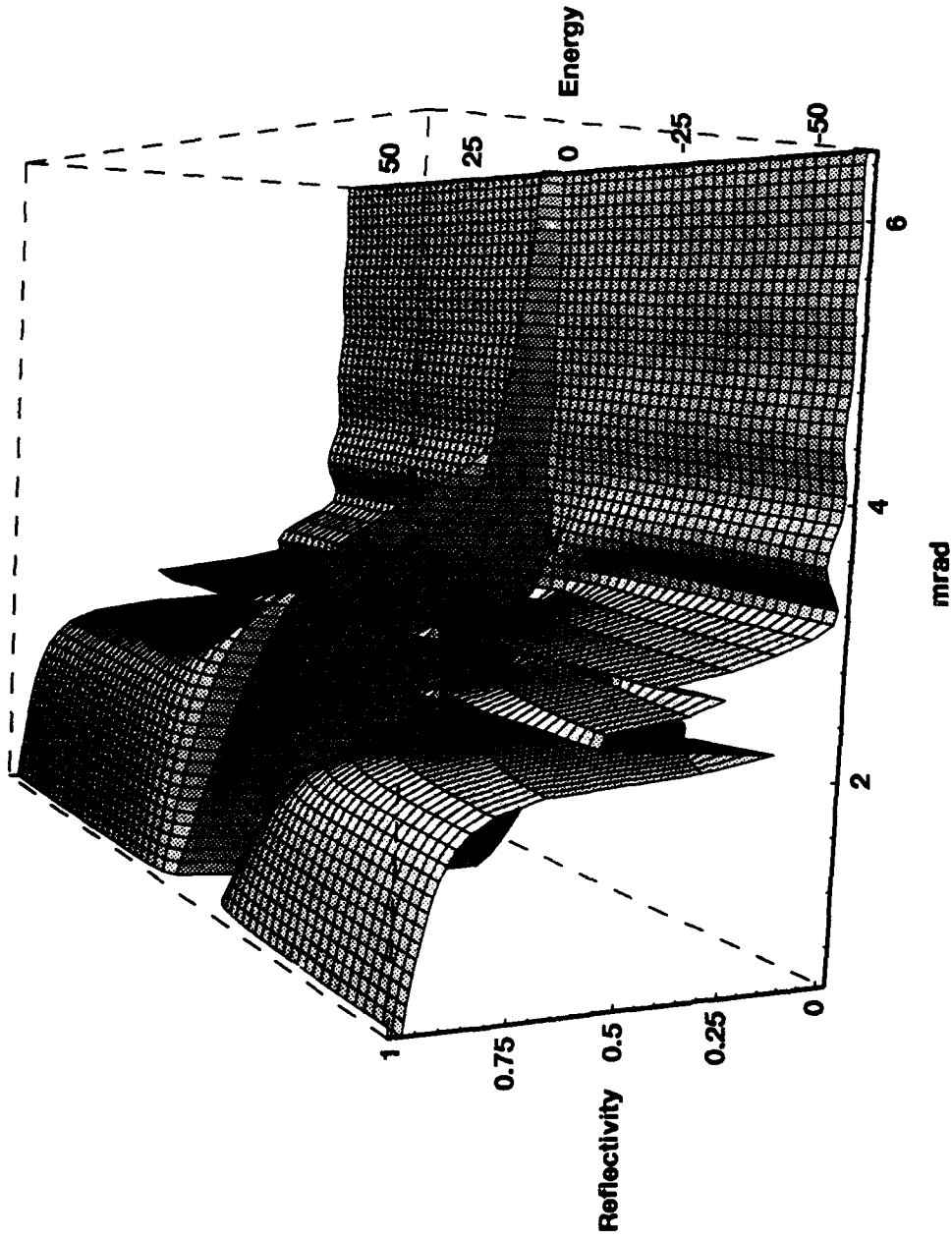
Growth and Structure 2

MD 7:30pm–10:45pm
Grand Room

Jeffrey B. Kortright, *Presider*
Lawrence Berkeley Laboratory

Application of *in-situ* ellipsometry to the study of ultrathinn layers and soft x-ray multilayers

Masaki Yamamoto

Research Institute for Scientific Measurements, Tohoku University
2-1-1, Katahira, Aoba-ku, Sendai, 980, Japan
Phone 022-227-6200, ext.3236

Ellipsometry is an accurate tool to study surface and thin-film phenomena[1]. It gives information of the dielectric boundary structures causing diffractions or reflections at the probed area of a surface down to the escape depth of the probe light. With a He-Ne laser light of a wavelength of 633nm, the probed depth for most metals are of an order of a few tens nm, being equivalent to several periods of a soft x-ray multilayer. The accuracy achieved for the single layers is at least a few tenths of nm in thickness[2,3].

When the fabrication processes are investigated at the high accuracy of ellipsometry, real ultrathin films exhibit characteristic ellipsometric response originating from various imperfections such as non-uniformity (island structure or pinholes), oxidation, chemical compound formation, and diffusion at the interfacial boundary. These are all important phenomena to be studied and controlled for realization of better soft x-ray multilayer optics.

For *in-situ* ellipsometry of soft x-ray multilayer fabrication, we developed a method to calculate complex refractive index and thickness of the growing films by using *in-situ* data taken during deposition[4]. With the method, we studied optical properties of growing single layers and multilayers of various materials.

Deposition systems and ellipsometers
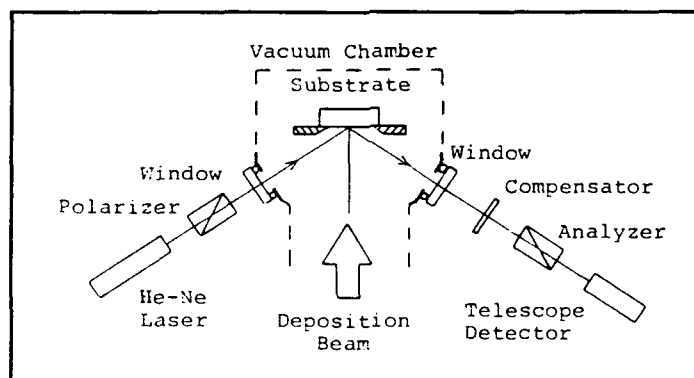

Figure 1 Schematic view of the *in-situ* ellipsometer

Ion beam sputtering system (Elionix Co. Ltd.,Japan)[2] and electron beam deposition system(Ulvac Co. Ltd., Japan) are used for the present study. The sputtering system is evacuated down to a base pressure of $<10^{-4}$ Pa by a diffusion pump with a liquid nitrogen trap and is operated with argon gas at 3.0×10^{-2} Pa.

The ion source is electron cyclotron resonance type and produce a 10-cm diameter ion beam of 1-mA/cm^2 current density at 1-kV acceleration. The electron beam deposition system is evacuated down to a base pressure of <10^{-7} Pa by a cryogenic pump. A 3-kW electron gun with four crucible is used for deposition. The deposition distances are about 30-cm for both system. Both systems have birefringence free glass windows for in situ ellipsometers.

Ellipsometric parameter $\rho=\tan(\psi)\exp(i\Delta)$ is a complex number and is defined by a ratio between p- and s-component amplitude reflectance Rp/Rs. In the standard extinction ellipsometry that we used at zone 3, ρ is calculated as $\tan(-P)\exp(i(2A-\pi/2))$ where P and A are the measured extinction azimuths of the polarizer and the analyzer, respectively. The computer records ρ and displays as a complex plane plot.

Single Layer
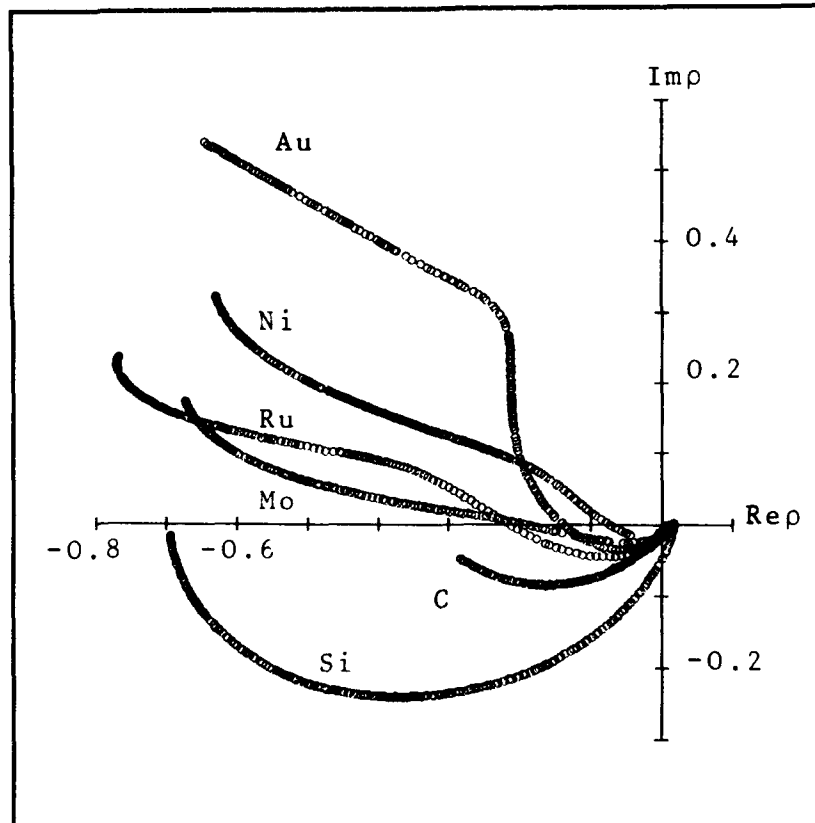
Figure 2 Growth curves plotted in the complex plane

Figure 2 shows the complex plane plot of the measured ρ during the growth of Au, Mo, Ru, Ni, C and Si layers on BK7 glass substrates. Each growth curve starts from the bare substrate point near the origin but show very different behavior depending on their optical constant. By using two ellipsometric data taken in sequence during deposition, we can analyze the refractive index n, extinction coefficient k and the two thicknesses at two data points. These growth curves have been analyzed with this method developed. Typical results are shown in Fig. 3, where n, k, and d are plotted as a function of the deposition time.
As the deposition proceeds, n and k start from those of the
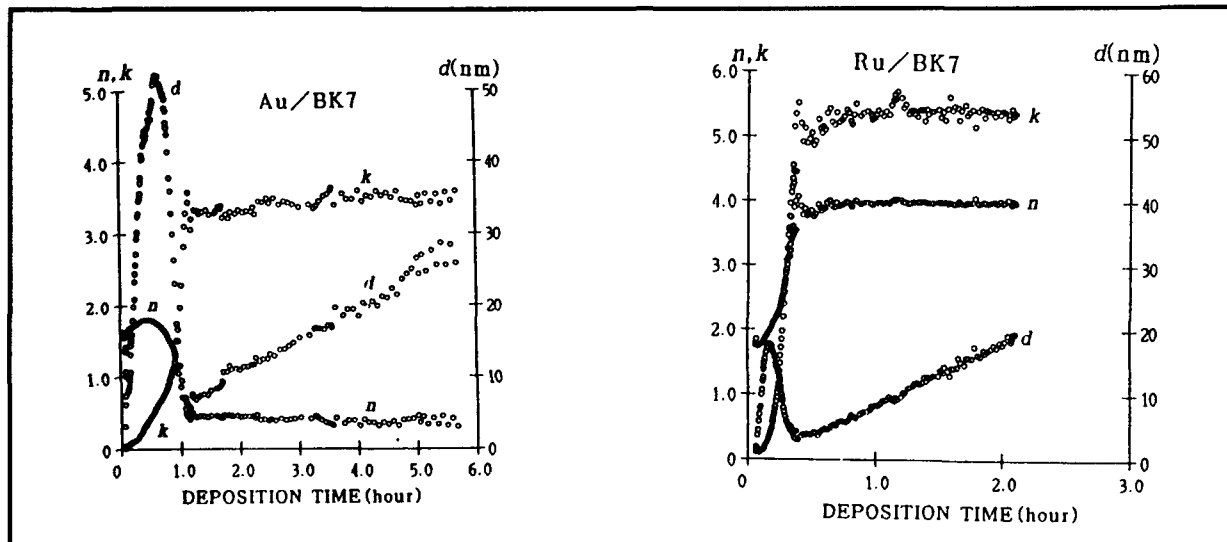
Figure 3 Refractive index *n*, extinction coefficient *k*, and thickness *d* analyzed with the relative amplitude attenuation ρ measured.

substrate, and change gradually towards the values for the bulk. With these changes, *d* goes through an anomalous peak. Then at around a certain deposition time t_c, the values of *n*, *k* and *d* behaves as an optically ideal layer. The layer thickness d_c at the deposition time t_c are the minimum critical thickness for optical isotropy. Above d_c, the optical constant is a good measure of crystallographical structure in the film such as impurity inclusion and crystallization.
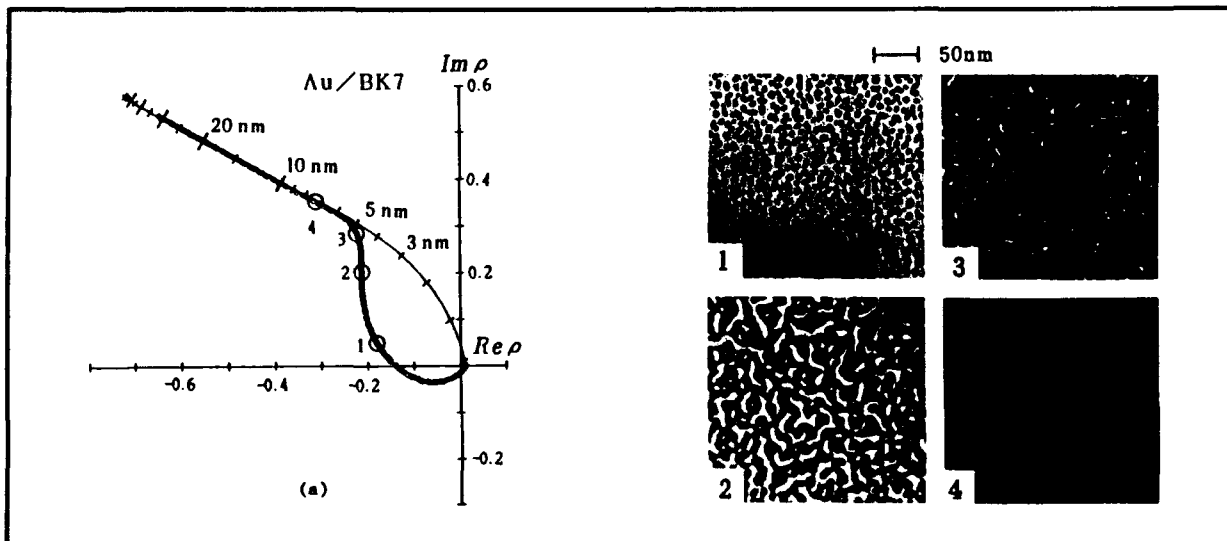
Figure 4 Au growth curve and four growth stages observed by electron micrographs. Layer reaches continuous stage between 3 and 4. The critical thickness d_c is 5.8-nm. The ideal growth curve is shown by the solid line.

The anomalous below d_c is very large for Au and Ag (not shown) layers as observed by others[5,6]. The plasma resonance absorption of Au layers has been intensively studied in respect to the island structure at a wavelength ~ 610nm, which is very near to our probe light of 633nm. We confirmed with electron

micrograph observation, that the critical thickness d_c is the thickness at which the layer reaches continuous stage as shown in Fig. 4. The ideal growth curve in the figure is calculated with $(n,k)=(0.44,3.50)[4]$. The anomalous behavior has close correlation to disappearance of pinholes or channels in the layer acting as scattering sources of the free electron. The critical thickness of Au thus tells minimum thickness of a continuous layer for the particular growth condition. We found the critical thickness of Au grown by ion beam sputtering was 5.8nm whereas by electron beam deposition, it was much thicker 12nm at room temperature. These are the good examples showing that the layer quality can be detected with a probe light near plasma resonance through the optical constant or the dielectric constant of the layer.

Multilayers
Figure 5 shows two examples of the growth curve of a Ru/C and an Ni/C multilayers.
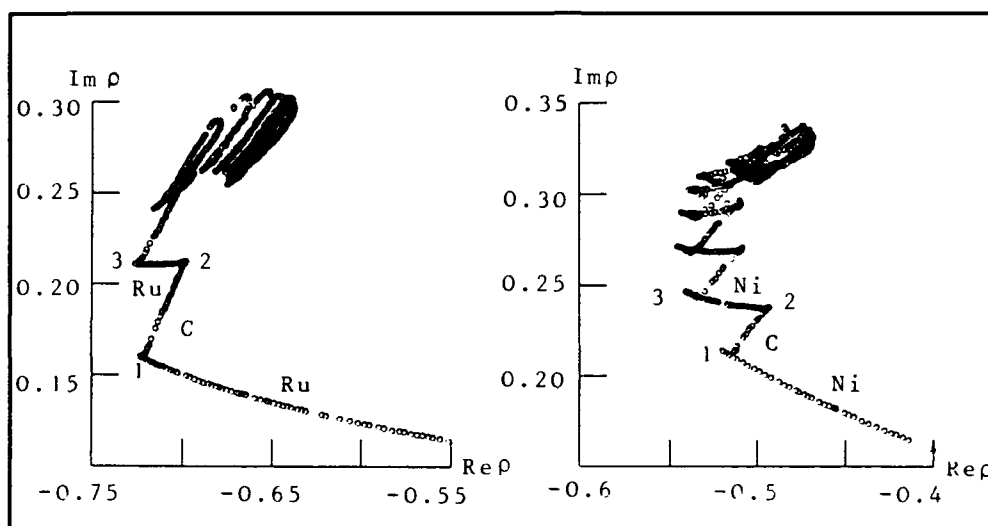
Figure 5 Ru/C (left) and Ni/C (right) growth curves.

In the Ni/C multilayer, C layer shows backward movement along the Ni growth curve at the initial growth stage till ~ 0.7nm, then makes near 90° left turn. This backward movement is very small in the Ru/C layer. These are the direct information on the behavior at the interfaces relating to carbide layer formation or mixed layer formation. These results indicate a sharper interface of Ru/C than the Ni/C.

Reference
[1] see for example, J. de Phy. Colloq. **C10**, suppl. No.12 (1983).
[2] M. Yamamoto, A. Arai, H. Shibata, and T. Namioka, Conf. Dig. 13th Cong. Intl. Comm. Opt. (Sapporo, 1984), pp. 626-627.
[3] P. Houdy, et al., Proc. SPIE, **688**, 122-125 (1986).
[4] M. Yamamoto and T. Namioka, Appl. Opt., in print.
[5] T. Yamaguchi, S. Yoshida, and A. Kinbara, Japan. J. Appl. Phys., **8**, 559-567 (1969).
[6] R. P. Netterfield and P. J. Martin, Appl. Surf. Sci., **25**, 265-278 (1986).

Optimization of Growth Conditions of Vapor Deposited Mo/Si Multilayers

M. B. Stearns, Department of Physics, Arizona State University, Tempe, AZ 85287

D.G. Stearns, University of California, Lawrence Livermore National Laboratory, Livermore, CA 94550

The dependence of the layer structure and interfaces of e-beam deposited Mo/Si multilayers (ML) on the growth conditions has been studied. The substrate temperature was varied over a range of 300-600°K at deposition rates of 1 and 3 Å/sec. The structure of the ML was determined using small-angle x-ray scattering, large-angle x-ray scattering, and cross-sectional high-resolution electron microscopy. The variation of the normal incidence reflectivity was measured as a function of soft x-ray wavelength using synchrotron radiation. We found that the ML structure has a strong dependence on the substrate temperature and a lesser dependence on the deposition rate. ML grown at a substrate temperature of 300°K have Mo layers composed of small crystallites and exhibit significant short wavelength roughness. The lateral extent of the Mo crystallites increases and the interfacial roughness decreases with increasing substrate temperature up to 525-550°K. We attribute the larger Mo crystallites, improved texture and suppression of columnar growth observed at higher substrate temperatures to the increased surface mobility of the adatoms. The optimum conditions to obtain smooth layers by e-beam deposition were found to be a substrate temperature of ~525°K and a deposition rate of ~1 Å/sec. Thus to a great extent the smaller adatom energies of e-beam deposition can be compensated for by increasing the substrate temperature. Above T_s~575°K interdiffusion is observed to significantly degrade the ML structure.

In a separate study Mo/Si ML were grown using dc magnetron sputtering in an Argon plasma. The layer roughness was found to decrease strongly at lower Argon pressure. This behavior can also be attributed to an increased surface mobility. A comparison of the e-beam and sputtered ML will be made and the important role of surface mobility in ML growth will be

discussed. The optimized e-beam ML have distinct differences in the interlayer thicknesses from those prepared by sputtering. The e-beam ML have interlayers which are ~5-6 Å thick for Si-on Mo while the Mo-on-Si interlayers are ~15Å for T_s = 300-400°K and increase to ~23 Å at T_s = 575°K. This behavior contrasts with that of optimized sputtered ML, deposited at pressure-distance products of ~15 mTorr cm, which have interlayer thicknesses of only 5 and 10 Å for Si-on-Mo and Mo-on-Si interlayers respectively.

From a comparison of the measured and calculated normal incident reflectivity for the optimal e-beam ML (T_s = 525°K) we estimate that a composition variation at the interfaces corresponding to the uniform thicknesses of the observed interlayers can account for only a ~5% reduction from the maximum ideal reflectivity. We conclude that the interface roughness, arising from the texture of the crystalline Mo layers and the variation in the thicknesses of the interlayers, is much more deleterious to the normal incidence reflectivity at soft x-ray wavelengths than the existence of the interlayers.

Pulse Laser Deposition of Layered Synthetic Microstructures

S. V. Gaponov, E. B. Kluenkov, Yu. Ya. Platonov, N. N. Salashchenko

Institute of Applied Physics, USSR Academy of Science,
46 Uljanov Street, 603600 Nizhny Novgorod, USSR

The deposition technique of LSM's efficiently reflecting in the soft x-ray region (SXR) should satisfy the following requirements: to be capable of depositing continuous superthin layers up to 5Å thick, to control thickness and crystal structure of superthin layers, to sustain the period thickness at the LSM depth with an accuracy to hundredth fractions of the period. Thus, the admissible rms height of interfacial LSM roughness should not exceed 2-5Å, while the accuracy of sustaining the period thickness in the shortwave part of the SXR region (where the structure period d=15-25Å and the number of efficiently reflecting periods 100) amounts to fractions of Ångstrom.

The are two methods for depositing superthin layers of definite thickness and multilayer structures synthesized from these layers, i.e. direct measurement of the layer thickness during the deposition procedure or stabilization of the target material sputtering and of the film deposition conditions. These two approaches are realized employing the electron-beam evaporation (EBE)[1,2] and magnetron sputtering (MS)[3]. We have mastered both the techniques and developed a new technological method of pulse laser deposition (PLD). PLD has three peculiar features determing its LSM deposition capability. The first peculiarity is associated with abnormally high rate of the condensate ingress on the substrate and affects the possibility of obtaining continuous superthin films. The condensate ingress rate is limited only by the substrate surface overheat and exceeds by far the escape rate of absorbed atoms from the interaction region, caused by surface diffusion, providing thereby the conditions of two-dimensional nuclei formation.

The second peculiarity is due to the energy spectrum of the laser plasma particles. According to their action on the surface and near-surface layers of the substrate, the particles can be

divided into two groups,i.e.the particles with the energy lower than 20-25 ev, which do not cause defects in the substrate and the particles with higher energy,which knock atoms out of the near-surface layer causing the "vacancy"-type defects in the substrate. The relation between the quantities of defect-producing particles and relatively slow ones governs the processes accompanying the irradiation of the surface by plasma. A typical energy spectrum of the laser plasma particles is shown in Fig.1.
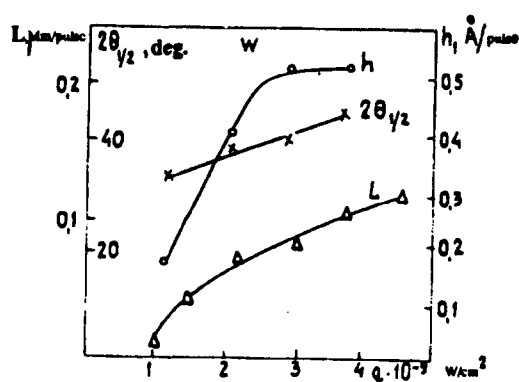
Fig.1. A typical energy spectrum of laser plasma particl__.Laser pulse duration $\tau=10ns, q=10^9 W/cm^2$.

In the case of monocrystal substrates the plasma irradiation produced a grid of additional cristalization centres. This ensures the epitaxial growth of films with limited mobility of adsorbed atoms, i.e. at lower temperatures than in other methods[4]. Bombardment of the substrate surface by high-energy plasma particles also stimulates the oriented growth of films on crystal surfaces covered with superthin nonoriented layers,permitting to obtain superstructures synthesized from monocrystal and nonoriented layers[5].

The third peculiarity of PLD concerns the layer thickness deposited per a laser pulse. Even the first experiments on the deposition of dimensional-quantized films of semiconductors, quantum superlatties and multilayer x-ray mirrors[6] have shown that the film thickness can be calculated rather accurately as the product of the pulse number and the layer thickness deposited per a pulse. The relation between the film thickness and the laser radiation density on the target surface (q) is mainly determined by the erosion product escape and their scattering in vacuum.The target surface screening by plasma provides some sta-

bilization of the mass escape. The layer thickness evaporated per a pulse is yielded by $H=(q-q_{th})^{1/2}$, where q_{th} is the intense evaporation threshold. The scattering diagram width depends on the residual thermal energy at the beginning of nondimensional scattering of plasma. The energy increases with q,which leads to strong acceleration of particles moving in the lateral directions and, thus, enhancement of the mass escape with q is compensated by the scattering diagram broadening. Figure 2 displays the typical relations of maximum metal film thickness h, the crater depth H on the target surface per a laser pulse and the half-height width of the erosion product scattering diagram to the radiation density q.It is readily seen from the figure that there is an intensity domain where the film thickness deposited per a laser pulse is stabilized.
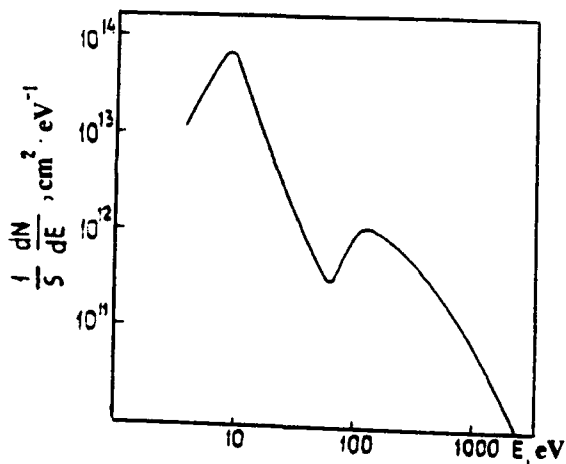
Fig.2. Dependence on the flux density q of the maximum thickness h of a tungsten film and the crater depth H on the target surface (both for a single pulse) and the width $\Delta\alpha$ (at half maximum) of the expansion cone of the erosion products.

Therefore, the stability of the layers deposited per a pulse enables one to use programmed pulse-number deposition of films of rigorously controlled thickness. High growth rate provides the continuity of the layers whose thickness is close to the monomolecular one. The joint action of these factors permits to synthesize multilayer periodic structures from superthin films, i.e. x-ray and neotron optics elements, semiconductor magnetic superlattices.

The PLD method is now employed mainly for depositing LSM made of metal-carbon LSM with minimum period up to 15Å and for rapid investigation of LSM made of new unstudied pairs of materials. The use of all the technologies (PLD,EBE,MS) has provided the

opportunity of free selection of materials and LSM period. The basic results obtained are presented in the Table 1.

TABLE 1.

EXPERIMENTAL CHARACTERISTICS

Radiation energy, eV	Wave-lengths Å	LSM	Period, Å	Angle of incidence, deg.	Reflectivity, %	Spectral resolution λ/Δλ
41[1),2)]	300	Mo-Si	176	4	22	10
70[1),2)]	175	Mo-Si	97	5	30	14
80[1),2)]	150	Mo-Si	80	5	50	17
95[1),2),3)]	130	Mo-Si[1),2)]				
		Rh-C[3)]			30	30
108[3)]	105	Rh-C	57	5	16	42
		Rh-C			10	50
132[3)]	93	Rh-Y	50	2,5	10	40
188[3)]	66	W-C	34	2,5	7	48
206[3)]	60	Fe-C	31	2,5	8	45
255[3)]	48,8	Fe-C	24,5	2,5	8	60
		Cr-C				
277[3)]	44,7	Ni-C	50	63,4	35	25
392[1),3)]	31,6	Cr-Sc[1)]	68	77	35	15
		W-Si[1)]	35	63	5	20
		Cr-Sc	18	30	0,8	55
452[3)]	27,3	Ni-Ti	58	77	22	15
525[1)]	23,6	W-Si	30	68	8	26
		W-Sb	30(12)		11,4(0,84)	(45)
572[3)]	21,6	Cr-C	23	63	20	40
677[1)]	18,3	W-Si	30	72	14	30
705[3)]	17,6	Fe-C	25	70	18	35
776[3)]	16,0	Co-C	22	69	9	55
1040[1)]	11,9	W-Si	30	79	22	30
1255[1)]	9,9	W-Si	30	81	25	30
1480[1),3)]	8,3	W-Si	30	83	28	30

1)Magnetron sputtering,2)E-beam evaporation,3)Pulse laser deposition

REFERENCES

1. E.Spiller, Eveporated multilayer dispersion elements for soft x-rays ,AIP Proc.,1981,v.75,p.124.
2. M.P.Bruijn,J.Verhoeven,M.I.van der Wiel,Optimization of multilayer soft x-ray mirrors,NIM,1984,v.219,p.603.
3. T.W.Barbee Jr.,Sputtered layered synthetic microstructure (LSM) dispersion elements,AIP Proc.,1981,v.75,p.131.
4. S.V.Gaponov,B.M.Luskin,B.A.Nesterov,N.N.Salashchenko,Low-tempera-ture film epitaxy condensed from laser-produced plasma,Pis'ma Zh. Tekh.Fiz.,1977,v.12,p.573.
5. S.V.Gaponov,B.M.Luskin,N.N.Salashchenko,Homoepitaxial superlat-tices with nonorier. ed barrier layers,Solid State Comm.,1981,v.39 p.301.
6. A.D.Akhsakhalyan,S.V.Gaponov,S.A.Gusev,et.al.,Synthetic multi-laer reflecting and selective elements for soft x-ray radiation. II.Fabrication of multilayer soft x-ray mirrors by laser pulse deposition,Sov.Phys.Tech.Phys.,1984,v.29(4),p.446.

Ion-Assisted Sputter Deposition of Mo-Si Multilayers

S.P. Vernon *Vernon Applied Physics, Torrance, CA 90505*

D.G. Stearns and R.S. Rosen
Lawrence Livermore National Laboratory, Livermore, CA 94550

Mo-Si multilayer (ML) structures fabricated using DC magnetron sputtering in an

Ar plasma show a transition from layer to columnar growth as the deposition pressure is

increased above ~1 mTorr. The dominant effect of the increased deposition pressure is the

increased thermalization of Ar neutrals, reflected in charge exhange collisions with the

sputtering target, striking the substrate surface. At high deposition pressure there is less

energy deposited at the substrate surface which, in turn, modifies the adatom mobility.

These effects markedly impact the layer morphology. The layers are observed to have

significantly increased roughness at higher deposition pressures. Consequently, the x-ray

optical properties of the ML coatings are strongly effected. The measured normal incidence

reflectivity at 130 Å decreases from ~60% to 14% as the deposition pressure is raised from

2.5 to 10 mTorr [1].

The application of a substrate bias during the deposition process, in principle,

allows direct modification of energy deposited onto the substrate surface by the extraction

and bombardment of accelerated Ar ions. Preliminary measurements of Mo-Si ML

fabricated at deposition pressures of 1.75 mTorr and Si and Mo powers of 280 and 110

Watts respectively, with substrate bias voltages between 0 and -500 VDC exhibit a

systematic contraction of the ML period with increased bias voltage. At bias voltages at or

above -400VDC there is a degradation in the ML structure inferred from decreased intensity

of all reflected orders in small angle x-ray diffraction measurments (at Cu Kα). The origin

of the observed contraction could be explained by a variety of effects ir cluding film

densification, enhanced compound formation at the interfaces or resputtering of the

deposited film due to ion bombardment. These effects will be further investigated using high-resolution electron microscopy and the studies will be extended to higher deposition pressures. The results will be correlated with measurements of normal incidence reflectivity.

References

1. D.G. Stearns, R.S. Rosen and S.P. Vernon, J.Vac.Sci. Technol. **A9**, 2662 (1991).

Simulation of Mixing at Mo/Si Interfaces

D. B. Boercker

Lawrence Livermore National Laboratory, Livermore, CA 94550

W. L. Morgan

Kinema Research, 18720 Autumn Way, Monument, CO 80132

Soft x-ray projection lithography is a rapidly emerging technology which will have enormous impact on the microelectronics industry, by providing faithful image reduction to a minimum feature size below 1000Å.[1] X-ray reduction cameras have already been designed and tested,[2,3] but the successful development of this new technology will depend heavily upon the production of efficient, durable x-ray optics[1].

A leading candidate for x-ray mirrors near 130Å is multilayer structures made of alternating thin layers of Mo and Si. The microstructure of these multilayers has been thoroughly studied,[4,5] and one of their most important features is an asymmetry in the thicknesses of the interfaces between layers. The interlayers produced by depositing Mo on Si are thicker than those produced by depositing Si on Mo. The ratio of the two interlayer thicknesses can vary from about 1.5 to 4, depending upon the details of the deposition process.[6] As currently envisioned, [1,2,3] x-ray lithography will require as many as seven reflections from multilayer mirrors. Therefore, even small improvements in the performance of the mirrors can lead to substantial increases in overall efficiency. Since the sharpness of the interlayers can significantly affect the performance of the multilayer mirror, the mechanisms which determine interlayer thickness are an important area of research.

We have performed molecular dynamics (MD) simulations of the deposition of Mo-on-Si and Si-on-Mo,[7] using interatomic potentials containing three-body terms.[11] These simulations reproduce the experimental asymmetry in the interlayer thickness. When Mo atoms are incident upon an Si substrate they penetrate several layers deep. In contrast, incident Si atoms make virtually no penetration into the Mo substrates. Figure 1 shows a side view of an α-Si slab upon which 192 Mo atoms have been deposited. Most of the Mo atoms initially deposited have mixed into the Si and those arriving later have begun to form a purely Mo layer. Figure 2 shows a crystalline Mo slab after the deposition of Si atoms. There is a very sharp transition from the crystalline Mo to the Si overlayer. Consistent with both experiment and previous calculations, the Si overlayer is amorphous. Experimentally, some

mixing at this interface is observed, but it is not reproduced in these simulations.

FIG. 1. 192 Mo atoms (dark circles) deposited on amorphous Si (gray circles).
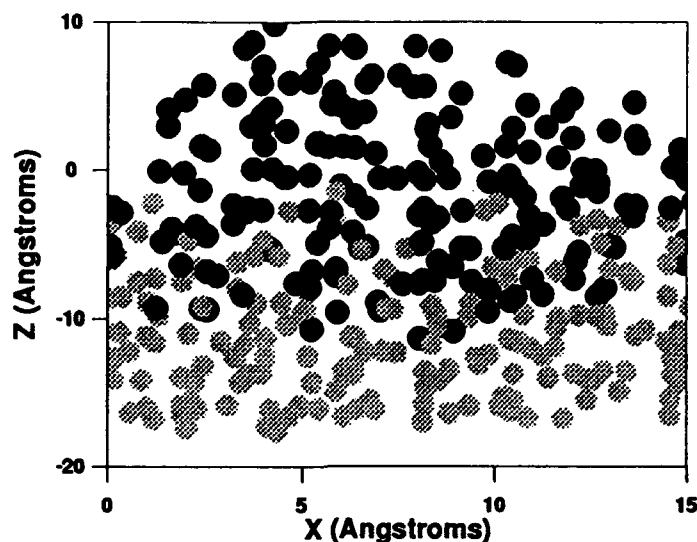
FIG. 2. Si atoms (gray cirles) deposited on the (110) face of bcc Mo (dark circles).
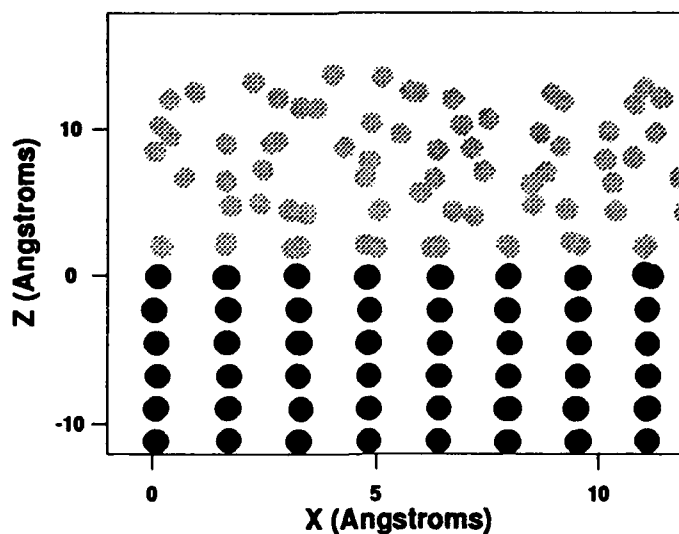
In order to investigate the mixing mechanism in more detail, we have also performed simulations in which five Mo atoms were placed on the (001) face of a Si crystal. The resulting penetration is shown in figure 3. A preliminary interpretation of our results is that the mixing is driven by the desire of the Mo atoms to be highly coordinated. When placed on the Si surface a Mo atom has few near neighbors, so it buries itself to increase its

coordination. In contrast Si likes to have only four near neighbors, so a Si atom is content to remain on a Mo surface. This hypothesis will be tested further by examining the mixing of Mo clusters into Si substrates. Presumably clusters in which the Mo atoms have a high initial coordination will mix less readily than the isolated atoms.

FIG. 3.   Penetration of Si (001) surface by Mo atoms.
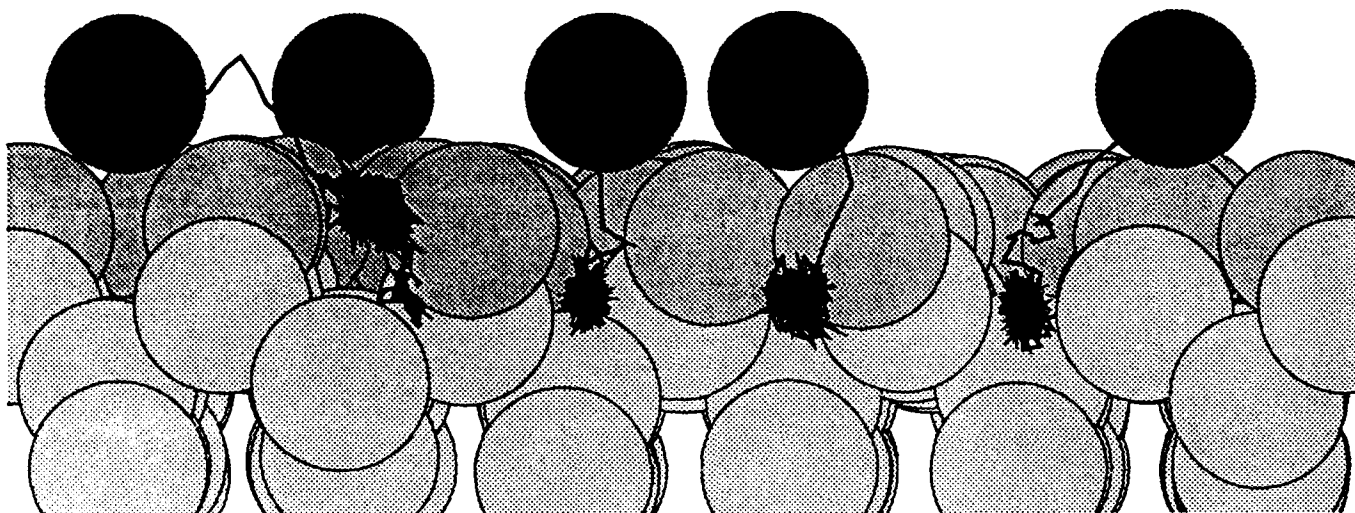
[1] D. G. Stearns, N. M. Ceglio, A. M. Hawryluk, R. S. Rosen, and S. P. Vernon, *Multilayer Optics for Soft X-ray Projection Lithography: Problems and Prospects*, preprint, 1991.

[2] A. M. Hawryluk and L. G. Sappala, J. Vac. Sci. Technol. B 6, 2162 (1988).

[3] H. Kinoshita, K. Kurihara, Y. Ishii, and Y. Torii, J. Vac. Sci. Technol. B 7, 1648 (1989).

[4] A. K. Petford-Long, M. B. Stearns, C.-H. Chang, S. R. Nutt, D. G. Stearns, N. M. Ceglio, and A. M. Hawryluk, J. Appl. Phys. 61, 1422 (1987).

[5] D. G. Stearns, M. B. Stearns, Y. Cheng, J. H. Stith, and N. M. Ceglio, J. Appl. Phys. 67, 2415 (1990).

[6] M. B. Stearns and C.-H. Chang, and D. G. Stearns, J. Appl. Phys. (to be published).

[7] W. L. Morgan and D. B. Boercker, Appl. Phys. Letts. 59, 1176 (1991).

[8]F. H. Stillinger and T. A. Weber, Phys. Rev. B **31**, 5262 (1985).

[9]K. M. Miller, J. Phys. F: Metal Phys. **11**, 1175 (1981).

[10]K. Ding and H. C. Andersen, Phys. Rev. B **36**, 2675 (1987).

·Roughness and Nonspecular Scattering 1

TuA   8:00am–9:45am
Grand Room

Jon M. Slaughter, *Presider*
University of Arizona

Roughness Evolution in Films and Multilayer Structures

M. G. Lagally

University of Wisconsin-Madison

Madison, WI 53706

(608) 263-2078 FAX: (608) 262-8353

Structures fabricated from multiple layers of very thin films make up an increasing component of our high-technology base in electronics, photonics, and x-ray optics. In particular, in x-ray optics, quite dissimilar materials are combined to create what are effectively one-dimensional diffraction gratings, in which the layers must have indices of refraction that are as different as possible. But that feature alone is not enough. The interfaces between the different layers affect the quality of the structure as an x-ray reflector, bringing into consideration questions of crystal growth and the kinetic and thermodynamic mechanisms of growth. This paper provides an overview of the most important kinetic mechanisms that control growth and illustrates then with scanning tunneling microscopy (STM) and diffraction measurements.

The limiting-case, equilibrium growth models that are usually invoked (1) to describe thin-film growth are 1) Frank-van der Merwe (FM), 2) Volmer-Weber (VW), and 3) Stranski-Krastanov (SK). X-ray optical multilayer structures fall, with few exceptions, into the category of VW growth. In this growth mode, the materials making up the layers are dissimilar either in size or in cohesive energy, causing a desire for each film to grow on the other as 3-D clusters rather than as a flat film. Quite the opposite is true for FM growth: here the materials are similar in lattice constant, size, and cohesive energy, so that the growth occurs epitaxially, layer-by-layer. Of course, these are ideal-case, equilibrium situations, in which kinetic mechanisms that limit transport, nucleus formation, or ordering are assumed not important. In fact, that assumption can never be completely true. At finite growth rates and finite temperatures, there is always a competition between arrival rate of atoms and the

attempt of the structure to reach equilibrium. Epitaxial (FM) films are grown near equilibrium; if they are not, they will develop a significant growth front roughness and internal disorder. Volmer-Weber films are grown far from equilibrium; if they are not, clusters or grains will form, causing a very rough morphology. However, growth far from equilibrium implies kinetic mechanisms are slow; hence atoms arriving from the gas phase do not move far before they are buried by more atoms. The implication is that such films will replicate roughness that exists on the substrate or in underlying films.

The most important kinetic mechanisms (2) affecting the morphological evolution of films are 1) in-plane transport, 2) level-crossing transport, implying interactions with steps and diffusional barriers at steps, 3) sticking to steps, islands, and clusters, and 4) desorption from steps, islands, clusters, or surfaces. The competition of these rates, combined with the desire of the film to seek its equilibrium structure, determines the morphology. Although these ideas have been known for many years, it has only recently been possible, with the advent of scanning tunneling microscopy, to observe these processes and their impact on film morphology at the atomic level. As yet, only few studies exist; these are chiefly on epitaxial films; in particular for Si growth on Si(001) (3) and more recently for GaAs(001) (4). The former system has been used to investigate in-plane diffusion and its anisotropy, level-crossing, and accommodation and desorption from steps, by investigating morphological features, such as the number density of islands and their distribution, during the very initial stages of growth (5). Both the activation energy for the diffusion of a single Si (or Ge) atom on Si(001) and the diffusional anisotropy have been measured. Barriers for crossing steps have been analyzed; they differ for the two different types of steps found on Si(001). The relative probabilities of sticking on different types of edges have been determined from growth shapes of islands. Films

of both GaAs(001) and Si(001) grown epitaxially show kinetic roughness of several monolayers over size scales of the order of 1000Å.

Multilayer films for x-ray optics do not grow in the same manner. Generally, transport properties are kept deliberately slow so that cluster formation does not occur. The implication is that atoms more or less "stick where they hit". In the limit, this would imply that growth front roughness grows Poisson-like. It also implies that roughness existing in the substrate will be replicated. For deposition at finite temperatures, additionally fluctuations can cause growth front morphology, which may also be replicated or partly replicated layer to layer and interface to interface. Although total interfacial roughness in x-ray optical multilayer films has been extensively investigated (6) attempts to determine the degree of correlation in the roughness and the correlation length, as well as the influence of growth conditions on these factors have only recently been made (7,8). These methods depend on a novel application of x-ray diffraction, namely the measurement of the reciprocal-space distribution of intensity through the use of transverse (rocking) scans with a narrow detector. These measurements show that a significant fraction of the roughness is correlated from layer to layer. It is also evident that growth parameters, such as the thickness of the individual layers, the number of layers, and the nature of the buffer layer grown on the substrate affect the degree of correlated roughness, so that it is not only the substrate roughness that one observes.

To make the connection with what is known from epitaxial growth about kinetic mechanisms of transport and growth front roughening, one must, in principle, perform depositions of multilayers at a variety of temperatures and deposition rates. An evaluation of changes in correlation with changing conditions can then be interpreted in terms of kinetic mechanisms. Only very preliminary work of this nature has been done. A direct measure of such roughness buildup can be obtained using the STM to determine directly the height-height correlation function of

the growth front. Such measurements are relatively straightforward in ultra-high vacuum molecular-beam epitaxy chambers if these are outfitted with STM, although even for such systems, little work has been done. For x-ray optical multilayer films grown by sputter deposition, in-air STM scans have been made of the final surface. These show a greater roughness than is determined from x-ray diffraction of the interfacial roughness. It is believed that this extra roughness is due to oxidation or other atmospheric contamination of the outer surface. More specific conclusions must await a detailed STM analysis of the evolution of roughness during growth.

References

1. E. Bauer, Z.f. Kristall. 110, 372 (1958).

2. W. K. Burton, N. Cabrera, and F. C. Frank, Phil. Trans. Roy. Soc. (London) A243, 299 (1951).

3. See, for example, papers in Kinetics of Ordering and Growth at Surfaces, ed. M. G. Lagally, Plenum, New York (1990).

4. E. J. Heller and M. G. Lagally, MRS Proceedings, 1991, submitted.

5. Y.-W. Mo and M. G. Lagally, Surface Sci. 248, 313 (1991); J. Cryst. Growth 111, 876 (1991); Y.-W. Mo, J. Kleiner, M. B. Webb, and M. G. Lagally, Phys. Rev. Letters 66, 1998 (1991).

6. See, for example, T. W. Barbee, Jr., SPIE 563, 2 (1985).

7. D. E. Savage, J. Kleiner, N. Schimke, Y.-H. Phang, T. Jankowski, J. Jacobs, R. Kariotis, and M. G. Lagally, J. Appl. Phys. 69, 1411 (1991).

8. D. E. Savage, N. Schimke, Y.-H. Phang, and M. G. Lagally, J. Appl. Phys., submitted.

X-ray Scattering Studies of Correlated Interface Roughness in Multilayers

S. K. Sinha
Corporate Research, Exxon Research & Engineering Company
Annandale, New Jersey 08801

M. K. Sanyal
Physics Department, Brookhaven National Laboratory
Upton, New York 11973

S. K. Satija and C. F. Majkrzak
National Institute for Standards and Technology
Gaithersburg, Maryland 20899

I. K. Schuller
Physics Department, University of California, San Diego
La Jolla, California 92093

H. Homma
Physics Department, Brooklyn College
Brooklyn, New York 11210

C. M. Falco and B. N. Engel
Physics Department, Optical Sciences Center
University of Arizona
Tucson, Arizona 85721

The specular and off-specular reflectivity of radiation from single surfaces possessing roughness has been extensively discussed both within the framework of the Born Approximation and the Distorted Wave Born Approximation (DWBA). The same ideas can be generalized to reflectivities from multilayer structures. An interesting effect arises due to the fact that the interface fluctuations between layers are usually highly correlated. This is shown to lead to structure in the off-specular reflectivity which mimics the structure found in the true specular reflectivity (e.g., Bragg peaks, etc.). In fact, such structure can persist due to interlayer height correlations for q_z values where the true specular Bragg peaks have vanished due to large global roughness.

The expressions we have derived for the specular and diffuse scattering at small angles from a multilayer in the Born Approximation are:-

$$R_{spec} = \frac{16\pi^2}{q_z^2} \sum_{ij} \Delta\rho_i \, \Delta\rho_j \, F_{ij} (q_z) \tag{1}$$

$$\left(\frac{d\sigma}{d\Omega}\right)_{diff} = \frac{A}{q_z^2} \sum_{ij} \Delta\rho_i \, \Delta\rho_j \, F_{ij} (q_z) \, S_{ij} (q) \tag{2}$$

where i,j refer to all the interfaces, $\Delta\rho_i$ is the electron density contrast across the interface i, q is the scattering (wavevector transfer) vector, z is the direction normal to the average surfaces, A is the illuminated surface area of the multilayer;

$$F_{ij}(q_z) = \exp(-iq_z [z_j - z_i]) \exp(-\tfrac{1}{4} q_z^2 [\sigma_i^2 + \sigma_j^2 + \delta^2 N_{ij}]) \qquad (3)$$

where z_j is the mean height of interface i, σ_i is its root-mean-square roughness amplitude, δ is the cumulative (layer thickness) error, and N_{ij} is the number of interfaces between i and j; and

$$S_{ij}(q) = \iint dxdy [\exp(q_z^2 P_{ij}(R)) - 1] \exp(-iq_x X - iq_y Y) \qquad (4)$$

$P_{ij}(R)$ is the correlation function between height fluctuations at lateral separation R,

$$P_{ij}(R) = < \delta z_i(o) \, \delta z_j (R) > \qquad (5)$$

Such correlation functions for self-affine rough surfaces may be characterized in terms of stretched exponentials involving a roughness exponent h, and a lateral correlation length ξ. To a good approximation, S_{ij} can be regarded as decaying with an interlayer correlation length ξ'.

We have carried out specular and off-specular reflectivity experiments on a variety of multilayers (Pb/Ge, GaAs/AlAs, Fe/Ti, and Mo/C) to study the validity of such a description. Figure 1 shows the measured specular reflectivity for a GaAs/AlAs multilayer together with the diffuse background. Figure 2 shows the true specular along with the fitted curve, as described in the text. Finally, Figure 3 shows a fit to a transverse diffuse scan for the same multilayer.
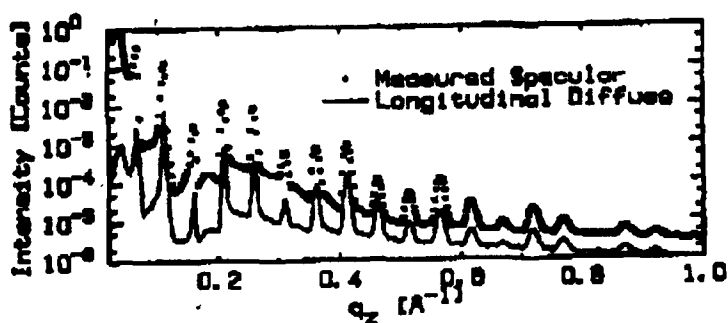
Fig. 1. As measured specular reflectivity and longitudinal diffuse scattering data for GaAs/AlAs multilayer.
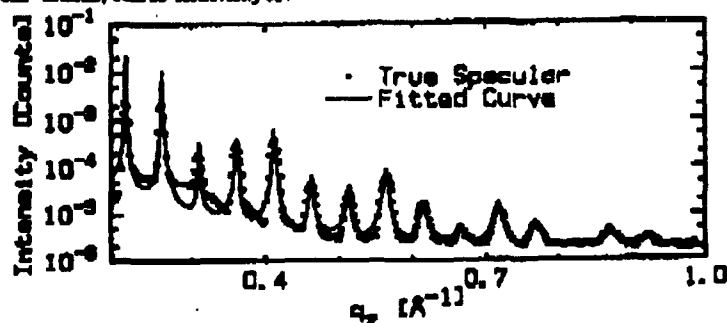
Fig. 2. Corrected true specular reflectivity data and the fitted curve as described in the text.
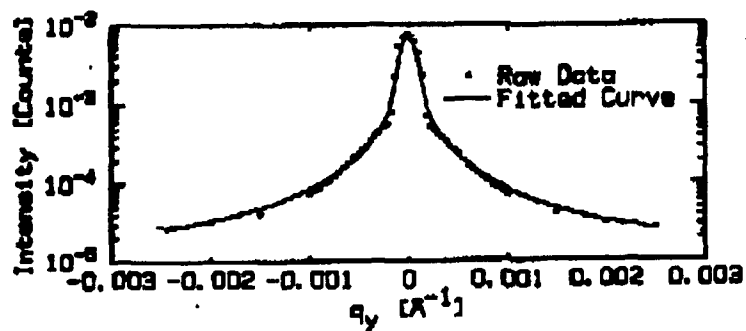
Fig. 3. Transverse diffuse scattering data across the fifth Bragg peak. The solid curve represents the calculated scattering.

Theory of Nonspecular X-ray Scattering from Multilayer Structures

D. G. Stearns
University of California, Lawrence Livermore National Laboratory
Livermore CA 94550
(510) 423-4938

One important type of structural imperfection that can affect the properties of multilayer (ML) structures is interfacial roughness. In x-ray optical ML, roughness both decreases the reflectivity and introduces a background halo that can degrade the resolution of imaging optics. A promising technique for characterizing the roughness of surfaces and interfaces in ML structures is x-ray scattering. The use of x-ray scattering as a structural probe has several important advantages. It is inherently a non-invasive technique, well-suited for dynamic measurements including *in situ* growth studies. The penetration of x-rays allows both surfaces and buried interfaces to be directly probed. Furthermore, due to the short wavelength of x-rays, x-ray scattering can provide structural information on spatial scales ranging down to atomic dimensions. There is increasing interest to use nonspecular x-ray scattering to study the roughness of interfaces in x-ray ML structures. The first experimental results indicate that the x-ray scattering can exhibit a rich variety of behavior associated with the structural correlations between interfaces[1-4]. We present a simple theory that, within the limitations imposed by certain simplifying approximations, can provide a straightforward means of relating realistic interface structures to measurements of nonspecular scattering.

The present theory is developed from previous work describing the scattering of x-rays from a non-ideal interface of arbitrary structure[5]. The treatment utilizes the first Born approximation and hence is only valid when the scattering is weak and refraction can be neglected, conditions generally satisfied for x-ray scattering provided that the incident and scattering angles (measured from the normal) are less than the critical angle for total external reflection. To treat the case of ML structures, a general model for interfacial

roughness is introduced that can account for an arbitrary amount of correlation between interfaces. The frequency spectrum of the ith interface, $\tilde{f}_i(s)$, is given by,

$$\tilde{f}_i(s) = \tilde{h}_i(s) + \tilde{a}_i(s) \tilde{f}_{i-1}(s) \qquad (1)$$

where $\tilde{h}_i(s)$ is the random roughness introduced at the ith interface. The correlation of the roughness between layers is described by a frequency-dependent replication factor,

$$\tilde{a}_i(s) = \frac{1}{1 + 4\pi^2 t_i v_i s^2} \qquad (2)$$

where t_i is the thickness of the ith layer and v_i is a diffusion-like parameter. Frequency components of the roughness that are greater than $1/\sqrt{v_i t_i}$ are damped, while lower frequency components propagate through the ML stack. The model imposes no constraints on the power spectrum of the roughness, and thus is compatible with both conventional correlation-length-type and fractal-type descriptions of surface roughness.

We present calculations of nonspecular x-ray scattering from ML structures for different hypothetical roughness configurations. In particular, it is shown that correlated roughness produces characteristic resonance behavior in the nonspecular scattering which occurs in reciprocal space in the vicinity of the set of planes defined by $|q_z|=2\pi m/\Lambda$. This "quasi-Bragg" scattering has already been experimentally observed[1-4], indicating that the interfacial roughness in some x-ray ML structures is at least partially correlated. We show that quantitative modeling of the resonance scattering can provide a sensitive measure of the existence and degree of correlation in the ML interfacial roughness.

Acknowledgement

References
1) A. Bruson, C. Dufour, B. George, M. Vergnalt, G. Marchal, Ph. Mangin, Solid St. Comm., 71, 1045 (1989).
2) D. E. Savage, J. Kleiner, N. Schimke, Y.-H. Phang, T. Jankowski, J. Jacobs, R. Kariotis and M. G. Lagally, J. Appl. Phys. 69, 1411 (1991).
3) J. B. Kortright, J. Appl. Phys 70, 3620 (1991).
4) O. Renner, M. Kopechy, E. Krousky, F. Shcafers, B. R. Muller and N. I. Chkhalo, Proc. 4th Inter. Conf on Synch. Rad. Instrum. (Chester, July, 1991) in press.
5) D. G. Stearns, J. Appl. Phys. 65, 491 (1989).

TEM Characterization

TuB 10:15am–11:30am
Grand Room

D. J. Eaglesham, *Presider*
AT&T Bell Laboratories

HIGH RESOLUTION ELECTRON MICROSCOPE IMAGING

AND QUANTIFICATION OF INTERFACE

STRUCTURE IN X-RAY MULTILAYERS

R. Hull, D.L. Windt, R. Kola and W.K. Waskiewicz

AT&T Bell Laboratories
600 Mountain Avenue
Murray Hill, NJ 07974

We discuss the applications and limits of high resolution electron microscopy (HREM) to quantifying atomic-scale structure in X-Ray mirror multilayer (XMM) structures. It is shown how detailed processing of HREM images can yield quantitative measurements of interface planarity and diffuseness, which are critical parameters in determining the reflectivity of XMM structures.

Application of HREM to the study of atomic-scale interface structure is established in a wide range of materials systems, see for example (1). For many classes of structures, including XMMs, absolutely abrupt, planar interfaces are desired. Deviations from ideality of such interfaces may be defined in terms of the interface roughness, σ_R and interface diffuseness, σ_D. In Figure 1 we illustrate a simple model which defines interface structure in terms of these concepts, and which is amenable to measurement by HREM (2). The interface normal is along the z direction and lies between two materials A and B. The reference position of the interface is arbitrarily defined as the limit of pure material A. The interface roughness, $f(x,y)$ is defined as the deviation of this reference position from a fixed (x,y) plane (e.g. at z=0). The interface diffuseness describes the compositional variation in the z direction such that the composition at a point (x_i,y_i,z_i) is given by the function $g(z') = g[x_i,y_i,(z_i - f(x_i,y_i))]$.

The apparent interface "width", $w(z)$, sampled over an area $A_{x,y}$ in the (x,y) plane, will arise from the sum of the diffuseness function, $g(z')$ and those components of the Fourier spectrum of $f(x,y)$ which are sampled within $A_{x,y}$. In the limit that $A_{x,y}$ tends to infinity, the interface width arises from the sum of the interface diffuseness, σ_D, and all components of the interface roughness, σ_R. In the limit $A_{x,y} \to 0$, $w \to g(z')$, i.e. only interface diffuseness σ_D, is sampled.

In conventional phase contrast HREM (PCHREM) imaging, the intent is to produce an interpretable two-dimensional image of the projected crystal structure via its projected potential. This is in general a complex process requiring extensive numerical simulations (1). With contemporary instruments a point resolution, r_p, < 2Å is routinely available. However, a more significant lower limit in sampling $A_{x,y}$ arises

from the minimum attainable and useable specimen thickness, t_{min}, which due to specimen preparation artifacts is typically of the order 50 Å. The minimum interface area which may be sampled is then $A_{min} \sim t_{min} r_p$. If we assume isotropicity of the interface roughness in the (x,y) plane, the largest spatial frequency of the roughness spectrum sampled within A_{min} is defined not by $\sqrt{A_{min}}$, but by the largest linear dimension sampled, which is in general the sample thickness. The magnitude of of the largest practical interface sampling area, A_{max}, will depend upon the resolution required in w(z). To attain information at the instrumental resolution, r_p, the constraints on specimen geometry and image interpretation are severe: the sample thickness must be typically no more than a few hundred Å (this quantity is very dependent upon the atomic numbers of the XMM constituents), and the lateral sampling length in the image plane must be no greater than the lateral spatial coherence length of the imaging electrons, typically again a few hundred Å. If the resolution in w(z) can be relaxed to say of the order of one nm these constraints may be relaxed and greater sample thicknesses of the order of thousands of Å may be accessed, and lateral sampling lengths as high as microns may be considered. Thus at ~ 2 Å resolution we may sample $A_{x,y}$ over the range $\sim 10^2 - 10^5$ Å^2 and at ~ 10 Å resolution in the range $10^2 - 10^8$ Å^2. For isotropic in-plane roughness, the range of roughness wavelengths which may be accessed are of the order $50 - 500$ Å at 2 Å resolution and $50 - 50000$ Å at 1 nm resolution.

We have applied the above technique to a wide range of Mo/Si, Ru/Si and Ru/C XMM structures (3,4). In Figure 2, we show measured values of w for magnetron-sputtered Ru-C structures in the limit of minimum interface sampling areas, corresponding to an upper bound to σ_D. For these particular samples, the magnitudes of interfacial roughness and diffuseness were found to be comparable (3). For Mo/Si and Ru/Si XMM structures we have studied, we observe $\sigma_D > \sigma_R$ at low Ar (~ 2 mT) pressure in the sputtering system, but $\sigma_R > \sigma_D$ at higher (~ 8 mT) sputtering pressures (4). The total interface widths, $w \sim \sigma_D + \sigma_R$, measured from PCHREM are consistent with interpretation of Cu-K_α and XUV reflectivities based upon non-specular scattering theory derived from a first-order Born approximation (5).

We shall address in some detail the possibilities and limitations of the HREM technique discussed above in assessing XMM interfacial structure. The primary experimental complications which need to be addressed are: interpretation of PCHREM image intensities in terms of projected crystal potential; accuracy of alignment of the electron beam to the interface orientation; effects of projector lens distortions (either in the electron microscope itself, or in post-microscope optical systems); effects of thin sample specimen preparation; and effects of intensity non-linearities. We shall also discuss other high resolution electron imaging techniques such as Fresnel contrast imaging (6) and correlation of the PCHREM technique with other experimental techniques which

can measure other regimes of the $f(x,y)$ functions, as illustrated by comparison of PCHREM and surface profilometer measurements in Figure 3.

REFERENCES

(1) See, for example, J.C.H. Spence, Experimental High Resolution Electron Microscopy (Clarendon Press, Oxford, England, 1981)

(2) R. Hull, K.W. Carey and G.A. Reid, Mat. Res. Soc. Proc. 77, 455 (1987)

(3) D.L. Windt, R. Hull and W.K. Waskiewicz, SPIE Vol. 1343, X-Ray/EUV Optics for Astronomy, Microscopy, Polarimetry and Projection Lithography (1990)

(4) D.L. Windt, R. Hull and W.K. Waskiewicz, submitted to Journal of Applied Physics

(5) D.G. Stearns, J. Appl. Phys. 65, 491 (1988)

(6) W. C. Shih and W. M. Stobbs, Ultramicroscopy, 32, 219 (1990)
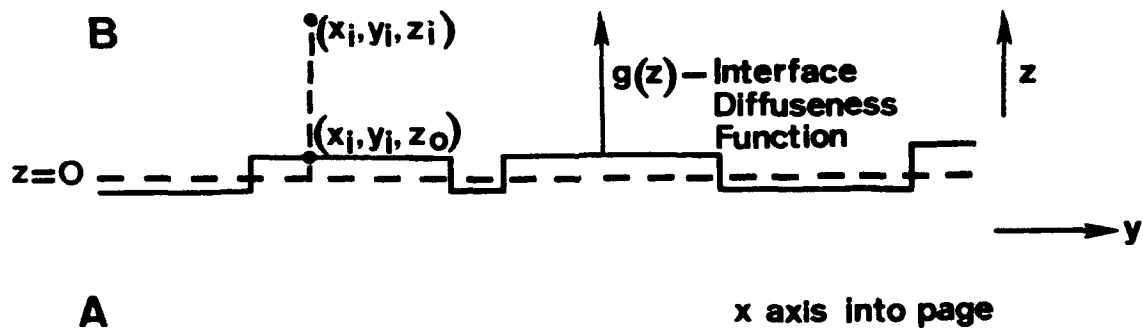
Figure 1: Geometry and orientation of interface structure used in text.

DERIVED INTERFACE WIDTHS
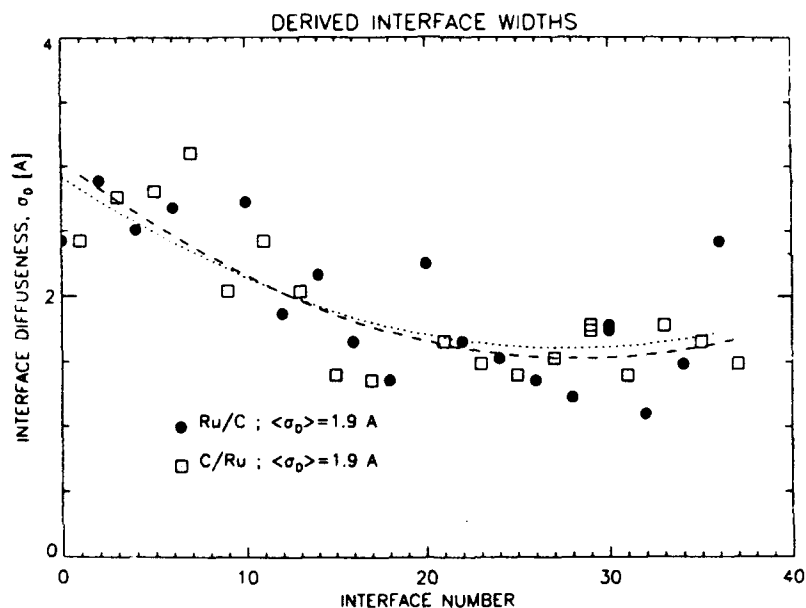
Figure 2: Interface number (counted from substrate) vs. measured σ_{D_o} (from the low area limit of interface width, $w(z) \rightarrow g(z)$ as $A_{x,y} \rightarrow 0$) for a 44.3 Å bilayer Ru/C sample.
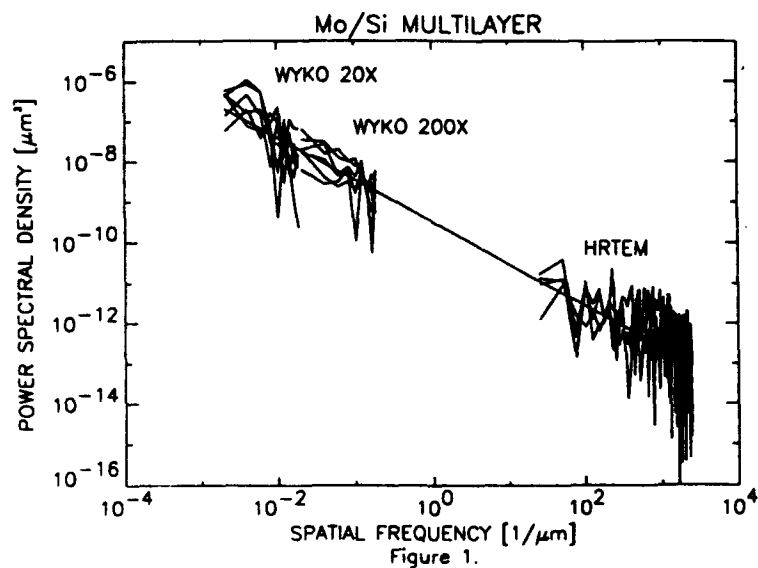
Mo/Si MULTILAYER

Figure 3: Power spectral density function computed from the measured surface topography (using a WYKO optical profilometer) and the measured interface topography (from digitized HREM images) for a Mo/Si multilayer sample.

Effects of Fresnel Fringes on TEM Images
of Interfaces in X-Ray Multilayers

Tai D. Nguyen,[1,2] Michael A. O'Keefe,[3] Roar Kilaas,[3] Ronald Gronsky,[2,3] Jeffrey B. Kortright[1]

[1]Center for X-Ray Optics, Lawrence Berkeley Laboratory, Berkeley, CA 94720,
Tel. (510) 486-4051 FAX (510) 486-4550,
[2]Department of Materials Science and Mineral Engineering, University of California, Berkeley, CA 94720,
[3]National Center for Electron Microscopy, Lawrence Berkeley Laboratory, Berkeley, CA 94720,

Cross-sectional High-Resolution Transmission Electron Microscopy (HRTEM) has been widely used to examine the structure and morphology at multilayer interfaces at an atomic scale. Assessment of the interfacial structures quantitatively from these TEM images however is difficult due to the Fresnel fringe effects, which produce different apparent structures with defocus values in the images. These fringes result from the electrons experiencing an abrupt change in the scattering potential parallel to the electron beam path. Imaging of multilayers in cross-section, in which the electrons travel parallel to the interfaces between the two layer materials, always results in such fringes. X-ray multilayers having alternating layers of very different atomic numbers or scattering powers are more prone to these fringes than the heterostructures having less contrast layers. The visibility of the fringes increases with increasing defocus away from the minimum contrast, while optimum resolution in bright-field imaging is obtained at the Scherzer defocus, which is about 100 nm from the minimum contrast for most high resolution microscopes. Fresnel fringes are thus present when imaging at optimum defocus. The effects of these fringes have been commonly overlooked in efforts of making quantitative interpretation of interfacial profiles. They however have also been employed to characterize the structures and compositional roughness at interfaces.[1-3] In this report, we present the observations of the Fresnel fringes in nanometer period Mo/Si, W/C, and WC/C multilayers in through-focus-series TEM images. Calculation of the Fresnel fringes of a Mo/Si multilayer using charge density approximation is used to illustrate the characteristics of the fringes from different interfacial structures.

Fresnel fringes are observed in many TEM through-focus-series images of W/C, WC/C, Ru/C, and Mo/Si multilayers.[4] The visibility of these fringes depends on the thickness of the specimen, and on the defocus value. The contrast of the fringes is higher with increasing defocus

both positive and negative values from the minimum contrast condition. The fringes in the W/C and Mo/Si appear symmetrical on the two interfaces of the W-rich and Mo-rich layers signifying similar structures at interfaces of the high-Z on low-Z and of the low-Z on high-Z materials. The fringes in the WC/C multilayers however show different characteristics at the two interfaces of the WC-rich layers, which likely indicates different shapes of the potentials and hence of the chemistry or the composition at the two interfaces. Micro-densitometry traces of the multilayers across the layers and interfaces of through-focus-series images show similar behaviors as those observed from the images. These traces can be used for quantitative comparison with calculation to determine the interfacial profiles.

Simulated Fresnel fringes of a 9 nm period Mo/Si multilayer is generated using charge density approximation method. The calculation produces line tracings of the a multilayer period, similar to the micro-densitometry traces of the experimental TEM images. The potentials of the Mo and Si layers are assumed to be uniform, and the transition layers have a finite linear slope at the interfaces. Comparison of structures of different potential difference (ΔP), transition layer thickness (d_{tr}) and slope (m_{tr}), and their combinations, are used to study the characteristics of the fringes. Similar to the experimental results, the fringes have higher contrast at higher defocus values, and change in sign from positive to negative defocus. The contrast or intensity is higher for larger potential difference between the layers. Change in ΔP with constant transition layer thickness, and hence change in the slope or abruptness in change of composition, does not result in significant difference in the spacings of the fringes. The profile however varies for different ΔP with the same slope from positive to negative defocus. For the same potential difference, the contrast increases with higher slope and shorter d_{tr}, while the spacing increases with lower m_{tr} and longer d_{tr}. Comparison of the fringe intensities and spacings of two different transition layer thicknesses with the same slope and hence of two different ΔP, reveals that the difference in the intensity is significantly higher for the shorter d_{tr} and higher ΔP, while the spacing is much wider in the longer d_{tr} and lower ΔP. This observation indicates that the potential difference and the abruptness of the interfacial composition change are a strong function of the fringe contrast, while the fringe spacing depends more strongly on the thickness of the transition or interfacial layer.

1. J.N. Ness, W.M. Stobbs, and T.F. Page, *A TEM Fresnel Diffraction-Based Method for Characterizing Thin Grain-Boundary and Interfacial Films*, Phil. Mag.A 54, 5 (1986) 679.

2. W.M. Stobbs, *Techniques for Characterizing Artificial Layer Structures using Transmission Electron Microscopy*, MRS Proc. 103 (1988) 121.

3. W.C. Shih and W.M. Stobbs, *The Measurement of The Roughness of W/Si Multilayers Using The Fresnel Method*, Ultramicroscopy 32 (1990) 219.

4. T.D. Nguyen, R. Gronsky, and J.B. Kortright, *Fresnel Fringe Effects at Interfaces of Thin Multilayer Structures*, Proc. Int. Congr. Elec. Microsc. Vol. 4 (1990) 442.

Roughness and Nonspecular Scattering 2

TuC 7:30pm–10:15pm
Grand Room

David L. Windt, *Presider*
AT&T Bell Laboratories

Surface Roughness and X-Ray Scattering

E. L. Church
Bldg 65N, USA ARDEC, Picatinny NJ 07806-5000
(201 724 7317)

P. Z. Takacs
Bldg 535, Brookhaven National Laboratory, Upton NY 11973-5000
(516 282 2824)

SUMMARY

1. Introduction

Interface roughness and diffusion limit the performance of x-ray multilayer (ML) stacks by generating unwanted scattering and reducing their efficiencies.

A number of routines for evaluating these effects are described in the literature [Eastman, Carniglia, Peterson, Bousquet, Stearns ...]. Their development involves two steps: the modelling of the properties of a single interface, and the combination of the effects of many interfaces to determine the performance of the stack. Our discussion here is concerned principally with the first step, the critical single-interface part of the problem.

2. Reflection and scattering from rough and diffuse interfaces

The radar/EM literature gives 'exact' vector expressions for the reflection, transmission and scattering by rough and graded interfaces which are useful for evaluating the scalar [Eastman, Carniligia, Peterson, Harvey, Zavislan ..] and vector [Elson, Gourley, Bousquet, Apfel, Stearns ..] approximations used in the multilayer literature.

First-order Rayleigh-Rice theory, for example, gives the (16) Stokes matrix elements for scattering in the simple form:

$$\frac{1}{I_i}\left(\frac{dI}{d\omega}\right)_{a,b} = \frac{16\pi^2}{\lambda^4} \cdot \cos\theta_i \cos^2\theta_s \cdot Q_{a,b} \cdot S_2(\vec{f})$$

where a,b refer to polarization states, the Q's are reflection-polarization factors, S_2 is the two-dimensional power spectral density of the topographic roughness, and $\vec{f}$ is the surface spatial frequency. In the case of s to s scattering, for example, Q_{ss} is the geometric mean of the Fresnel intensity reflection coefficients evaluated at the incident and scattering angles for arbitrary surface permittivity. (Rayleigh-Rice theory is an improved and extended version of first-order Born-approximation analysis.)

3. One- and two-dimensional power spectral densities

The power spectral density S_2 appearing above is the two-dimensional Fourier transform of the surface autocovariance function (ACF). In contrast, the power spectrum of a linear profile, S_1, is its one-dimensional transform. The two spectra are different but related. In the case of isotropic surfaces (considered hereafter) they are Abel transforms of each other [Church,79].

4. Models of surface topography

The ACFs of surface topography are usually taken to be Gaussians and/or exponentials, parameterized by intrinsic surface roughnesses σ and transverse correlation lengths ℓ . We have found, however, that three-parameter K-correlation or ABC model is more realistic and versatile:

$$ACF(\vec{\tau}) = F(A,B,C) \cdot \left(2\pi \frac{\tau}{B}\right)^{(C-1)/2} \cdot \mathbb{K}_{\frac{c-1}{2}}\left(2\pi \frac{\tau}{B}\right)$$

The corresponding one- and two-dimensional power spectra are

$$S_1(\xi_x) = A / \left[1 + (B\xi_x)^2\right]^{C/2} \quad , \quad S_2(\vec{\xi}) = A' / \left[1 + (B\xi)^2\right]^{(C+1)/2}$$

The parameters A and $A' = AB/2\, \beta(C/2, 1/2)$ have the dimensions of length-cube and length-fourth, $B/2\pi$ is a correlation length, and C determines the power-law fall-offs of the spectra at high frequencies. (K = Bessel function and β = beta function) [See Church and Takacs, Proc SPIE 1530 71-86 (1991)].

5. Experimental observations

We have measured the profile spectra of many mirror surfaces using a Wyko profiling microscope for spatial wavelengths between 10 μm and 5 mm and the Brookhaven Long Trace Profiler (LTP) for wavelengths between 2 mm and 1 m, and find reasonable fits to the ABC model with $C \sim 1.2 - 1.5$ and B values corresponding to correlation lengths which are often comparable with the size of the part being measured -- up to tens of cm [Takacs]. On the short wavelength end of the spectrum, the few profile and scattering measurements that are available show surface spectra approximating a power-law form with $C \sim 1 - 2$ down to almost atomic dimensions [Windt, Spiller, Andrews, Kunieda, et al.]

Such surfaces are 'fractal-like' in that their spectra show the inverse power-law or self-affine forms

$$S_1(\xi_x) = \frac{K_m}{\xi_x^m} \quad , \quad S_2(\vec{\xi}) = \frac{1}{2\,\beta(m/2, 1/2)} \cdot \frac{K_m}{\xi^{m+1}}$$

over a wide range of surface frequencies. These are limiting forms of the ABC model for large B, where $K_m = A/B^{\wedge}(C)$ and $n = C$. K_m and n are the intrinsic finish parameters of fractal models, corresponding to σ and ℓ of conventional models [cf Church, Appl. Opt. 27 1518-1526 (1989)].

6. Application to ML stacks

Three roughnesses are involved in ML stacks: the substrate roughness, the 'extrinsic' roughness of an interface -- i.e. the print-through of the roughness of the previous interface -- and the 'intrinsic' roughness generated on the top of a given layer in the deposition process [Harvey].

Stearns has recently made the ingenious suggestion that the smoothing of the print-through can be described in terms of a transfer function determined by a diffusion process operating during deposition. He evaluates this using (in ABC language) a C = 1 model for the diffusion process and C = 2 models for the

substrate and intrinsic roughnesses, with correlation lengths between 0.2 - 20 Angstroms in the first and 10 - 100 Angstroms in the second.

C = 1 models are common for noise-driven processes such as growth, spontaneous roughening and thermally-excited capillary-gravity waves [Kardar, Weeks, Bak].

In contrast, our results suggest that $C \sim 1.2 - 1.5$ processes might be more realistic, and that the effects of larger correlation lengths should be explored -- so large, in fact, that the spectra and transfer functions have the fractal form over the coherence length of the stack illumination. Windt has already considered such fractal forms in a study of multi-wavelength stack efficiencies [Windt et al. Proc SPIE 1343 292-308 (1991)].

7. Effects of system parameters

Calculations of stack performance are usually idealized in that they assume infinite plane waves in and out and point detectors in the far field. Real systems, however, involve two finite length parameters -- the coherence length W , and the size of the illuminated area, L . Roughly speaking, spatial wavelength components with $\lambda < d = 1/f < W$ diffract, and their relevant statistics are their height-distribution function and power spectral density -- while those with $W < d = 1/f < L$ reflect, and their relevant statistic is their slope distribution function. The effective coherence length is determined by the source and detector sizes:

$$W \sim \lambda / t \cos \theta_i$$

where t is their half angular width subtended at the surface. Values of W depend on system parameters but can lie between a fraction of a micrometer and a few millimeters.

We have developed a simple scalar scattering theory which automatically includes the effects of these system parameters on the imaging and scattering properties of a single surface. For the glancing-incidence slit-detector geometry of synchrotron mirrors this is a one-dimensional theory, but it gives insight into the two-dimensional version appropriate for arbitrary incidence. [Church and Takacs, Proc SPIE 1160 323-336 (1989)].

8. Conventional and fractal forms of the Debye-Waller factor

A particular feature of interest is the DWF -- the factor by which the specular intensity is reduced by surface errors. In this calculation the DWF appears as the convolution of diffraction and slope terms. For conventional surfaces -- ie those with $\ell << W$ -- the diffraction term is the square magnitude of the Fourier transform (characteristic function) of the roughness height distribution function, and is independent of the surface spectrum. For a Gaussian height distribution, for example,

$$DWF_d = Exp \left[- \left\{ 2\pi (\cos \theta_i + \cos \theta_s) \sigma / \lambda \right\}^2 \right]$$

This is the standard result except for the fact that the rms roughness involved includes contributions only from surface components with spatial wavelengths in the range $\lambda < d < W$.

In the case of fractal-like surfaces -- ie those with ℓ > W -- the ergodic approximation breaks down and the diffraction factor in the DWF depends on L, W, and S(f) as well as the height distribution, and its functional form is no longer Gaussian for a Gaussian height distribution [Church,88, Sinha.88].

The slope term in the DWF is the slope distribution function of the surface for components with spatial wavelengths in the range W < d < L, modified in an obvious way to account for the doubling of the deflection angle on reflection. For single surfaces one must also account for the fact that the tilt of the illuminated area of the surface is removed by the selection of the optic axis as the direction of the peak specular reflection.

The simplest computational approximation is to take the slope distribution to be Gaussian (instead of, say, the more general gamma distribution) with an rms slope, μ, determined from the measured surface spectrum as described below.

9. Measured finish parameters

The effects of surface topography on system performance are expressed in terms of band-width limited values of its rms roughness and slope. In the one-dimensional case these are given by

$$\sigma^2 = \int_{1/w}^{1/\lambda} d\xi_x \, S_1(\xi_x) \quad , \quad \mu^2 = \int_{1/L}^{1/w} d\xi_x \, (2\pi\xi_x)^2 S_1(\xi_x)$$

where S_1 is the measured/modeled profile spectrum. Their values are finite for fractal surfaces since any divergences are cut off by the lower and upper frequency limits.

All measurements of surface properties are bandwidth limited by instrumental parameters. Measurements of the ACF involve that instrumental bandwidth convolutionally and it is possible to misinterpret their effects as an exponential function. However, the value of the apparent ACF at zero lag depends on the instrumental bandwidth, and its apparent correlation length reflects the low-frequency cut-off of the measuring instrument rather than the longer (infinite) correlation length the surface itself.

Measurements of the surface spectrum are least susceptible to confusion by measurement bandwidth effects since they enter multiplicatively, in the form of a measurement transfer function for linear measurement systems.

10. Statistical fluctuations

Discussions above refer to the average (mean) properties of an ensemble of statistically equivalent surfaces or stacks. How accurately those averages represent an individual member of the ensemble depends on higher-order statistical properties (the variance) of the quantity being examined. The differences can be significant for fractal surfaces for quantities such as the DWF and small-angle scattering which may depend on a relatively few long-wavelength degrees of freedom. [Church 88, Church and Takacs, 91]

11. **Recommendation** The royal road to understanding roughness effects is through their power spectra. More measurements of ML substrates and interfaces are needed.

Substrate effects on x-ray specular reflectance

# and non-specular scattering from x-ray multilayers

J.B. Kortright,[1] T.D. Nguyen,[1] I.M. Tidswell,[2] C.A. Lucas[2]

[1]Center for X-ray Optics and
[2]Materials Science Division
Lawrence Berkeley Laboratory
Berkeley, CA 74720
(510) 486-5960
(510) 486-4550 FAX

It is common knowledge that substrate roughness plays an important role in limiting the specular reflectance of x-ray multilayers. However, there have been relatively few systematic experimental studies of the effects of substrate roughness on x-ray multilayer reflectivity. We have begun to investigate these effects by measuring the specular and off-specular scattering from a set of substrates with different roughness and from tungsten/carbon multilayers deposited simultaneously onto an identical set of substrates.

The substrates were polished fused-silica and were flat to better than $\lambda/10$ (λ visible) at low spatial frequencies. The higher spatial frequency microroughness was varied during the polishing process, and was quantified by the optical polisher[1] using a ZYGO Model 5500 Heterodyne Profiler at visible wavelengths to yield an rms roughness ($\sigma_{visible}$) and a peak-to-valley roughness (PV). Substrates with four distinct microroughness levels were studied. The $\sigma_{visible}$ values for these substrates were roughly 0.2 Å, 2.0 Å, 5.0 Å and 10.0 Å, and the corresponding PV values were 1.4 Å, 12 Å, 32 Å, and 65 Å, respectively. Tungsten/carbon multilayers were deposited by magnetron sputtering to have 40 periods each 30 Å thick in which the tungsten layers comprised roughly 0.4 of each period.

X-ray measurements were made using $\lambda = 1.38$ Å radiation from a synchrotron source. The intensity from the synchrotron is especially useful for measuring diffuse scattering from the substrate surfaces, which is one of the weaker components to the scattering measured here. Three types of
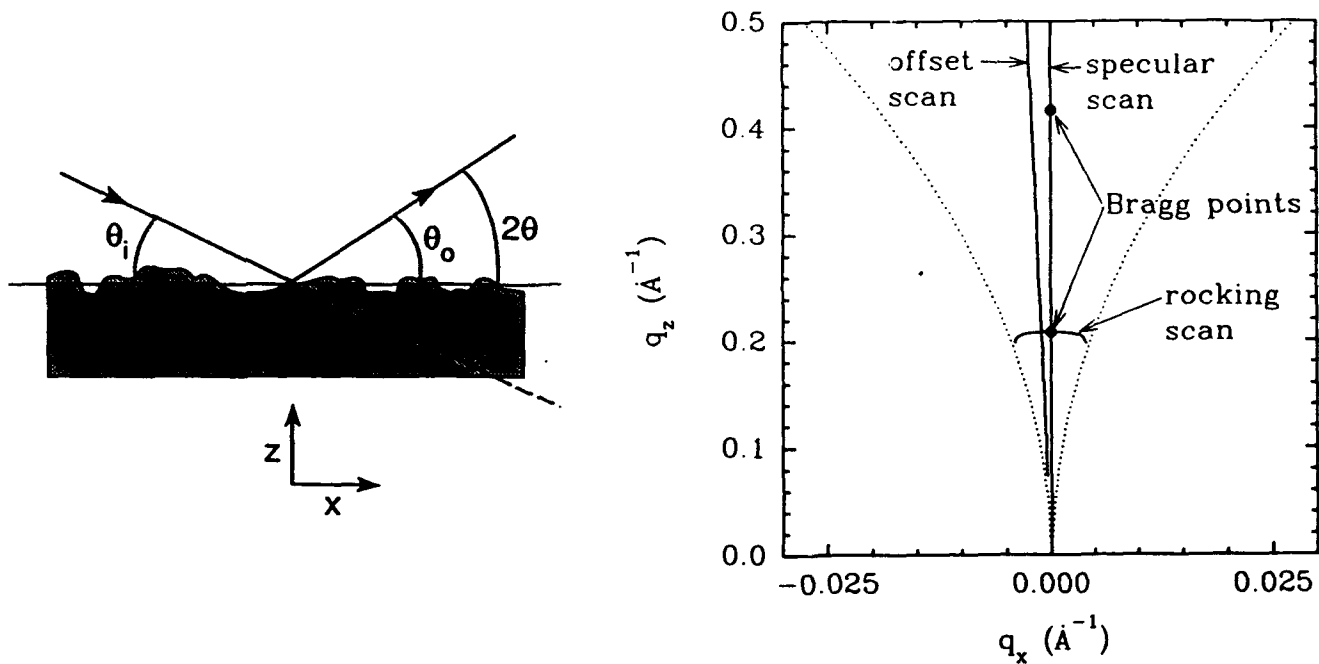
The scattering geometry at left imposes limits on the region of scattering vector space available for measurement between the dotted lines in the plot on the right. Different types of angular scans make different trajectories through momentum transfer space. The position of the first two specular multilayer Bragg peaks is indicated.

Specular scans are directed along the surface normal at zero in-plane momentum transfer, rocking scans are predominantly orthogonal to specular scans, and offset scans are nearly parallel to the specular scan at some non-zero in-plane momentum transfer.

Scattering from the substrates includes several common components, some of which show pronounced trends with surface roughness. Common features include the specular (delta-function) component, a diffuse non-specular component originating from surface roughness, a diffuse component originating from bulk density fluctuations, and an oscillation in the specular component resulting from a thin surface layer having different density than the substrate bulk. The intensity and shape of the surface diffuse component is strongly correlated with $\sigma_{visible}$, confirming that each of these quantities is a sensitive measure of surface roughness over relevant length scales. Likewise the specular component depends sensitively on the differing levels of roughness, with the x-ray Debye-Waller rms roughness (σ_{x-ray}) larger than that obtained from the optical profilometer measurement ($\sigma_{visible}$). The ratio of the specular to diffuse intensity components decreases with increasing momentum transfer, as expected. At a given momentum transfer the specular to diffuse ratio is

strongly correlated with $\sigma_{visible}$, and ranges from over 10^3 to less than 1 even at relatively small values of momentum transfer.

The multilayers also show specular and diffuse components in the low scattering vector region. A multilayer diffuse component arising from interface roughness within the multilayer can be identified, as can a bulk diffuse component originating probably in the substrate. Scans offset from the specular scan show that the multilayer diffuse scattering has essentially identical multilayer interference features compared to those in the specular scan. Thus roughness in the multilayer structure has the same vertical correlations as do the layers of the multilayer stack. Rocking scans show that the shape of the multilayer diffuse intensity for a given substrate roughness is similar to that of that substrate's surface diffuse intensity. Thus the spectral density function of the roughness in the multilayers appears to be the same as that of the substrates. This suggests that conformal growth of the sputter-deposited multilayers to the roughness of the substrate has occurred over the measured range of spatial frequencies. The similarity of the specular to diffuse intensity ratios at the same momentum transfer for the substrates and the multilayers further confirms this growth mode.

These qualitative results show that the roughness of the substrate plays a predominant role in determining the relative amounts of specular and diffuse intensity of these multilayers, and indeed in limiting specular reflectance of multilayers. Since the relative specular to diffuse intensity decreases with increasing momentum transfer, the effect of substrate roughness becomes more important for shorter period structures. Quantitative modeling of these data is underway. Specific emphasis will be given to questions relating to what extent the measured multilayer scattering is determined by the substrate roughness, as opposed to structural inhomogeneities intrinsic to the multilayer structure itself.

Footnotes
1. General Optics, Moorpark, CA.
2. J.B. Kortright, J. Appl. Phys., **70**, 3620, (1991).

Synchrotron Study of Roughness in Fe-Cr Multilayers

B.M. Clemens and A.P. Payne, Department of Materials Science and Engineering,
Stanford University, Stanford, CA
S. Brennan, Stanford Synchrotron Radiation Laboratory, Stanford, CA

Introduction

Many advances in the characterization of roughness in artificially layered structures have grown out of interest in their x-ray optical properties. In the present work we apply these techniques to a different application of layered media: magnetic multilayers. Recent reports have shown that the antiferromagnetic order and giant magnetoresistance in layered magnetic materials are mediated by interface quality and roughness, and several reports claim layer roughness *enhances* giant magnetoresistance. The objective of the current work is to characterize interface roughness and correlate it to the magnetic properties in these materials. We have fabricated structurally distinct Fe/Cr layered structures and examined both the exchange coupling and electrical transport properties. We correlate this with quantitative measurements of the character and magnitude of the structural perturbations.

X-Ray Scattering from Rough Surfaces

X-ray scattering from metallic surfaces can be adequately treated with the Kirchhoff integral formulation for diffraction[1]. Here, a randomly rough surface is characterized by a height-height correlation function, $C(X,Y)$, describing the average height difference between two points separated by distance $R = \sqrt{X^2 + Y^2}$. This function typically describes the roughness in terms of an rms value, σ, and characteristic in-plane length scale ξ. We have employed an exponential correlation function for a randomly rough, planar surface [2].

$$C(X,Y) = \langle z(x-X, y-Y)z(x,y) \rangle = \sigma^2 \exp(-|R|/\xi)$$

where $z(x,y)$ is the height of the surface at point (x,y).

By inserting this correlation function into the Kirchoff integral it can be shown that the scattered intensity assumes the following form [2]:

$$I(q_x, q_z) = \frac{2\pi I_0}{q_z^2} e^{-q_z^2 \sigma^2} \times \left[2\pi \delta(q_x) + \sum_{m=1}^{\infty} \frac{2\xi \left(\sigma^2 q_z^2 \right)^m}{m(m!)\left(1 + q_x^2 \xi^2/m^2 \right)} \right]$$

where the delta function in the first term in the brackets describes the specularly reflected beam and the second term describes the non-specular diffuse scattering as a sum of Lorentzians. If, in a multilayer structure, the roughness is conformally mapped from one layer to another, one dimensional periodicity persists, and the diffuse scattering is confined to planes of constant q_z passing through Bragg points. Thus, through investigations of diffuse scattering from multilayer materials, conformal and non-conformal roughness can be differentiated. Quantitative information regarding the magnitude and lateral length scale of both types of roughness can be obtained.

Film Preparation

We have found that by varying the pressure we are able to repeatably and controllably alter the layer quality. A series of Fe/Cr multilayers (20x[25 ÅFe/40ÅCr]) was fabricated by sputter deposition

at a four different argon pressures (1.4, 2.0,5.0 and 10.0 mT). The base pressure of the system was 4×10^{-9} and the multilayers were grown at a rate of 1 Å/s. The films were deposited on 1 inch diameter oxidized Si(100) wafers which were 5mm thick to avoid substrate bowing due to intrinsic stresses.

X-Ray Measurements

X-ray measurements were performed on a Huber 4-circle diffractometer at beamline 7-2 of the Stanford Synchrotron Radiation Laboratory. An energy of 9985 eV ($\lambda_x = 1.2418$ Å) was used for all measurements. Three types of scans were employed, each having distinct paths through reciprocal space shown in Fig. 1[2, 3]. The vector components q_x and q_y of the scattering vector $\vec{q}$ are given by:

$$q_x = \frac{2\pi}{\lambda_x}(\cos\theta_o - \cos\theta_i)$$

$$q_z = \frac{2n\pi}{\lambda_x}\left(\sqrt{1 - \cos^2\theta_o/n^2} + \sqrt{1 - \cos^2\theta_i/n^2}\right)$$

where θ_i and θ_o are the incident and exit angles and n is the index of refraction. In a symmetric Bragg scan the $\theta_i = \theta_o$ so that $q_x = 0$, while q_z varies from roughly .05 to 0.9 Å^{-1}. By fitting this spectrum with numerical model, a variety of structural parameters can be determined, including the bilayer period, component ratio, index of refraction, standard deviation of the statistical fluctuation in layer thicknesses, and fraction of alloyed material at the interface. However, since $q_x = 0$ in these scans, no information on lateral structure or roughness can be obtained.
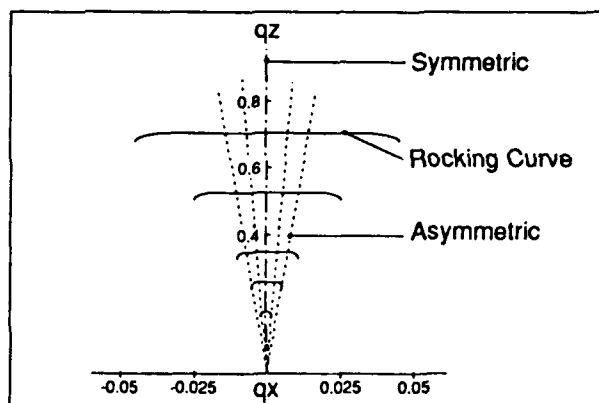
Figure 1: Schematic of reciprocal space paths for the various scans performed in this study.

In order to study in-plane roughness, rocking curves were performed which investigate the scattering behavior as a function of q_x. The detector is held at a fixed 2θ while the sample is rotated in the beam ($\theta_i \neq \theta_o$) resulting in scans with nearly constant q_z and varying q_x. The range in q_x is limited by the surface of the sample interfering with either the incident or exit beam. As this limit is approached, total external reflection from the sample reduces q_z, as shown in Fig. 1.

The third scan used in this study is the offset Bragg scan. This is performed in an identical manner to a symmetric Bragg scan except that θ_i and θ_o are not longer equal but differ by a constant value. In reciprocal space this scan can be represented as a radial line passing through the origin with both q_x and q_z components. Such trajectories allow us to differentiate the conformal and non-conformal components of the total roughness.

Fitting Procedures

Symmetric Scans

The bilayer period and index of refraction were extracted from the spectra by fitting the positions of the Bragg and finite thickness peaks to the expression:

$$\sin^2 q_z = \left(\frac{2\pi}{\Lambda}\right)^2 n_p^2 + \left(\frac{\pi}{\lambda_x}\right)^2 2\delta$$

where n_p is the diffraction peak order, which takes on fractional values for the finite thickness fringes, Λ is the bilayer period, and δ is the difference from one of the real part of the refractive index. The similarity in electron density for the Fe/Cr leads to scattering which can be adequately treated with kinematic models. Our model produces the diffraction pattern from stacks of a and b layers with electron densities ρ_a, ρ_b in which the thickness of each layer vary around mean values t_a, t_b with standard deviation σ_a, σ_b. A linearly varying alloyed region of constant thickness t_i is also included. The average intensity scattered from this structure is calculated from the ensemble average over all possible bilayer configurations using a mathematically compact formalism [4].

Rocking Curves

Rocking curves were fit to the theoretical profile for diffuse scattering presented earlier. Because of enhanced scattering near the critical angle, Yoneda wings were observed in almost all of the rocking scans [5]. These features were circumvented in the fitting by limiting the q_x range of the fit to a region between the inflection points of the Yoneda peak and the diffuse peak. Corrections to account for sample illumination, path length change, and reciprocal space trajectory were applied to the theoretical profile before fitting.

Results

Results from the symmetric Bragg scattering showed a strong influence of sputtering pressure on the quality of the multilayer. The lowest pressure sample exhibited up to seven well defined Bragg harmonics as well as sharp finite thickness submaxima between peaks. The highest pressure sample shows only one wide Bragg peak. Fitting indicates that this difference is due to increased thickness fluctuations around the mean bilayer period as well as interfacial alloying.

Figure 2 shows the symmetric scan as well as several offset scans for the 1.4mT multilayer. Bands of diffuse scattering through the Bragg locations are clearly evident, indicating the presence of conformal roughness. The ratio of specular to diffuse scattering decreases in q_z so that for the 5th harmonic and beyond the Bragg scattering is almost purely diffuse. In general, samples showing strong modulation in the symmetric scans showed larger levels of peaked diffuse scattering through the Bragg peaks. Rougher samples exhibited more diffuse scattering between Bragg harmonics, resulting in less distinct enhancement of the diffuse scattering at the Bragg peaks. We conclude that the increased sputtering pressure leads primarily to an increase in non-conformal roughness.

As predicted by the theoretical expression, the rocking curves exhibit an instrument limited spike at $q_x = 0$ in addition to a much broader diffuse peak. Collections of narrowly spaced rocking curves through the Bragg peaks confirmed the presence of peaked of diffuse scattering. This is shown for the third harmonic in the 1.4 mT sample in Figure 3. The intensity of the diffuse scattering grows near the Bragg harmonic, but becomes a maximum at a slightly higher q_z. Rocking curves through q_z values slightly higher than the Bragg peak exhibit a square profile before refraction corrections are applied. The corrected scans in Fig. 3 show that this is caused by the tails of the scans passing

Mosaic Reflectivity of X-ray Multilayer Structures

F.E. Christensen and H.W. Schnopper
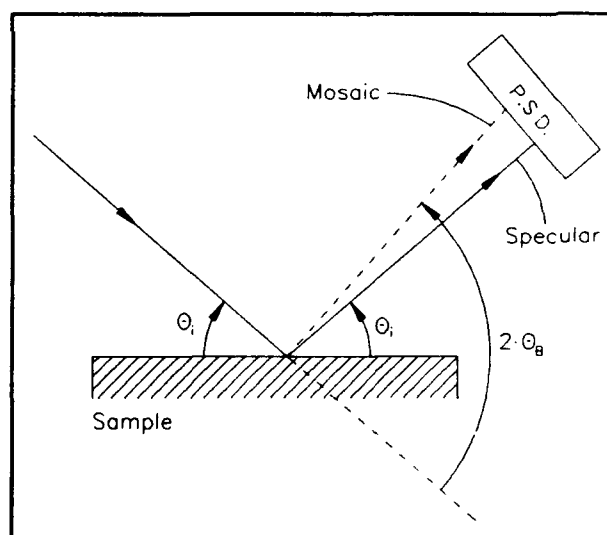Danish Space Research Institute, Gl. Lundtoftevej 7, DK-2800 Lyngby, Denmark
Telephone : +45 42 88 22 77

SUMMARY

Mosaic reflectivity from multilayer structures has previously been detected[1] but only in a limited angular range close to the Bragg angle (θ_B) and only at a single energy. In this paper, a systematic study of the mosaic reflectivity is performed at five line energies (B-K_α (0.183 keV), Cr-L_α (0.573 keV), Ni-L_α (0.852 keV), Pd-L_α (2.838 keV), Cu-K_α (8.048 keV)) for a series of Ni/C multilayers with similar d-spacings and similar ratio between Ni-content and C-content but different deposition methods. The mosaic reflectivity is measured in the complete angular range from zero to 2 θ_B around the first order Bragg peak. Several interesting and novel effects are revealed. First of all, it is observed that the mosaic reflectivity increases linearly as the angle of incidence is decreased. Secondly, the mosaic reflectivity is observed to decrease sharply as one enters the total reflection region. Thirdly, the mosaic reflectivity disappears completely as the angle of incidence approaches twice the Bragg angle. Finally, the mosaic reflectivity varies in a characteristic way with the energy.

The experimental arrangement is shown in Figure 1. This figure defines the relevant experimental parameters and shows the distinction between specular and mosaic reflection. The measurement of mosaic reflection is performed by positioning the arrangement on the 1 order Bragg peak and rotate the sample so that the angle of incidence (θ_i) is varied from ~ 0 to $2\theta_B$ while recording the counts in the few channels in the P.S.D., where the mosaic reflectivity must occur. Specular reflectivity was also measured. This is done by performing a θ-2θ scan with the sample and detector.

Figure 1 Experimental geometry. θ_i is glancing angle of incidence. θ_B is Bragg peak. In the Position Sensitive Detector (P.S.D.) the specular and mosaic peak may be separated with a resolution which depends on the position resolution of the detector and the distance between the sample and the detector.

The multilayers studied are Ni/C multilayers with d-spacings close to 45 Å and a thickness of the Ni-layer ~ 0.33 · d. This type of multilayer will be used as a dispersive element in an objective crystal spectrometer for X-ray astronomy[2]. The presence of mosaic reflectivity will contribute to the diffuse background during the low countrate observations and must therefore be minimized. The same holds true in any application of multilayer X-ray optics.

Figure 2 Specular (filled circles) and mosaic (open circles) reflectivity of 1. order Bragg peak of Ni/C multilayer with d ≃ 49 Å, Γ ≃ 0.31 and number of periods = 70 provided by Ovonics Synthetic Materials Co. Cu-K_α was used in this case. Data has been obtained from θ_i ~0.3° to θ_i ~ 1.5°. Incident beam on multilayer had a divergence of ~ 0.004°. Full line is fit to eq. (2) of mosaic reflectivity well away from the Bragg peak as described in the text.
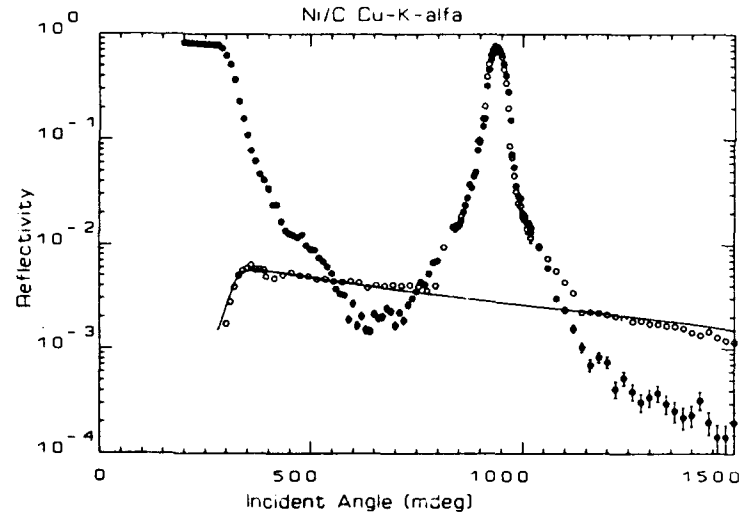

Figure 2 shows an example of the experimental data. Both the mosaic and specular reflectivity is presented and shown in the figure. The angle of incidence (θ_i - see Figure 1) is varied from close to 0° and up to 1.5°. The mosaic reflectivity of interest here is the one showing up well away from the Bragg peak and it clearly displays most of the features listed earlier. A theoretical model of the mosaic reflectivity well away from the Bragg peak, taking into account total external reflection and absorption, yields the following expression for the mosaic reflectivity :

$$R_{MOS} \; \alpha \; M \; (\; | \; \theta_i \; - \; \theta_B \; | \;) \cdot [\; 1 \; - \; R_F \; (\theta_i) \;] \cdot \frac{e^{-\Delta x \cdot G}}{(1- \; e^{-\Delta x \cdot G})} \cdot \left[1 - e^{\frac{- \; dN}{\sin \theta_i} \cdot G} \right]$$

where   (1)

$$G = \mu \left[1 + \frac{\sin\theta_i}{\cos(90 - 2\theta_B + \theta_i)} \right]$$

(2)

In these expressions, R_F is total external reflectivity, μ is linear absorption coefficient, d is d-spacing, N is number of periods, θ_i is angle of incidence and Δx is a basic length scale ≤ $1/\mu$.

M ($| \theta_i$ - $\theta_B |$) is the mosaic reflection at an offset angle of $| \theta_i$ - $\theta_B |$. Using this model, assuming M ($| \theta_i$ - $\theta_B |$) to be constant for the range of θ_i studied here, we get the full line shown in the figure. Obviously, the model describes the data well in this case.

Conclusively, the combined study of specular and mosaic reflection over a large range of angles of incidence and as a function of energy provides an extremely detailed characterization of multilayers.

REFERENCES

1) F.E. Christensen, A. Hornstrup, P. Frederiksen, P. Grundsøe, S. Henrichsen, E. Jacobsen, P. Jonasson, M.M. Madsen, C. Nilsson, H.W. Schnopper, N.J. Westergaard, and P. Ørup,
"Studies of Multilayers and Thin-Foil X-Ray Mirrors Using a Soft X-Ray Diffractometer",
J. of X-Ray Science and Technology, 2, 81-94 (1990).

2) F.E. Christensen, B.P. Byrnak, A. Hornstrup, Z. Shou-hua, H.W. Schnopper,
"Objective Crystal Spectrometer (OXS) for the SPECTRUM-X-γ Satellite",
SPIE-Proc., vol 1344, p. 14 (1990).

Growth and Structure 3

WA   8:00am–11:45am
Grand Room

R. E. Somekh, *Presider*
University of Cambridge, United Kingdom

Morphology of Thin Film Growth, R.W. Collins, Ilsin An, and Y.M. Li

275 Materials Research Laboratory, The Pennsylvania State University,

University Park PA 16802; Tel: (814) 865-3059; Fax: (814) 865-2326.

Thin films prepared by vapor deposition methods have a range of applications which demand control over the microstructural, electronic, and/or optical properties. Empirical classification schemes for the morphology of vapor-deposited thin films have been developed over the years in attempts to provide physical insights into the relationships between preparation parameters and resulting film properties.[1-3] A variety of computational techniques have also been applied to model film growth and to elucidate the physical principles that account for the observed morphological development. These include continuum,[4] molecular dynamics,[5] Monte Carlo,[6] and ballistic aggregation[7] techniques. In continuum models of film growth, many authors have studied the stability of one-dimensional surface profiles in response to sinusoidal perturbations of wavelength, λ_r.[4,8-10] Effects of finite atomic size[4] and shadowing by asperities[8] have been proposed to enhance the perturbations, whereas adatom surface diffusion damps them. A smooth profile can be regained for $\lambda_r < \lambda_o$, where λ_o is the adatom diffusion length. When $\lambda_r > \lambda_o$, a modulated profile develops that appears analogous to experimentally-observable columnar morphology. In the experimental situation, clustering associated with initial nucleation is the dominant surface perturbation for thin film deposition on dissimilar substrates. It is technologically important to determine and control the evolution of surface morphology with subsequent film growth. Of direct importance here is the ability to fabricate multilayered structures with atomically smooth interfaces.

Non-invasive probes are required to observe thin film nucleation and, in particular, the surface smoothening associated with microstructural coalescence. Optical ellipsometry is one of the few techniques with sufficient sensitivity to characterize such phenomena.[11] Until our most recent work,[12] such measurements have been performed at a fixed wavelength, and the data have been presented as trajectories in the plane of the two ellipsometric angles, (ψ,Δ), that are swept out as a function of time during film growth. From an optical standpoint, a two-layer model (see Fig. 1) with three key microstructural variables characterizes thin film coalescence: (1) d_s, the thickness of a surface layer of low bond-packing density; (2) d_b, the thickness of an underlying layer of bulk bond-packing density; and (3) f_v, the surface layer density deficit (expressed as the void volume fraction). The surface layer simulates either the clusters in the early stages of growth or the residual surface roughness after the first bulk monolayer forms. In order to apply this optical model, the dielectric functions of the bulk material and all substrate components as well as any substrate structural parameters must be known. The dielectric function of the surface layer is then calculated from f_v with an effective medium theory (EMT); in our case the Bruggeman EMT is appropriate.[11]

It is clear that the time evolution of the three parameters $\{d_s, d_b, f_v\}$ cannot be obtained from the time evolution of the two ellipsometry angles $\{\psi,\Delta\}$ at a single wavelength. Even if simplifications are made, for example expressing f_v as a function of d_s by assuming an initial cluster and roughness geometry (e.g. hemispheres on a square grid that increase in radius with time),[11] there is still no extra information to verify the validity of the two-layer model. In contrast to the one-layer model, which is appropriate for perfect layer-by-layer growth, the two layer model is appropriate when clustering occurs, as long as the bond-packing density at the substrate interface reaches the bulk value. The two layer model, however, is invalid under conditions of columnar microstructure in which the near-substrate void structure is not filled in, but rather propagates through the film leaving inverted-cone-shaped columns of material.[13] Such a structural evolution requires a more complex optical model having at least three layers so that the buried gradation in the void volume fraction can be simulated.

With the development of real time spectroscopic ellipsometry (RTSE) and the associated linear regression procedures for data analysis, it is possible to overcome the limitations of single wavelength ellipsometry.[12] In this paper, RTSE is applied in a study of the coalescence

behavior of amorphous semiconductor films. A photodiode array detector is the unique feature of our rotating polarizer spectroscopic ellipsometer. It permits acquisition of 128-point (ψ,Δ) spectra from 1.5 to 4.5 eV in a minimum time of 40 ms. Here (ψ,Δ) are defined as usual by $r_p/r_s \equiv \tan\psi \exp(i\Delta)$, where r_p and r_s are the complex reflection coefficients for p- and s-polarizations. In the present experiments, which involve film growth at low rates, signal averaging was employed to obtain (ψ,Δ) spectra with sub-monolayer precision in a time of 3.2 s. Ambient light correction and real time graphics extended the full data cycle to 15 s.

The amorphous semiconductors studied here were deposited onto the native oxides of c-Si wafers under conditions optimized for microstructural uniformity (assessed by RTSE as described below). For pure PVD amorphous Si (a-Si) or Ge (a-Ge), low pressure magnetron sputtering was utilized to ensure that unthermalized, energetic Si or Ge atoms impact the substrate for an enhanced adatom surface diffusion. Substrate temperatures were 300°C for a-Si and 25°C for a-Ge. For plasma-enhanced CVD (PECVD) hydrogenated a-Si (a-Si:H), a remote He plasma was used to excite downstream-injected SiH_4. The substrate temperature in this case was 250°C. A vacuum chamber with a base pressure of 10^{-8} Torr, having windows oriented for optical access to the film at a 70° angle of incidence, was used for all depositions.

As the initial step in the interpretation of RTSE data, expressed as $\{\psi(h\nu,t), \Delta(h\nu,t)\}$, the substrate structure (i.e. native oxide thickness) and optical properties at the deposition temperature were determined. Then the dielectric function of the deposited film and the evolution of the two-layer model parameters $\{d_s,d_b,f_v\}$ were obtained using two different procedures, both giving equivalent results. These procedures are discussed in detail elsewhere.[12] It suffices to note here that once the dielectric functions of all the components of the structure are known at the deposition temperature, linear regression analysis (LRA) can be performed to extract $\{d_s,d_b,f_v\}$ since the unknown parameters are all wavelength independent.[14] Figures 2 shows the results of the two-layer analysis for (a) PVD a-Si, (b) PVD a-Ge, and (c) PECVD a-Si:H, concentrating on the first 35 Å of bulk film growth. The solid circles and open triangles denote d_s and d_b for the two-layer model versus time, all on the same scale. In each case f_v was also determined but is not shown. The open circles represent the thickness deduced from the one-layer model over the cluster growth regime. This regime is defined by $t<t_b$, where t_b is the time at which the first bulk monolayer forms (designated by the vertical broken lines in Fig. 2 at the approximate bulk layer thickness of d_b=2.5 Å).

Figure 2(d) shows the quantity $\sigma(t)$, which is a measure of the quality of the LRA fit,[14] for the one- and two-layer film growth models for the PECVD film of Fig. 2(c). It clearly shows that the two-layer model is an overinterpretation of the data for $t<t_b$=3.5 min, as would be expected since d_b<2.5 Å in this regime. The two layer model becomes appropriate for $t>t_b$, and here $\sigma(t)$ is as low as can be expected, considering our experimental precision and accuracy. As a result, a third layer is not required to interpret these data. A similar conclusion applies to the two PVD films. For other growth conditions, for example, PVD at high pressure, $\sigma(t)$ for the two layer model also increases significantly, indicating that additional layers must be included to simulate the columnar morphology that is anticipated under such conditions.

Now we concentrate on the implications of Figs. 2 for the nucleation and coalescence process. In this regard, the behavior of d_s and d_b is clear. For $t<t_b$ the high void fraction surface layer simulates the growth of nuclei. Here, d_b≡0, and f_v versus d_s from the one-layer model provides insights into the nuclei geometry. In all cases in Fig. 2, the nuclei geometry in the first few partial monolayers is consistent with disc-shaped structures. For $t=t_b$, the first *bulk* monolayer has formed, which completely covers the substrate surface, and from that point onward, the deposited flux adds predominantly to the bulk layer. This effect is substantiated by a change in the growth behavior of the surface layer also observed precisely at $t=t_b$. *Once the first bulk monolayer forms, the evolution of d_s is a direct indication of the ability of subsequent flux to smoothen the nucleation-related surface morphology.* Thus, an experimental connection is made to the stability analyses of film growth models.

For PVD a-Si, a 13 Å surface roughness layer which originates from the initial nucleation process gradually increases in thickness by 3 Å as the bulk film grows to 35 Å. In contrast for

a-Ge, a 9 Å roughness layer gradually decreases by 2 Å over the same range. For PECVD a-Si:H, the initial surface layer is larger, 20 Å, but its decrease is most significant, 7 Å, and the film continues to smoothen as the bulk layer increases in thickness beyond 35 Å. In the case of the PECVD material, because its growth involves H, we estimate that d_s includes a constant 4-6 Å contribution from a weakly polarizable surface layer of Si hydrides (in addition to a microstructural modulation of the surface). The hydride layer is eliminated from the surface of the film when a second film is deposited on top of it.

The differences between the results in Fig. 2(a) and (c) are intuitively clear and reveal interesting trends in the surface adatom diffusion length and the post-nucleation microstructural scale. The lower value for the cluster thickness at $t=t_b$ for the PVD film indicates a higher nucleation density. If we were to assume (1) that the disc-shaped nuclei evolve into hemispheres as they increase in size and (2) that these nuclei are located on a square grid, then nuclei spacings and densities of 40 Å and 5×10^{12} cm^{-2} for PECVD a-Si:H and 26 Å and 1.5×10^{13} cm^{-2} for PVD a-Si are calculated. The lower nucleation density for PECVD a-Si:H probably arises as a result of a higher adatom diffusion length on the substrate surface, in turn indicating a homogeneous component of nucleation in the case of the a-Si:H. We would expect that when the first bulk monolayer is formed, the wavelength distribution for the nucleation-related roughness, would be centered at $\lambda_r=40$ Å and $\lambda_r=26$ Å for the PECVD and PVD a-Si(:H), respectively. Appealing to the stability arguments,[4] the diffusion length λ_0 of precursors on the a-Si:H surface must be greater than 40 Å in order for the material to smoothen in the bulk film growth regime, as is observed experimentally. Similarly λ_0 must be less than 26 Å for the PVD a-Si in order for that material to roughen in the bulk film regime.

The origin of the differences in the results between PVD a-Si and a-Ge is less clear. Interpretation must take into account the fact that the a-Ge nuclei spacing and density, 18 Å and 3×10^{13} cm^{-2} (deduced as above), are smaller than the corresponding values for a-Si. This would indicate either a shorter diffusion length for Ge atoms on the oxide of the substrate or a higher density of substrate sites that can form stable bonds with Ge. Both may be possible owing to the lower temperature of Ge deposition. However, observation of weak smoothening in Fig. 2(b) indicates that the lower temperature does not appear to reduce significantly the diffusion length of Ge atoms on the a-Ge surface (i.e. $\lambda_0 > 18$ Å). The lower Ge-Ge bond strength or a higher energy for the incoming Ge atoms may compensate for the lower T.

In summary, we have developed techniques that provide sub-monolayer sensitivity to the coalescence of ultrathin films, relying on real time spectroscopic ellipsometry observations. An investigation of amorphous materials has provided new insights into the role of adatom surface diffusion and initial nucleation density in determining the ultimate atomic scale roughness on the film surface. The surface roughness is expected to translate into interfacial roughness when such films are deposited as components of multilayer structures.

1. B.A. Movchan and A.V. Demchishin, Phys. Met. Metallogr. 28, 83 (1969).
2. J.A. Thornton, Ann. Rev. Mater. Sci. 7, 239 (1977).
3. R. Messier, A.P. Giri, and R.A. Roy, J. Vac. Sci. Technol. A 2, 500 (1984).
4. A. Mazor, D.J. Srolovitz, P.S. Hagan, and B. Bukiet, Phys. Rev. Lett. 60, 424 (1988).
5. H.J. Leamy, G.H. Gilmer, and A.G. Dirks in: Current Topics in Material Science, edited by E. Kaldis (North Holland, Amsterdam, 1980) p. 309.
6. B. Lewis and J.C. Anderson , Nucleation and Growth of Thin Films, (Academic, New York, 1978) p. 206.
7. H.J. Leamy and A.G. Dirks, Appl. Phys. Lett. 25, 641 (1978).
8. R.P.U. Karunasiri, R. Bruinsma, and J. Rudnick, Phys. Rev. Lett. 62, 788 (1989).
9. C.H.J. van den Brekel and A.K. Jansen, J. Cryst. Growth 43, 364 (1978).
10. G.S. Bales, A.C. Redfield, and A. Zangwill, Phys. Rev. Lett. 62, 776 (1989).
11. J.B. Theeten and D.E. Aspnes, Ann. Rev. Mater. Sci. 11, 97 (1981).
12. I. An, H. Nguyen, N. Nguyen, and R.W. Collins, Phys. Rev. Lett. 65, 2274 (1990).
13. R. Messier and J.E. Yehoda, J. Appl. Phys. 58, 3739 (1985).
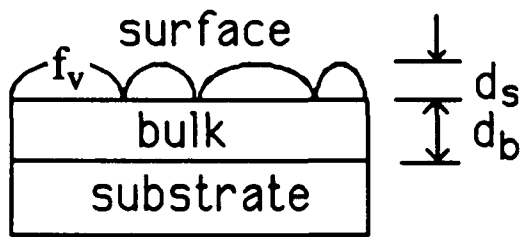14. D.E. Aspnes, Proc. Soc. Photo-Opt. Instrum. Eng. 276, 188 (1981).

Fig. 1 Two-layer optical model for film growth (left) with the associated free parameters.

Fig. 2 (a-c) Surface (solid circles) and bulk layer (triangles) thicknesses deduced from a two-layer optical model for the growth of (a) PVD a-Si, (b) PVD a-Ge, and (c) PECVD a-Si:H. The open circles are the thicknesses deduced from a one-layer optical model with $d_b \equiv 0$. (d) Quality of the LRA fit to data for the PECVD a-Si:H film of (c).
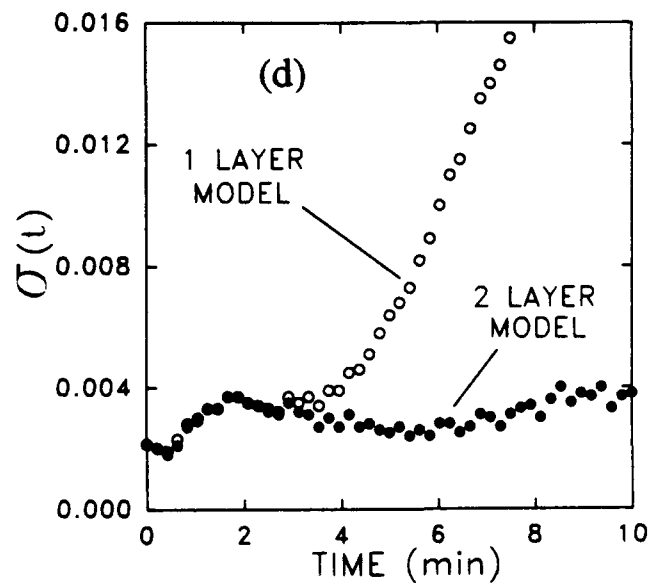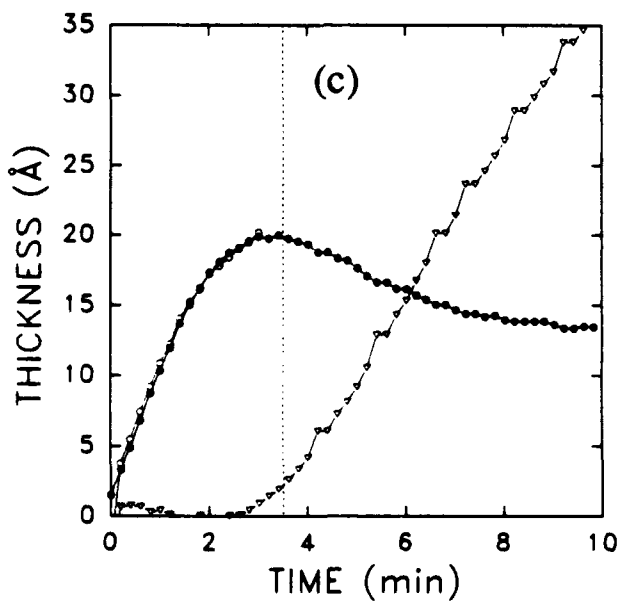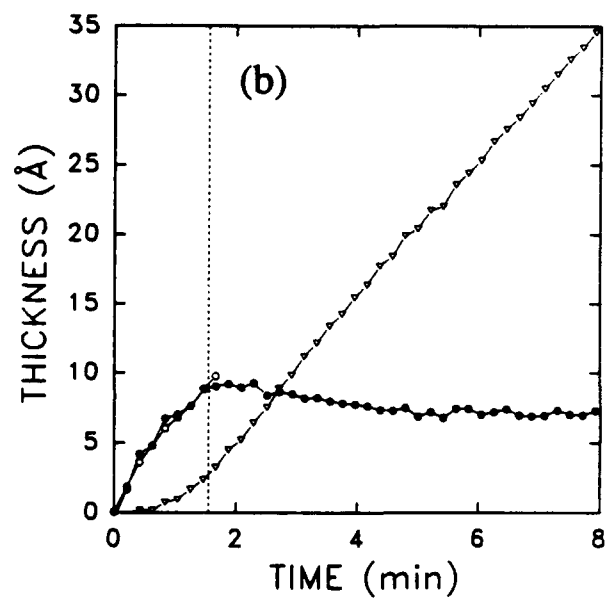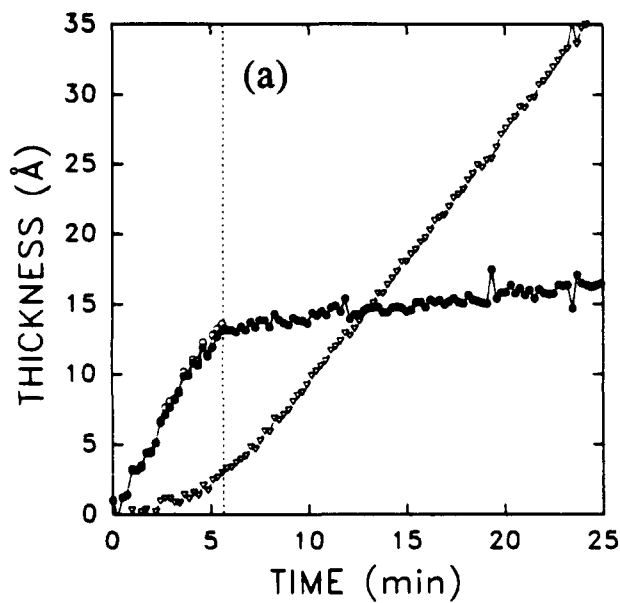
Growth and Epitaxy of Materials for Multilayer X-ray Optics

Jon M. Slaughter, Patrick A. Kearney, Judith A. Ruffner, and Charles M. Falco

Laboratory for X-Ray Optics, Optical Sciences Center
University of Arizona, Tucson, AZ 85721
Telephone: 602 621-2878   FAX: 602 621-4356

New material pairs are needed to provide useful mirrors at wavelengths where currently none exist, and to improve on performance at wavelengths where there are existing mirrors. In this paper we discuss our studies of selected new materials. Our studies take a surface analysis approach toward characterizing reactions at interfaces, the sharpness of interfaces, and the effect of the thin film growth mode on roughness. The studies were carried out in molecular beam epitaxy systems for two reasons: to study epitaxial growth of promising materials as a step toward single-crystal multilayer mirrors, and to exploit the powerful analytical tools available for surface analysis in a UHV environment. Growth of Be-, and B-based materials pairs have been studied with a wide variety of techniques including Auger, XPS, RHEED, LEED, and STM with the goal of determining interface structure, overlayer morphology, and crystal structure.

B-based

The Ag/B material pair is of interest as a candidate for a superlattice x-ray mirror. Attempts to grow epitaxial B, the first step toward growing a superlattice, have been unsuccessful. Amorphous B films were formed upon deposition of B onto various substrates at temperatures < 200 °C. Although this amorphous structure has precluded further progress toward B-based superlattices, high-quality amorphous multilayers would also be useful. We have found that Ag tends to deposit in rough crystallites on B, however, since lattice match is not important for amorphous materials, a variety of other metals can be considered.

The Pd/B system attains a high theoretical reflectivity (~60%) over a wide range of wavelengths above the B K-edge (at 67 Å). Although the binary phase diagram for the Pd/B system contains several compounds, calculations show that B based mirrors layered with Pd_5B_2, the most B-rich phase in the diagram, have an ideal reflectivity almost as high as that of Pd/B.[1] We have grown several test multilayers by alternately depositing Pd and B. Characterization during growth with RHEED indicates that the layers are nearly amorphous, i.e., they have very small crystallites. In addition, initial characterization with low angle x-ray diffraction indicates

that the multilayers are of good quality with interfacial roughness on the order of a few Ångstroms. Separate growth mode studies, using AES, indicate that the Pd is deposited on B at ~50 °C, they react to form a compound Pd_xB, with $x \approx 2.4$. The reaction is very temperature dependent. Annealing at temperatures as low as 80 °C causes an increase in the B concentration in the Pd_xB overlayer but it seems to saturate quickly. Further experiments are underway to determine if the reaction stops at Pd_5B_2. Work remains to be done on this material system, but our initial results make the Pd_xB/B system look very promising.

A growth study of Si on B indicates little intermixing. This has encouraged us to make Si/B multilayers for $\lambda > 125$ Å where Si is the spacer and B acts as the absorber. Since the absorption of B is lower than that of most absorber materials used with Si, more layer pairs can contribute resulting in a narrow bandpass optic.

Be-based

Our studies of Be epitaxy were motivated by the desire to grow single-crystal multilayer x-ray mirrors. Such mirrors would have many advantages over the typical amorphous and polycrystalline multilayers. Epitaxial growth of Be thin films on single-crystal substrates is a first step toward single crystal multilayers.

Al_2O_3 (001) has a close 2:1 lattice match with hcp Be. A cut perpendicular to the [001] axis of sapphire reveals a triangular net of oxygen atoms with a spacing very nearly twice that of the spacing between the Be atoms in the hcp-Be (001) planes. The in-plane lattice mismatch between them is only 3.9%. Although such a mismatch is large by semiconductor standards, there are many examples of epitaxial metal growth with such mismatches present.[2,3]

Be films were grown in a Riber-1000 MBE growth chamber at a pressure of 2×10^{-10} torr. An effusion cell with a pyrolitic boron nitride (PBN) crucible was used to evaporate Be onto the sapphire substrates. The Be was deposited at a rate of 4.1 Å/minute onto substrates held at 10, 250, and 500 °C, and at 9 Å/minute onto substrates held at 10 °C for a total thickness of 1200 ± 200 Å for each sample. RHEED was used for *in situ* analysis of the samples before, during, and after deposition. The samples were analyzed *ex situ* with θ-2θ x-ray diffraction, x-ray rocking curve analysis, Seemann-Bohlin (S-B) x-ray diffraction, optical microscopy, and ion beam analysis with He^{++} and proton backscattering. The RHEED patterns indicate that the Be forms an epitaxial overlayer.

X-ray diffraction studies of these films also indicate that the Be has grown epitaxially on the sapphire substrates. High-angle θ-2θ diffraction showed only the Al_2O_3 (006) substrate peak

and Be (002) peak. The Be peak for the sample deposited at 10 °C and 4.1 Å/min had a full-width-at-half-maximum of 0.12°, which is only slightly larger than the measured instrumental broadening (FWHM = 0.07°). This narrow linewidth of the Be peak is consistent with the structural coherence of the film being limited only by its finite thickness. Furthermore, the rocking curve taken about the same Be peak has a FWHM of only 0.7° θ, demonstrating a very small mosaic spread for a metal film. Finally, analysis with our S-B diffractometer shows that the films have no polycrystalline component.

Films deposited onto ambient temperature substrates (10 °C) at rates of up to 9 Å/minute were epitaxial, structurally coherent, and smooth. Films deposited at temperatures at or above 250 °C are also epitaxial and coherent, but are rough due to islanding. The surface roughness increases with increasing temperature. The SEM reveals islands, some hexagonal in shape, making up the film deposited at 500 °C. Apparently the increased Be mobility afforded by the higher substrate temperatures promotes a three-dimensional growth mode. The discovery of a technique to grow Be epitaxially, coupled with its favorable optical constants give Be-based multilayers great potential for the development of superlattice x-ray optics.

REFERENCES

1. Patrick A. Kearney, J.M. Slaughter, and Charles M. Falco, Opt. Eng. 30, 1076 (1991).

2. B. Schmiedeskamp, B. Kessler, B. Vogt, and U. Heinzmann, Surf. Sci. 223, 465 (1989).

3. Hitoshi Homma, Kai-Y. Yang, and Ivan K. Schuller, Phys. Rev. B 36, 9435 (1987).

INTERFACE ROUGHNESS AND VOID FORMATION IN Si DEPOSITION AT LOW TEMPERATURES

D.J. Eaglesham and D.L. Windt,

AT&T Bell Laboratories, Murray Hill, NJ 07974

X-ray scattering from multilayers (such as Mo-Si) is to a large extent controlled by interface quality, which in turn is frequently controlled by surface morphology. Here we present a study of interface and surface morphology in both crystalline and amorphous Si layers deposited by evaporation in UHV at low substrate temperatures. For simplicity, the interfaces investigated are single monolayers of Ge, so that chemical effects are avoided. Amorphous Si films undergo morphological roughening and void formation, leading to apparent Si-Ge interface widths ≈5nm. In crystalline Si grown at the same temperature and deposition rate the roughness is considerably less marked, although localised void formation still occurs. Both the void density and the apparent interface width of single monolayers of Ge appears under these conditions to be linked to the thickness of crystalline Si deposited.

Si deposition onto clean Si substrates by evaporation in UHV from solid sources can lead to either amorphous or crystalline films depending on the deposition conditions. It has long been thought that there should be a minimum "epitaxial temperature" T_{epi} for crystalline deposition. The standard view of this transition in deposition behaviour [1] is a trade-off between deposition and surface diffusion: if the deposition rate exceeds the surface diffusion rate (weighted by some density of appropriate sites N_0) then the film will be amorphous:

$$N_0^2 D_0 \exp\{-E_{act}/k_B T\} < R: \text{Amorphous}$$

Given a thermally activated diffusion process, this leads to an epitaxial temperature:

$$T > -E_{act}/\{k_B \ln[R/N_0^2 D_0]\}: \text{Epitaxy}$$

(Note that the $1/\ln R$ gives a rather slow rate dependence of this critical temperature). Surprisingly (given the significance of T_{epi} in limiting our ability to suppress segregation of dopants in Si MBE, the so-called "doping problem") the reported values of T_{epi} vary over a wide range. We have recently shown that this is a consequence of a previously-unsuspected phenomenon, limited-thickness epitaxy [2]. In fact, for a given temperature and deposition rate Si films on clean Si(100) substrates are always initially crystalline, and epitaxial growth proceeds up to an epitaxial thickness at which the amorphous phase forms. We have shown elsewhere that this phenomenon is widespread in semiconductor MBE [3] and has important applications in totally suppressing dopant segregationphenomena [4]. Here we use the effect as a tool which allows us to investigate interface quality in crystalline and amrphous films grown under identical deposition conditions (rate

and substrate temperature) by looking both above and below the transition from epitaxial to amorphous deposition.

Si films were grown in a UHV chamber with a base pressure typically $\approx$1-3x10^{-10} Torr and a pressure during deposition of $\approx$1-5x10^{-9} Torr (depending on the deposition rate). Si(100) substrates were cleaned either by the usual desorption of a chemical oxide or by desorption of H from a Si surface H-passivated *ex-situ* with an HF dip [5], but in both cases the starting surface for low-temperature deposition was grown by standard Si MBE at "high" temperature ($\approx$550°C). Deposition rates varying from 0.1Å/s to $\approx$50Å/s were obtained using electron-beam evaporation of a Si charge in the usual way. The role of growth mode and morphology in controlling interface quality was investigated by the deposition of single monolayers of Ge. Ge deposition on Si follows a Stranski-Krastanow growth mode, in which Ge islands will form only after the surface has been wetted by 3 monolayers of Ge [6], so that regardless of the surface diffusion coefficient Ge should follow the Si surface morphology. For the low temperatures we are concerned with here (150-300°C) Ge segregation to the Si surface is a measureable but small effect [7] so that the final buried layer of Ge represents the degree to which Si surface morphology controls the interface in the absence of significant chemical effects. Buried Ge layers were then studied using cross-sectional transmission electron microscopy (XTEM) on samples prepared by mechanical polishing to 3Γ μm and subsequent ion-beam milling to perforation using 2-5kV Ar$^+$ ions.

FIG. 1. Ge monolayers either side of the amorphous-crystalline interface showing the large increase in surface roughness for a-Si over c-Si for a given deposition rate and temperature. Roughness produced by geometric shadowing in a-Si appears to dominate this increase.
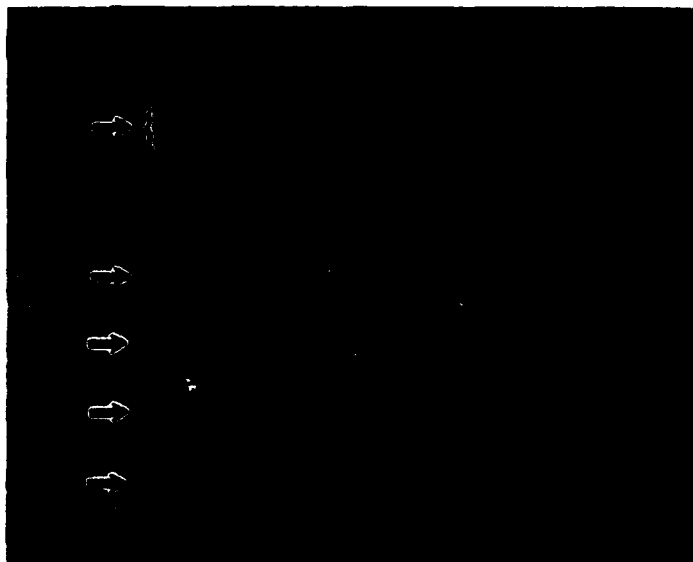
The difference between Ge monolayers in a-Si and c-Si is strikingly seen in Fig. 1. We associate the abrupt increase in the width of the Ge monolayers after the transition from crystalline to amorphous with the very rough morphology known to occur in a-Si films deposited under these conditions. This well-known phenomenon has been investigated by a number of authors and has been attributed to the catastrophic roughness achieved by a surface growing under diffusionless conditions where the deposition flux forms a slightly-collimated beam at an angle to the substrate normal [8,9]. The combination of negligible diffusion and non-

isotropic incident atom flux leads first to statistical roughness and then to local shadowing of any valleys that form: since the lower regions see less incident flux, surface roughness should then increase without limit. Ultimately this catastrophic roughness can lead to the formation of chains of voids in the film, and TEM analysis of deposited a-Si has shown these to be present in high densities. It is interesting to note that the interface width seen in these Ge monolayers ($\approx$5nm) is well in excess of that usually seen in a-Si/Mo multilayers. Since the latter are generally deposited by sputtering, it could be inferred that this is a consequence of the greater collimation of the deposition flux in an MBE system: however, the theoretical treatments show a rather weak dependence on the angular spread in the beam. It should also be noted that while theoretical models show a surface roughness that increases without limit during deposition, the observed Ge monolayer width (and hence presumably the height deviations of the a-Si surface) are all constant once the amorphous phase has formed.

In c-Si growth at the same rate and temperature the Ge monolayers always appear sharper. Although Si surface diffusion coefficients on a-Si are not known, it might be expected that the lower dangling bond density of a reconstructed c-Si surface would increase diffusion rates. Measurements of the width of the monolayers suggest that surface roughness is increasing during low-temperature deposition from the original (100) facet prepared at high temperature. Since diffusion is extremely limited even on the crystalline surface at these temperatures, we might expect to see some roughness arising from similar mechanisms to those in a-Si. Indeed, it could be argued that roughness on a length scale well in excess of the diffusion length should not be hindered by diffusion, so that this surface should also get rougher without limit. This does not appear to be the case, and surface roughness remains lower than that seen in a-Si up to the point at which the amorphous phase forms (probably the surface energy terms stabilising the (100) facet are sufficient to reduce this effect), but void chains are observed in c-Si deposition at low temperature (see [10] and Fig. 2), the density of these features increasing as the film gets thicker.

FIG. 2 Void chains in c-Si deposited at low temperature, showing that although the surface remains far smoother, similar shadowing mechanisms are present in this system.

Surface roughness linked to geometric shadowing thus follows the broad trend expected, with a-Si showing far more marked roughness than that seen in c-Si, but several details of the phenomenon remain confusing. In both a-Si and c-Si the tendency for roughness to increase once geometric shadowing has become significant is far less strong than expected, and in a-Si the apparently reduced roughness seen for sputtered films differs from theoretical predictions. It is fairly clear that even in the absence of interfacial reactions or interdiffusion geometric roughness can become large enough to dominate X-ray scattering from multilayers, but a deeper understanding of the phenomenon is required to improve the predictive capabilities of existing models.

REFERENCES

[1]   J. A. Venables in *Epitaxial Growth, Part B*, Ed. J.W. Matthews, Academic Press, New York, 1975, p. 389.

[2]   D.J. Eaglesham, H.-J. Gossmann and M. Cerullo, *Phys. Rev. Lett.* **65**, 1227 (1990).

[3]   D.J. Eaglesham, H.-J. Gossmann, M. Cerullo, L.N. Pfeiffer and K.W. West, J. Cryst. Growth **111**, 833 (1991).

[4]   H.-J. Gossmann, E.F. Schubert, D.J. Eaglesham, and M. Cerullo, *Appl. Phys. Lett.* **57** 2440 (1990)

[5]   D.J. Eaglesham, G.S. Higashi and M. Cerullo, Appl. Phys. Lett. 59 685 (1991)

[6]   H.-J. Gossman, L.C. Feldman, and W.M. Gibson, *Surf. Sci.* **155**, 413 (1985).

[7]   S. Fukatsu, K. Fujita, H. Yaguchi, Y. Shiraki, and R. Ito, *Appl. Phys. Lett.* **59**, 2103 (1991) and references therein.

[8]   R.P.U. Karunasira, R. Bruisma, and J. Rudnick, *Phys. Rev. Lett.* **62**, 788 (1989).

[9]   G.S. Bales and A. Zangwill *Phys. Rev. Lett.* 63, 692, (1989), and *J. Vac. Sci. Technol.* **A9** 145 (1989).

[10]   D.D. Perovic, J.-P. Noel, D.C. Houghton and G.C. Weatherly, *Proc. 1st Topical Symp. on Si based heterostructures*, AVS Toronto (1990).

In-Situ Grazing Incidence X-Ray Diffraction During Sputter Deposition

B.M. Clemens, A.P. Payne, T.C. Hufnagel, J.A. Bain,
Department of Materials Science and Engineering, Stanford University, Stanford, CA
S. Brennan,Stanford Synchrotron Radiation Laboratory, Stanford, CA

Many aspects of thin film growth can be studied most directly using *in-situ* techniques. These include a host of critical phenomena which are only observed for very thin layers and are no longer available for study if the film is grown to bulk levels. Although sputter deposition is a very widely used deposition technique both in research and industry, *in-situ* studies of film growth during sputter deposition are rare. This is primarily because the sputtering gas precludes the use of conventional electron diffraction techniques. Photon based diffraction techniques, on the other hand, are immune to the deleterious effects of the argon sputtering gas and offer a powerful method for investigating film structure provided a source of sufficient brightness is used. We recently performed experiments in which grazing incidence x-ray scattering (GIXS)[1] using synchrotron radiation was implemented *in-situ* to study film growth by sputter deposition . A special UHV deposition chamber was developed with appropriate x-ray windows and precision sample positioning mechanisms needed in performing a diffraction experiment[2]. During the initial test of this new technique and apparatus, we examined two metal/metal systems: gadolinium/cobalt and molybdenum/nickel.

Though a number of rare earth/transition metal binary systems have been found to react in the solid state at interfaces to form an amorphous product[3, 4], the mechanism by which this occurrs is not fully understood. The large negative heat of mixing and atomic size mismatch associated with the Gd/Co system suggest that it is an likely candidate for solid state amorphization[5]. We set out to observe the dynamics of such a reaction *in-situ*. Crystalline films of both Gd and Co were deposited examined using the GIXS technique. Small amounts of the complementary element were subsequently deposited and the effect on the crystallinity of the underlayer was studied. It was found that while Gd deposited on Co has no significant effect on the crytallinity of the Co, Co deposited onto Gd rapidly diminished crystallinity in the Gd producing an amorphous structure. This demonstrated

a strong diffusional asymmetry between the constituents and that Co is the active diffusing species during the reaction. The *in-situ* nature of the experiment clearly elucidated another important feature of the amorphization reaction: it occurs concurrently with deposition. Comparison of the time needed to form an amorphous alloy by bulk diffusion suggests that the diffusivity of Co is strongly enhanced by the high surface mobility of arriving Co atoms at the free surface of the Gd.

In-situ work on the Mo/Ni system was stimulated by the sudden disappearance of high angle supperlattice lines in multilayers as the bilayer period is reduced from 20 to 15 Å (1/1 component ratio)[4]. Since the presence of high angle superlattice lines is contingent upon sharp crystalline interfaces between the constituents[6], their sudden disappearance suggested the presence of a disordered interface phase existing only during the first few monolayers of growth. In-situ examination of this ultra-thin regime of film growth revealed an entirely different mechanism. Large, compressive, crystallographically anisotropic strains were observed in molybdenum films which would suddenly vanish as the Mo layers were grown past approximately 14Å. Correlated broadening of the peaks indicated a significant degree of inhomogeneous straining. In contrast, strains in the Ni films were essentially constant as a function of thickness. We suspect that this behavior is caused by epitaxial island growth of Mo on Ni during the inital stages of Mo deposition, a growth mode confirmed in other studies[7]. The dramatic relaxation observed in the Mo is associated with island coalescence. Because of the relaxation available at the free surface of an island, in-plane epitaxial strains will lead to inhomogeneous straining both parallel and perpendicular to the interface through the Poisson effect. Modeling of superlattice spectra confirms that a variation in d-spacing through the thickness of individual Mo layers leads to the same quenching of the high angle peaks observed experimentally[8].

References

[1] P.H. Fuoss and S. Brennan. *Annu. Rev. Mater. Sci.*, 20:365, 1990.

[2] A.P. Payne, B.M. Clemens, and S.M. Brennan. *Rev. Sci. Instr.*, accepted for publication, 1991.

[3] F. Spaepen. *Mat. Sci. Eng.*, 97:403–8, 1988.

[4] B. M. Clemens. *J. Less. Comm. Met.*, 140:57–66, 1988.

[5] B.M. Clemens and R. Sinclair. *MRS Bulletin*, XV(2):19–38, 1990.

[6] B. M. Clemens and J. G. Gay. *Phys. Rev. B*, 35:9337, 1987. Rapid Communication.

[7] Y.H. Lee, R.P. Burns, J.B. Posthill, K.J. Bachmann. *Mat. Res. Soc. Symp. Proc.*, 160:215–220, 1990.

[8] E.E. Fullerton, I.K. Schuller, H. Vanderstraeten, Y. Bruynseraede. submitted, *Phys. Rev. B*, 1991.

STABILITY OF METALLIC SUPERLATTICES

P. E. A. Turchi and M. Sluiter, LLNL, Condensed Matter Division (L-268), P.O. Box 808, Livermore, CA 94550 (tel: 510-422-9925).

With the constant progress made in designing and manufacturing materials with composition modulation in one dimension on an atomic scale [1], artificial superlattices have opened up new opportunities to study both theoretically and experimentally a wide range of properties. This new class of materials consist of a sandwich of layers of different species or mixtures thereof, and with the development of atom by atom deposition techniques, composition, layer repeat period, growth orientation and chemical order may be controlled. Such atomic engineering has led to the discovery of new phenomena such as the supermodulus effect [2], giant magneto-resistance effect [3] and also complex phenomena at or near interfaces such as solid state amorphization [4]. Moreover, unusual properties are expected in one dimensional quasiperiodic multilayers [5].

Despite these attractive phenomena, little is still known about the thermodynamic state of these materials. It is widely acknowledged that most superlattices are in states far from equilibrium and that effects pertaining to strain and chemistry play a major role. Strain effects are revealed on an atomic scale near interfaces or in the presence of composition gradients, on a mesoscopic scale due to the presence of extended defects such as dislocations, and finally, on a macroscopic scale, due to external stress, thermal gradients and inhomogeneities. On the other hand, chemical effect, as discussed in the present study, pertains to short range interactions between like or unlike species. The knowledge of these interactions allows one to study the well known phenomena of ordering or clustering in bulk alloys. Retaining effects on an atomic scale, strain and chemical order effects can be well described within a so-called generalized 3-dimensional Ising model. Such a model has been very successful in studying the thermodynamics of bulk alloys, starting from a first principles description of their electronic structure properties [6]. Although the present work pertains to idealized superlattices, in the sense that interfaces are considered sharp and perfect, lattice mismatch, relaxation effects and magnetism are ignored, the theoretical predictions can already serve as guidelines for further experimental investigations in the field, before a more complete treatment is proposed.

Let us first show how the formalism developed for bulk systems may apply for a 3-dimensional multilayer topology by describing its stability properties with a one dimensional Ising model.

METHODOLOGY

Let us specify a particular configuration of a bulk alloy $A_{1-c}B_c$ by a set of occupation numbers $\{p_n\}$ (where $p_n=1(0)$ if site n is occupied by a B(A) species). By applying a perturbation technique, the so-called Generalized Perturbation Method (GPM) to an appropriate reference medium, namely the completely chemically disordered state, as described by the Coherent Potential Approximation (CPA), the total energy of a specific alloy configuration can be expressed as the sum of two terms: (1) the energy of the random state $E_{dis}(c)$ which is concentration dependent but configuration independent, and (2) the ordering energy $\Delta E_{ord}(\{p_n\})$ which is associated with the deviation from randomness, i.e. the degree of long or short range order.

Within this approach, the ordering energy is written as an expansion in terms of pair and many-body interactions, which are concentration dependent and derived from the electronic structure properties of the random medium within, for example, the multiple scattering formalism of the Korringa Kohn Rostoker (KKR)-CPA [6]:

$$\Delta E_{ord}(\{p_n\})= \frac{1}{2}\sum_{nm} V_{nm}\, \delta c_n\, \delta c_m + \frac{1}{3}\sum_{nml} V_{nml}\, \delta c_n\, \delta c_m\, \delta c_l + ...$$

where $\delta c_n = p_n - c$ is the concentration deviation at site n

Usually the many-body interactions are negligible and the pair interactions converge rapidly with distance. For a perfectly ordered configuration, at T=0 K, the ordering energy takes the simple form:

$$\Delta E_{ord}(\{p_n\}) \approx \sum_s q_s V_s \quad \text{with } q_s = \frac{c}{2}(n_s^{BB} - c n_s)$$

where the sum runs over the neighbor shells s, n_s^{BB} and n_s refer to the number of BB pairs and total number of pairs, per site, associated with the sth neighbor shell. V_s is a sth neighbor effective pair interaction given by: $V_s = V_s^{AA} + V_s^{BB} - 2V_s^{AB}$ Therefore a positive (negative) V_s favors unlike (like) species betwen an atom at origin and its neighbors in the sth shell.

Since artificial superlattices are materials in which layers are alternately occupied by different species, it is meaningful to describe them one-dimensionally. Each crystallographic plane, normal to the direction of the composition modulation ñ is labeled with an integer j. Let α_s^j be the number of sth neighbors of a site on the plane $j = j_0$ that are located on the plane with $j = j_0 + i$. Note that these numbers depend on the direction ñ of the composition modulation and on the lattice under consideration. Hence the ordering energy can be rewritten as:

$$\Delta E_{ord}(\{p_n\})= \frac{N_{plane}}{2N_{cryst}} \sum_{j_0} \sum_s \sum_j \alpha_s^j V_s\, \delta c_{j_0}\, \delta c_{j_0+j}$$

where N_{plane} and N_{cryst} are the number of sites on the particular crystallographic plane which characterizes the growth orientation and the number of sites in the crystal, respectively. Let us define an interplanar interaction P_j as follows:

$$P_j = \frac{1}{2}\sum_s \alpha_s^j V_s \text{ for } j=0 \text{ and } P_j = \sum_s \alpha_s^j V_s \text{ for } j \geq 1$$

Since the configuration of the superlattice is periodic, summations may be restricted to those planes within one period of L planes, and:

$$\Delta E_{ord}(L)= \sum_{j \geq 0} \beta_j(L) P_j \quad \text{where } \beta_j(L)= \frac{1}{L} \sum_{j_0=1}^{L} \delta c_{j_0}\, \delta c_{j_0+j}$$

If the repeat period L=2n, where n is the number of layers occupied by A species, then $\beta_j(n) = (n-2j)/4n$, $n \geq j$ and $\beta_{j+n}(n) = -\beta_j(n)$. It can also be shown that for large value of n, the ordering energy becomes a linear function of 1/n [7].

Hence, by mapping the effective pair interactions V_s of a 3d-lattice to interplanar interactions P_j, one can use the ground state analysis for the linear chain [8] to determine which particular composition modulation is the most stable. Except for high index ñ (not of great interest, in practice), the properties of α_s^j combined with the fast convergence of the V_s with s, lead to a rapid decay of the interplanar interactions with

distance; for example, for ñ=<110> on the bcc lattice, V_{10} is the first interaction to contribute to P_6.

Let us now consider a coherent interface between two pure components A and B. The corresponding interfacial energy per unit area can be expressed in terms of the previously introduced configurational parameters as follows:

$$E^{\{hkl\}}=\frac{1}{S^{\{hkl\}}}\sum_s q_s^{\{hkl\}}V_s$$

where $S^{\{hkl\}}$ is the area per atom pertaining to the interfacial plane specified by the indices {hkl}, and:

$$q_s^{\{hkl\}}=-\frac{1}{4}\sum_{i\geq1} i\ \alpha_s^i$$

where i refers to a particular plane parallel to the interface.

RESULTS

The first principles KKR-CPA-GPM [6] approach was used to compute effective pair interactions for a number of bcc-based equiatomic alloys, in their non-magnetic state. The interactions V_s up to s=7 and the resulting ordering energies of superlattices with composition modulations in the <100>, <110> and <111> directions, and layer thicknesses n from 1 to 7 as well as n infinity (phase separation case) were thus obtained. Note that many observed bulk ordered structures can be viewed as superlattices with composition modulation in one direction only; for example B2 (of CsCl type): ñ=<100> or <111> and n=1, B32 (of NaTl type): ñ=<111> and n=2, B11 (of PbO type): ñ=<100> and n=2. For c=1/2 and interactions P_j extending to the fourth neighbor distance, there exists 5 possible ground states for the linear chain [8], namely those configurations associated with n ranging from 1 to 4 and AABABBAB (referred to as n=4/3). We show in the Figure, as an example [7], the ordering energies, in mRy/atom, as a function of 1/n for (a) TiFe and (b) TiCr, and 3 low-index composition modulation directions of the bcc lattice: <100> (solid line), <110> (dash dotted line) and <111> (dash triple dotted line).
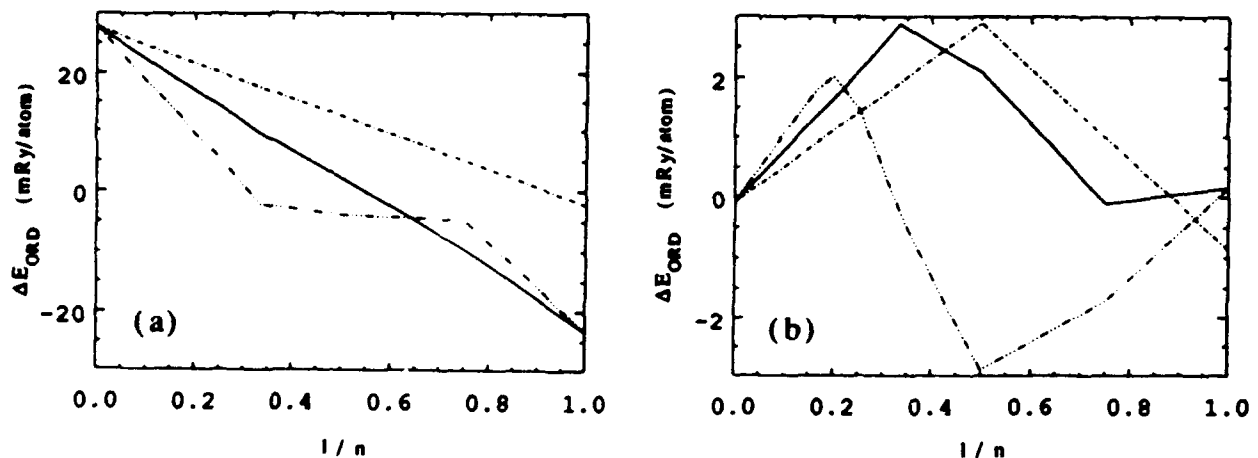
Among the interesting features of the $\Delta E_{ord}(1/n)$ curves, note the local minimum for TiCr at n=2 (ñ=<111>) corresponding to a predicted bulk ordered phase B32, and the flat region for n ranging from 4/3 to 3 (ñ=<111>) for TiFe. These typical behavior can be interpreted as follows: in the case of TiCr, superlattices characterized with e.g.

ñ=<100> and n=2 will be relatively unstable and should transform easily. On the contrary, for TiFe, any metastable superlattice for ñ=<111> and n ranging from 4/3 to 3 have little driving force for a transformation. Note, however, that in the case of a strongly ordered bulk alloy such as TiFe, a large amount of energy can be stored by producing a highly unstable superlattice with e.g. ñ=<110> and n=5 which, by comparison with the ground state energy of the alloy, corresponds to about 40 mRy/atom. Such an artificially ordered superlattice, preferably obtained by depositing on a cold substrate, could very exothermally transform to the stable B2 structure or become amorphous. In a more broader context, atom by atom deposition techniques may offer a unique way of designing metastable ordered configurations which are not accessible by conventional metallurgical approaches.

The effective interactions were used to estimate interfacial energies (in mRy/a^2, where a is the lattice parameter) for selected equiatomic bcc-based alloys and for some low-index planes (see Table below). It was found that: (1) strong tendencies toward order in bulk alloys lead to the existence of energetically favorable interfaces, (2) interfacial energies weakly depend on the orientation of the interfacial plane as a result of a similar property for the geometrical ratio $q_s^{\{hkl\}}/S^{\{hkl\}}$.

alloy	interfacial plane 100	110	111	311	331	210
AlNi	-55.7	-43.2	-51.2	-53.4	-48.3	-52.4
TiFe	-53.9	-43.1	-51.9	-51.7	-48.4	-50.6
VFe	-18.6	-17.9	-19.1	-18.8	-19.0	-18.8
TiCr	8.81	8.59	6.71	7.36	7.97	8.36
VCr	-6.03	-4.28	-5.37	-5.57	-4.91	-5.43
TiNi	-15.5	-17.4	-18.0	-16.8	-18.1	-16.7
TiV	6.36	5.47	5.36	5.70	5.60	5.99
CrFe	2.65	-1.47	0.44	0.90	-0.65	0.73

An approach has been presented for the study of the thermodynamic stability properties of artificial superlattices. General expressions have been derived for the configurational energy as a function of the superlattice parameters, and also for the interfacial energy. Finally, the relationship between some artificial superlattices and naturally occurring ordered phases has been briefly discussed.

REFERENCES

1. see e.g. T. W. Barbee in MRS Bulletin XV, no. 2, p. 17 (1990).
2. M. L. Huberman and M. Grimditch, Phys. Rev. Lett. **62**, 1403 (1989) and references therein.
3. M. N. Baibich et al., Phys. Rev. Lett. **61**, 2472 (1988).
4. R. B. Schwarz and W.L. Johnson, Phys. Rev. Lett. **51**, 415 (1983).
5. J. Birch et al., Phys. Rev. B **41**, 10398 (1990).
6. P. E. A. Turchi et al., Phys. Rev. Lett. **67**, 1779 (1991) and references therein.
7. M. Sluiter and P. E. A. Turchi, submitted to Phys. Rev. B (1991).
8. M. Kaburagi and J. Kanamori, Prog. Theor. Phys. 54, 30 (1975); A. Finel, Thèse d'Etat es Sciences Physiques, University Paris VI, unpublished (1987).

Elastic Properties of Strained Metallic Superlattices

D.Ariosa

Institut de physique, Université de Neuchâtel,
Rue A.-L. Breguet 1
CH-2000 Neuchâtel, Switzerland
(fax:41-38-244913)

Due to the improvement of metal deposition techniques in the last ten years, high quality epitaxial metallic superlattices made from non soluble materials with different crystal structures and important lattice mismatches are now available for varied applications. One exciting aspect of this kind of superlattices,among others, is their novel elastic properties (different from those of the constituents or their eventual alloys) due to the lattice deformation caused by epitaxial stress. As an example, one can cite the average lattice expansion in the growth direction and the softening of the sound velocity that have been reported for Mo/Ni superlattices[1, 2]. The above papers have been chosen because, as we will see later, they illustrate some controversial interpretation of X-Ray diffraction data and sound velocity measurements.

Indeed, in ref.[1], the authors compare the intensity of satellite diffraction peaks with two model calculations assuming, respectively, uniform strain in Ni layers and localized strain at the Mo/Ni interface. The calculated behavior in function of the modulation wavelength is almost the same regardless of the initial assumption. However, they have chosen the lattice expansion interpretation in view of the abrupt correlated collapse of structural and transport parameters observed below a certain critical wavelength, in the framework of a model of structural transformation induced by the uniform deformation of the Ni lattice.

On the other hand, authors in ref[2], interpret the same behavior in a completely opposite way. They introduce a model of interfacial localized strain, and they fit the linear behavior of the relative average lattice expan-

sion in function of the inverse modulation wavelength. Furthermore, they fit also the wavelength dependence of the sound velocity, relating interface expansion to metallic adhesion. In the present contribution, we propose an alternative interpretation, based on our earlier model[3, 4] of partially coherent growth of metallic superlattices. In ref.[3, 4], an interplay between coherency strain, interdiffusion and misfit dislocations was assumed. One important result in this work was the prediction of a crossover between coherent to partially coherent growth at some critical wavelength, presumably related to the structural changes reported in refs[1, 2]. Here we will calculate the relative lattice expansion in function of the modulation wavelength $r(\Lambda)$ and the related sound velocity $v(\Lambda)$ assuming uniform deformation. A simplified version of the model can be used when dealing with sharp interfaces (no interdiffusion) as in the Mo/Ni samples of refs.[1, 2]. Let us consider a uniformly strained superlattice with sharp interfaces. It is clear that, depending on the relative stiffness and Poisson ratio of the materials, the relative expansion r can range from $-\epsilon_0$ to $+\epsilon_0$, where ϵ_0 is the relative mismatch defined by:

$$\epsilon_0 = \frac{d_0^A - d_0^B}{d_0^A + d_0^B} \tag{1}$$

d_0^A and d_0^B being the unstrained lattice constants in the growth direction. Since our purpose is just to reproduce the $r(\Lambda)$ behavior qualitatively, we will use a very easy set of assumptions: symmetric strain and identical elastic modulii.

The strategy consists in minimizing the total elastic energy density u including dislocations. One can write for u [3, 4] :

$$u = \frac{E}{1 - \nu}\epsilon_{xy}^2 + \frac{4u_0}{\Lambda\delta} \tag{2}$$

where E is the Young modulus, ν the Poison ratio, ϵ_{xy} the in-plane strain, u_0 the energy per unit length of a line dislocation and δ the average spacing of the dislocation network depending on the actual mismatch (reduced from ϵ_0 via the strain). By identifying δ with the coincidence lattice spacing, one can express it in terms of ϵ_{xy} as follows:

$$\delta = \frac{d_0(1 - \epsilon_0^2)(1 - \epsilon_{xy}^2)}{2(\epsilon_0 - \epsilon_{xy})} \tag{3}$$

Reporting this last expression in the energy density, and minimizing with respect to the strain, we obtain:

$$\epsilon_{xy} = \frac{B}{2\Lambda} \frac{1 - 2\epsilon_0\epsilon_{xy} - \epsilon_{xy}^2}{(1 - \epsilon_{xy}^2)^2} \tag{4}$$

with $B = \frac{8u_0(1-\nu)}{d_0(1-\epsilon_0^2)E}$. The equation for ϵ_{xy} admits no solution below a certain critical wavelength, and gives the almost linear behavior of ϵ_{xy} in function of $\frac{1}{\Lambda}$ as observed experimentally [see figure 1]. Since r is proportional to ϵ_z, which is proportional to ϵ_{xy}, we can fit, above the critical wavelength, the relative expansion with:

$$r(\Lambda) = \gamma/\Lambda \tag{5}$$
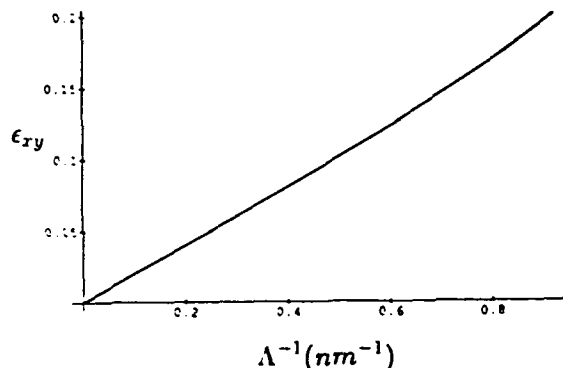
Fig. 1

We now introduce a simple model in order to relate the uniform expansion with the stiffness constant, and thus with the sound velocity:

let us take a Lennard-Jones potential for the ion- ion interaction in the growth direction:

$$V_0(z) = -U(\frac{2}{a_0 z} - \frac{1}{z^2}) \tag{6}$$

When the crystal is uniaxially expanded, one can calculate the 1-dimensional resulting potential for the ion at the origin:

$$V(z) = V_0(z + a) + V_0(z - a) \qquad ; \quad a = a_0(1 + \epsilon_z) \tag{7}$$

The resulting stiffness constant is calculated as the second derivative at the origin and takes the value:

$$E(\epsilon_z) = E(0)\frac{1 - 2\epsilon_z}{(1 + \epsilon_z)^4} \tag{8}$$

thus for the sound velocity one obtains the relation:

$$\left(\frac{v(\epsilon_z)}{v(0)}\right)^2 = \frac{1 - 2\epsilon_z}{(1 + \epsilon_z)^4} = \frac{1 - 2\gamma\Lambda^{-1}}{(1 + \gamma\Lambda^{-1})^4} \tag{9}$$

From the diffraction data of ref[2]: $\gamma = 2.75 \ 10^{-2} nm$; the behavior of the sound velocity, depicted in figure 2, is in excellent agreement with the experimental data.
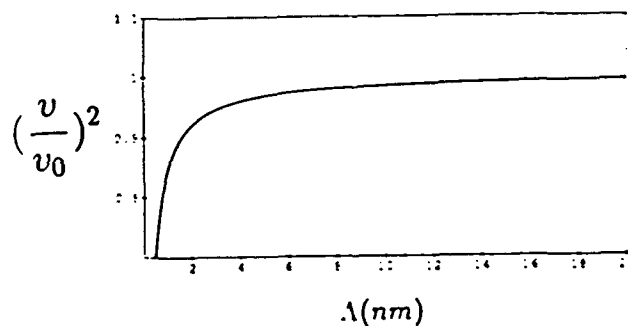

Fig. 2

In conclusion, we have shown that diffraction data and sound velocity measurements on metallic superlattices can be interpreted within a model of partially coherent growth, admitting strain in the center of the pure layers. Furthermore, the observed structural change below the critical wavelength was already predicted in our earlier work[4].

References

[1] M.R. Khan, C.S.L. Chun, G.p. Felcher, M. Grimsditch, A. Kueny, C.M. Falco, and Y.K. Schuller, Phys. Rev. B 27, 7186 (1983)

[2] B.M. Clemens and G.L. Eesley, Phys. Rev. Lett. 61, 2356 (1988)

[3] D.Ariosa, Ø. Fischer, M.G. Karkut, and J.-M. Triscone, Phys. Rev. B 37,2415 (1987)

[4] D.Ariosa, Ø. Fischer, M.G. Karkut, and J.-M. Triscone, Phys. Rev. B 37,2421 (1987)

X-ray Characterization

WB 7:30pm–10:15pm
Grand Room

Takeshi Namioka, *Presider*
NASA Goddard Space Flight Center

Multilayer X-Ray Mirror Absolute reflectivity,

Energy Band Pass and Overlapping Order Determination

Using an X-Ray tube and a Si(Li) Detector.

P. Dhez, LSAI and LURE, Université Paris Sud F-91405 ORSAY (France).
Present address: University of Arizona, Dept. of Physics,PAS81, TUCSON AZ 85721 (USA).
                Fax: (602) 621 4356 Tel: (602) 621 9716
H. Duval, Laboratoire de Physique des Solides, Bat.503, Université Paris Sud F-91405 ORSAY (France).
J.C. Malaurent, Laboratoire de Physique des Solides, Bat.503, *Université Paris Sud F-91405 ORSAY (France)*.

I. Introduction.

X-ray interference mirrors are a particular case of artificial multilayered media for which the wanted property is a high intensity of the diffraction phenomena itself. For such applications one needs to know the performance of the mirrors at different wavelengths. We would like to demonstrate here how such X-ray reflectivity tests can be achieved on a laboratory apparatus to get absolute reflectivity and without the need of a synchrotron source.

II. Angular and energy dispersive methods for multilayer reflectivity tests.

Considering the Bragg relation, it is useful to look on a plot showing the variation of the Bragg peak angles θ_N for each Bragg order N versus the photon energy E. For a periodic medium having a periodicity $d = 50\text{Å}$ that we will consider later, the curves on figure 1 illustrate the case of the 5 to 35 KeV energy range. On the horizontal plane are drawn curves corresponding to the projected top of the peaks of the different Bragg order positions. Typical reflectivity Energy and Angular Dispersives curves are schematically represented in figure 1 by using the vertical axis to plot the reflected intensity variation.
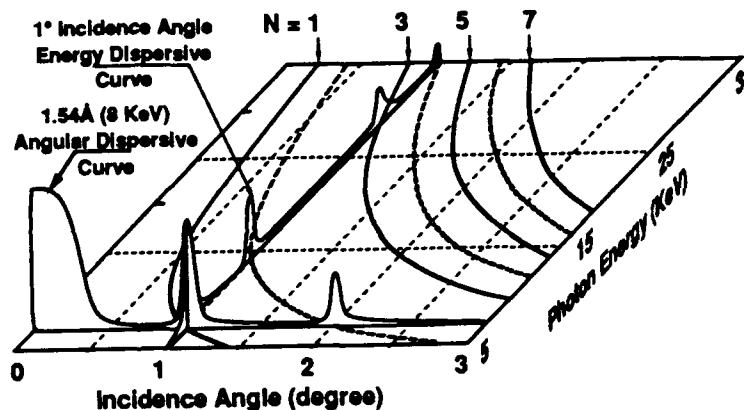
In the most used diffraction method for multilayers, which we call Angular Dispersive mode, one mesures, in a $\theta/2\theta$ mode, the specular reflected intensity of a monochromatic beam. On our graph, that appears like the curve drawn on a vertical plane parallel to the E axis. Another possibility, called Energy Dispersive, is to keep a fixed incidence angle θ. In such a case one measures the reflected intensity versus the energy E, but only for a single 2θ specular angular direction. On our graph that corresponds to the curve drawn on a vertical plane which is parallel to the θ axis. In fact these curves are two cuts of a 3D volume made of succesive curved chains of peaks and valleys.

In principle, from experimental data obtained by both methods one can deduce the structural characteristics of the multilayer if one is able to compare experimental reflectivity results to theoretical diffraction calculations. The different reflectivity calculation methods especially adapted to multilayered media have been compared elsewhere (1). Most of them are considering the case of Angular Dispersive experimental results and are oriented toward layering qualities determination. Using a monochromatic light one just needs to introduce two pairs of optical index values to optically characterize the constituents. Next, from the deduced structure, one can predict reflectivity at other wavelengths and incidence angles; but that supposes one knows the deposited material indice over all the energy range under consideration. By comparison, the data obtained by the Energy Dispersive method poses a quite opposite problem. We will show one can directly obtain experimentally the peak reflectivity, the band pass and overlapping order contribution at any energy of the spectra and at any angle of incidence. All this information is obtained experimentally and so does not need any optical index knowledge or structural hypothesis.

The main difference between the Angular and Energy Dispersive methods for collecting data is the way to record the reflected beam intensity.

For the Angular Dispersive measurements one needs a monochromatic beam. During the $\Theta/2\Theta$ scanning, one should continuously record the specular reflected beam intensity. That is difficult for two reasons. First, at grazing incidence angles, any slight misalignment of the sample on the rotation axis will appear on the reflected beam like a noticeable angular shift of the specular direction. In addition, during grazing incidence Θ scans, the illuminated surface of the sample changes noticeably. So, if the sample surface is not perfectly flat and has any slope errors, the reflected beam width fluctuates in an unpredictable manner. In consequence the photon intensity collected through a detector slit could change without link to a real reflectivity variation, and that perturbs the registred reflectivity curve. A large detector slit can avoid such errors but that is paid by a lower contrast on the reflectivity curves because scattered and fluorescence X-rays are collected. Systematic 2Θ scans for each incidence Θ angle can be used also to detect that, but they are time consuming. It seems the best way is to use no detector slit but rather a 1D position sensitive detector having a convenient spatial resolution (2, 3).

In the Energy Dispersive measurements one uses an incident polychromatic beam at fixed incidence Θ and one analyzes the energy distribution of the reflected beam in the corresponding, but fixed, 2Θ direction. In this mode one records a reflected spectrum without a moving source, sample or detector. For a given incidence Θ and a periodicity d, Bragg peaks corresponding to order N appear at energies E_N satisfaying the Bragg relation:

$$E_N(KeV) = 12400 \ N \ / \ 2d(\text{Å}) \ \sin\Theta.$$

To get such a spectrum versus energy it is better to avoid a scanning monochromator because that is time consuming. As demonstrated in 1968, by B.C. Giessen and G.E. Gordon on X-ray diffraction experiments, a Si(Li) detector coupled to a multichannel is an energy analyzer able to work over a large photon energy range (4). Compared to the multilayer band pass, a Si(Li) detector as energy analyzer has a convenient energy resolution. Energy Dispersive reflectivity tests using a Si(Li) detector were earlier achieved on surfaces and single layer coatings. These preceding experiments were not performed to get absolute reflectivity because the goal was only to evaluate the critical energy of total reflecting mirrors (5). More recently the method has been also used for relative reflectivity measurements on synthetic multilayers (6) and for magnetic multilayer period determination (7).

III. Energy dispersive reflectivity set up adapted to multilayered media tests.

We are interested in absolute reflectivity measurements, so as usually in such a case it is necessary to take care to: beam aperture, alignment and detector linearity response versus flux variation.

Our slit system set in the incident arm of a vertical axis goniometer provides a 0.3 degree divergence polychromatic beam which is convenient to cover a few centimeter long samples under glancing incidences. Our X-ray source is a Silver anode tube with a vertical focus line 8 mm height, and a 0.04 mm apparent width when seen under a 6° take off angle. After aligment, an X-ray film set on the detector entrance is used to check the symmetry of the obtained image and its vertical uniformity intensity distribution. An uniform vertical distribution is necessary because we are using different vertical height collimators like a neutral attenuator versus wavelength. That is because our goal is to make absolute reflectivity spectra so we need to keep the detector working in the linearity range of response for any direct or reflected beam intensity.

Figure 2a on the left is an example of a reflected spectrum and its corresponding direct spectrum; for presentation convenience both have been normalized to the top of the Ag characteristic line. Figure 2b on the right is the channel to channel ratio of the two preceding spectra but after having taken into account the slit height ratio used for each spectrum. In this figure the vertical scale corresponds to an absolute reflectivity coefficient versus energy.
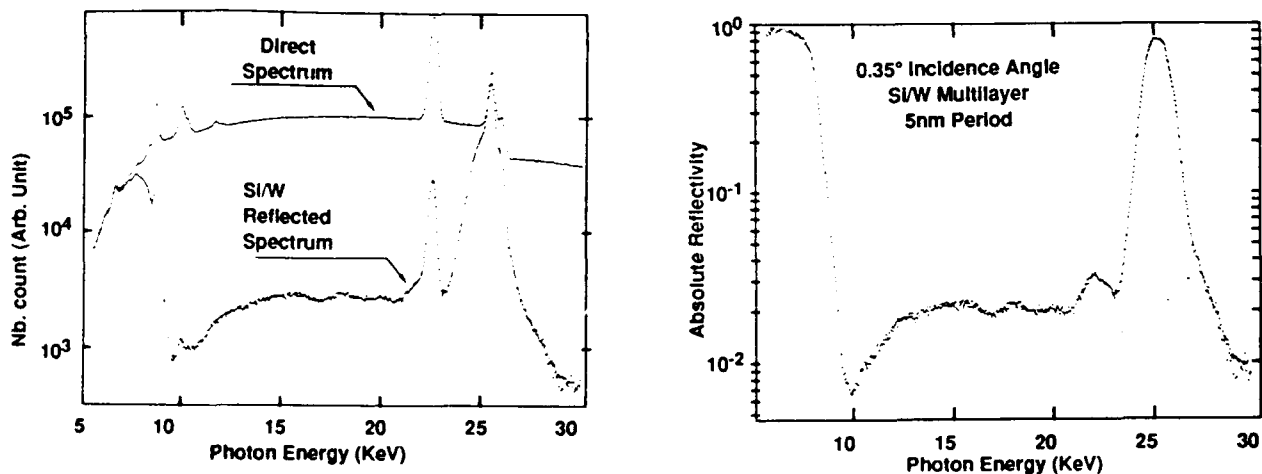
For very soft X-ray or extreme U.V mirrors it is not always possible to use an X-ray tube and a Si(Li) detector to evaluate the reflectivity for the designed wavelength, but the X-ray range is useful to study the deposited stack qualities. Like for the precedent W/Si mirror, the figure 7 is an example of Angular Dispersive reflectivity curve achieved at 1.54Å on a Mo/Si multilayer coated for an extreme U.V launchable telescope. Because this stack has a designed changing thickness of the absorbing layer from period to period, the peak to peak intensity variation of the secondary maxima is complicated. For this mirror, figure 8 shows the corresponding Energy Dispersive reflectivity curve. One time more one seen almost the same details. That confirm the two methods have potentially the same sensitivity and are able to bring the same amount of information.

We also used this multilayer to demonstrate how to measure the reflectivity variation around an atomic threshold of one of the constituent. Figure 9 is a detail of the Energy Dispersive reflectivity curve for which the incidence angle on this multilayer have been chosen in such manner that the center of the second Bragg peak corresponds to the Mo_K threshold energy. Because the Mo optical index is varying largely over an energy range much smaller than the half width of the Bragg peak, the reflectivity variation is seen directly as a step. In this case it is the Si(Li)resolution which determinates the energy width of the observed Mo index variation.
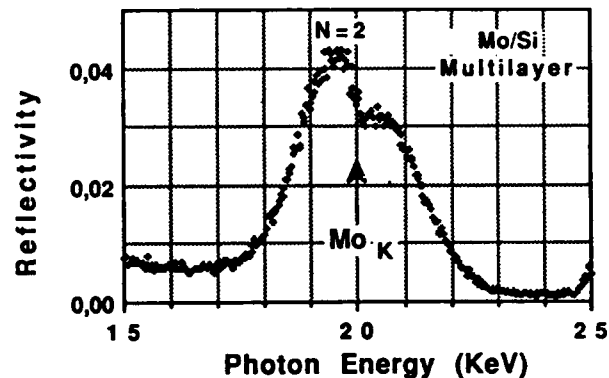
V. Conclusions.

Until to now the tests of the multilayered media structure by X-ray diffraction have been usually achieved by the Angular Dispersive method. This one is quite delicate to handle, but well adapted to structure studies. That is because the inverse calculation permitting to deduce the multilayer structure through the diffraction curve is done at a single energy and so need a single pair of optical index values. We demonstrated here that for multilayer studies another method, the Energy Dispersive Method, has the same potentially and is much easier to manage. Related theoretical methods for inverse calculation applied to the Energy Dispersive method are under development (8).

The Energy Dispersive Method is a very sensitive method. It could be very helpful close to a coating system, for comparing from multilayer to multilayer the progress achieved for period reproducibility and interfaces improvement. Inserting a multilayer at a reproducible incidence angle in a Energy Dispersive system, just looking to the Bragg peaks and to their relative intensities need few minutes to decide about qualities. Coating uniformity is also very easy and fast to study by this method. Last but not least, the Energy Dispersive method is certainly a good candidate to make an in-situ X-ray reflecting test inside a coating system. None movement is necessary for the incident beam or the detector and a classical X-ray tube provide enough photons. That is convenient to be use on sputtering systems because, using kapton windows, the X-ray tube and Si(Li) detector could be set at air pressure outside the vaccuum tank.

Concerning X-ray mirror calibration the Energy Dispersive Method seem the best. Without prior knowledge of any optical index values of the deposited materials it can directly provide experimental reliable values of the absolute peak reflectivity, band pass and overlapping order over all the X-ray range. Such calibration of X-ray multilayer mirror is especially important in case of use with a continuum source like synchrotron radiation or hot plasmas.

References.

1. B. Pardo, T. Megademini and J.M. André, Revue Phys. Appl., 23 (1988) 1579-1597.
2. P. Dhez, S. Megtert, M.F. Ravet and E. Ziegler, SPIE Proceedings Vol. 984 (1988) 89.
3. J. Corno, E. Dartyge, P. Dhez, A. Fontaine, A. Jucha, Y. Lepetre, SPIE Proceedings Vol. 733 (1986) 398.
4. B.C. Giessen and G.E. Gordon, Science 159 (1968) 973-975.
5. D.H.Bilderback, Proceedings SPIE Vol 315 (1981) 90-102.
6. J.C. Malaurent, H. Duval and A. Fert, J. Appl. Crystal.,20 (1987) 491-498.
7. J.C. Malaurent, H. Duval and P. Dhez, J. Magn. and Magn. Mat.,93 (1991) 164-168
8. J.C. Malaurent and H. Duval, accepted in Nouvelle Revue d'Optique.

## IV Experimental results and comparison between Angular and Energy Dispersive methods.

IV.1. X-ray mirrors.

Figure 4 is a reflectivity curve obtained by the classical Angular Dispersive method in the case of the same W/Si interferential X-ray mirror than before. This absolute reflectivity curve has been achieved at the most frequently used 1.54Å Cu K_α line (8 KeV) selected by a crystal monochromator. Figure 5 is the Energy Dispersive reflectivity curve corresponding to the same multilayer. In this case, the incident angle has been chosen to get the first Bragg peak centered on the Cu K_α emission line energy used on the previous Angular Dispersive test. These two reflectivity curves correspond to those of figure 1 where the two indicated sections intersect on the top of the first Bragg peak at 8 KeV.
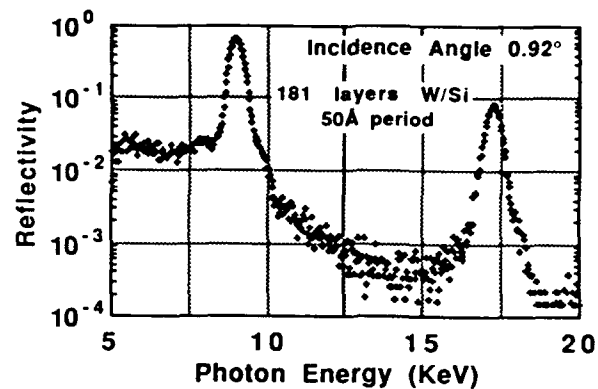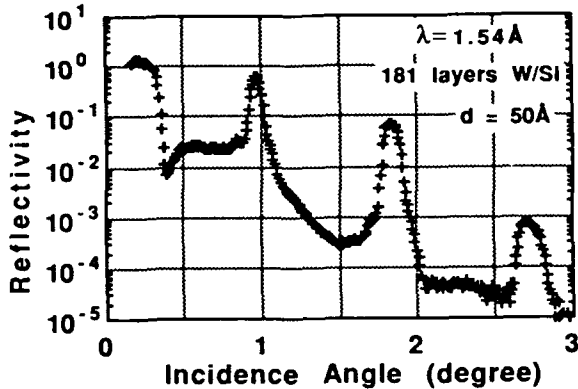
The Energy Dispersive curves provide directly: the peak reflectivity, the band pass and the overlapping order. On must to note that such an information could be gotten at any incidence angle.

Figure 6 is an example of a reflectivity curve obtained on the same multilayer, with a larger grazing angle than the previous. That gives high Bragg orders on the X-ray tube energy range. It also demonstrates how to achieve calibrations over all the energy range covered by the prepared incident beam. Collecting a set of spectra at different incidence angle offers also the possibility to get the variation of the performance of the multilayer versus the energy. This is a key information for the use of a multilayer mirror in a scanning monochromator mode or for optics used with a continuum spectra.
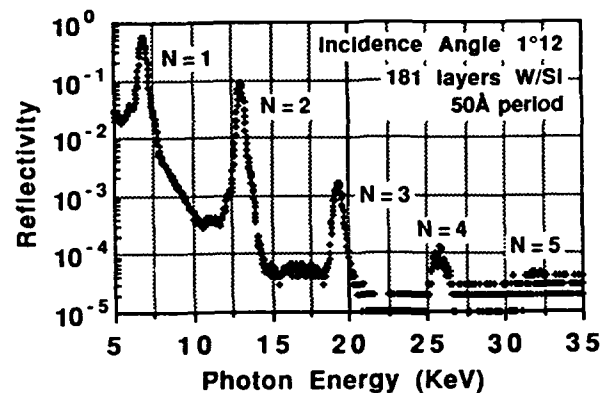
IV.1. Extreme U.V mirrors.

Extreme U.V multilayer stacks needs few periods to reach its maximum efficiency. In such a case Bragg peaks are quite large because widths are proportional to 1/N, where N is the number of working periods. In addition one can easely observe N-2 secondary maxima between two successive Bragg peaks.
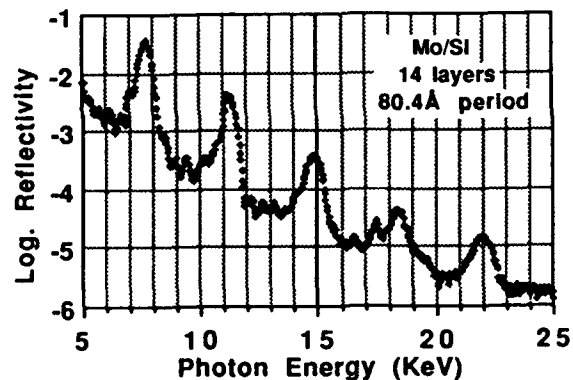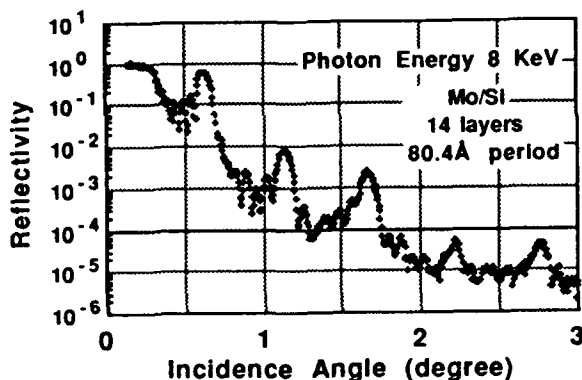
A Soft X-ray and Extreme U.V. Reflectometer Using a Laser
Produced Plasma Source and a High Throughput Monochromator.

E. M. Gullikson, J. H. Underwood, P. C. Batson, V. Nikitin.
Center for X-ray Optics
Lawrence Berkeley Laboratory
Berkeley, Ca. 94720

Measurements in the soft x-ray and extreme ultaraviolet regions of
the spectrum have historically been hampered by the lack of a
bright, tunable source. Although synchrotron radiation sources are
gradually filling this need, such facilities are not sufficiently
compact and inexpensive to be within the reach of an average
laboratory. The commercial availability of compact, inexpensive
pulsed lasers has changed this picture. The high temperature plasma
produced when the light from such a laser is focused upon a suitable
metal or dielectric target emits x-rays and extreme ultraviolet
radiation that can either be a rich line spectrum or a smooth and
intense continuum, depending upon the target material. Such a
source needs only monochromatization to make it useful for a wide
variety of measurements and calibrations.

In this paper we describe the LBL laser reflectometer. The laser is
a Continuum, Inc. Model YG 661-10 Nd:YAG laser which operates at a
frequency of 10 Hz. The output is frequency doubled to 532 nm, at
which the laser gives about 300 mJ per pulse of 7 ns. The light is
focused onto a cylinder of the chosen target material. This
cylinder is stepped between pulses to bring new surface into the
focus on each pulse.

The x-ray emitting plasma is positioned at the focus of a high
throughput monochromator (HTM) using a spherical grating (Hettrick
and Underwood, 1986). This slitless monochromator design
incorporates a cylindrical mirror to collect radiation in the
grating sagittal direction and to control astigmatism. This design
has approximately 2×10^{-4} steradians of collection solid angle
and thus delivers a high soft x-ray flux to the sample chamber. At
the highest throughput the spectral resolution of the instrument is
100 or 200 over the wavelength region 30 – 400 angstroms. This is
sufficiently high for most reflectivity measurements measurements on
multilayers having 100 or fewer periods.

The output of the monochromator passes through a chamber containing
an I_o detector into the reflectometer. Two computer controlled
Huber goniometers drive the sample and detector arms separately
through a dual coaxial feedthrough. Thus in addition to simple
theta- two theta scans, the instrument can be programmed to scan the
two arms in a variety of ways appropriate to the type of measurement
being made. Detectors used for this instrument include Si surface
barrier diodes and proportional counters.

In this paper we present the performance of the instrument using a variety of different target materials. The precautions taken to ensure stability and reproducibilty of the measurements are illustrated with data obtained from various multilayers, filters and gratings.

REFERENCES.

M. C. Hettrick and J. H. Underwood, Appl. Opt. 25, 4228 (1986)

Preparation and Characterization of Platinum-Carbon Multilayers

K. Yamashita, G.S. Lodha, and T. Suzuki
Institute of Space and Astronautical Science
3-1-1 Yoshinodai, Sagamihara, Kanagawa 229, Japan
Tel:0427-51-3911 ext.2536

I. Hatsukade
Department of Electronic Engineering, Miyazaki University
1-1 Kibanadai-nishi, Gakuen, Miyazaki 889-21, Japan

M. Ohtani
NIKON Corporation
1-6-3 Nishi-ooi, Shinagawa, Tokyo 140, Japan

Development of platinum-carbon(Pt/C) multilayers is aimed at applying to grazing incidence x-ray optical systems such as x-ray telescope, x-ray microscope and x-ray beamline optics of synchrotron radiation.

Pt/C multilayers were synthesized on a float glass, silicon wafer and laminar grating by an electron beam deposition method. The thickness(2d) and number(N) of layer pairs are 50-150A and 5-25, respectively. The thickness ratio of Pt to C was 1/2 and 1/1. The temperature of substrates during the deposition was controlled at liquid nitrogen(LN_2), room temperature or 100°C.

The x-ray reflectivity measurement was carried out in the energy range 0.9-8keV by using characteristic x-rays of Cu-Kα and Al-Kα and monochramatized synchrotron radiation at UVSOR, Institute for Molecular Science. A thin window proportional counter was used for all these measurements. The detailed description of reflectivity measurement system is given by Yamashita et al[1]. Observed reflectivities(R_{obs}) are fitted with calculated ones(R_{cal}), following an equation,

$$R_{obs} = R_{cal} \exp(-(4\pi\sigma_i \sin\theta / \lambda)^2),$$

where σ_i is rms interfacial roughness, θ incident angle against the reflecting surface and λ wavelength of incident x-rays. R_{cal} is calculated with Fresnel equation, taking into account the thickness of each layer obtained by a thickness monitor during the deposition. We can derive the 2d value and σ_i of multilayers from this fitting.

Observed reflectivities of Pt/C(2d=80A, N=15) for Al-Kα are shown in Fig.1 together with calculated values. 2d value and σ_i are derived to be 78.8A and 3.7A, respectively. The substrate was cooled down by LN_2 during the deposition.

Peak reflectivities of 1st order Bragg reflection of Pt/C(2d=83.7A, N=15) against x-ray energies are shown in Fig.2, which were measured by using monochromatized synchrotron radiation. Solid curve shows calculated values without interfacial roughness, which is estimated to be 5A. This sample was deposited at room temperature, so that σ_i becomes larger than that shown in Fig.1.
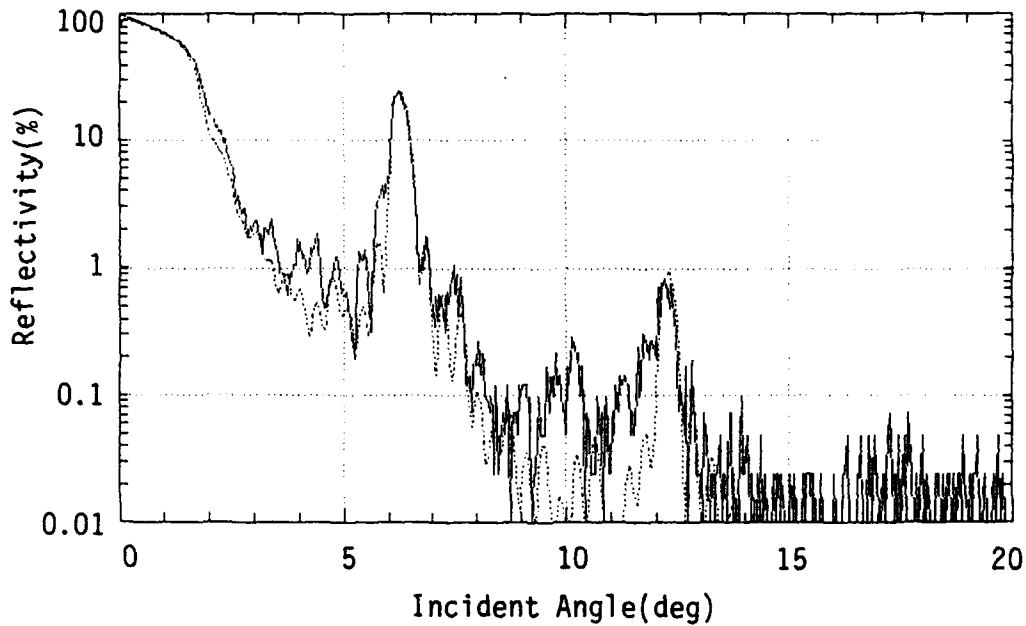
Fig.1 Reflectivity of Pt/C(2d=78.8A, N=15) for Al-Kα. Solid curve: observed, dashed curve: calculated with σ_1=3.7A.
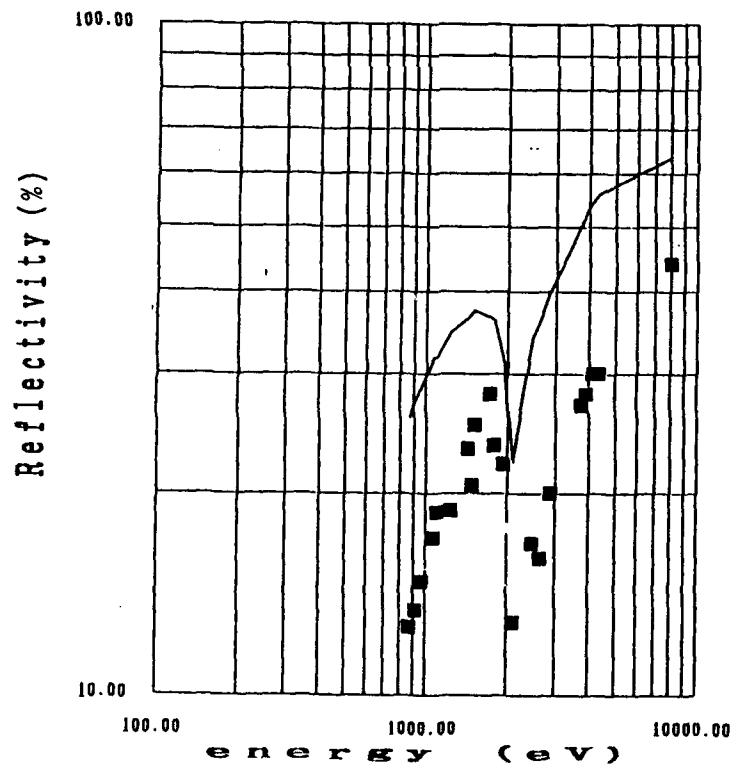

Fig.2 1st order peak reflectivity of Pt/C(2d=83.7A, N=15) vs. x-ray energy. Solid curve: calculated with σ_1=0A.

Pt/C multilayers were fabricated by changing 2d=50-150A, N=5-25, thickness ratio of 1/2-1/1, and substrate temperature of LN_2-100°C, which were evaluated by the measurement of x-ray reflectivity. The surface roughness of substrates and multilayers was measured with Wyko profilometer and STM, which was obtained to be 3A. Selected samples with N=15 and 2d=50-100A are plotted in Fig.3.
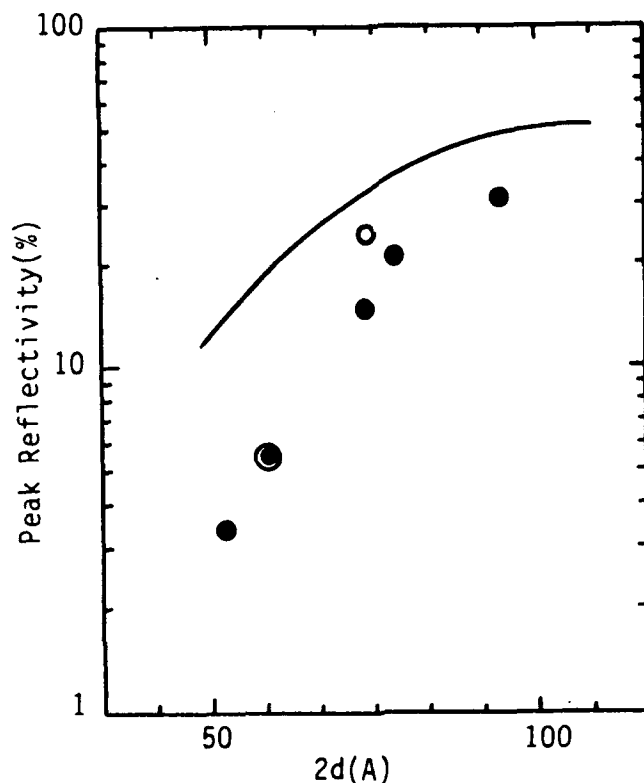
Fig.3 1st order peak reflectivity of Pt/C(N=15) for Al-Kα vs. 2d value. Filled circle: room temperature, open circle:LN_2, double circle : 100°C, solid curve: calculated with N=15 and σ_i=0A.

The interfacial roughness increases from 4.5A to 5.5A with decreasing 2d value except for LN_2 sample. When the number of layer pairs increases up to 25, the interfacial roughness still remains in above range.

The interfacial roughness is obviously different from the surface roughness and depends on the material combination and deposition method. We also investigated this problem for other multilayers such as Ni/C, Mo/Si, Mo/C, W/Si and W/B_4C. Anyway, Pt/C multilayer is useful for grazing incidence x-ray optics, which shows rather high reflectivity with small number of layer pairs.

Reference

1. K. Yamashita et al., Rev. Sci. Instrum., 60, 2006(1989).

Experimental and Theoretical Soft X-Ray Reflectivities for Mo-B₄C Multilayer Structures

D.B. Brown, J.V. Gilfrich,[†] R.K. Freitag, H.B. Rosenstock,[†]
J.H. Konnert, P. D'Antonio, P.B. Burkhalter, and C.M. Dozier

Naval Research Laboratory, Washington, DC 20375
(202)767-2154

[†] Also at SFA, Inc., Landover, MD 20785

Introduction

The use of artificial multilayer structures (MLS) as wavelength dispersive elements has proven of great importance in soft x-ray (2 to 15 nm) spectroscopy. Much of the early work in this field has concentrated on structures consisting of alternating layers of a pair of materials, one of high atomic number (most commonly tungsten) and one of low atomic number (most commonly carbon). Although the *ideal* performance of multilayer pairs can be calculated,[1] the performance of a MLS can be substantially degraded by imperfections introduced in their manufacture. In particular, it has become clear that optimum performance of MLS is strongly dependent upon the quality of the interfaces (roughness, interdiffusion, etc.) between the two materials. These interface properties are dependent upon the chemical-metallurgical properties of the materials chosen. Since such properties are typically not amenable to theoretical prediction, the choice of good layer pairs is typically an Edisonian process. The purpose of this paper is to explore the soft x-ray diffracting properties of the material pair Mo-B₄C. We will concentrate on the ways in which the measured diffraction behavior deviates from ideality and, especially, possible reasons for this non-ideality.

MLS Manufacture

The Mo-B₄C structures were obtained from Ovonic Synthetic Materials. They were deposited on either polished Si wafers or on supersmooth quartz substrates. The roughness of the substrates, measured optically, was 0.5 to 0.6 nm for the Si substrates and better than 0.2 nm for the quartz substrates. Two sets of MLS were obtained, one with 2d (twice the bilayer thickness) equal to 6.7 nm and one with a 2d value of 13.4 nm. In both cases the nominal ratio of the thickness of the light layer and the dense layer was 1:1.

Experimental Methods

The properties of the MLS as wavelength dispersive elements were determined in a vacuum double crystal spectrometer. The first crystal was TAP which, because of its narrow rocking curve, gave a negligible contribution to the line breadth measured for the MLS. The line breadth, integral reflection, and line shape were determined. Data for the first three orders of reflection were obtained using Fe L radiation (1.76 nm). Measurement of additional data using Al K radiation (0.834 nm) is currently in progress.

Atomic force microscope (AFM) data were taken using a Digital Instruments Nanoscope II AFM with a 12 μm scanning tip.

Theoretical Methods

Diffraction efficiency has been predicted using three theoretical approaches:
(a) Predictions of the diffracted intensity versus angle of diffraction were made using a model based on optical theory -- that is, a theory where each material is represented as a homogeneous layer with a particular complex index of refraction.
(b) As a modification of method "a", above, the effects of interfacial roughness have been simulated by introducing layers with optical constants graded smoothly between those of the two actual material layers. (This will be referred to as the "graded layer" calculation.)
(c) In addition, a related prediction has been performed using a kinematical model for x-ray diffraction -- that is, a theory where each material is represented as having a particular electron density and x-ray absorption coefficient.

Table I. Comparison of First Order Diffraction From Mo-B$_4$C and W-C MLS at 1.76 nm.

		Measured Integral Reflection (mr)	Theoretical Integral Reflection (mr)	Measured Full Breadth at Half Maximum	Theoretical Full Breadth at Half Maximum
W-C	2d = 5.5 nm	0.98	2.4 (a) 1.6 (b)	0.53 °Θ	0.29 °Θ (a) 0.28 °Θ (b)
W-Si	2d = 5.28 nm	1.3	2.1 (a) 1.7 (b)	0.44 °Θ	0.23 °Θ (a) 0.23 °Θ (b)
Mo-B$_4$C	2d = 6.7 nm	1.4	1.8 (a)	0.58 °Θ	0.37 °Θ (a)
	2d = 13.4 nm	2.6	3.9 (a)	1.05 °Θ	0.73 °Θ (a)

(a) optical theory - perfect MLS calculation
(b) optical theory - "graded layer" calculation

This third calculation differs in associating the diffracted intensity at a particular angle with particular diffraction h00 node.

Results

Table I shows the first order diffracting properties of Mo-B$_4$C. These are compared with recently published data for a W-C MLS and a W-Si MLS.[2] Note, in Table I, that the measured integral reflection for the Mo-B$_4$C MLS with 2d = 6.7 nm is about 40% greater than that for a W-C MLS with 2d = 5.5 nm. [Perhaps 20% of the relatively enhanced performance of the Mo-B$_4$C MLS tested here is due to its slightly greater interplanar spacing (2d). Thus the true enhancement of this Mo-B$_4$C MLS, in comparison to W-C, was about 20%.] Note that the relatively superior performance of the Mo-B$_4$C MLS is in contrast to the fact that the predictions for ideal (perfect) MLS are in the opposite order. It appears that this results from the measured integral reflection being closer to the "perfect" value. The measured line breadth (full breadth at half maximum) for the 6.7 nm Mo-B$_4$C MLS is about the same (but slightly inferior) in comparison to that for the 5.5 nm W-C MLS. Additional detail, giving the predicted and measured peak shapes for first order diffraction from Mo-B$_4$C at 1.76 nm can be seen in Figure 1 and Figure 2.
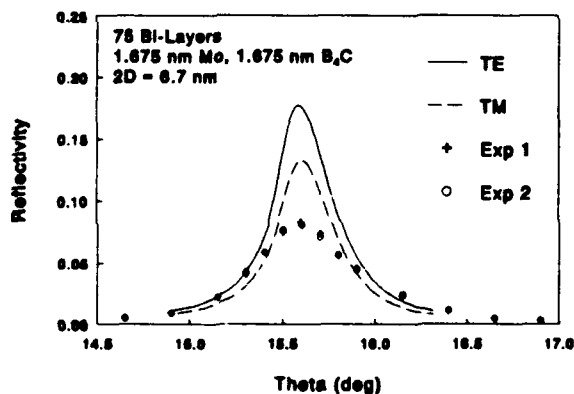
Figure 1. Line shape for 6.7 nm Mo-B$_4$C MLS at 1.76 nm.
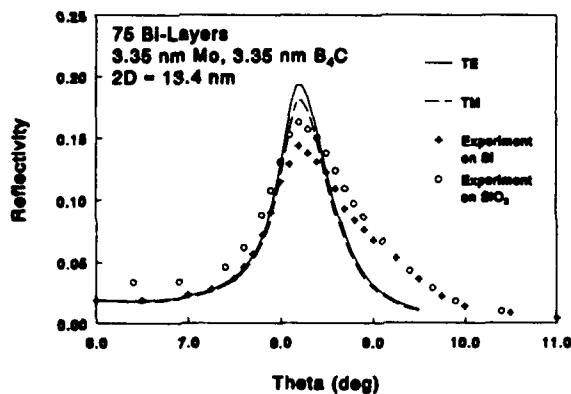
Figure 2. Line shape for 13.4 nm MLS at 1.76 nm.

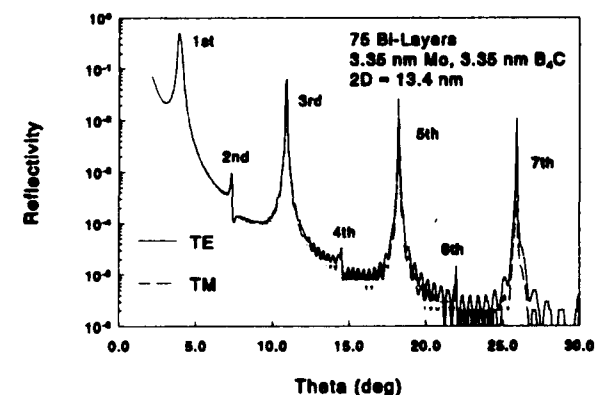**Table II.** Experimental and Theoretical Diffraction Parameters For Three Diffraction Orders at 1.76 nm.

		1st Order	2nd Order	3rd Order
2d = 6.7 nm	R, Exp.	1.4 mr	0.0060 mr (a)	0.012 mr (a)
	R, Theor.	1.8 mr	0.0035 mr	0.10 mr
	W, Exp.	0.62 °Θ	0.42 °Θ (a)	0.48 °Θ (a)
	W, Theor.	0.37 °Θ	(b)	0.31 °Θ
2d = 13.4 nm	R, Exp.	2.6 mr	0.097 mr	0.057 mr
	R, Theor.	3.9 mr	0.031 mr	0.14 mr
	W, Exp.	1.05 °Θ	0.69 °Θ	0.72 °Θ
	W, Theor.	0.73 °Θ	0.38 °Θ	0.26 °Θ

(a) uncertain due to low intensity
(b) uncertain due to confusion created by interference fringes

Predictions for several diffraction orders based on optical theory of the diffracted intensity versus diffraction angle can be found in Figure 3 and Figure 4 for the 13.4 nm MLS. Comparison of these predictions with experimental measurements, for the case of 1.76 nm radiation, for three orders of diffraction can be found in Table II. Note in Table II that (as expected) for the most part the experimentally measured integral reflection, R, is somewhat smaller than predicted by the theoretical calculation for a perfect MLS. The data for the second order reflections are exceptions. The theoretical calculation predicts a very low reflectivity for even orders of diffraction in cases where the ratio of the thickness of the light layer and the dense layer is 1:1.[3] The fact that the experimentally measured second order R values are anomalously large suggests that there is some deviation from the nominal 1:1 layer thickness ratio.

The differences between the experimental and theoretical integral reflection is thought to be largely due to interfacial roughness between the differing material layers.[4] To gain additional insight into this roughness, we have measured the top surface roughness of two of our MLS (one each of 6.7 nm and 13.4 nm interplanar spacing) using the AFM. A topographic presentation of the data for the 2d = 13.4 nm MLS can be seen in Figure 5. The data for the 6.7 nm MLS is similar. The AFM data (as represented by Figure 5) corresponds to a r.m.s. roughness of 0.24 ±0.4 nm for the 2d = 6.7 nm MLS, and 0.24 ±0.3 nm for the 2d = 13.4 nm MLS. This degree of surface roughness is similar to the 0.24 nm r.m.s. roughness recently reported for a W-C MLS with 2d = 5.5 nm.[5]
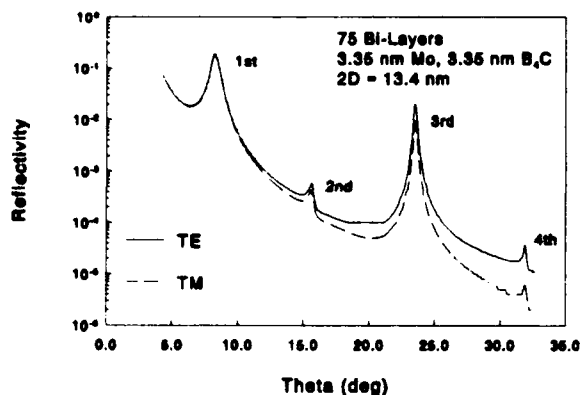
| **Figure 3.** | Predicted reflectivity for four diffraction orders at 1.76 nm. | **Figure 4.** | Predicted reflectivity for seven diffraction orders at 0.834 nm. |

It has previously been shown, by comparing perfect MLS calculations with "graded layer" calculations, that the widths of the diffraction peaks are almost insensitive to the degree of roughness.[2] (See, for example, the W-C data in Table I.) As a result, it has been suggested that the differences between the experimental and theoretical values for the diffraction line breadth are most probably largely due to variability in the interplanar spacing. To test this hypothesis, a rough calculation using the data presented in Table II has been made. This calculation suggests values of $\Delta d/d$ lying between 2% and 4% for the 2d = 13.4 nm MLS.

Figure 5. Topographic presentation of surface roughness. AFM data for a MLS with a bilayer spacing corresponding to 2d = 13.4 nm.

Discussion and Summary

This work has shown that MLS of Mo-B_4C show a superior integral reflection and a comparable line breadth, as compared with W-C MLS. In the full presentation we will provide additional detail by: (a) presenting further experimental data on multiple orders of diffraction using Al K radiation, (b) presenting further results using the kinematical model for diffraction, and (c) presenting an interpretation, based on the AFM data, of the reduction (non-ideality) of the integral reflection.

References

1. See, for example, the work of A.E. Rosenbluth quoted by Troy W. Barbee, Jr., Optical Engineering 25, 898 (1986).
2. P.G. Burkhalter, J.V. Gilfrich, R.K. Freitag, H.B. Rosenstock, and D.B. Brown, SPIE Conf. 28, *Multilayer and Grazing Incidence X-Ray/EUV Optics*, 21-26 July 1991, San Diego, CA.
3. See, for example, Fig. 4 in Alan E. Rosenbluth and J. M. Forsyth, "The Reflecting Properties of Soft X-Ray Multilayers", in *Low Energy X-Ray Diagnostics*", AIP Conference Proceedings No. 75, David T. Attwood and Burton L. Henke, Eds. (Am. Inst. Physics, New York, 1981).
4. D.L. Rosen, D. Brown, J. Gilfrich and P. Burkhalter, J. Appl. Cryst. 21, 136 (1988).
5. D.B. Brown, J.H. Konnert, J.V. Gilfrich, P. D'Antonio, R.K. Freitag, H.B. Rosenstock, and P.G. Burkhalter, Pacific-International Congress on X-Ray Analytical Methods, August 12-16, 1991, Honolulu. Submitted for publication in Advances in X-Ray Analysis, Vol. 35 (Plenum, New York).

SOFT X-RAY MULTILAYER MIRRORS

Fan Zhengxiu   Shao Jianda
Shanghai Institute of Optics and Fine Mechanics,
Academia Sincia, P.O. Box 800-211,
Shanghai, P.R. China

ABSTRACT

The present status of studies on soft x-ray multilayer mirrors in our institute are described. These include the optinum design, deposiion technique and the preliminary characterizations. W/C, Ta/Si, Mo/Si, Mo/Al multilayers, which are designed as mirrors at 105A, 135A and 234A respectively, have been fabricated with DC- and RF- plane magnetron sputtering system. Small Angle Diffraction with Cu-Ka radiation, Transmission Electron Microscopy and Auger Electron Spectroscopy have been applied to investigate the informations about the interfaces and the layer thickness monitor random errors and the roughness of the layer systems. Our reflectometer have also given us some informations about the optical constants.

Stability

ThA 8:00am–11:45am
Grand Room

Eric Ziegler, *Presider*
European Synchrotron Radiation Facility, France

Thermal Stability of Mo-based Multilayers Fabricated by rf Sputtering

Yoshikazu Ishii, Hisataka Takenaka, Tomoaki Kawamura and * Hiroo Kinoshita
NTT Interdisciplinary Research Laboratories
3-9-11, Midori-cho, Musashino-shi, Tokyo 180 Japan
*NTT LSI Laboratories
3-1, Morinosato Wakamiya, Atsugi-shi, Kanagawa 243-01 Japan

Introduction

Mo-based periodic multilayers such as Mo/Si and Mo/B4C show great promise as reflectors for soft x-ray reduction lithography[1-3]. The thermal stability of multilayers is one of the most important factors for ensuring the reliable performance. The Mo/Si and Mo/B4C multilayers show high reflectivity in the 8 nm - 15 nm region at normal incidence. The purpose of this paper is to present the resulting changes of layered and crystal structures of the Mo/Si and Mo/B4C multilayers upon thermal annealing.

Experiment

The deposition of Mo/Si and Mo/B4C multilayers on Si substrates was carried out by a new rf magnetron sputtering method[4,5]. The structural characteristics of these multilayers are listed in Table 1. These multilayers were annealed at $400^\circ C$ and $600^\circ C$ for 1 hour in an Ar atmosphere. The layered and crystal structure of as-deposited and annealed multilayers were evaluated by both x-ray diffraction using a θ -2 θ diffractometer and transmission electron microscopy.

Table 1. Structural characteristics of as-deposited multilayers.

Materials	Substrate	d(nm)	d_{Mo}(nm)	d_{Si}ord_{B4C}(nm)	No.of periods
Mo/Si	silicon	6.5	2.6	3.9	30
Mo/B4C	silicon	6.7	2.7	4.0	30

Results

Table 2 lists the Cu-K α first order Bragg peak reflectivity for as-deposited and annealed multilayers. The reflectivity of the Mo/Si multilayers markedly decreases above $400^\circ C$ and is 8% at $600^\circ C$. On the other hand, the reflectivity of Mo/B4C multilayers slightly decreases with increasing annealing temperature, and maintains 67% even after annealing at $600^\circ C$ for 1 hour. These results indicate Mo/B4C multilayers are superior to Mo/Si multilayers in terms of thermal stability.

Table 2. Thermal annealing effects on x-ray reflectivity.

Materials	as-deposited	400°C, 1hour	600 C, 1hour
Mo/Si	78%	44%	8%
Mo/B4C	78%	72%	67%

Figure 1 shows the changes in the first order Bragg profiles for the Mo/Si multilayer as a function of annealing temperature. Annealing causes a decrease in periodic lengths shown by the peak shift to higher Bragg angle.

Figure 2 shows the changes in first order Bragg profile for the Mo/B4C multilayer as a function of annealing temperature. The peak position shifts toward lower angle with a shift of about half that of the Mo/Si multilayer. These results indicate annealing induces periodic length expansion of the Mo/B4C multilayer, and the variation of periodic length of the Mo/B4C is smaller than that of the Mo/Si multilayers. The peak shift directions of the Mo/Si and the Mo/B4C multilayer are analogous to W/Si and W/C multilayers[6-8], respectively.

Figure 3 (a) and (b) is the transmission electron micrograph cross-section for the as-deposited and 600°C annealed Mo/Si multilayer, respectively. The micrograph of the as-deposited Mo/Si multilayer clearly indicates the existence of well formed layers. However, the micrograph of the annealed Mo/Si multilayer indicates a diffuse layer structure with crystallization of the Mo layers. The x-ray diffraction results suggest the formation of Mo_5Si_3 or $MoSi_{0.65}$.

From the calculation based on the Fresnel equation incorporating Mo_5Si_3 intermediate layers, the decrease in the periodic length can be explaned by the formation of these intermediate layers. The periodic length of the annealed Mo/Si multilayer decreases with increasing the intermediate layer thickness.
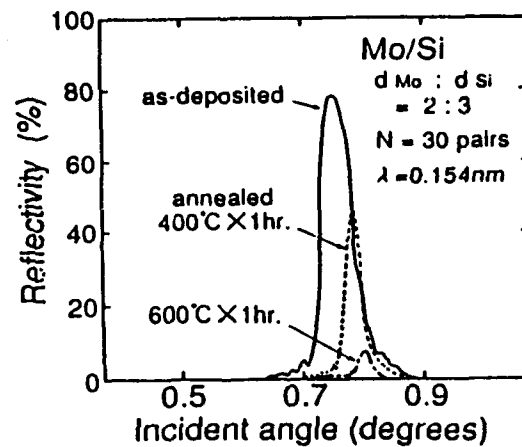

Figure 1, The change in first order Bragg profile for the Mo/Si multilayer on annealing temperature.
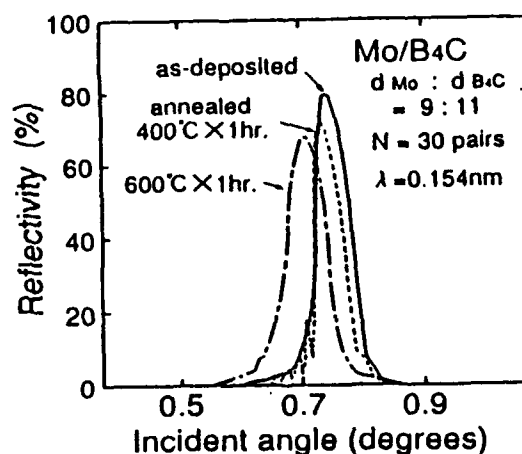

Figure 2, The first order Bragg peak reflectivity for various annealing temperatures.

(a)   (b)

Figure 3, The transmission electron micrograph cross-section for the as-deposited(a) and 600°C(b) annealed Mo/Si multilayer.

On the other hand, the as-deposited and 600°C annealed Mo/B4C multilayer both have a well-defined discrete multilayer structure by the transmission electron micrograph observation. Because of this, the Mo/B4C multilayer maintains a higher reflectivity than the Mo/Si multilayer for both annealing temperatures of 400°C and 600 °C.

Conclusion

The reflectivity of the Mo/Si multilayer markedly decreases above 400°C. On the other hand, the reflectivity of the Mo/B4C multilayer slightly decrease at every annealing temperature. From the TEM observation, the thermally induced deteriorations of Mo/B4C multilayer is smaller than that of the Mo/Si multilayer. This means that the Mo/B4C multilayer is superior to the Mo/Si multilayer in terms of thermal stability. Moreover, the reflectivity of the Mo/B4C multilayer is higher than that of the Mo/Si multilayer under the 12 nm region. These results suggest the Mo/B4C multilayer is suited as a reflector for x-ray reduction lithography.

References

1)H.Kinoshita,K.Kurihara,Y.Ishii and Y.Torii, J.Vac.Sci.Technol.B3,1581(1989)

2)H.Kinoshita,K.Kurihara,T.Mizota,T.Haga Y.Torii. H.Takenaka and Y.Ishii . Proceedings of OSA (1991)

3)J.E.Bjorkholm,J.Boker,L.Eichner,R.R.Freeman,J.Gregus,T.E.Jewell,W.M.Mansfield. A.A.Mac Dowell. E.L.Raab. W.T.Silfvast,L.H.Szeto,D.M.Tennant, W.K.Waskiewics. D.L.White,D.L.Windt. O.R.Wood II. and J.H.Bruning, J.Vac.Sci.Technol.B8,1509(1990)

4)Y.Ishii, H.Takenaka and H.Takaoka. Proceedings of the International Meeting on Advanced Materials of MRS. Tokyo. 1988

5)H.Takenaka, Y.Ishii, K.Kurihara and H.Kinoshita. Proceedings of SPIE. 1345. 213 (1990)

6)Y.Takagi, S.A. Flessa, K.L.Hart, D.A. Pawlik, A.M.Kadin, J.L.Wood. J.E.Keem. and J.E.Tyler. Proceedings of the International Society of Optical Engineering, 563, 66 (1985)

7)Y.Lepetre, E.Ziegler, I.K.Shuller, and R.Rivoira,J.Appl.Phys.60, 2301 (1986)

8)J.B.Kortright, St.Joksch and E.Ziegler,J.Appl.Phys.69, 168 (1991)

Interdiffusion Kinetics in Mo/Si Multilayers

R. S. Rosen and D. G. Stearns, *Lawrence Livermore National Laboratory Livermore, CA 94550.*
Phone (510) 422-9559.

M. A. Viliardos and M. E. Kassner, *Department of Mechanical Engineering, Oregon State*
University, Corvallis OR 97331

S. P. Vernon, *Vernon Applied Physics, Torrance, CA 90505*

Mo/Si multilayers (ML's) are attractive for x-ray optics due to the relatively high associated reflectivity. However, the reflectivity is known to decrease with the formation of diffuse interlayer regions resulting from interdiffusion at the Mo-Si interfaces [1–2]. Most of the previous studies have reported interdiffusion coefficients [1–5] and effective activation energies [2–4] over a range of temperature assuming that the interdiffusion coefficient is invariant with annealing time. At temperatures of 560–580 °C, hexagonal molybdenum-disilicide (h-$MoSi_2$) grows with a square-root time dependence at the Mo-Si interface [6]. This suggests diffusion-limited growth with a time-invariant interdiffusion coefficient. However, at temperatures of 300–400 °C, the interlayer structure is known to change with annealing time from amorphous to crystalline [1–3], suggesting the possibility that the rate-controlling mechanism(s) for interdiffusion may also change with annealing time and/or temperature. Therefore, it is the objective of this study to perform a series of annealing treatments of Mo/Si ML's at temperatures lower than those previously reported to determine the Mo-Si interdiffusion kinetics as a function of time.

The multilayers in this study consisted of 40 bilayers of Mo and Si sputter deposited onto polished single crystal Si wafers. The nominal bilayer spacing was 7.0 nm and the ratio of the Mo layer thickness to the bilayer thickness was ~0.4. A detailed description of the vacuum system and deposition procedures is presented elsewhere [7]. The coated Si substrates were then annealed at temperatures of 216–342 °C and times from 1–1000 hours. The structure of the as-deposited (unannealed) and annealed multilayers were examined using small and large angle x-ray diffraction (XRD), normal incidence x-ray reflectance (NIR) measurements using a synchrotron source, selected area electron diffraction, and high resolution electron microscopy (HREM).

The unannealed multilayer consists of amorphous Si layers and crystalline Mo layers. These pure layers are separated by thin amorphous interlayer regions of $MoSi_2$ stoichiometry [8]. Small angle XRD measurements of the bilayer spacing indicated that annealing causes a contraction of the multilayer structure. HREM confirmed that this contraction corresponds with growth of the Mo-Si interlayer regions, consistent with the formation of higher density silicides from the pure layers.

At relatively short annealing times, the amorphous interlayer regions grow thicker without any (observable) crystallization. After a sufficient annealing time, the ML structure consists of relatively thick layers of h-MoSi$_2$ separated by thin layers of "unreacted" crystalline Mo. The pure Si layers are completely consumed by the formation of h-MoSi$_2$.

The NIR of the ML's was found to decrease with annealing time and increased annealing temperature. The measured NIR of the ML's were compared with the theoretical reflectance that was calculated using a matrix method modified to incorporate nonideal interfaces [9]. Theoretical fits of the experimental reflectance data were obtained using interlayer regions of uniform MoSi$_2$ stoichiometry, abrupt interfaces (no roughness), and thicknesses obtained from the HREM and small-angle XRD data. The decrease in measured reflectance of ML's annealed at different temperatures and times were found to correlate with the growth of the interlayer regions over the temperature ranges of this study.

The growth kinetics of the Mo-Si interlayers were determined by assuming that the interlayer growth is diffusion limited with constant concentrations at the interfaces between the Mo-Si interlayer and elemental layers, and that the concentration gradient across the interlayer is linear. The interlayer width w(t) after annealing time t can then be related to the interdiffusion coefficient, D(t'):

$$w^2(t) = w^2(0) + 2\Delta C \int_0^t D(t')dt' \qquad (1)$$

where w(0) is the initial interlayer width and ΔC is the change in concentration across the interlayer. Results of the annealing experiments of this study have shown that the interlayer thickness increases with annealing time according to the relationship

$$w^2(t) \propto t^\alpha, \qquad (2)$$

where α is >1. Combining Eqs. 1 and 2 and differentiating with respect to time indicates that D(t') increases with annealing time. This result can be explained by an increase in the diffusion rate due to an increasing percentage of h-MoSi$_2$ as the interlayer thickness increases, assuming that diffusion through h-MoSi$_2$ is faster than through amorphous MoSi$_2$.

In conclusion, annealing Mo/Si ML's at temperatures of ~200–350 °C for 1–1000 h can result in decreased reflectivity. This loss of reflectivity may be the result of interdiffusion of Si and/or Mo in the (principally) amorphous Mo-Si interlayer region, causing growth of this interlayer region that eventually crystallizes to h-MoSi$_2$. The silicide appears to continue to grow until all of the Si

is consumed. A plot of the square of the interlayer thickness vs. annealing time indicates an increasing interlayer growth rate with time. This implies that the interdiffusion coefficient increases with annealing time and, also, that the effective activation energy for interdiffusion is overestimated when interdiffusion coefficients are evaluated at constant annealing times.

References

1. D. G. Stearns, M. B. Stearns, Y. Cheng, J. H. Stith and N. M. Ceglio, "Thermally induced structural modification of Mo-Si multilayers," J. Appl. Phys. vol. 67, pp. 2415–2427, March 1990.

2 R. S. Rosen, M. A. Viliardos, M. E. Kassner, D. G. Stearns, and S. P. Vernon, "Thermal Stability of Mo/Si Multilayers," *Proc. Optical Applied Science and Engineering,* SPIE Symposium, San Diego, CA in press.

3. K. Holloway, K. B. Do and R. Sinclair, "Interfacial reactions on annealing molybdenum-silicon multilayers," J. Appl. Phys. vol. 65, pp. 474–480, Jan. 1989.

4. H. Nakajima and H. Fujimori, "Interdiffusion and structural relaxation in Mo/Si multilayer films,"
J. Appl. Phys. vol. 63, pp. 1046–1051, Feb. 1988.

5. W. G. Sloof, O. B. Loopstra, Th. H. de Keijser and E. J. Mittemeijer, "Diffusion and structural relaxation in amorphous Mo/Si multilayers," Scripta Metall. vol. 20, pp. 1683–1687, Dec. 1986.

6. J. Y. Cheng, H. C. Cheng, and L. J. Chen, "Cross-sectional transmission electron microscope study of the growth kinetics of hexagonal $MoSi_2$ on (001)Si," J. Appl. Phys. vol. 61, pp. 2218–2223, Mar. 1987.

7. D. G. Stearns, R. S. Rosen, and S. P. Vernon, "Fabrication of high-reflectance Mo-Si multilayer mirrors by planar-magnetron sputtering," J. Vac. Sci. Tech. A vol. 9, pp. 2662–????, Sept./Oct. 1991.

8. D. G. Stearns, R. S. Rosen, and S. P. Vernon, "High Performance Multilayer Mirrors for Soft X-ray Projection Lithography," Invited Paper in *Proc. Optical Applied Science and Engineering,* SPIE Symposium, San Diego, CA in press.

9. D. G. Stearns, "The scattering of x-rays from nonideal multilayer structures" J. Appl. Phys., vol. 65 pp. 491–506, Jan. 1989.

Comparison of Microstructure and Thermal Stability of
Short Period X-Ray Multilayers

Tai D. Nguyen,[1,2] Ronald Gronsky,[2,3] and Jeffrey B. Kortright[1]

[1]Center for X-Ray Optics, Lawrence Berkeley Laboratory, Berkeley, CA 94720
Tel. (510) 486-4051 FAX (510) 486-4550
[2]Department of Materials Science and Mineral Engineering, University of California, Berkeley, CA 94720
[3]National Center for Electron Microscopy, Lawrence Berkeley Laboratory, Berkeley, CA 94720

detail studies of x-ray multilayer microstructures and stability are essential to a complete understanding of these nano-scali metastable materials, and may lead to synthesis of multilayers of improved performance. The microstructures and phases inside the layers depend upon the period, and show different behaviors for different materials systems.[1,2] Their response to thermal treatment likewise depends on the materials combinations and the period. In this project, the microstructures and their thermal stability of various period W/C, WC/C, Ru/C and Ru/B$_4$C multilayers are investigated by High-Resolution Transmission Electron Microscopy (HRTEM) and x-ray diffraction.

Multilayers were prepared by magnetron sputtering at floating temperature. The periods of the multilayers range from 2 to 12 nm. Low angle x-ray reflectance measurements of the first several multilayer Bragg peaks were used to determine the periodicity of the multilayers. Microstructural characterization of the multilayers were performed by cross-sectional and plan-view TEM. Thermal treatment of the multilayers were performed in a tube furnace under a vacuum of 10^{-6} torr.

The microstructures of the layers in the W/C, Ru/C, and Ru/B$_4$C systems show similar development with period to each other, and different from those of the WC/C system. The low-Z layers in all multilayers are observed to be amorphous. The microstructures of as-prepared WC/C multilayers are predominantly amorphous for all periods, while those of the metal-rich layers in the W/C, Ru/C, and Ru/B$_4$C multilayers depend on the period. The 2 nm period as-prepared multilayers of these three systems have amorphous microstructures, and the metal-rich layers in the longer periods show the presence of the elemental crystalline

structures along with the amorphous phase. The layers in all as-prepared multilayers are quite "well-formed", even at periods as short as 2 nm.

Changes in the microstructures and phases have been observed in some of the multilayers upon annealing at 500°C for 4 hours. Annealed WC/C multilayers of all periods show amorphous microstructures. The 2 nm period W/C multilayer remains amorphous after annealing, while the elemental W crystallites in the longer period as-prepared samples react and recrystallize to form a carbide W_2C. A minor trace of elemental BCC tungsten is still detected in the annealed 12 nm period W/C multilayer, which indicates that the reaction has not completed under this annealing condition. Annealing of the Ru/C multilayers leads to crystallization or grain growth of the elemental Ru crystallites, in contrast to the formation of the carbide phase in the W/C system. Upon annealing, the Ru crystallites in the as-prepared 10 nm Ru/C sample grow to sizes of tens of nanometers in lateral direction, which are of the same order as the Ru-rich layer thickness in the multilayer. They have a strong texture in [101] perpendicular to the layer interfaces, and no preferred orientation in the layer plane. The structures of the longer period annealed Ru/C multilayers remain layered, while the amorphous Ru layers in the as-prepared 2 nm period have agglomerated to form almost-spherical Ru crystallites that are larger than the initial period. The layered structure in the short period multilayer hence is destroyed, in contrast to the stable structure of the annealed W/C and WC/C multilayers of the same period. This agglomeration probably results from the driving force to lower the interface to volume energy, which is largest in this sample. Preliminary studies of Ru/B_4C multilayers indicate that the layered structure of a 2.6 nm period sample is also stable after annealing, and the Ru crystallites in the longer periods react and recrystallize to form a boride phase (RuB_2), as predicted from the appropriate equilibrium phase diagram. These results suggest that the layered structure remain intact after annealing for multilayers that their materials components react to form compounds. Agglomeration of the Ru layers in the Ru/C system, in contrast to the stable layered structure in the W/C and the Ru/B_4C systems, appears to be related to the immiscible region in its phase diagram, which reflects the driving force for phase separation between the Ru and the C constituents.

X-ray measurements of the low-angle Bragg peaks of all the W/C, WC/C, and Ru/C multilayers reveal the expansion of the multilayer periods upon annealing. All three systems show higher relative expansion ($\Delta d/d$) for shorter periods than for longer periods. The relative expansions of the WC/C and Ru/C multilayers appear almost linear with period, and are significantly higher than those of the W/C multilayers. The expansion of the period upon annealing in these metal/carbon multilayers has also been observed by many other groups.

Possible explanations for this expansion include agglomeration of the metal-rich layers,[3] or expansion of the amorphous carbon layers to a more graphitic structure.[1,4,5] Our x-ray reflectivity[6] and Raman spectroscopy measurements[7] of thin carbon films (5 to 40 nm) show conclusively that the carbon expansion is the mechanism. This conclusion is consistent with the observations on the metal/silicon and metal/B_4C multilayers that their periods do not expand like those of the metal/carbon systems. The metal/silicon multilayers contract,[5] while the those of Ru/B4C show small expansions upon annealing. Stability of the multilayer period on annealing is important to practical applications since the effects of thermal annealing are similar to that of intensive radiation.

1. T.D. Nguyen, R. Gronsky, and J.B. Kortright, *Microstructure and Stability Comparison of Nanometer Period W/C, WC/C, and Ru/C Multilayer Structures*, in: Thin Film Structures and Phase Stability (MRS Proc. 187, 1990) 95.

2. T.D. Nguyen, R. Gronsky, and J.B. Kortright, *The Microstructural Evolution of Nanometer Ruthenium Films Between Carbon Layers with Thermal Treatments*, in: Phase Transformation Kinetics in Thin Films (MRS Proc. 230, 1990).

3. Y. Lepetre, E. Ziegler, I.K. Schuller, and E. Spiller, Appl. Phys. Lett. 48 (1986) 1354.

4. X. Jiang, D. Xian, and Z. Wu, *Expansion of Amorphous Carbon in W/C Multilayers after Annealing*, Appl. Phys. Lett. 57, 24 (1990) 2549.

5. J.B. Kortright, St. Joksch, and E. Ziegler, *Stability of Tungsten/Carbon and Tungsten/Silicon Multilayer X-Ray Mirrors under Thermal Annealing and X-Radiation Exposure*, J. Appl. Phys. 69, 1 (1991) 168.

6. C. Lucas, T.D. Nguyen, and J.B. Kortright, *X-ray Reflectivity Measurements of the Expansion of Carbon Films upon Annealing*, Appl. Phys. Lett. 59,17 (1991) 2100.

7. J. Ager, C.A. Lucas, and T.D. Nguyen (unpublished).

Modeling of Multilayer Mirror Damage by a Short Pulse of X-Rays

D. C. Eder, B. J. MacGowan, L. B. DaSilva, S. Mrowka, and T. Barbee Jr.

Lawrence Livermore National Laboratory
P. O. Box 808, Livermore, California 94551
(510) 423-3483

SUMMARY

Multilayer mirrors can have a dramatic reduction in reflectivity as a result of large optical and x-ray fluxes incident on the surface of the mirror. We consider the effect of a short pulse of x-rays on the reflectivity of a variety of mirrors including W/C, WC/C, Cr_3C_2/C, Mo/Si, and $MoSi_2/Si$ multilayers. We use the measured x-ray spectrum from a gold target heated by a 0.5 ns laser for the case of no filter between the gold and the mirror and when various low energy filters are used. One tool we use to determine the reduction in reflectivity is a multilayer damage code ROMULS.[1] We have modified the code to allow non-normal incidence and for a spectrum of x rays In the figure we show the calculated normal incidence reflectivity of a W/C multilayer mirror at 44.8 Å. The x-ray flux from the gold target is incident at 50° from normal and we show the reflectivity for three values of integrated fluence. The temporal dependence of the x-ray flux used in the calculation is shown. Two of the curves use an x-ray spectrum measured with no filter and one uses the spectrum after passing through a low energy filter. In all cases, the calculated reflectivity is reduced dramatically during the x-ray pulse. The calculated reflectivities with no damage are approximately a factor of four larger than measured. The calculation assumes smooth layers and no diffusion between the layers. We will discuss the reduction of reflectivity as a result of rough surfaces and diffusion between layers. Our modeling results will be compared with recent experiments that measured the reflectivity both temporally and spectrally.

1. K. J. Gray, L. V. Knight, B. G. Peterson, J. M. Thorne, T. W. Barbee, Jr., and A. Toor, Journal of X-Ray Science and Technology 1, 99 (1989).
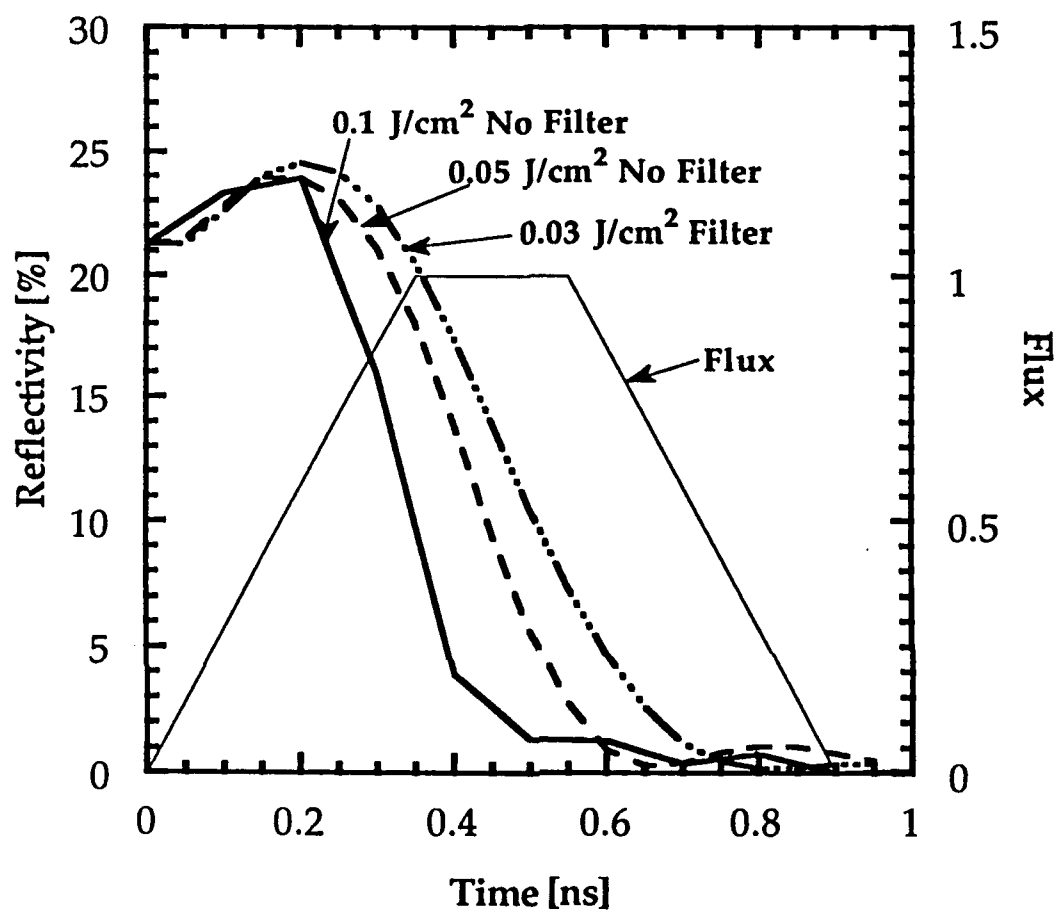
Figure: The calculated reflectivity as a function of time for an incident x-ray flux with an integrated fluence of 0.1, 0.05, and 0.03 J/cm^2. The 0.3 J/cm^2 calculation uses the measured spectrum after passing through a low energy filter consisting of 250 Å of Al and 1000 Å of CH.

Low-radiation-damage multilayer coatings for the soft x-ray region

W. R. Hunter and J. F. Seely*

SFA, Inc.

1401 McCormick Drive

Landover, MD 20785 (202-767-2545)

*Naval Research Laboratory

Washington, D. C. 20375 (202-767-3529)

INTRODUCTION

Highly reflecting multilayer coatings (MLC), used to form resonant cavities for soft x-ray lasers(1) in which double- and triple-pass amplification occurs, can be destroyed by strong electric fields generated at the multilayer boundaries by intense soft x-ray radiation, rather than plasma debris from which the coatings are shielded. Any multilayer coating used in high field strength applications, FEL, x-ray projection lithography, etc., are subject to such damage. Electric field strengths can be reduced at the boundaries in MLCs by altering slightly the layer thicknesses of the final, or topmost, layers. Ca¹ᵤulations are presented showing reduced field strengths caused by altering final layer thir ᵢesses. The optical constants used in the calculations were obtained from Henke et al(2) ᵢd Palik(3) so similar computations may vary depending on the actual n,k values used but the basic concepts discussed herein are independent of the optical constants.

DISCUSSION

When designing MCLs the ratio of nodal layer thickness to period thickness (nodal layer plus spacer layer thickness), γ, is adjusted for maximum reflectance. Calculation of the volumetric absorptance, the number of photons absorbed per unit volume in the coating divided by the number of incident photons, shows that the maximum absorptance occurs at the nodal layer boundaries. Figure 1 shows the calculated reflectance of a tungsten/carbon multilayer with a period thickness of 22.5 Å and a γ of 0.4 at normal incidence. The maximum reflectance of approximately 15% (normal incidence) occurs at 44.83 Å, the most interesting region for imaging and holography of biological specimens, just longward of the C K edge at 43.7 Å. The coating is composed of 50 periods of C and W with W uppermost at the vacuum interface.

Figure 2a shows the time-averaged total electric field intensity at 44.83 Å in a portion of the coating close to the vacuum interface and in the vacuum region just above the coating. The nodal layers are designated by H and the spacer layers by L. The units depend on the incident radiation intensity and are arbitrary. Although the nodes occur in the nodal layers they are not centered, consequently the field is rather intense near the interface closest to vacuum. Shown in Figure 2b is the volumetric absorptance which is much larger in the nodal layers than in the spacer layers, as expected because of the larger extinction coefficient. In addition, the volumetric absorptance peaks at the vacuum side of each nodal layer interface, being largest at the vacuum interface. Since radiation damage occurs in regions were the electric field is most intense, where the volumetric absorptance is largest, the topmost interfaces of the nodal layers are most susceptible.

Reducing damage susceptibility can be done by changing the γ values of the topmost

periods during fabrication or adding periods with appropriate γ values. For the wavelength under consideration, 44.83 Å, extinction coefficients are sufficiently small so that the reflectance is hardly affected by additional periods. However, at longer wavelengths addition of periods reduces the peak reflectance somewhat.

Figure 3 shows the volumetric absorptance of the coating of Figures 1 and 2 after addition of a C/W period with C thickness 11.5 Å and W thickness 9 Å. The thickness of the additional C layer was adjusted so that the node of the standing wave occurs at the midpoint of the W layer which reduced the volumetric absorptance by almost a factor of two. Adding a second period with the same W thickness but a C thickness of 13 Å to place the node at the midpoint of the added W layer results in a maximum reflectance of approximatly 15%, the same value as for the coatings of Figure 1 and 2, and with reduced volumetric absorptance in the upper two periods, as shown in Figure 4.

At 130 Å, the region of most interest for soft x-ray projection lithography, Mo and Si are the present choices for the nodal and spacer layers, respectively. This wavelength is just longward of the Si $L_{2,3}$ absorption edge so the Si is relatively transparent. Shown in Figure 5 is the volumetric absorptance of a coating composed of 20 Si/Mo periods with period thickness of 67 Å and a γ of 0.5. For this coating the topmost interface of the nodal layer almost coincides with the maximum electric field and the volumetric absorptance shows that almost all absorptance takes place at the topmost nodal interfaces. Adding a Si/Mo period with Mo and Si thicknesses of 25 Å centers the node in the nodal layer and reduces the volumetric absorptance by more than a factor of three without reducing the reflectance significantly. It is possible to add more Si/Mo layers without reducing the reflectance significantly.

The most widely developed soft x-ray laser is the Ne-like Ge laser operating at 232 and 236 Å(ref). Calculations show that optimum reflectance for 10 periods of Si/Mo is about 41% with a period thickness of 125 Å and γ of 0.3. As at 130 Å, the topmost Mo interface is close to the maximum electric field strength and most of the absorptance occurs at that interface. An additional Si/Mo period with Si thickness of 70 Å adjusted to center the node in the Mo layer, and an Mo thickness of 50 Å to maximize the reflectance reduces the volumetric absorptance at the topmost Mo boundary by about 30%. Because of the additional absorptance of the Si the reflectance was reduced from 41% to 36%.

REFERENCES
1. C. Montcalm, B. T. Sullivan, H. Pepin, J. A. Dobrowolski, and G. D. Enright, "Multilayer mirrors for xuv Ge-laser wavelengths" Proc. SPIE 1547, (1991). to be published
2. B. L. Henke, J. C. Davis, E. M. Gullickson, and R. C. C. Perera, "Photoabsorption coefficients and atomic scattering factors for 92 elements in the 10-10,000 eV region", Lawrence Berkeley Laboratory Report LBL-26259 (1988).
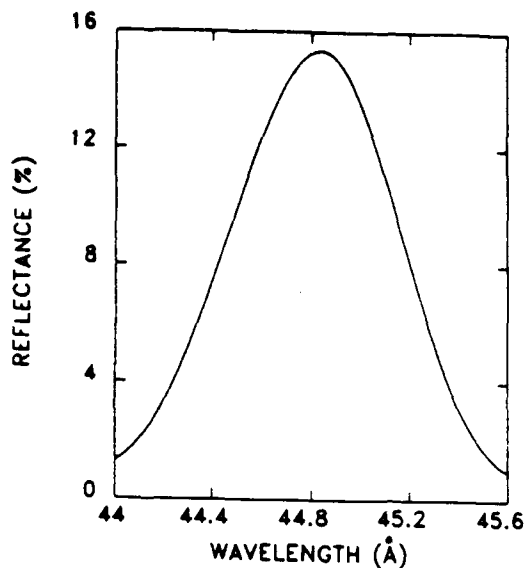3. E. D. Palik, Handbook of Optical Constants of Solids (Academic Press, San Diego, 1985).

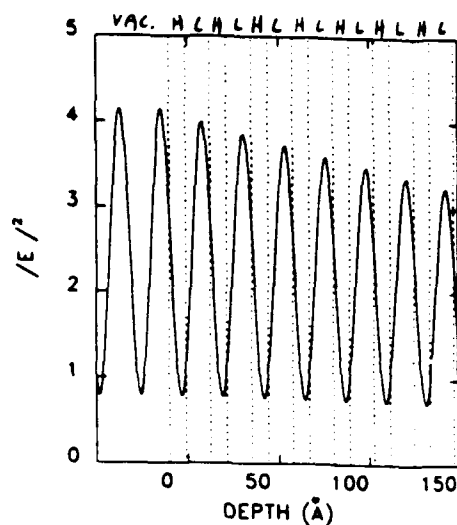Figure 1. Reflectance at normal incidence of a W/C multilayer of 50 periods

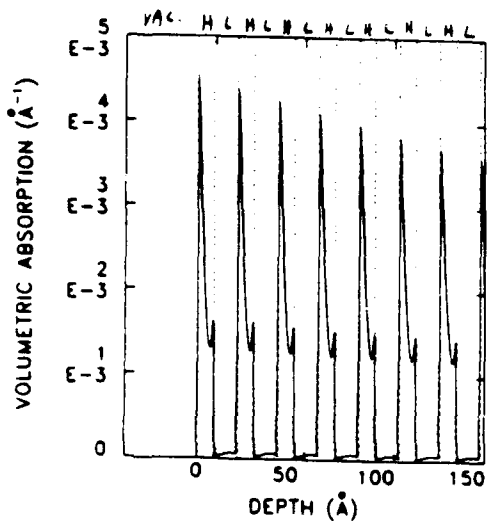Figure 2. Electric field in the multilayer of Figure 1

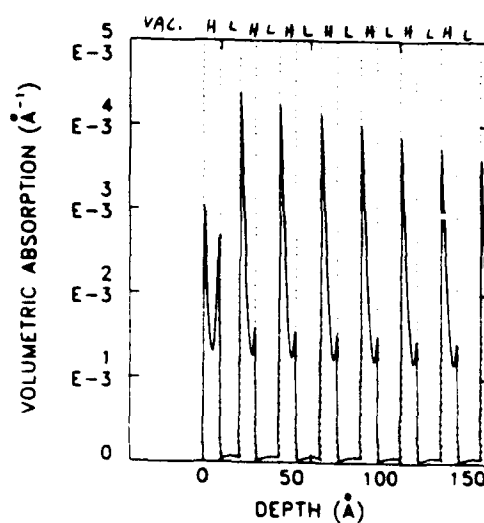Figure 3. Volumetric absorptance in the multilayer of Figure 1

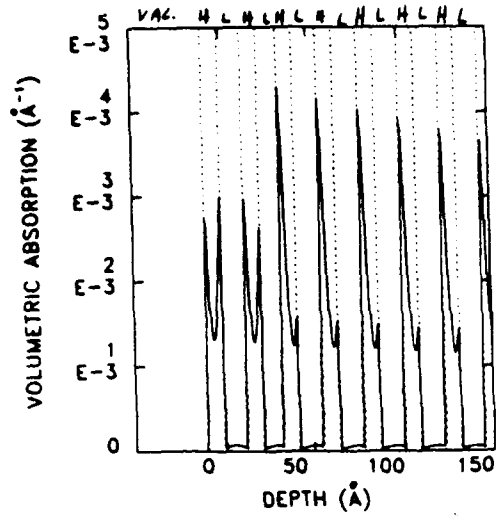Figure 4. Effect of adding a period to the multilayer of Figure 1 to reduce volumetric absorptance

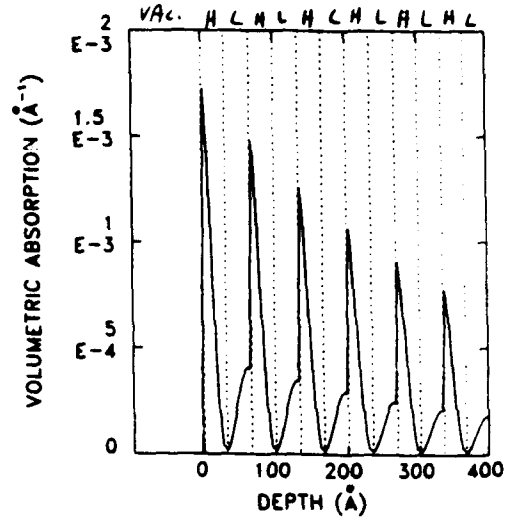Figure 5. Volumetric absorptance in the multilayer of Figure 1 with two periods added

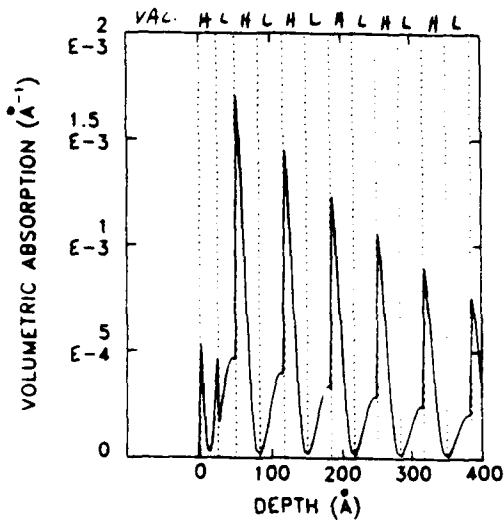Figure 6. Volumetric absorptance in a Si/Mo multilayer of 20 periods (normal incidence)

Figure 7. Effect of adding a period to the multilayer of Figure 6 to reduce volumetric absorptance

Novel Properties

ThB   7:30pm–9:45pm
Grand Room

Natale M. Ceglio, *Presider*
Lawrence Livermore National Laboratory

BRAGG-FRESNEL MULTILAYER OPTICS FOR X-RAY
MICROSCOPY AND SPECTROSCOPY.

B.Vidal[1], M.Brunel[2], A.Erko[3], D.Rochtchoupkine[3] J.Susini[4],
P.Vincent[1].

[1]Laboratoire d'Optique Electromagnetique, Universite de Mar-
seille, URA CNRS N 843 FACULTE DES SCIENCES ET TECHNIQUES
DE SAINT JEROME (case 262) 13397 Marseille, Cedex 13 France.
Fax number 33. 91. 67. 44. 28

[2]Laboratoire de Cristallographie CNRS, 166X, 38042 Grenoble
Cedex, France. Fax number: 33. 76. 88. 10. 38

[3]Institute of Microelectronics Technology USSR Academy
of Sciences, Chernogolovka, Moscow dist. Box 1957, 142432
USSR. Fax number 7. 095 292. 65. 11

[4]European Synchrotron Radiation Facility, BP 220 - F-38043
Grenoble Cedex , France.Fax number 33. 76. 88. 20. 20.

ABSTRACT.

Application of metallic multilayer mirrors for construc-
tion of different components of x-ray optical schemes became
more and more frequent. Number of publications gives an examp-
les of objective lenses, monochromators, focusing and imaging
devices, based on figured multilayer mirrors. One of the most
exited application of such optics in future can be projection
X-ray lithography and local analyses of microstructures with
submicron resolution for microelectronics technology.

Recently, focusing and imaging by the use of some kinds
of "grooved" diffraction optics on flat surfaces instead of
the curved substrate had been reported in several papers. This
optics is now known as Bragg-Fresnel Multilayer Optics (BFMO)
[1,2]. Compared to grazing incidence optics and figured multi-
layers optics, BFMO can provide higher spatial and spectral
resolutions. That is say, till to spot value up to 0.1μ spati-
al resolution of BFMO is limited only by the flatness of the
plane substrate and accuracy of the lithographic process [3].
In principle BFMO combines the high spatial resolution of
Fresnel zone plates and the high radiation stability of multi-

layer X-ray mirrors.

This report gives an examples of fabrication, computer simulation and tests for two kind of BFMO: Lamellar Multilayer Gratings (LMG) and Linear Bragg-Fresnel Multilayer Lenses (LBFML). LMG, used here as the first step for the understanding of diffraction property of LBFML, can be very interesting themselves as by spectroscopic instruments with relatively high dispersion and efficiency.

I. Fabrication of Multilayer Bragg-Fresnel Optics.

BFMO can be made by conventional methods of microelectronics technology, such as thin metallic and semiconductor film deposition, optical and electron-beam lithography, ion and reactive ion etching techniques.

A W/Si and W/C multilayer mirror prepared by a magnetron sputtering technique have been used as a substrate for LMG and BFML. Period of the W/Si bilayers was 32Å and 181 layers have been coated. Period of the W/C bilayers was 30Å, 201 layers have been coated. BFML procedure preparation follows. First, a Fe O mask on glass substrate was obtained by electron beam lithography and etching. Next, this mask have been used for UV lithography on the multilayer substrate,coated with photoresist. Finally, an RF-excited ion-beam source was used to etch the multilayer through the photoresist mask. For this etching, the ion energy was in the 0,5 to 1 KeV range and the etching rate about 5 layers per minute. All optical designing and technological part of work where done at IPMT (USSR Academy of Sciences). Several specimens having different etching depths were prepared for experimental tests. Optical interferometer and tally-step measurements have been used to control the etching depth.Control of profile were done at ESRF (France) by WYKO interferometer, at IPMT (USSR) and Institute d'Optique (France) by tally-step instrument.

II. Linear Multilayer Gratings simulation and tests.

Computer simulation of diffraction on LMG was performed using program, developed at Laboratoire d'Optique Electromagnetique (LOE)University of Marseille III (France). Transition matrix of bilayers are computed using a differential method

(4) taking into account the refractive index of each layer and grating parameters. Then, for the total LMG, efficiency of diffraction orders are determined with the suitable power of the transition matrix (5). LMG were made by electron-beam lithography and argon ion etching at IPMT on the multilayers, prepared at LOE. Thick silicon substrate (3 mm thickness) provided flat surfaces for mirror with RMS in order of 7.5 $\overset{\circ}{A}$. Aperture of iach LMG is 1mm x 1 mm, variation of the depth profile range from 200$\overset{\circ}{A}$ to 1600$\overset{\circ}{A}$.

LMG tests were performed at the Laboratoire de Cristallographie CNRS using rotating anode X-ray generator.

III. Bragg-Fresnel Multilayer Lenses.

LBFML were made by combination of optical and e-beam lithography argon ion etching at IPMT USSR Academy of Sciences on the multilayers, prepared at LOE University of Aix-Marseille III. Aperture of the LBFML 1mm x 8 mm, focal length 10 cm at 1.5 $\overset{\circ}{A}$ wavelength, expected spatial resolution 0.5 μm.

IV. Conclusion

Computer simulations and experimental tests of LMG with variable thickness shows, that diffraction efficiency strongly dependent on lumellar grating period and profile depth.The strong "volume" phenomena in short-period gratings, gives gives possibility to increase diffraction efficiency of LMG practically till to 30% - 40% of input energy in first diffraction order with totally suppressed zero order. Application of this phenomena to acoustic waves surface modulation of multilayer mirrors will open new class of X-ray acousto-optical devices for ultra fast modulation, time-resolved spectroscopy and scanning X-ray lithography. All theoretical calculations are verified by experimental tests.

References

1. Aristov V.V., Erko A.I., Martynov V.V., Revue de Physique Appl., 23, pp.1623-1630 (1988).
2. Erko A. I., Journal of X-ray Science and Technology Vol.2, 297-316 (1990).
3. Chevallier P., Dhez P., Erko A., Khan Malek C., Khzmalian E., Panchenko L., Redkin S., B. Vidal, in Proceedings of the 3 International Conference on X-Ray Microscopy,", London, England, 3-7 Sept. (1990).

4. Vincent P., in "Electromagnetic Theory of Gratings" (Topics in Current Physics, 22) ed. by R.Petit, Spriger-Verlag, 101-121, 1980.

5. Vidal B., Vincent P., Appl. Opt., 23, n 11, 1794-1801, (1984).

A multilayer quarter-wave plate of transmission type at a wavelength of 12.4nm

Hiroaki Kimura

Department of Synchrotron Radiation Science, The Graduate University for Advanced Studies,
PF, KEK, 1-1 Oho, Tsukuba 305, Japan
Phone 0298-64-1171 Fax 0298-64-2801

Masaki Yamamoto, Hiroshi Nomura, Ko Mayama and Mihiro Yanagihara
Research Institute for Scientific Measurements, Tohoku University,
2-1-1 Katahira, Aoba-ku, Sendai 980, Japan
Phone 022-227-6200(Ex. 3236) Fax 022-211-9119

In order to measure or to transform the polarization state in the soft x-ray region, we need a suitable quarter-wave plate. Kortright and Underwood[1] have shown theoretically that the transmission type multilayer has a good potential for a quarter-wave plate in the soft x-ray region. They demonstrated as a good example, the Mo/Si multilayer which has a periodicity of 9.0 nm and 20 periods at the wavelength of 13.8 nm, has the retardation $\Delta_p-\Delta_s=86°$, the polarizance $(T_s-T_p)/(T_s+T_p)=42\%$ and the throughput for s-component of 39% at the incident angle of 39.7° measured from the sample normal. The best quarter-wave plate should have the retardation equal to $\pm90°$, the polarizance close to zero, and the high throughput over 50%. The multilayer designs presented here achieve these conditions necessary for good and useful quarter-wave plates.

We have simulated the response of Ru/Si multilayer quarter-wave plate of transmission type using a computer program based on an optical scheme with complex Fresnel reflection coefficients[2]. We have optimized the retardation, the polarizance and the throughput (transmittance) for Ru and Si multilayer at wavelength 12.4 nm. The refractive indices used for Ru and Si are (0.9185-

0.00565i) and (0.9985-0.000433i), respectively, as measured by our group.

Figure 1 shows the performance of two quarter-wave plates as a function of the angle of incidence. One optimized at 35° incident angle is presented by the solid line, and the other optimized at 50° by the broken line. For both designs, 90° retardation, zero polarizance and approximately 50% throughput were obtained. The retardation curves show large retardation at two angle regions to be common for the transmission multilayers. One near the critical angle (75° incident angle) is of no use as the transmittance is very poor. Near the Bragg angle (30°, 45°), the maximum is much useful than the minimum because of the asymmetry to the zero line. Then we optimized the retardation at the maximum peak near the Bragg angle. In this case, however, the retardation and the polarizance are very sensitive to the angle of incident around the principal angle(Δ=90°).

More interesting design from experimental point of view is to find a transmission type quarter-wave plate which would be much insensitive to small shifts or errors of the angle of incidence of light. This is very important in practice because free standing multilayers are difficult to make flat and also the light may have large divergence. In the following simulation we optimized at the plateau region between two peaks to achieve an average value of retardation of 90°. Figure 2 shows two results of such design. One optimized at 45° incident angle is presented by the solid line and the other at 50° by the broken line. For both designs, 90° retardation, 20% polarizance, 15% throughput were obtained. In

fig. 2, much smoother variations in retardation and polarizance curves are evident for angles of incidence around the principal angle.

These simulations will play an important role in the development of quarter-wave plates in the soft x-ray region.

Reference

[1] J. B. Kortright and J. H. Underwood, Nucl. Instrum. Methods A291,272(1990).
[2] J. H. Underwood and T. W. Barbee, Jr., Appl. Opt. 20, 3027(1981).
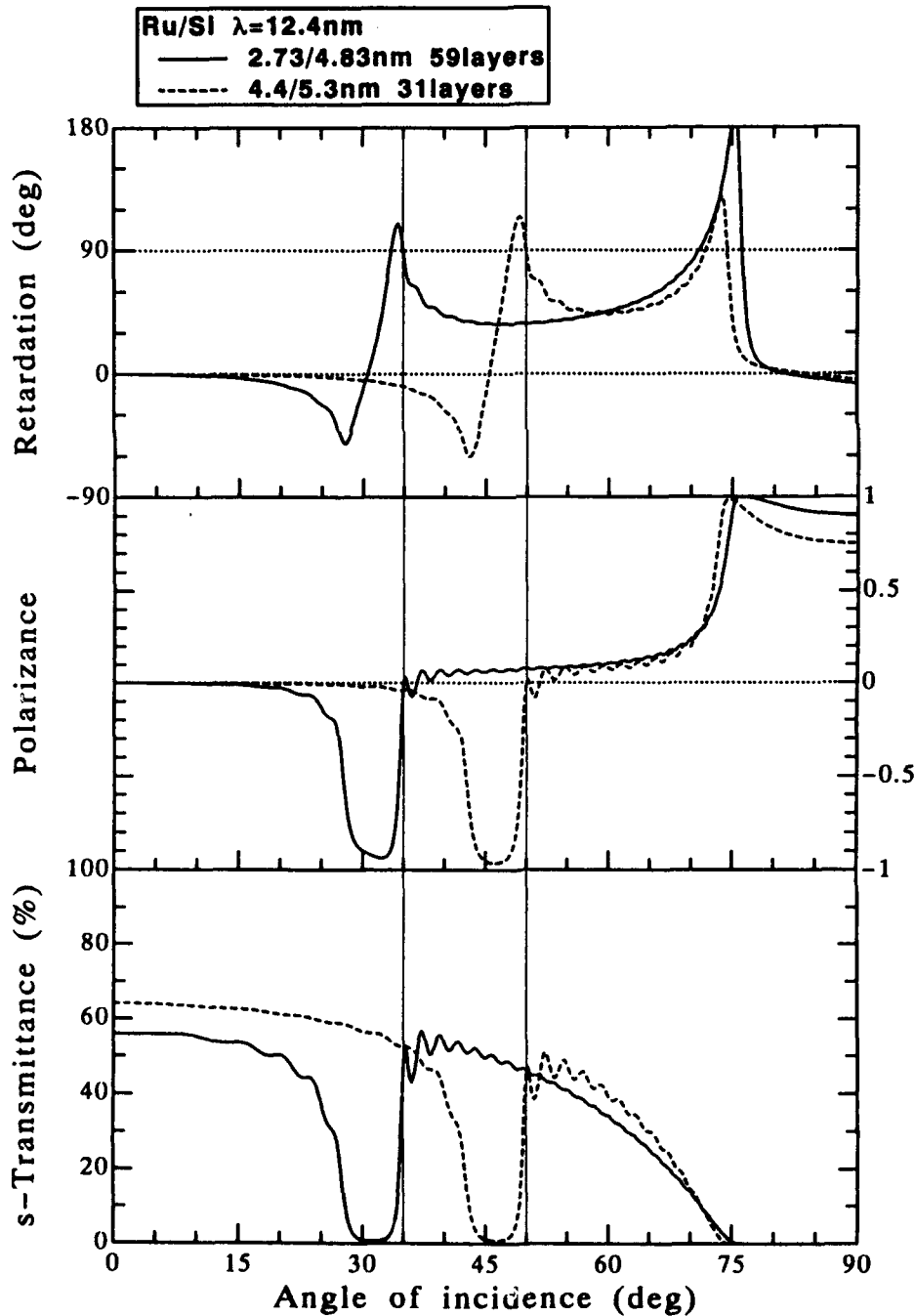
Fig. 1
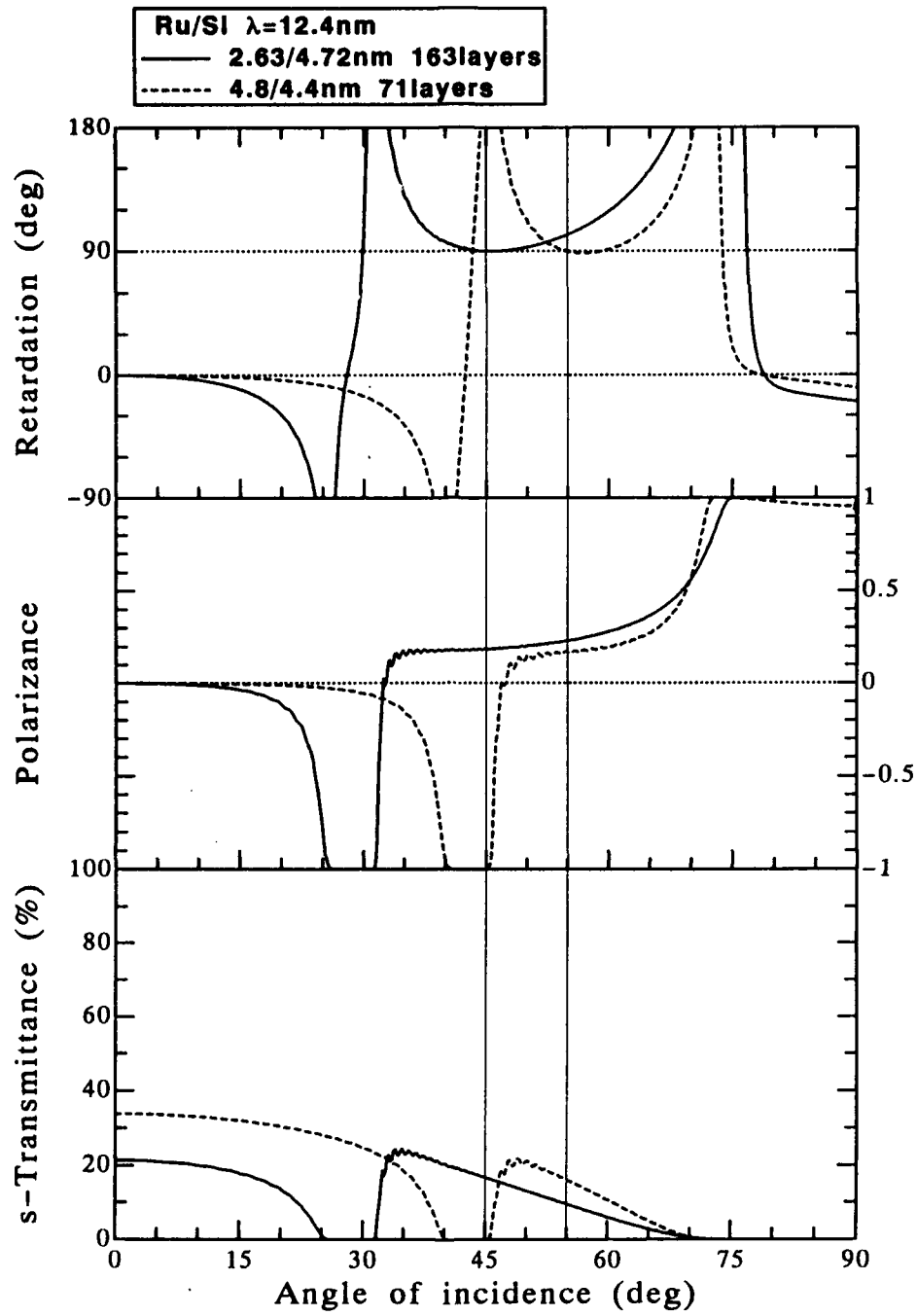
Fig. 2

Observation of nuclear diffraction from multilayers containing ^{57}Fe

R. Röhlsberger, E. Witthoff, E. Lüken, E. Gerdau

II. Institut für Experimentalphysik, Luruper Chaussee 149, D-2000 Hamburg 50
Phone: (040) 8998 2229/2241

The small resonance width Γ_0 of Mößbauer transitions allows monochromatization of synchrotron radiation down to a bandwidth of $10^{-7} - 10^{-9}$ eV by nuclear resonant diffraction. Up to now, the Mößbauer isotopes ^{57}Fe (E_0 = 14.4 keV, Γ_0 = 4.7 · 10^{-9} eV) and ^{169}Tm (E_0 = 8.4 keV, Γ_0 = 1.2 · 10^{-7} eV) have been used in this field [1-5]. In order to observe nuclear resonant diffraction, the competing contribution of electronic scattering with a bandpass of at least a few meV has to be strongly reduced. Precise determinations of hyperfine interactions can be made by observation of quantum beats in the collective decay of the nuclei excited by synchrotron pulses. Most of the experiments have been done with single crystals which have a pure nuclear reflection. In these cases the structure factor for the electronic reflection is zero because of the symmetry of the crystal. The structure factor for the nuclear reflection is nonzero, because subgroups of the Mößbauer nuclei are distinguished by a symmetry breaking hyperfine interaction or by isotopic arrangement [6]. In a layered crystal of ^{56}Fe and ^{57}Fe atoms obviously the electronic and nuclear lattice constant differ by a factor of two, so that a superstructure appears with a pure nuclear reflection. Such a crystal has not been grown up to now, since the preparational requirements are very hard to meet. However, an isotopic superstructure can easily be realized in a multilayer, which need not be a single crystal. Alternating layers containing ^{56}Fe and ^{57}Fe give rise to a multilayer Bragg peak of pure nuclear origin. Such a multilayer will be described here.

To avoid magnetic level splitting and to keep photoabsorption as low as possible, the Fe was embedded in a B_4C matrix, resulting in Fe_5B_4C as layer material.

The energy dependence of the multilayer reflectivity is determined by the refractive index of the layers containing the resonant nuclei [7]. The refractive index for $^{56}Fe_5B_4C$ and for $^{57}Fe_5B_4C$ in the vicinity of an unsplit nuclear resonance is shown in Fig.1.
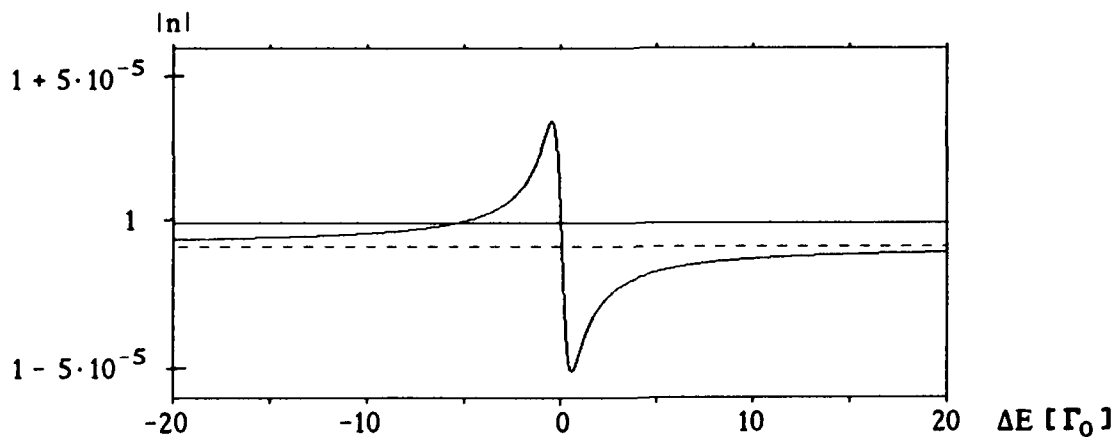
Fig.1   The refractive index of $^{56}Fe_5B_4C$ (– – –) and $^{57}Fe_5B_4C$ (———) around the 14.4 keV nuclear resonance of ^{57}Fe.

Obviously, in a $^{56}Fe_5B_4C$ / $^{57}Fe_5B_4C$ multilayer there is a very strong contrast in the refractive indices between both layer materials near the resonance. Therefore strong reflectivity occurs in a small energy range around the resonance. Far off the resonance both refractive indices are equal and only the Fresnel reflectivity from the surface boundary is present. To illustrate this behaviour, a theoretical calculation of the reflectivity of a nuclear resonant multilayer consisting of 80 * (1.5 nm $^{57}Fe_5B_4C$ / 2.5 nm $^{56}Fe_5B_4C$) is shown in Fig.2. The double peak structure appearing in the reflectivity is a general phenomenon in resonance scattering and was already observed in nuclear resonant Bragg scattering from single crystals [8]. The peak reflectivity is 0.64, while the electronic reflectivity far off the resonance is 10^{-3}. The energetic width of the reflection is about 20 Γ_0 = 0.1 μeV, and the angular width of the Bragg peak is 0.3 mrad.
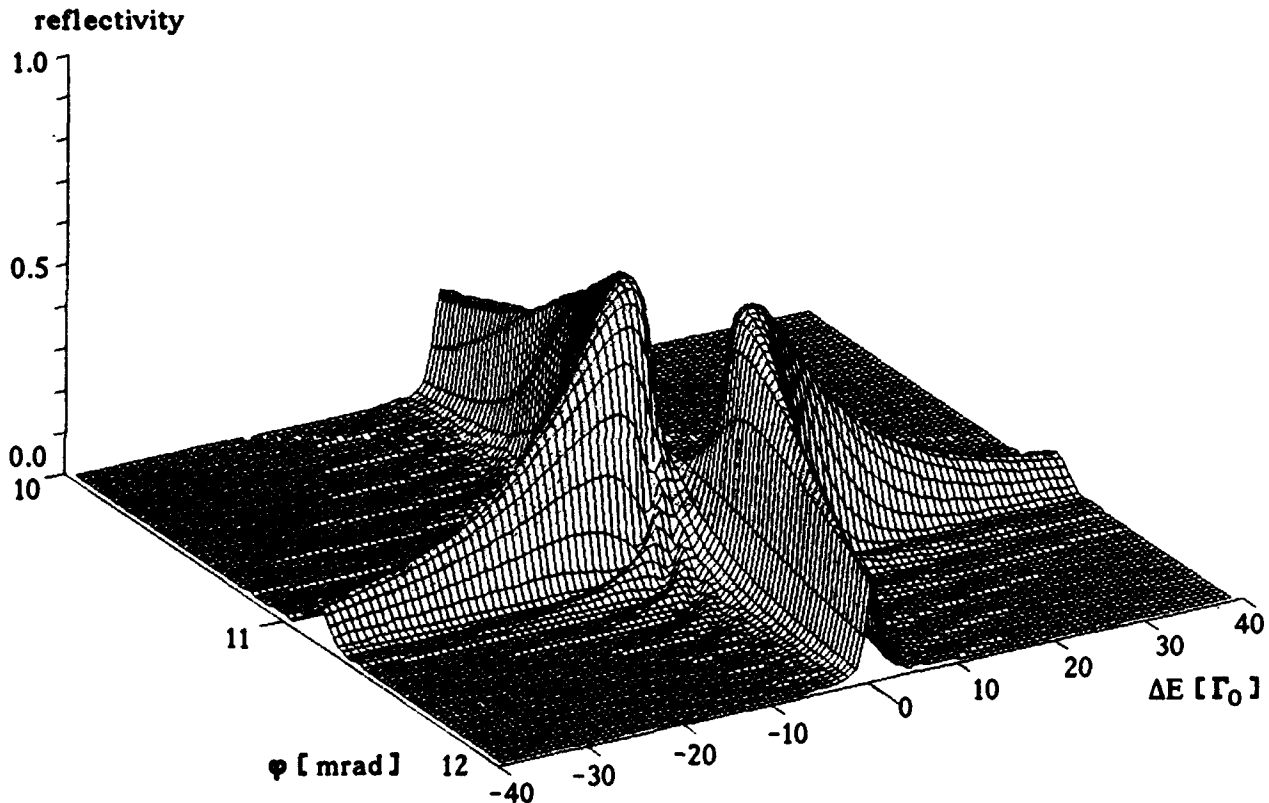
Fig. 2 Reflectivity of a resonant multilayer as a function of the angle of
incidence φ and the deviation ΔE from the resonance energy. The
data of the multilayer used for the calculation are given in the text.

This multilayer was found to be the optimum one for the given d-spacing of 4 nm. No substantial increase in peak reflectivity and bandwidth can be achieved by increasing the number of layers or by changing the thickness ratio between both layers.

First experimental results have been achieved from a multilayer consisting of 10 * (4.8 nm $^{56}Fe_5B_4C$ / 3.9 nm $^{57}Fe_5B_4C$). The multilayer was produced by RF-sputtering from B_4C targets covered with ^{56}Fe and ^{57}Fe foil pieces, respectively. The substrate was a Si-wafer with a microroughness of 0.3 nm. The Fe content in the layers could be adjusted by the amount of Fe foil pieces on the target. The ^{56}Fe and ^{57}Fe content was the same in both layers within a margin of 2%, since the rockingcurve of the multilayer at 17.5 keV showed no Bragg peak.

The rockingcurve of the nuclear reflectivity of the multilayer was measured with the 14.4 keV radiation from a $^{57}Co(Pd)$ Mößbauer source, see Fig.3. The source was mounted on a Mößbauer drive and moved periodically from Doppler shifts of $-10\Gamma_0$ to $+10\Gamma_0$ around the resonance during the measurement. The beam divergence was 0.3 mrad. The expected nuclear Bragg peak at 5.7 mrad can clearly be seen.
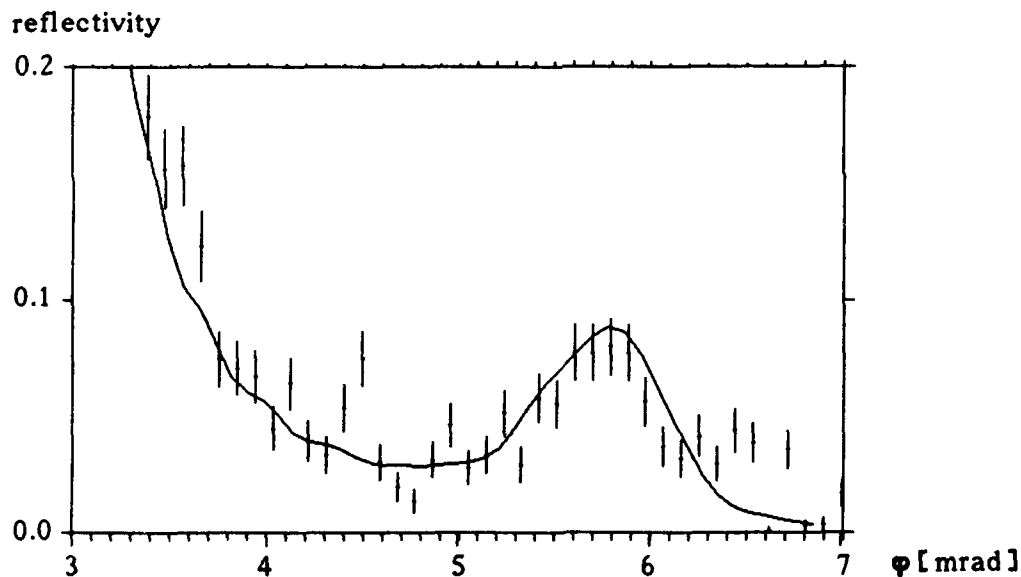
Fig. 3 Rockingcurve of the resonant multilayer measured with 14.4 keV radiation from a ^{57}Co source. The solid line is a theoretical simulation.

The energy dependence of the reflectivity with the angle of incidence fixed at the Bragg position is shown in Fig.4. Clearly the two peaks lying below and above the exact resonance energy can be seen. The maximum reflectivity is 0.13, whereas the reflectivity far off the resonance is about 0.02. The solid line is a theoretical simulation with the parameters used for the calculation in fig.3.
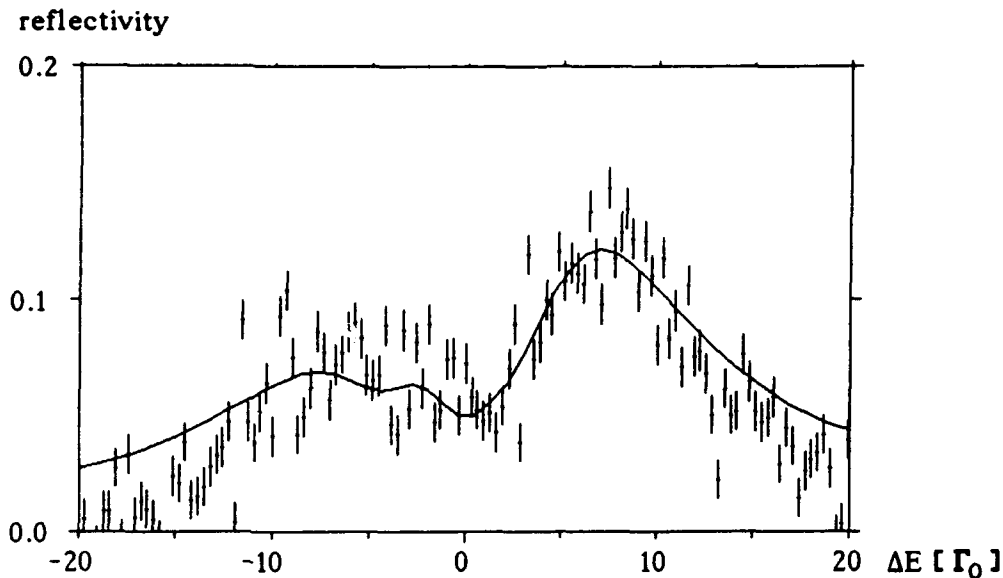
reflectivity

Fig.4 Energy dependence of the multilayer reflectivity in the nuclear Bragg peak of Fig.3.

The experiments have shown, that the concept of nuclear resonant multilayers can be realized. For further suppression of the nonresonant reflectivity the d-spacing of the multilayer has to be decreased, resulting in higher angles of incidence for the Bragg peaks at which the non-resonant reflectivity from the surface is much smaller.

References

[1] R. Rüffer, E. Gerdau, M. Grote, R. Hollatz, R. Röhlsberger, H. D. Rüter, W. Sturhahn; Nucl. Instr. Meth. A303, 495 (1991)

[2] J. B. Hastings, D. P. Siddons, G. Faigel, L.E. Berman, P.E. Haustein, J.R. Grover; Phys. Rev. Lett. 63, 2252 (1989)

[3] J. Arthur, G.S. Brown, D.E. Brown, S.L. Ruby; Phys. Rev. Lett. 63, 1629 (1989)

[4] A.I. Chumakov, M.V. Zelepukhin, G.V. Smirnov, U. van Bürck, R. Rüffer, R. Hollatz, H.D. Rüter, E. Gerdau; Phys. Rev. B41, 9545 (1990)

[5] W. Sturhahn, E. Gerdau, R. Hollatz, R. Rüffer, H.D. Rüter, W. Tolksdorf; Europhys. Lett. 14, 821 (1991)

[6] E. Gerdau, R. Rüffer; Hyp. Int. 27, 59 (1986)

[7] J.P. Hannon, N.V. Hung, G.T. Trammell, E. Gerdau, M. Mueller, R. Rüffer, H. Winkler; Phys. Rev. B32, 5081 (1985)

[8] U. van Bürck, G.V. Smirnov, R.L. Mößbauer, H.J. Maurus, S. Semioschka; J. Phys. C 13 (1980) 4511

Multilayer Structures Traversed by Electron Beams
as Narrow Line X-Ray Sources

(410) 516-7018

A. E. Kaplan and C. T. Law

Department of Electrical and Computer Engineering

The Johns Hopkins University, Baltimore, MD 21218

When an electron beam traverses the interface between two media with different dielectric constants, the so called transition radiation are generation [1]. In a periodic structure with multiple interfaces, the radiation is greatly enhanced around a spatial region in a conical pattern for certain wavelength. In previous research [1,2] structures with the thickness of each layer is much longer than the wavelength are used. As a result, ultra-relativistic electrons with energies 100 Mev to 50 Gev [2] are required. However, with advent of new technologies, periodic multilayer structures can be constructed with a spatial period less then 100 $\mathring{A}$. The generation of soft x rays with a low-energy electron beam that passes through such a multilayer structure was recently proposed [3]. In solid-state structures, the losses due to photoabsorption, and electron scattering may be the main obstacles in x-ray generation with these structures. We showed [4] that the energy of the electron beam from $\sim$ 200 Kev to a few Mev is sufficient to compensate for the loss due to electron scattering. We further demonstrated that above the electron energy of $\sim$ 200 Kev for most of the materials radiating soft x-ray frequency range, the photoabsorption is the limiting factor and electron scattering can be neglected. The phtotoabsorption imposes an energy "ceiling" above which further increase in beam energy is rewarded with diminishing radiation. Based on these results, we prescribe the optimal geometric configuration for maximum radiation from multilayer structures composed of certain materials at certain frequency and electron beam energy.

For transition radiation, electromagnetic field is generated due to the difference in dielectric constants between the neighboring layers and the power of the radiation is proportional to $|\Delta\epsilon(\lambda)|^2$ where $\Delta\epsilon$ is the difference between dielectric constants. Therefore, dispersion of dielectric constants of the materials strongly affects the optimal radiation and the spectral distribution. By choosing appropriate combination of

2

materials as the spacer and radiator for the multilayer structures, we demonstrate that electron beams passing through these structures can generate narrow line x-ray radiation. These lines are attributed to the extremely narrow resonance of dielectric constants of materials in the vicinity of atomic absorption edges. The available data for atomic scattering factor f for all elements in the periodic table show that only K, L, and M absorption edges have sharp resonances, and therefore, may significantly reduce the spectral width of transition radiation. Since various K, L, and M absorption edges of the elements in periodic table occur in the soft x-ray range between 10 $\overset{\circ}{A}$ to 100 $\overset{\circ}{A}$, narrow-line x-ray sources are feasible in the same range. To take advantage of this effect, maximize radiated power and reduce photoabsorption, we have formulated a "rule of thumb" in material selection: the radiator should be a heavy element with large atomic number and have its resonant frequency (i.e. frequency of one of its absorption edges) in the vicinity of the desired frequency whereas the spacer should be a light element with large atomic number and be nonresonant in the same frequency range. Typical examples for spacer are B, Be and C; we perform specific calculations for Ba, Ce and Eu as examples for radiator.

This research is supported by AFOSR.

References

1. V. L. Ginzburg and I. M. Frank, Zh. Eksp. Theor. Fiz. <u>16</u>, 15 (1946) [J. of phys. <u>9</u>, 353 (1945)]; M. L. Ter-Mikaelian, *High Energy Electromagnetic Processes in Condensed Media* (Wiley Interscience, New York, 1972).

2. M. L. Cherry, G. Hartmann, D. Muller and T. A. Prince, Phys. Rev. <u>D10</u>, 3594 (1974); P. J. Ebert, M. J. Maran, B. A. Dahling, B. L. Berman, M. A. Piestrup, J. O. Kephart, H. Park, R. K. Klein and R. H. Pantell, Phys. Rev. Lett. <u>54</u>, 893 (1985).

3. A. E. Kaplan and S. Datta, Appl. Phys. Lett. <u>44</u>, 661 (1984); S. Datta and A. E. Kaplan, Phys. Rev. <u>A 31</u>, 790 (1985).

4. C. T. Law and A. E. Kaplan, Opt. Lett. <u>12</u>, 900 (1987).

PHYSICS OF X-RAY MULTILAYER STRUCTURES

ADDENDUM AND POSTDEADLINE PAPERS

MARCH 2–5, 1992
JACKSON HOLE, WYOMING

PHYSICS OF X-RAY MULTILAYER STRUCTURES

POSTDEADLINE PAPERS
AND
ADDENDUM

JACKSON HOLE, WYOMING
MARCH 2-5, 1992

Postdeadline poster presentations
Monday 7:00 p.m. - 7:30 p.m.

PD1   Atomic Layer Epitaxy of Tungsten and Boron for Multilayer X-Ray Optics, J. K. Shurtleff, J. Phillips, MOXTEK, D. D. Allred, R. T. Perkins, L. V. Knight, J. M. Thorne, Brigham Young University.   No abstract available.

PD2   Characterization of Etched Laminar Multilayer Amplitude Gratings in the Soft X-Ray Region, Philippe Troussel, D. Schirmann, Centre d'Etudes de limeil-Valenton, France, S. Bac, R. Barchewitz, CNRS URA, France, Pierre Boher, Phillips Electronic Laboratory, France, C Kahn Malek, CNRS, France.   No abstract available.

PD3   Status of the Soft X-Ray/XUV Optical Metrology Program at the National Institute of Standards and Technology, Richard Watts, David L. Ederer, Thomas Lucatorto, Charles Tarrio, Natl. Inst. Standards & Tech.   We describe the final design parameters and expected performance of a new monochromator/reflectometer optical characterization facility being built at NIST.

PD4   Image Quality and Scattering by Multilayer X-Ray Mirrors and its Implication for the Fabrication of Diffraction Limited Large X-Ray Optics, Eberhard Spiller, IBM, T.J. Watson Research Center, Daniel Stearns, Lawrence Livermore National Laboratory. Analysis of image quality and scattering of our normal incidence soft x-ray telescope suggests that diffraction limited large x-ray mirrors with 0.01 arcsec resolution can be built.

Postdeadline oral presentations (Times to be announced)

PD5   Imaging X-Ray Multilayer Structures with Cross-Sectional Hrem, Yuanda Cheng, M. B. Stearns, D. J. Smith, Arizona State Univ., Daniel Stearns, Lawrence Livermore National Laboratory. No abstract available.

PD6   Limits to Ion Beam etching of Mo/Si Multilayer Coatings, R. Schlatmann, FOM Institute for Atomic and Molecular Physics, The Netherlands, C. Lu, Changchun Institute of Optics and Fine Mechanics, P.R. China, J Verhoeven, FOM Institute for Atomic and Molecular Physics, E. J. Puik, Shell Research, The Netherlands, M. J. Van Der Wiel, FOM Inst. for Plasma Physics, The Netherlands.   No abstract available.

ADDENDUM

MC12 **Layered Optics for Nuclear Monochromatization of Synchrotron Radiation,** E E. Alp, E Witthoff, T Mooney, Argonne National Lab., H Homma, M Kentjana, CUNY-Brooklyn. Originally scheduled as poster will be presented as an oral presentation.

Atomic Layer Epitaxy of Tungsten and Boron for Multilayer X-ray Optics. J.
K. Shurtleff and J. Phillips. MOXTEK, Box 7070, University Station, Provo,
UT 84602. D.D. Allred, R.T. Perkins, L.V. Knight and J.M. Thorne, Center
for X-ray Imaging, Brigham Young University, Provo, UT 84602.

The demand for high quality multilayer x-ray optics (MXOs) has
increased as x-ray imaging applications have developed. MXOs must be
uniform and smooth with precise periods. The period of the MXO
determines the angle and wavelength of the x-ray which can be reflected.
Current preparation techniques are limited to a period of approximately 40
Å. To reflect harder x-rays at near normal incidence, smaller periods must
be achieved.

We are investigating a new technique for producing MXOs. Atomic
layer epitaxy (ALE) is a chemical vapor deposition (CVD) technique which
can deposit a monolayer of atoms during each cycle of the deposition
process. The total thickness of the deposited film is determined by the
number of cycles and can be controlled to within a monolayer. A   ⁀
produce crystalline superlattice structures. Our theoretic⁀
show that the x-ray reflectivity of a crystalline superl⁀
approximately twice as large as a similar amorphous multilayer. ⁀
deposit multilayers on large or figured substrates, since the rea⁀   ⁀e
gaseous and diffuse rapidly. This is not possible with current multilayer
preparation techniques.

ALE can deposit a monolayer of atoms during each cycle, because a
surface exposed to a reactant can only chemisorb a monolayer of the
reactant. Reactant which is weakly physisorbed onto the strongly
chemisorbed layer can be removed. There are four steps in the ALE
process. First, the surface is exposed to the first reactant. The surface
chemisorbs a monolayer of the reactant. Second, any excess reactant is
removed by evacuation and nitrogen purging. Third, the surface is exposed
to the second reactant which reacts with the chemisorbed layer to produce
a monolayer of the desired material and gaseous products. Fourth, any
excess reactant and the reaction products are removed by evacuation and
nitrogen purging. This process is repeated until the sired thickness of
the material has been achieved. The key to ALE is that the reactants are
introduced sequentially, not simultaneously as in conventional CVD.

ALE has been used to deposit many of the II-VI and III-V
semiconductors. We have successfully deposited zinc sulfide by ALE;
however, these materials are not very useful for the preparation of MXOs.
Our theoretical calculations show that the x-ray reflectivity of a
tungsten/carbon multilayer is approximately thirty times greater than a
similar zinc sulfide/zinc selenide multilayer. We have pioneered the
deposition of single element materials by ALE. We have investigated the
deposition of tungsten and boron by ALE. We are confident that rhenium,
carbon and silicon can also be deposited by ALE.

We have investigated the deposition of tungsten by ALE using tungsten hexafluoride and hydrogen. The overall reaction is shown in [1].

$$WF_6 + 3H_2 \longrightarrow W_{(s)} + 6HF \quad [1]$$

During the deposition, we monitored the gaseous reactants and products using in situ mass spectroscopy. The total thickness of the film was measured using optical profilometry. The crystal structure was determined using thin film x-ray diffraction. The composition was measured using x-ray fluorescence spectroscopy and electron microprobe. We performed a statistical experiment to determined the optimum deposition parameters.

We have investigated the deposition of boron by ALE using diborane and chlorine. The overall reaction is shown in [2].

$$B_2H_6 + 3Cl_2 \longrightarrow B_{(s)} + 6HCl \quad [1]$$

We analyzed the boron samples using the same techniques we used for the tungsten depositions.

We are confident that rhenium can also be deposited by ALE using rhenium hexafluoride and hydrogen. Our theoretical calculations show that the x-ray reflectivity of a rhenium/carbon multilayer is larger than a similar tungsten/carbon multilayer. Rhenium does not form a stable compound with carbon which means that the interface between rhenium and carbon layers should be sharper than for tungsten and carbon layers. Rhenium sputter targets are expensive which has limited the use of rhenium for MXOs. ALE allows rhenium to be accessible for MXOs.

We are confident that carbon and silicon can also be deposited by ALE using methane, silane and chlorine. As we continue our research, more materials will become available for producing MXOs by ALE.

We have studied the deposition of materials by ALE which are useful in preparing MXOs. The next phase of our research will be to combine the materials into a MXO. This will require matching of the deposition parameters and crystal structures of the materials.

CHARACTERIZATION OF ETCHED LAMINAR MULTILAYER AMPLITUDE GRATINGS IN THE SOFT X-RAY REGION

P. TROUSSEL [(1)] - D. SCHIRMANN [(1)]
S. BAC [(2)] - R. BARCHEWITZ [(2)] - P. BOHER [(3)]
C. KAHN MALEK [(4)]

(1) Commissariat à l'Energie Atomique, Centre d'Etudes de limeil-Valenton,
94195 Villeneuve Saint Georges Cédex (France) - tél. (1) 45 95 62 50 -
(2) Laboratoire de Chimie-Physique, CNRS URA. 176,
11 rue Pierre et Marie Curie, 75231 Paris + Laboratoire pour l'Utilisation du
Rayonnement Electromagnétique (LURE),
Paris Sud (France)
(3) Laboratoire d'Electronique PHILIPS,
3 avenue Descartes, BP 15, 94451 Limeil-Brévannes Cédex (France)
(4) Laboratoire de Microstructures et de Microélectronique, CNRS,
196 avenue Ravera, 92220 BAGNEUX (France)

1. INTRODUCTION

The fabrication of lamellar multilayer gratings has permitted a number of results on the performances of these devices.(1)
The results obtained on a 3.µm pitch grating patterned by electron beam lithography, tested at 97 eV photon energy are presented. These are compared to a Kinematical theory for lamellar multilayer grating.
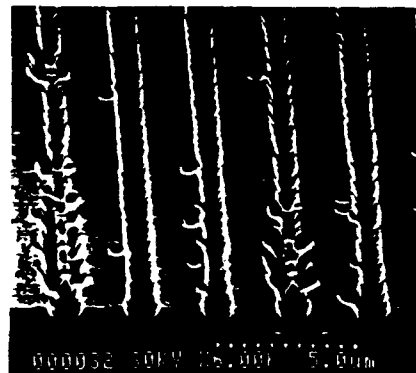
2. EXPERIMENTAL

2.1. Fabrication

The approach used for the fabrication of the multilayer gratings was first to coat the silicon wafer substrate with diode RF sputtering multilayer mirror (2) then to define the grating pattern by a lithographic technique and then to transfer the grating pattern inside the multilayer coating by etching (3). It presents advantage such as better definition of patterns such as higher accuracy and edge acuity.
Mo/Si multilayer mirror consisting of 40 bilayers of 4.76 nm of Mo and 7.64 nm of Si was optimized at 97 eV photon energy. Grating patterns with a 3 µm pitch (333 lines/mm) over an 3 x13 mm^2 area were generated by electron beam lithography. A grating with 1 um resist lines was patterned on the Mo26 multilayer mirror. An intermediate 30 nm thick aluminium layer was electron beam evaporated and transfered by the lift-off process in order to improve the selectivity and fedelity of the pattern during reactive ion etching in a plasma SF_6. The grating was etched through the multilayer mirror down to the substrate. Figure 1. shows a scanning micrograph of the multilayer grating: the grating pitch D and the groove cyclic ratio Γ (width multilayer/pitch) were measured to be approximately 3000 nm and 2/3 respectively.

Figure 1: Scanning electron micrograph of a fabricated multilayer etched grating

2.2) description of test station

Experiments were performed at SA23 X-ray beamline station of SUPER-ACO storage ring at the LURE.

The experimental set-up consists of two principal elements:
- a high flux monochromator, the wavelength of which is scanned by rotating holographic grating.
- a θ-2θ goniometer with possibility of independent rotation of the sample and of the detector. It is equipped with the following modules: an adjustable slit which limits the Synchrotron Radiation angular divergence, a pair of plane BK7 mirrors used as high-frequency cutoff.

The monochromator is vertically dispersing and accepts 4 mrad, and 3 mrad in the horizontal and vertical plane of the synchrotron radiation, s polarized. The absolute intensities are determinated by the ratio of the intensity in each order of the multilayer grating to that of the incoming beam.

2.3) results:

The diffraction pattern of the multilayer grating is recorded by three different modes:
- the grating scan mode by rocking the grating with a θ outgoing angle and with the detector fixed in a θ_d direction. θ is the measured outgoing angle referred to the mirror plane as defined in Figure 2(a).
- the detector scan mode by scanning the detector while keeping the sample at an θ_0 incoming angle. θ is defined as before (Figure 2b).
- the grating rule mode obtained by first optimizing the position of the grating at the expected incoming angle for each order and then by optimizing the position of the detector at the diffraction angle for that order in such a way that the grating rule is fullfilled.

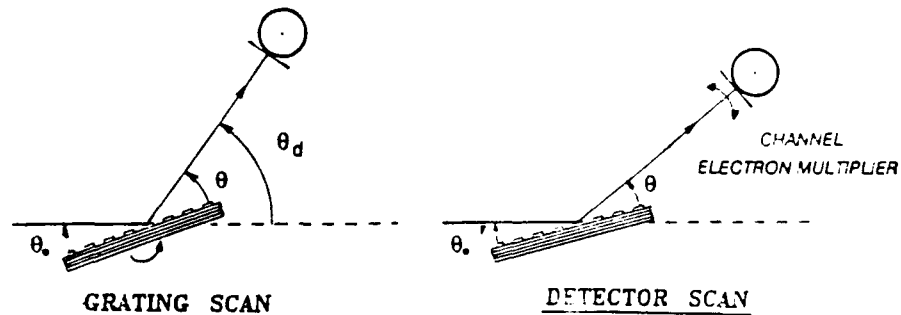GRATING SCAN   DETECTOR SCAN

Figure 2: Angular configuration for the grating scan mode and for the detector scan mode

The experimental diffraction patterns for the Mo26 multilayer grating are shown in Figure 3(a,b,c,d) obtained with a 1mrad incident radiation angular divergence. Figure 3(a) represents a grating scan, while the detector is fixed in θ_d= 65.1°. We observe several orders. Figure 3(b) and Figure 3(c) are two detector scan spectra with the grating fixed in direction θ_0= 32.55° and θ= 32.65° respectively. In Figu. 3(c), the grating is holding at the zeroth order Bragg angle. The ratio between the ±1 orders and the zeroth order in the detector scan mode is relatively less intense than in that in the grating scan mode. Figure 3(d) represents the three grating rule scans modes corresponding to the zeroth and ±1 orders. We

have a partial overlapping of the various grating orders, because the period is too great. A smaller period is necessary to ensure a good dispersion by the grating.
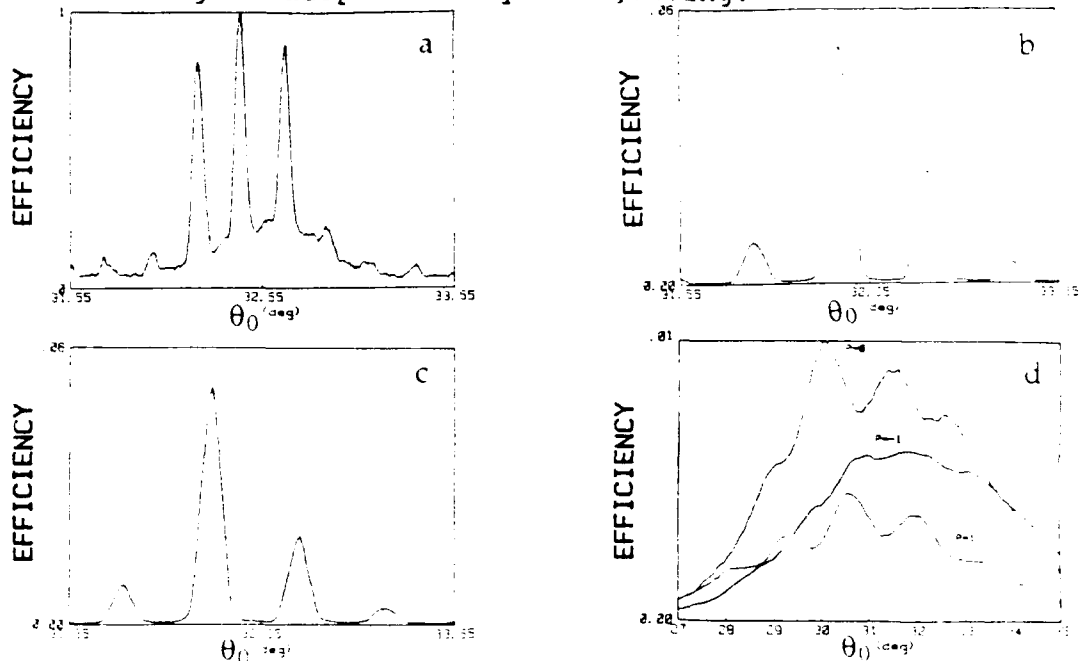

Figure 3: Experimental diffraction pattern of the grating at 97 eV in the grating scan mode (a), in the detector scan mode (b) (c), and in the grating rule mode (d).

Figure 4 represents two detector scan modes keeping the sample at $\theta=32.5°$ with a better collimated beam: 0.5 mrad vertical divergence in figure 4a and 0.3 mrad in Figure 4b: we observe several orders in the spectra which can be attribuated to the slight divergence of the incoming angle , to the lack of flatness of the sample surface, and to the spatial profile of the incident beam.
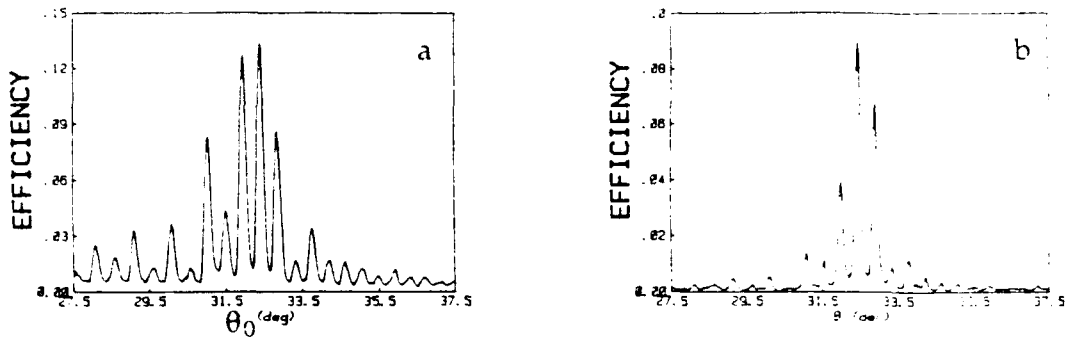

Figure 4: Experimental diffraction pattern of the grating in the detector scan mode with a 0.5 mrad divergence (a) and 0.3 mrad (b)

3.THEORETICAL MODEL

The main features of the diffraction pattern can be determined within the framework of the kinematical approach. In particular, the shape of the diffraction spectra is well described by the Fourier transform of the spatial distribution

of the coherent scattering factor on a bidimensionnal lamellar multilayer grating. A standard calculation gives for the diffraction pattern of a multilayer lamellar grating:

$$I = Io\ \sin^2_c(u\Gamma D)\sin^2_c(v\gamma d) . \left[(\sin(N_r\pi uD)./N_r\sin(\pi uD)).(\sin(N_{bi}\pi vd)/N_{bi}\sin(\pi vd))\right]^2$$

with $u = (\cos\theta - \cos\theta_0)/\lambda$ and $v = (\sin\theta + \sin\theta_0)/\lambda$

λ is the radiation wavelength in vacuum, d is the period of the multilayer mirror. The average refractive index of the grating medium value(n) has been taken to the corresponding vacuum value.N_{bi} is the number of bilayers (40), N_g is the number of illuminated grating period. The relationship (1) shows that a necessary condition for obtaining diffraction by the whole system, i.e. both laterally and in depth is that the two denominators vanish at the same time. The condition contains both the Bragg law written in a general form:

$$m\lambda = d(\sin\theta + \sin\theta_0)$$

and the grating rule: $p\lambda = D(\cos\theta - \cos\theta_0)$

Figure 5 is a detector scan computed with the formule (1). The agreement with the experimental spectrum (Figure 3c) is relatively good
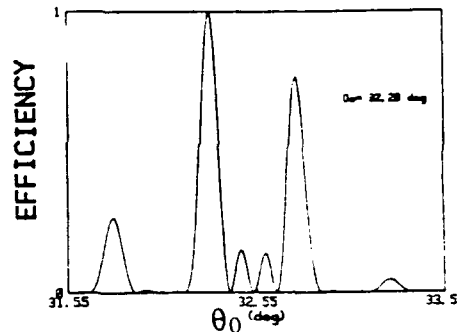

Figure 5: Theoretical diffraction pattern of the grating in the detector scan mode

4.CONCLUSION

One laminar multilayer amplitude grating patterned by electron beam lithography, and etched down to the substrate, was tested at 97 eV. The importance of the divergence value on the quality of the spectra is shown. The shape of the diffraction spectra is well described by a simplified kinematical theory, but the efficiencies could only be explained with a dynamical theory diffraction.

REFERENCES
1. T.W. Barbee, J.C.Rife and P.Pianatta Opt.Eng 29, 738 (1990)
2. P.Boher et al San diego July (1991) conf.1547.
3. C.Khan Malek, F.R.Ladan, M.Carré, and R.Rivoira, Proc.Microcircuit Eng., 90, 283, 1991.

Status of the Soft X-ray/XUV Optical Metrology Program at the National Institute of Standards and Technology

Richard Watts, David Ederer, Thomas Lucatorto and Charles Tarrio
Division of Electron and Optical Physics
Physics Laboratory
National Institute of Standards and Technology
Gaithersburg, MD 20899
(301) 975-6892;   fax (^^1) 975-3038

The National Institute of Standards and Technology (NIST) has initiated a program devoted to the characterization of soft x-ray optics at the wavelength of use. Although NIST has an operational XUV characterization facility which it is using to make measurements for users across the country, that facility suffers from several deficiencies that will limit its usefulness in the coming years. Therefore, we are constructing an improved monochromator/ reflectometer beamline that will upgrade and extend our XUV measurement capabilities.

We will describe the optical properties of the new monochromator, shown schematically in Fig. 1 and detailed in Table 1, and discuss the state of the design of the the new reflectometer. The monochromator is based on a varied line spaced plane grating that uses simple optical elements in a fixed entrance slit/fixed exit slit geometry. Important features of the new instrument include high throughput, simple wavelength scanning, resolutions in excess of 1000, and the ability to characterize large (in excess of 30 cm diameter) optical surfaces with small radii of curvature.
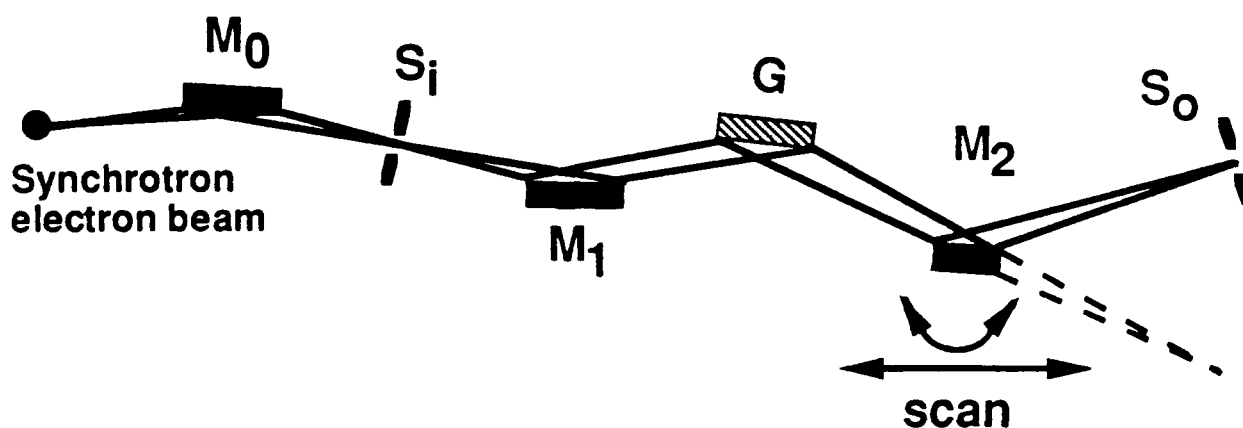

Figure 1. Optical setup for NIST varied line spaced monochromator with entrance slit S_i, toroidal 1:1 focussing mirrors M_0 and M_1, plane varied line spaced grating G, plane scanning mirror M_2, and exit slit S_0.

Table 1
Design Parameters for NIST VLS monochromator (dimensions in cm)

Dimensions:

Source to M_0	254
S_i to M_1	325
M_1 to G	40 (G_1), 50 (G_2)
G to S_o	285 (G_1), 275 (G_2)

Transfer mirror (M_0):

Material:	Nickel coated toroid on Glidcop blank
Blank size:	6.5 x 15
Illuminated area:	5 x 15
Acceptance angle (h x v):	20 mrad x 3 mrad
Grazing angle of incidence:	
Radii of curvature	$R_m = 4,853$ $R_s = 13.3$

Focus mirror (M_1):

Material:	Nickel coated toroid on Glidcop blank
Blank size:	8.5 x 20
Illuminated area:	7 x 20
Acceptance angle (h x v):	20 mrad x 3 mrad
Grazing angle of incidence:	3°
Radii of curvature:	$R_m = 6,210$ $R_s = 17.0$

Grating (G):

	G_1	G_2
Material	Gold coated ULE blank	
Ruling Size:	6 x 14	6 x 10
Nominal line density $1/d_0$:	1500 l/mm	600 l/mm
Grazing angle of incidence:	3.5°	5°
Blaze angle:	2.5°	2.6°

Plane scan mirror:

Material:	Nickel coated silica
Blank size:	5 x 12.5
Grazing diffraction angle scanned:	3° - 15°
Grazing angle of incidence:	3° - 15°

Focal spot properties at 100 Å:

Size (max)	2 mm x 2 mm
Divergence (h x v, max)	20 mrad x 7 mrad
Resolving power	100 - 2000
Flux (photons/s/0.2 Å)	8×10^{10}

Image Quality and Scattering by Multilayer X-Ray Mirrors
and its Implication for the Fabrication of Diffraction Limited
Large X-Ray Optics

Eberhard Spiller

IBM Research Division, T. J. Watson Research Center
P.O. Box 218, Yorktown Heights, NY 10598

Daniel Stearns

Lawrence Livermore National Laboratory, Livermore CA 94550

Roughness of the boundaries presents a severe limitation for the performance of multilayer x-ray mirrors with small periods $\Lambda < 50\mathring{A}$, and makes it difficult to produce efficient multilayers with periods approaching the size of the atoms in the coating. Reflectivities are reduced by a large factor from the theoretical smooth boundary value, for example nearly a factor 10 for a coating with period $\Lambda = 30\mathring{A}$. If all the loss in reflectivity would appear as scattered light within the field of view of an instrument, one would not be able to obtain high contrast images of extended objects; each image element would be surrounded by a halo of scattered light of much higher total intensity.

However, no indication of scattering has been observed in any imaging experiment up to now [1-4]; There is a list of arguments to explain the reduction in scattering:

1. Near the reflectivity maximum of a properly designed multilayer mirror, the amplitudes of all periods add in phase resulting in a reflectivity increase proportional to N^2, where N is the number of contributing periods, while scattered light adds up with random phases producing only an increase proportional to N. Thus the relative amount of scattering is reduced by a factor N.

2. The multilayer coating near its maximum has reduced absorption, because the absorbing layers are located near the nodes of the standing wave within a coating. The reduction in the absorption is smaller for scattered light, which propagates with more randomized phases or angles through the structure. A large fraction of the internally scattered light will therefore be absorbed and not contribute to scattering outside the coating.

3. In a multilayer, where the heavy material is much thinner than the low absorption spacer material, the boundaries are close to the nodes of the standing wave within the coating, where intensities are low thus reducing scattering

4. A large contribution to the measured roughness of the boundaries occurs at high spatial frequencies which scatter into evanescent waves or waves propagating at large angles outside the field of view of our instruments. These spatial frequencies reduce the specular reflectivity but have no detrimental effect on the imaging performance.

The arguments 1) and 2) implicitly assume that roughnesses of different boundaries are uncorrelated in a multilayer stack. This is expected to be true for very high spatial frequencies in the roughness spectrum, where roughness is caused by randomness in the positions of few atoms. Such fluctuations are averaged out for very sm·" frequencies (large periods with a ...ge number of atoms per period). Replication of the surface topography from layer to layer is therefore expected for long spatial periods, making the arguments in points 1) and 2) above invalid.

We have measured scattering of the multilayer coatings used for our normal incidence soft x-ray telescope at $\lambda = 63.5\text{Å}$ at $\lambda = 1.54\text{Å}$ and grazing angles of incidence and at soft x-rays near normal incidence. Rocking curves and detector scans around the first order reflectivity maximum are obtained at $\lambda = 1.54\text{Å}$, and the detector scans show drastically reduced scattering as expected from the arguments 1-3 above. Furthermore, the edge of the moon is used as a known test target to estimate the amount of scattering in the arcsec range from images obtained on the date of the solar eclipse on July 11, 1992. The internal surfaces of the coating are inspected by high resolution electron microscopy. Tunnel microscopy and optical profilometry have been used previously to characterize the top surface of the mirror[4].

We compare our results with data that are theoretically obtained from a model of the multilayer structure. We find, to our surprise, that we can describe the measurements at small scattering angles only, if we assume that the roughness of the internal boundaries is much smaller than that of the top surface for large spatial periods in the roughness spectrum. The roughness (figure error) of the internal boundaries has to be less than 0.5Å for spatial periods in the 0.1 to 1mm range in order to fit the data. This result make us optimistic about our capability to fabricate large diameter optical elements with diffraction limited performance.

Interferometers[5] and profilometers[6] which can measure figure errors in the 1Å range for spatial periods above 1mm have become commercially available in the last few years and historically the fabrication capabilities for optical surfaces has always been equal to the measurement capabilities. We expect that this match will continue in the future. One way to fabricate such a surface is the thin film deposition methods which we use to produce our multilayer coatings. We have been able to produce coatings with accumu-

lated thickness errors under 3Å, thickness uniformity better than 0.5% over a 25cm diameter and no accumulation of roughness over total thicknesses up to 0.5μm . Properly shaped masks between the evaporation sources and the mirror surfaces were used to obtain this uniformity. We can also shape these masks to produce a thickness distributions which corrects the figure errors in a surface. For example, starting with a mirror with figure errors in the 200Å range and a map of the deviations from the desired surface with an accuracy in the Angstrom range, we could deposit a corrective thin film structure on the mirror which reduces the errors by about a factor 100 in only one deposition run. Repeats of the cycle could be used for further reduction of the errors.

Up to now this method has been tested for rotationally symmetric corrections. It can be applied to transform a perfect sphere into a perfect paraboloid or hyperboloid. We are confident that we can produce a telescope mirror with 0.01 arcsec resolution.

References

[1] J. Henry, E. Spiller, and M. Weisskopf, "Imaging Performance of a Normal Incidence Soft X-Ray Telescope," Appl. Phys. Lett. **45**, 25-27 (1982).

[2] A. B. Walker, T. W. Barbee, R. B. Hoover, and J. F. Lindblom, "Soft   lar corona with a normal-incidence Cassegrain multilayer telescope."
Science **241**, 1781-1787 (1988).

[3] L. Golub, M. Herant, K. Kalata, I. Lovas, G. Nystrom, E. Spiller, and J. Wilczynski, "Sub-Arcsecond Observations of the Solar X-ray Corona," Nature **344**, 842-844 (1990)

[4] E. Spiller, R. McCorkle, J. Wilczynski, L. Golub, G. Nystrom, P. Takacz, and C. Welch, "Imaging Performance and Tests of Soft X-Ray Telescopes," Proc. SPIE **1343**, 134-144 (1990).

[5] M. M.Küchel, "The new Zeiss interferometer," Proc. SPIE **1332**, 655-663 (1990)

[6] P. Glenn, "Angstrom level profilometry for sub-millimeter to meter scale surface errors," Proc. SPIE **1333**, 326-336 (1990).

[7] E. Spiller, J. Wilczynski, L. Golub, and G. Nystrom, "The normal incidence soft x-ray, $\lambda = 63.5$Å telescope of 1991," Proc. SPIE **1546**, 168-174 (1991)

IMAGING X-RAY MULTILAYER STRUCTURES WITH CROSS-SECTIONAL HREM

Y. Cheng, M.B. Stearns and D.J. Smith*, Physics Department, Arizona State University, Tempe, AZ 85287
*Also at Center for Solid State Science, Arizona State University, Tempe, AZ 85287
D.G. Stearns, University of California, Lawrence Livermore National Laboratory, Livermore, CA 94550

High-resolution electron microscopy (HREM), with a resolution below 2Å, is the best tool for observing the actual detailed structure for ML. This gives direct atomic scale information about the film structure, including the bilayer thickness, the crystalline structure and the roughness of the individual layers and the interlayers.

In order to maximize the contrast, the HREM images of multilayers are typically recorded with the objective lens close to the Scherzer defocus. For the JEM-4000EX microscope used in this study, the Scherzer defocus is -320Å below the in focus position. The question has been raised as to how trustworthy are the multilayer micrographs and in particular how sensitive are the observed multilayer parameters to different defocus conditions of the objective lens. Further questions concern the effects due to the orientation of the cross-sectional specimen. The specimen is usually aligned with a double-tilt sample holder to the edge-on orientation so that the specimen is viewed with the electron beam direction parallel to the layers as well as to one of the zone axes of the single crystal substrate. Such alignment can be accomplished using the selected area electron diffraction (SAED) pattern from an area containing both some of the substrate and the multilayer area of interest. In order to exam how the apparent ML parameters change with the imaging conditions of the objective lens focus and ML orientation, we have prepared a cross-sectional specimen of a high quality ML composed of Mo and Si layers. A set of through focus TEM images of the ML cross-section were taken at edge-on orientation using a JEM-4000EX HREM. The point-to-point resolution of the microscope is better than 1.7Å. To determine the sensitivity of the images off-axis alignment an image of the ML was also taken at Scherzer defocus with the specimen slightly tilted from the edge-on orientation.

From measuring the multilayer parameters on the HREM images taken at exact edge-on orientation with different objective lens focus, we found that there is no significant change in the bilayer thickness of the multilayer for the objective lens focus range of +320Å to -1280Å. The pure Mo and Si layers and the Mo-on-Si and Si-on-Si interlayers thicknesses were also

seen to be same over the focus range of +320Å to -640Å. These measured multilayer parameters were found to be in good agreement with those obtained from small and large angle x-ray scattering spectra. However, the micrographs taken with defocus of 960Å or more were found to be unreliable with significant deviation in multilayer parameters from those of the Scherzer defocus. Thus the "safe range" of the objective lens defocus was found to be ≤ 640Å for our JEM-4000EX microscope.

The ML image taken with the specimen slightly tilted from the exact edge-on orientation showed a thicker Mo and thinner pure Si layers with much fewer Mo crystallites visible. The apparent bilayer thickness of the ML measured on this image was also found to be unreliable. This shows that precisely tilting the ML specimen to the exact edge-on orientation is necessary in order to obtain the true layer thicknesses. Such alignment is not difficult to achieve by observing the behavior of the Laue circle.

Limits to Ion Beam etching of Mo / Si multilayer coatings

R. Schlatmann, C. Lu + *and J. Verhoeven*

FOM Institute for Atomic and Molecular Physics, Kruislaan 407, 1098 SJ Amsterdam, The Netherlands.

+*Present address: Changchun Institute of Optics and Fine Mechanics,Academica Sinica, P.O.Box 1024, Changchun, Peoples Republic of China.*

E.J. Puik ++ *and M.J. van der Wiel*

FOM Institute for Plasma Physics, P.O. Box 1207, 3430 BE Nieuwegein, The Netherlands.

present address: Shell Research , P.O.Box 3003, 1003 AA Amsterdam, The Netherlands.

Recently ion beam etching of electron beam deposited metal layers on C has resulted in higher x-ray reflection coefficients[1]. In spite of the widely recognized importance of Mo/Si multilayer coatings for projection lithography, little work has been done to use the etching technique on multilayer mirrors made of this combination of materials. As Mo/Si multilayer mirrors of d-values greater than 12 nm. have already been made with reflectivities very close to the theoretical maximum[2], our main interest is in multilayers with smaller d-values.

We have investigated the effect of ion beam etching on the morphology and surface smoothness of Mo on top of Si layers and of Si on top of Mo layers. In this study we varied the species of the etching ions (Ar and Kr) and the ion energy (from 200 up to 1500 eV). Increased x-ray reflectivities could be observed for every combination of ion species and energy.

The techniques we used in this study were Auger Electron Spectroscopy (AES), Transmission Electron Microscopy (TEM) and *in situ* soft x-ray reflection. Soft x-rays of 3.16 nm. were used (the N-Kα line), incident at an angle of 35 degrees with the surface. The reflected x-ray was detected with a proportional counter. For the combination of wavelength and angle used, the well known Bragg formula gives an (interference) period of 2.8 nm in the reflection signal that is measured *during* deposition or etching of material. Furthermore the average of the oscillations of the reflected signal is a measure for the roughness of the surface layer.

The layers were deposited by e-beam evaporation at a rate between 0.01 and 0.03 nm per s., at a substrate temperature of 300 K for Si on Mo and 350 K for Mo on Si. For the ion beam etching a 3 cm Kaufman gun was used, with the ions incident on the 1 cm² substrate at an angle of 45 degrees with the surface. The intensity of the ion beam was kept constant at 15 μA/cm² for all energies of the Ar and Kr ions.

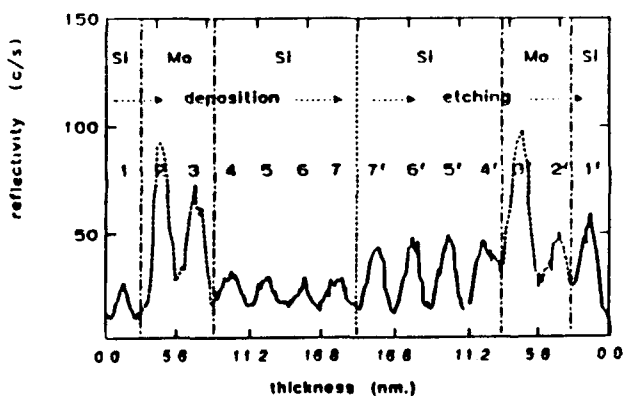In the case of Si evaporated onto Mo, the resultant films were amorphous according to TEM. The average reflection signal remained constant up to the maximum thickness investigated of 11.2 nm. Etching with 300 or 800 eV Ar ions resulted in a rapid increase in average reflectivity, within the first 1.4 nm of etching. Further etching hardly affected the reflectivity, which only decreased when the last 1.4 nm of Si on Mo were reached. Fig. 1 shows the reflectivity curve as a function of layer thickness during growth and during sputtering with 300 eV Ar+ ions.

fig. 1 Reflectivity during growth of Si on Mo and during etching with 300 eV Ar+ ions.

To study the growth of Mo on Si we deposited 11.2 nm of Mo on Si, prior to ion beam etching. According to TEM, the Mo grows as amorphous islands to an average layer thickness

of 4.0 nm, after which small crystallites begin to appear. These crystallites grow as the layer thickness increases. The average reflectivity signal collapses as the Mo layer grows to 11.2 nm.
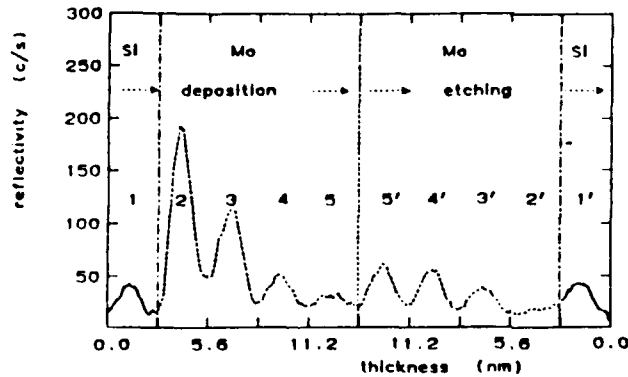

fig. 1 Reflectivity during growth of Si on Mo and during etching with 300 eV Ar+ ions.

During etching we observe an initial increase in average reflectivity, followed by a decrease. The initial increase as well as the subsequent decrease is visible for all ion energies of both Ar and Kr. The onset of the decrease of average reflectivity with etching depth depends on the ion energy, ion species and film thickness. Fig. 2 shows the reflectivity curve as a function of layer thickness during growth and during sputtering with 300 eV Ar+ ions.

Finally, we compared etching a thin layer to etching a thicker layer, both with 300 eV Ar ions. When etching a thin Mo film of 5.6 nm back to 2.8 nm, reflectivity increases by a factor 2 and TEM shows a complete disappearance of the crystallites. However when etching thicker films (11.2 nm), the initially growing average reflectivity collapses and TEM reveals that crystallites do not disappear until 8.4 nm of Mo has been etched off. The residual 2.8 nm film, according to TEM, then has an amorphous character and is not closed any more.

The constant average reflectivity signal of Si growing on Mo in our opinion indicates that Si grows with the same surface roughness as the underlying Mo layer. We ascribe the rapidly increasing average reflectivity, when etching, to a decreased roughness that quickly reaches its minimum and then stays constant. The subsequent decrease in reflectivity when etching off the last 1.4 nm of Si is caused by mixing at the interface, which is confirmed by AES.

For Mo growing on Si we think the growth of the crystallites causes a strong increase in surface roughness, leading to the collapse of the average reflectivity. We attribute the observed increased average reflectivity upon etching to surface smoothing as a result of the removal of the top ends of the crystallites. The subsequent decrease can be explained by two effects, depending on the ion energy and mass: Ion beam induced crystallization and interface mixing. For the lower ion energies (200 and 300 eV) we observe the collapse of the average reflectivity after a constant ion dose of approx. $4 * 10^{16}$ ions/cm^2 for both Ar and Kr. We think that after this dose crystallization occurs in the layer, with the remaining crystallites acting as nucleation centres. The crystalline Mo is then etched at a rate different from that of the amorphous Mo. This gives rise to an increased surface roughness causing the observed decrease of the average reflectivity. This hypothesis is supported by the observation that the 5.6 nm layer could be etched off to a smooth amorphous 2.8 nm layer with increased reflectivity, whereas etching the 11.2 nm layer down to 2.8 nm resulted in an amorphous layer with large holes in it and no reflectivity left. Therefore, within this explanation the effect of the ion beam etching is determined by the deposition morphology.

For the higher ion energies (1100 and 1500 eV) the average reflectivity started to decrease before the critical dose of ions was reached. In these cases we think the decrease was caused by interface mixing. The residual layer thicknesses when average reflectivities started to drop are in good agreement with the calculated values for the penetration depths for ions of that mass and energy (using the analytical program VG SUSPRE). For 800 eV ions and an initial layer thickness of 11.2 nm, interface mixing and crystallization are expected to occur at approximately the same residual layer thickness of 4.5 nm.

In conclusion, improvement of reflectivity by ion beam etching of Mo/Si multilayer coatings is observed for all ion energies of Ar and Kr, but it is limited by interface mixing and the deposition morphology of the Mo layer. Interface mixing requires the film thickness be greater than the ion penetration range, and the deposition morphology puts a maximum to the layer thickness that can be removed uniformly. Nevertheless improvement of the reflectivity by

a factor of 2 is expected for multilayers with d-values between 5 and 10 nm as a result of ion beam etching.

References

1.   E.J. Puik, M.J. van der Wiel, J. Zeijlemaker and J. Verhoeven, Appl. Surf. Sci. 47, 63 (1991)
2.   D.G. Stearns, R.S. Rosen, S.P. Vernon, J. Vac. Sci. Technol. A 9 (5), 2662 (1991).

PHYSICS OF X-RAY MULTILAYER STRUCTURES

Key to Authors

Allred, D D. - PD1
Bac, S - PD2
Barchewitz, R - PD2
Boher, Pierre - PD2
Cheng, Yuanda - PD5
Ederer, David L. - PD3
Kahn Malek, C - PD2
Knight, L V. - PD1
Lu, C - PD6
Lucatorto, Thomas - PD3
Perkins, R T. - PD1
Phillips, J - PD1
Puik, E J. - PD6
Schirmann, D. - PD2
Schlatmann, R - PD6
Shurtleff, J K. - PD1
Smith, D J. - PD5
Spiller, Eberhard - PD4
Stearns, Daniel - PD4, PD5
Stearns, M B. - PD5
Tarrio, Charles - PD3
Thorne, J M. - PD1
Troussel, Philippe - PD2
Van Der Wiel, M. J. - PD6
Verhoeven, J - PD6
Watts, Richard - PD3
Witthoff, E - PD7